takece.com
Continuing Education Simplified!

Echocardiography: Clinical Applications

Topic List:-

Chapter

Clinical Benefits of New Echocardiographic Methods

Teja Seneković Kojc and Nataša Marčun Varda

Abstract

The main goals of a good echocardiographic examination are an accurate assessment of myocardial function and precise presentation of cardiac morphology. Therefore, some new echocardiographic methods, such as functional echocardiography, cardiac deformation imaging, and 3D echocardiography, are becoming increasingly useful. The main advantages of each method, the possibilities for clinical use, and the most important limitations are presented in this paper. Functional echocardiography enables real-time evaluation of cardiac performance, identifying the nature of cardiovascular compromise, guiding therapeutic decisions, and monitoring response to treatment. A better understanding of the cardiac function and hemodynamic changes in critically ill patients is a crucial clinical benefit of the method. Myocardial deformation imaging could be beneficial for the detection of early ventricular dysfunction, especially where classical methods are unreliable. The new methods do not rely on geometric assumptions and can quantify regional as well as global ventricular function. 3D echocardiography allows understanding of complex spatial cardiac relationships; furthermore, it can be valuable in understanding functional anatomy and help planning interventions.

Keywords: echocardiography, congenital heart disease, functional echocardiography, myocardial deformation imaging, speckle-tracking imaging, three-dimensional echocardiography, four-dimensional echocardiography

1. Introduction

Congenital heart diseases (CHD) are highly variable, ranging from simple to complex lesions. Therefore, pediatric echocardiography faces different challenges, especially in demonstrating complex anatomy and assessing myocardial function in ventricles with variable morphology [1]. At the same time, there is a desire to detect early changes in ventricular function in cardiac patients as well as in patients with systemic diseases potentially affecting the heart. Furthermore, bedside techniques are increasingly used in clinical medicine, which is also seen in pediatric echocardiography. Consequently, the development of new methods or the upgrade of existing ultrasound techniques is urgently needed.

Recent advances in pediatric echocardiography include functional imaging, myocardial deformation imaging, and 3D echocardiography. Advances in ultrasound techniques, especially in pediatric probes, allow imaging with high temporal and

spatial resolution, which opens a new perspective on the mechanics and function of the myocardium. 3D echocardiography can help understand complex anatomy with associated functional changes, which is valuable for appropriate intervention planning. For pediatric cardiac patients, a highly variable ventricular morphology is typical, therefore, assessment of myocardial function may be challenging, especially assessment of right ventricular function and function of a single ventricle. Deformation imaging with strain and strain-rate quantification enables quantitative assessment of myocardial function independent of underlying morphology [1, 2]. Strain imaging also enables detecting minimal changes in the global and regional systolic function of the ventricles and allows recognition of the preclinical stage of different diseases affecting the heart [3].

Functional echocardiography has become increasingly useful in everyday clinical practice; nowadays it plays a central role in understanding and managing hemodynamics in critically ill patients [4]. Functional echocardiography facilitates real-time evaluation of cardiac performance, identifying the nature of cardiovascular compromise, guiding therapeutic decisions, and monitoring response to treatment [5]. Namely, early detection of cardiac dysfunction may help to choose an appropriate inotropic or vasopressor support. Good collaboration with pediatric cardiologists taking care of the patient is essential in the performance and interpretation of functional echocardiography [6].

2. Functional echocardiography

Bedside functional echocardiography provides physiological information and is a useful real-time noninvasive method among other monitoring tools for critically ill children. It is being increasingly used in making therapeutic clinical decisions and assessing response to treatment in unstable patients in the intensive and emergency units [7].

Functional echocardiography allows bedside use of cardiac ultrasound that brings fast and efficient investigation and recognition of the key hemodynamic changes, an assessment of cardiac function, pulmonary hypertension, pericardial effusion, and evaluation of the shunts. It provides insights into pathophysiology that leads to significant hemodynamic instability, and in addition, therapeutic interventions could be better planned and targeted. It also enables monitoring responses to treatment, which allows rapid therapeutic adjustments [7–10].

Functional echocardiography is also called targeted echocardiography, point-of-care cardiac ultrasound, or clinician performed ultrasound. It is being used to assess preload, afterload, and cardiac contractility while choosing inotropic or fluid therapy [4, 7].

Functional echocardiography performed in the newborn differs significantly from that performed in older children, because of the increased risk of critical or significant CHD. Therefore, the first echocardiography performed on a newborn should be accurate and structured with sequential segmental analysis of the heart. The subsequent scans can be functional, focused, or targeted to address specific clinical questions [7, 11–13].

Table 1 summarizes the recommendations for the practice of functional echocardiography including neonatologist-performed echocardiography.

Clinical benefits of functional echocardiography are well seen in patients with hypotension and shock, which are common conditions in critically ill children, both likely to have high mortality. Furthermore, echocardiography is crucial in identifying

Parameter	Recommendations
Left ventricular systolic function	• Qualitative assessment (eye-balling) • Quantitative assessment (M-mode measurements of LVEDD and LVESD with a thickness of the septal and posterior wall) • Shortening fraction can be measured by M-mode if there is no regional wall motion abnormality or abnormal septal motion • Ejection fraction should be calculated using biplane volumetric Simpson's measurements
Left ventricular diastolic function	• Doppler mitral or tricuspid inflow flow and pulmonary venous flow • TDI velocities at the mitral or tricuspid annulus
Right ventricular systolic function	• Qualitative visual assessment • Quantitative assessment (TAPSE and FAC)
Volume status	• IVC size and collapsibility • Measurement of LVEDD
Pulmonary artery pressure	• Estimation of RVSP and SPAP, MPAP and DPAP (Doppler measurement of tricuspid regurgitation and pulmonary regurgitation jets) • Pressure gradient across the PDA
Cardiac output	• Left ventricular output method with pulsed Doppler tracing of TVI in the left ventricular outflow tract and measurement of the cross-sectional area of the left ventricular outflow tract (in the presence of a PDA, the left ventricular output method does not reflect systemic blood flow)
Pericardial effusion	• Measurements of effusion at the end of diastole • Assessment of the hemodynamic significance
PDA	• The presence of a PDA • Direction of the shunt and pressure gradient between the aorta and pulmonary arteries • Hemodynamic significance in the case of left-to-right shunt by studying the degree of volume overload and left ventricular dimensions
PFO	• The presence of a PFO • Shunt direction and the pressure gradient between the right and the left atrium

DPAP, diastolic pulmonary artery pressure; FAC, fractional area change; LVEDD, left ventricular end-diastolic dimension; LVESD, left ventricular end-systolic dimension; MPAP, mean pulmonary artery pressure; PAP, pulmonary artery pressure; PDA, patent ductus arteriosus; PFO, patent foramen ovale; RVSP, right ventricular systolic pressure; SPAP, systolic pulmonary artery pressure; SVC, superior vena cava; TAPSE, tricuspid annular plane systolic excursion; TDI, tissue Doppler imaging; TVI, time velocity integral.

Table 1.
Recommendations for functional echocardiography.

the underlying pathophysiology, evaluating hemodynamics, and managing the response to treatment in patients with shock [7, 14].

Information from functional echocardiography in conjunction with other clinical parameters and monitoring tools can be used in choosing fluid resuscitation therapy and appropriate inotropic, vasopressor, or vasodilator therapy [15–17]. Early recognition of increased pulmonary pressure may help in the early institution of pulmonary vasodilators, especially in neonates with pulmonary hypertension [7, 9, 11, 17].

Functional echocardiography offers the potential for novel insights into cardiovascular impairment. Specifically, whether the concern relates to preload, afterload,

or myocardial contractility. Serial echocardiography evaluation to monitor treatment response may provide a better understanding of physiology and guide the duration of treatment, which minimizes drug exposure [11].

Assessment of volume status is usually made with inferior vena cava (IVC) size and collapsibility, which is also the method of choice to evaluate right heart filling pressure. This can be done easily in spontaneously breathing children, but some limitations exist in ventilated patients. In the presence of cardiogenic shock and increased right heart filling pressure, the IVC will appear dilated with no respiratory variation [15].

Qualitative estimation of the severity of pulmonary hypertension can be made by assessing the shape of the left ventricle and interventricular septum (IVS) motion, which is obtained from the parasternal short-axis view. With rising pulmonary artery pressure (PAP), the left ventricle begins to lose its circular shape and IVS starts to flatten, furthermore, paradoxical septal movement may occur in severe pulmonary hypertension [7, 9]. The shunt across the patent foramen ovale (PFO) is generally bidirectional in the presence of pulmonary hypertension but can sometimes be left-to-right even in the presence of severe pulmonary hypertension. An exclusively right-to-left shunt across the PFO is always abnormal and suggests elevated right heart filling pressure [6]. Direct assessment of the pulmonary artery pressures can be done by a peak velocity of the tricuspid insufficiency jet using the modified Bernoulli equation. The pulmonary artery systolic pressure (PASP) may be estimated by adding right atrial pressure to the peak systolic pressure gradient between the right ventricle and right atrium. The mean pulmonary artery pressure (MPAP) is assessed by using the peak diastolic velocity of the pulmonary regurgitation jet. The end-diastolic velocity of the pulmonary regurgitation jet is used to estimate diastolic pulmonary artery pressure (DPAP) [6, 7]. Functional echocardiography is useful in the initiation of vasodilator treatment (such as inhaled nitric oxide) and monitoring the response to treatment [6].

Pericardial effusion is a common condition in intensive care units; functional echocardiography allows easy diagnosis and timely echo-guided pericardiocentesis [18]. The hemodynamic effect of pericardial effusion does not depend solely on the amount of pericardial fluid. A large amount of pericardial fluid can be well tolerated when the fluid accumulates slowly. However, rapidly increasing pericardial effusion is more dangerous and may lead to cardiac tamponade. The main echocardiographic signs of cardiac tamponade are distended IVC with no respiratory variation, right atrial collapse at the end of diastole, right ventricular free wall collapse during diastole, and respiratory variation of Doppler mitral inflow for more than 10% and tricuspid inflow for more than 25% [7].

Patent ductus arteriosus (PDA) is an independent risk factor for intraventricular hemorrhage, necrotizing enterocolitis, bronchopulmonary dysplasia (BPD), and acute pulmonary hemorrhage [19, 20]. The hemodynamic significance of a PDA may not be directly related to the size of the PDA but depends upon the magnitude of the shunt and the ability of the myocardium to adapt to a left-to-right shunt [7, 20–22]. PDA causes pulmonary hyperperfusion and systemic hypoperfusion, which could be assessed with functional echocardiography. The duration of the shunt and the level of diastolic flow reversal in the descending aorta are good indicators of the significance of PDA and can be used for follow-up. An additional factor in assessing the PDA is pulmonary artery pressure, which can be monitored based on PDA Doppler velocity magnitudes. A low-pressure gradient between the aorta and pulmonary artery may be associated with pulmonary hypertension. Non-restrictive PDA has a low peak systolic velocity with a high systolic to diastolic velocity gradient, while restrictive shunt is

characterized by a high peak systolic velocity and a low systolic to diastolic velocity gradient [21]. Functional echocardiography has also been reported to improve the outcomes in infants being treated for PDA, the impact of this echocardiographic method is still the subject of ongoing research [23, 24]. Furthermore, it has been found that the performance of bedside echocardiography reduces the number of indomethacin doses used for treating PDA [25, 26]. The introduction of a functional echocardiography screening program for hemodynamically significant PDA on day 3 of life with the targeted intervention was associated with a reduction of severe intraventricular hemorrhage and ventilation duration [25, 27]. Serial echocardiography was associated with earlier identification and treatment of PDA, lower rates of severe intraventricular hemorrhage, and reduced ventilator days [11, 25].

3. Myocardial deformation imaging

Conventional methods for assessment of regional and global ventricular function, such as fractional shortening and ejection fraction, are largely dependent on loading conditions and geometric assumptions [28, 29]. Myocardial deformation imaging has introduced a new global parameter of left ventricular longitudinal deformation GLS (global longitudinal strain), which has turned out to be more sensitive for early detection of myocardial impairment compared to conventional echocardiographic systolic function parameters. Myocardial deformation parameters have diagnostic as well as prognostic values in several cardiac diseases [3].

Recent developments in the assessment of ventricular function are the measurement of myocardial tissue Doppler velocities (tissue Doppler imaging, TDI) and deformation imaging (strain and strain-rate quantification). TDI has some advantages over traditional echocardiographic techniques in providing measurements of cardiac tissue movements [7, 30]. Myocardial deformation analysis is a quantitative technique that helps define a global and regional function of both ventricles. Tissue deformation is measured by cardiac strain, and there is an additional parameter called strain rate that defines the rate of myocardial deformation in time [7].

Compared to traditional methods that measure cardiac function mainly in the radial direction, strain imaging does not rely on geometric assumptions and can quantify function in the longitudinal, radial, and circumferential direction of motion. Therefore, regional as well as global ventricular function may be better estimated. Strain rate measures the extent of shortening of the myocardium in the longitudinal and circumferential directions and thickening in the radial direction. These newer methods of myocardial function assessment have already shown great promise in several areas of pediatric echocardiography, but their use in clinical practice is still limited by the lack of data from large patient cohorts [1].

Recently, two-dimensional (2D) and three-dimensional (3D) speckle-tracking echocardiography (STE) has been introduced as a new method to quantify myocardial strain [29]. STE tracks the motion of speckles within the scan volume, allowing a more complete and accurate assessment of myocardial deformation in all three spatial dimensions [29, 31]. Strain imaging is a promising method for assessing left ventricular function for diagnosis, prognosis, and risk stratification of various congenital and acquired heart diseases; it is also useful for monitoring treatment outcomes before and after medical, percutaneous, and surgical interventions [29].

Strain and strain rate can be measured either from tissue Doppler velocities or with speckle-tracking techniques together with final analysis at the workstation. It

Vendor	Software	Average value of GLS (%)	Lower limit of normal GLS (%)	Average value of GCS (%)	Average value of GRS (%)
GE	EchoPAC BT12	−19.40 (−20.06 to −18.74)	−18	−19.47 (−20.49 to −18.45)	50.41 (47.96 to 52.87)
Philips	QLAB 7.1	−19.67 (−21.27 to −18.08)	−14	−22.13 (−26.73 to −17.52)	59.24 (41.91 to 76.56)
Toshiba	UltraExtend	−17.04 (−17.91 to −16.17)	−15	−28.79 (−32.90 to −24.68)	33.17 (24.38 to 41.97)

Data are mean (95% CI—confidence interval); GLS, global longitudinal strain; GCS, global circumferential strain; GRS, global radial strain.

Table 2.
Normal left ventricular global longitudinal strain (GLS), global circumferential strain (GRS), and global radial strain (GRS) values for specific vendors' equipment based on data from the literature (adapted from Truong et al., Lang et al.).

is necessary to be aware of the wide variability of the strain and strain rate measurements that depend on vendors, software packages, and echocardiographic laboratories, as shown in **Table 2** [32, 33]. Broad clinical use of the strain is still limited due to the intervendor differences and related difficult comparison of the results, thus, standardization is urgently needed [1, 34]. Higher heart rates, especially in younger children, require higher frame rates, particularly for strain rate imaging; therefore, this aspect of use requires further development. Another challenge for the implementation of strain imaging in everyday clinical practice is the availability of reference values for different age groups of children [1, 35].

3D speckle-tracking provides a more comprehensive evaluation of ventricular mechanics from pyramidal 3D datasets. Furthermore, it enables also more precise mechanical activation mapping compared to 2D strain, by being maximum opposing wall delay and SD (standard deviation) still significantly correlated with similar 2D strain measurements. 3D loops of regional strain are color-coded and divided into 16 or 18 segments for time-strain curves. The results are presented in a 16- or 18-segment polar map with segmental systolic strain values displayed in the bull's eye. GLS value is defined as the average peak longitudinal strain of the left ventricle [36, 37]. Future development and expansion of applications for 3D speckle tracking are anticipated.

Strain imaging has also been used to gain a greater understanding of the pathophysiology of cardiac ischemia and infarction, primary diseases of the myocardium, the effects of valvular disease on myocardial function, and understanding of diastolic function, as seen in **Table 3**. Strain imaging has also been used for heart failure patients undergoing cardiac resynchronization pacing therapy providing important quantitative information on the timing of mechanical activation. Strain imaging has become increasingly used for research purposes, in addition, it shows great potential for routine clinical practice in the light of the improved treatment of cardiovascular patients [37]. Therefore, deformation imaging also plays a role in the risk stratification of young individuals with a potentially increased risk for heart failure and sudden cardiac death [1, 38]. Strain imaging has also been used to help to differentiate between athlete's heart and individuals with potential cardiomyopathy [1, 39]. While multiple studies have shown the usefulness of strain quantification for risk stratification in various diseases, such as arterial hypertension, diabetes mellitus, metabolic

Area of use	Clinical applications
CHD	• The effects of valvular disease on myocardial function • Understanding of the diastolic function • Timely treatment decisions
Primary diseases of the myocardium (cardiomyopathies)	• Early detection of ventricular dysfunction • Potential need for additional diagnostics • Timely treatment decisions
Cardiac ischemia and infarction	• Extent of the ischemic myocardium • Assessing ventricular function, especially in patients with preserved LVEF
Cardiac resynchronization therapy	• Quantify abnormalities in the timing of mechanical activation of the left ventricle
Myocarditis	• Evaluation of ventricular function in patients with preserved LVEF • Evaluation of regional myocardial dysfunction
Cardiotoxicity	• Recognition of subclinical myocardial dysfunction • Adjustment of therapy
Risk stratification for heart failure and sudden cardiac death in children with a systemic disease	• Early detection of ventricular dysfunction in patients with arterial hypertension, diabetes mellitus, metabolic syndrome, chronic kidney disease, neuromuscular diseases • Potential need for additional diagnostics • Timely treatment decisions

CHD, congenital heart disease; LVEF, left ventricular ejection fraction.

Table 3.
Main clinical applications of myocardial deformation imaging.

syndrome, chronic kidney disease, neuromuscular diseases, and others, the main limitation remains that strain values vary among methods, modalities, and software versions [40–42].

Ventricular morphology can be highly variable in CHD, and therefore traditional methods of assessment of ventricular function that rely on geometry are unreliable. Assessment of right ventricular function and evaluation of functional changes in patients with a single ventricle are particularly challenging. Assessment of regional function is also important in pediatric patients with coronary artery abnormalities [1]. Subtle impairment in myocardial function, detectable with strain imaging, can be used to identify asymptomatic patients who progress to require valve surgery, which improves timely planning of the appropriate treatment [43].

Due to geometric factors, strain imaging better reflects systolic function in patients with preserved ejection fraction (EF), which is also common in cardiomyopathies. Particularly, longitudinal shortening may vary in patients with cardiomyopathies significantly, as it has less effect on EF than circumferential shortening. Therefore, longitudinal shortening might potentially be a more sensitive marker of systolic dysfunction, which typically affects the subendocardial region first, and could be assessed with longitudinal strain [44]. Deformation parameters, especially global longitudinal strain, have better accuracy in detecting cardiac amyloidosis in patients with thickened hearts [45].

Strain imaging is a beneficial additional echocardiographic method in assessing the extent of the ischemic myocardium and ventricular function. Postsystolic shortening is an important feature of the ischemic myocardium as a marker of tissue viability, and when associated with systolic hypokinesis or akinesis, it indicates actively contracting myocardium. When combined with dyskinesis, however, postsystolic shortening seems to be a nonspecific marker of severe ischemia [46]. Semiautomated calculation of GLS is significantly related to all-cause mortality or heart failure in patients with myocardial infarction and left ventricular ejection fraction (LVEF) > 40% [47].

Strain imaging is effective in monitoring cardiac function in patients with the multisystem inflammatory syndrome in children (MIS-C), which occurs after COVID-19 infection. Patients with preserved LVEF in myocarditis within MIS-C had significantly lower GLS; furthermore, regional myocardial dysfunction may also be presented, as seen in **Figure 1**. Hence, even preserved EF patients show subtle changes in myocardial deformation, suggesting subclinical myocardial injury. During a follow-up of the patients with MIS-C, there was a good recovery of systolic function but the persistence of diastolic dysfunction [48, 49]. Speckle-tracking imaging can help in the diagnosis of acute myocarditis when cardiovascular magnetic resonance (CMR) is not readily available or cannot be performed. There is a good correlation between speckle-tracking imaging-based LVEF, global strain and magnetic resonance imaging (MRI) calculated LVEF [50].

Segmental strain curves in a four-chamber view (top left), two-chamber view (top right), three-chamber view/APLAX—apical long-axis view (bottom left), and

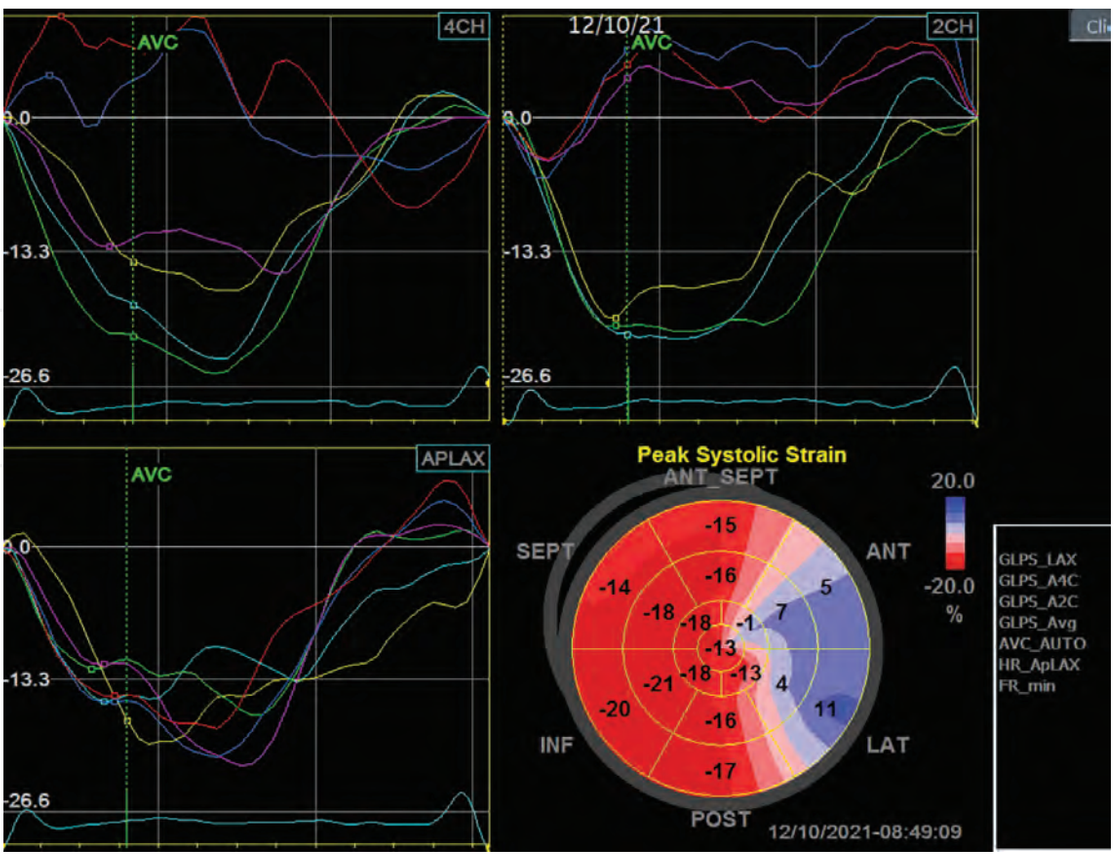

Figure 1.
Lower global longitudinal strain and regional myocardial dysfunction in the patient with myocarditis within multisystem inflammatory syndrome in children (MIS-C).

18-segment model or bull's eye (bottom right). The numbers in segments in the bull's eye are the peak longitudinal strain values in systole. The calculated value of global longitudinal strain (GLS) is −13.3%. Systolic values of the longitudinal strain are reduced in basal and mid-cavity segments of the anterior and lateral wall (blue color).

The recognition of early left ventricular dysfunction in cancer patients after cardiotoxic therapy may allow the identification of individuals at risk of future heart failure, allowing targeted monitoring and possibly institution of potential therapies such as angiotensin-converting enzyme inhibitors. The potential of strain imaging to prevent future cardiac toxicity by modulating cancer therapy and the institution of cardiac protective therapy is promising [51, 52].

GLS is the preferred indicator of left ventricular global systolic function. Strain measurements have proven to be more reproducible than LVEF due to minor dependency on segmental variability than LVEF calculations. Additionally, strain measurements should be obtained with the same analysis system and software version [42, 53–55].

Strain imaging is designed for the echocardiographic assessment of regional and global myocardial function, and has been well studied in the adult population, however, its use in pediatrics appears to be limited [56–58]. The duration of the investigation and the need to perform post-processing are major barriers to the more widespread implementation of the strain. Fully automated analysis with algorithms validated in the pediatric population may remove this problem [58].

4. 3D echocardiography

3D echocardiography (3DE) allows imaging and analysis of cardiovascular structures as they move in time and space, which enables the creation of 4D datasets (3D in real-time). Real-time 3DE is a major innovation in the history of cardiovascular ultrasound [59].

3DE is increasingly used in patients with congenital heart disease, as it allows the visualization of lesions in three dimensions, with opportunities for increased appreciation of complex spatial relationships. Alternative imaging modalities such as CMR or computed tomography (CT) have, compared to 3DE, some disadvantages, such as expense, general anesthesia (CMR), or exposure to radiation (CT) [1].

Clinical benefits of 3DE are evident in three main areas: better visualization and understanding of the spatial relationships and 3D morphology of congenital heart defects; quantification of cardiac mass and volumes; planning and guiding therapeutic interventions, as seen in **Table 4** [1, 60].

However, 3DE scanning modalities that use the ECG for gating, and then collect the data acquired over several heartbeats are often problematic in younger patients, as there is a large potential for movement artifact, especially with higher respiratory rates. The main shortcomings of 3D imaging have been the lower spatial and temporal resolution compared with 2D imaging, and the requirement for offline analysis [1, 60].

Compared to cross-sectional imaging methods 3DE does not use the same geometric assumptions, which allows a more accurate assessment of the cardiac function. At the same time, with better visualization also comes a better understanding of the anatomy of CHD, such as atrial and ventricular septal defects, atrioventricular (AV) septal defects, and atrioventricular valve or outflow tract abnormalities. In addition, 3DE enables better volumetric assessment of cardiac chambers in patients with borderline sized ventricles, it can also work as an important diagnostic tool for cardiac mass. 3DE findings correlate well with surgical findings, and can significantly improve the planning of therapeutic interventions, sometimes may also reduce the operative time [1].

Area of use	Clinical applications
Morphology of CHD	• Atrial septal defects • Ventricular septal defect • Atrioventricular septal defects • Atrioventricular valve abnormalities • Outflow tract abnormalities
Quantification of cardiac mass and volumes	• Ventricular volume and mass quantification (borderline left ventricle, right ventricle) • Atrial volume and mass quantification • Dyssynchrony assessment (regional LV volumes)
Planning and guiding therapeutic interventions	• Presurgical imaging (including 3D printing of atrioventricular valves) • Intraprocedural imaging (intraoperative epicardial and transesophageal 3DE, transcatheter procedures, endomyocardial biopsy)
Fetal echocardiography	• Spatial relationship of the cardiac structures and great vessels • Quantification of cardiac volumes

CHD, congenital heart disease; LV, left ventricle.

Table 4.
Main clinical applications of 3D echocardiography.

3DE offers the additional advantage to estimate the AV valve regurgitant volume, the mechanism, and the origin of regurgitation with clear visualization of the valves, which makes 3DE an ideal imaging modality to evaluate these structures and plan interventions [61–64]. 3DE is also a promising modality for 3D printing of AV valves, structures that are largely missing from cardiac models using exclusively MRI or CT data [64–66].

The 3DE and 4DE with spatiotemporal image correlation allow obtaining fetal cardiac volumes and their static and real-time analysis [67], and multiple two-dimensional images are stacked one behind the other to create a volume dataset [68–70]. 4DE is used mainly in the field of fetal echocardiography for the dynamic assessment of fetal cardiac structures and large vessels. The main challenge of fetal echocardiography is still a profound understanding of the spatial relationships and connections of the cardiac structures and great vessels, which 4DE overcomes with more accurate anatomic information. Although traditional 2D echocardiography is the basic modality for prenatal diagnosis of CHD, 3DE and 4DE should be considered as very useful additions [71].

5. Conclusions

Recently, the focus of the development of pediatric echocardiography has shifted toward accurate assessment of myocardial function and precise presentation of cardiac morphology. As in other areas of ultrasound examinations, there is an increasing need for bedside targeted echocardiography that provides fast answers to major clinical challenges. Therefore, some echocardiographic methods becoming increasingly useful, such as functional echocardiography, cardiac deformation imaging, and 3D echocardiography.

Functional echocardiography enables real-time evaluation of cardiac performance, identifying the nature of cardiovascular compromise, guiding therapeutic decisions, and monitoring response to treatment. An additional advantage of functional echocardiography is the noninvasiveness of the method. The decision-making process is easier with further information provided by targeted echocardiography, which also reduces a substantial proportion of interventions. Standardized training and close collaboration with pediatric cardiologists are essential for ensuring patients' safety and quality of examination, especially in neonatal units where the risk of a critical or major CHD is higher compared to older children. Future research should address short-term cardiovascular effects and long-term outcomes of functional echocardiography.

Myocardial deformation imaging may be beneficial for the detection of early ventricular dysfunction, especially where classical methods are unreliable. A better understanding of patterns of dysfunction may help clinicians to identify causative factors for global and regional ventricular dysfunction. Patients with progressive heart disease or systemic disease affecting the heart may be identified and treated timely. Furthermore, closer monitoring of the effects of therapy is also an important advantage of myocardial deformation. New methods of myocardial function assessment have already shown great promise in several areas of pediatric echocardiography, but the main limitation remains that strain values vary among methods, modalities, and software versions. Further investigation is warranted for the potential clinical applications in a pediatric population, especially in defining the normal range and maturational changes in strain.

3DE is a very promising and topical new echocardiographic method; recently, it has become more popular in patients with CHD, as it allows the visualization of defects in three dimensions, with opportunities for increased appreciation of complex spatial relationships. A current limitation of 3DE is a restriction of spatial and temporal resolution. Based on 3D modeling, virtual surgery may even be possible, to optimize device design for individual patients, or to determine the optimal surgical technique. In a near future, we are likely to see increased use of 3DE during transcatheter interventions and heart surgeries.

Conflict of interest

The authors declare no conflict of interest.

Author details

Teja Senekovič Kojc* and Nataša Marčun Varda University Medical Centre Maribor, Maribor, Slovenia

References

[1] Bharucha T, Mertens L. Recent advances in pediatric echocardiography. Expert Review of Cardiovascular Therapy. 2013;**11**:31-47. DOI: 10.1586/erc.12.168

[2] Smiseth OA, Torp H, Opdahl A, Haugaa KH, Urheim S. Myocardial strain imaging: How useful is it in clinical decision making? European Heart Journal. 2016;**37**:1196-1207. DOI: 10.1093/eurheartj/ehv529

[3] Kalam K, Otahal P, Marwick TH. Prognostic implications of global LV dysfunction: A systematic review and meta-analysis of global longitudinal strain and ejection fraction. Heart. 2014;**100**:1673-1680. DOI: 10.1136/heartjnl-2014-305538

[4] Harabor A, Soraisham AS. Utility of targeted neonatal echocardiography in the management of neonatal illness. Journal of Ultrasound in Medicine. 2015;**34**:1259-1263. DOI: 10.7863/ultra.34.7.1259

[5] Lavie-Nevo K, Dinur G, Almagor Y, Barzilay B, Rotschild A, Gover A. Functional echo in preterm infants—Past, present and future. Harefuah. 2020;**159**:759-763

[6] de Waal K, Kluckow M. Functional echocardiography; from physiology to treatment. Early Human Development. 2010;**86**:149-154. DOI: 10.1016/j.earlhumdev.2010.01.030

[7] Tissot C, Singh Y. Neonatal functional echocardiography. Current Opinion in Pediatrics. 2020;**32**:235-244. DOI: 10.1097/MOP.0000000000000887

[8] Groves AM, Singh Y, Dempsey E, Molnar Z, Austin T, El-Khuffash A, et al. Introduction to neonatologist-performed echocardiography. Pediatric Research. 2018;**84**:1-12. DOI: 10.1038/s41390-018-0076-y

[9] Singh Y. Echocardiographic evaluation of hemodynamics in neonates and children. Frontiers in Pediatrics. 2017;**5**:201. DOI: 10.3389/fped.2017.00201

[10] Beaulieu Y. Bedside echocardiography in the assessment of the critically ill. Critical Care Medicine. 2007;**35**:S235-S249. DOI: 10.1097/01.CCM.0000260673.66681.AF

[11] El-Khuffash AF, McNamara PJ. Neonatologist-performed functional echocardiography in the neonatal intensive care unit. Seminars in Fetal and Neonatal Medicine. 2011;**16**:50-60. DOI: 10.1016/j.siny.2010.05.001

[12] Mertens L, Seri I, Marek J, Arlettaz R, Barker P, McNamara P, et al. Targeted neonatal echocardiography in the neonatal intensive care unit: Practice guidelines and recommendations for training. Journal of the American Society of Echocardiography. 2011;**24**:1057-1078. DOI: 10.1016/j.echo.2011.07.014

[13] Singh Y, Gupta S, Groves AM, Gandhi A, Thomson J, Qureshi S, et al. Expert consensus statement 'Neonatologist-performed Echocardiography (NoPE)'—Training and accreditation in UK. European Journal of Pediatrics. 2016;**175**:281-287. DOI: 10.1007/s00431-015-2633-2

[14] Brierley J, Carcillo JA, Choong K, Cornell T, DeCaen A, Deymann A, et al. Clinical practice parameters for hemodynamic support of pediatric and neonatal septic shock: 2007 update from the American College of Critical

Care Medicine. Critical Care Medicine. 2009;**37**:666-688. DOI: 10.1097/CCM.0b013e31819323c6

[15] de Boode WP, van der Lee R, Horsberg Eriksen B, Nestaas E, Dempsey E, Singh Y, et al. The role of Neonatologist Performed Echocardiography in the assessment and management of neonatal shock. Pediatric Research. 2018;**84**:57-67. DOI: 10.1038/s41390-018-0081-1

[16] Landry DW, Oliver JA. The pathogenesis of vasodilatory shock. New England Journal of Medicine. 2001;**345**:588-595. DOI: 10.1056/NEJMra002709

[17] Wynn JL, Wong HR. Pathophysiology and treatment of septic shock in neonates. Clinics in Perinatology. 2010;**37**:439-479. DOI: 10.1016/j.clp.2010.04.002

[18] Pérez-Casares A, Cesar S, Brunet-Garcia L, Sanchez-de-Toledo J. Echocardiographic evaluation of pericardial effusion and cardiac tamponade. Frontiers in Pediatrics. 2017;**5**:79. DOI: 10.3389/fped.2017.00079

[19] Noori S, McCoy M, Friedlich P, Bright B, Gottipati V, Seri I, et al. Failure of ductus arteriosus closure is associated with increased mortality in preterm infants. Pediatrics. 2009;**123**:e138-e144. DOI: 10.1542/peds.2008-2418

[20] Noori S. Patent ductus arteriosus in the preterm infant: To treat or not to treat? Journal of Perinatology. 2010;**30**:S31-S37. DOI: 10.1038/jp.2010.97

[21] van Laere D, van Overmeire B, Gupta S, El-Khuffash A, Savoia M, McNamara PJ, et al. Application of Neonatologist Performed Echocardiography in the assessment of a patent ductus arteriosus. Pediatric Research. 2018;**84**:46-56. DOI: 10.1038/s41390-018-0077-x

[22] Arlettaz R. Echocardiographic evaluation of patent ductus arteriosus in preterm infants. Frontiers in Pediatrics. 2017;**5**:147. DOI: 10.3389/fped.2017.00147

[23] Sehgal A, McNemara PJ. Does point-of-care functional echocardiography enhance cardiovascular care in the NICU? Journal of Perinatology. 2008;**28**(11):729-735. DOI: 10.1038/jp.2008.100

[24] Sehgal A, Francis JV, James A, McNemara PJ. Patent ductus arteriosus ligation and post-operative hemodynamic instability: Case report and framework for enhanced neonatal care. Indian Journal of Pediatrics. 2010;**77**(8):905-907. DOI: 10.1007/s12098-010-0137-7

[25] O'Rourke D, El-Khuffash A, Moody C, Walsh K, Molloy E. Patent ductus arteriosus evaluation by serial echocardiography in preterm infants. Acta Paediatrica. 2008;**97**:574-578. DOI: 10.1111/j.1651-2227.2008.00745.x

[26] Carmo KB, Evans N, Paradisis M. Duration of indomethacin treatment of the preterm patent ductus arteriosus as directed by echocardiography. The Journal of Pediatrics. 2009;**155**:819-822. e1. DOI: 10.1016/j.jpeds.2009.06.013

[27] Poon W, Wong K. Neonatologist-performed point-of-care functional echocardiography in the neonatal intensive care unit. Singapore Medical Journal. 2017;**58**:230-233. DOI: 10.11622/smedj.2017036

[28] Dragulescu A, Mertens LL. Developments in echocardiographic techniques for the evaluation of ventricular function in children. Archives of Cardiovascular Diseases. 2010;**103**:603-614. DOI: 10.1016/j.acvd.2010.09.004

[29] Zhang L, Gao J, Xie M, Yin P, Liu W, Li Y, et al. Left ventricular

three-dimensional global systolic strain by real-time three-dimensional speckle-tracking in children: Feasibility, reproducibility, maturational changes, and normal ranges. Journal of the American Society of Echocardiography. 2013;**26**:853-859. DOI: 10.1016/j.echo.2013.05.002

[30] Nestaas E, Schubert U, de Boode WP, El-Khuffash A. Tissue Doppler velocity imaging and event timings in neonates: A guide to image acquisition, measurement, interpretation, and reference values. Pediatric Research. 2018;**84**:18-29. DOI: 10.1038/s41390-018-0079-8

[31] Gayat E, Ahmad H, Weinert L, Lang RM, Mor-Avi V. Reproducibility and inter-vendor variability of left ventricular deformation measurements by three-dimensional speckle-tracking echocardiography. Journal of the American Society of Echocardiography. 2011;**24**:878-885. DOI: 10.1016/j.echo.2011.04.016

[32] Truong VT, Phan HT, Pham KNP, Duong HNH, Ngo TNM, et al. Normal ranges of left ventricular strain by three-dimensional speckle-tracking echocardiography in adults: A systematic review and meta-analysis. Journal of the American Society of Echocardiography. 2019;**32**(12):1586-1597.e5. DOI: 10.1016/j.echo.2019.07.012

[33] Lang RM, Badano LP, Mor-Avi V, Afilalo J, Armstrong A, Ernande L, et al. Recommendations for cardiac chamber quantification by echocardiography in adults: An update from the American Society of Echocardiography and the European Association of Cardiovascular Imaging. European Heart Journal Cardiovascular Imaging. 2016;**17**(4):412. DOI: 10.1093/ehjci/jew041

[34] Lorch SM, Ludomirsky A, Singh GK. Maturational and growth-related changes in left ventricular longitudinal strain and strain rate measured by two-dimensional speckle tracking echocardiography in healthy pediatric population. Journal of the American Society of Echocardiography. 2008;**21**:1207-1215. DOI: 10.1016/j.echo.2008.08.011

[35] Marcus KA, Mavinkurve-Groothuis AMC, Barends M, van Dijk A, Feuth T, de Korte C, et al. Reference values for myocardial two-dimensional strain echocardiography in a healthy pediatric and young adult cohort. Journal of the American Society of Echocardiography. 2011;**24**:625-636. DOI: 10.1016/j.echo.2011.01.021

[36] Tanaka H, Hara H, Saba S, Gorcsan J. Usefulness of three-dimensional speckle tracking strain to quantify dyssynchrony and the site of latest mechanical activation. The American Journal of Cardiology. 2010;**105**:235-242. DOI: 10.1016/j.amjcard.2009.09.010

[37] Gorcsan J, Tanaka H. Echocardiographic assessment of myocardial strain. Journal of the American College of Cardiology. 2011;**58**:1401-1413. DOI: 10.1016/j.jacc.2011.06.038

[38] Printz BF. Noninvasive imaging modalities and sudden cardiac arrest in the young: Can they help distinguish subjects with a potentially life-threatening abnormality from normals? Pediatric Cardiology. 2012;**33**:439-451. DOI: 10.1007/s00246-012-0169-z

[39] Butz T, van Buuren F, Mellwig KP, Langer C, Plehn G, Meissner A, et al. Two-dimensional strain analysis of the global and regional myocardial function for the differentiation of pathologic and physiologic left ventricular hypertrophy: A study in athletes and in patients with hypertrophic cardiomyopathy. The

International Journal of Cardiovascular Imaging. 2011;**27**:91-100. DOI: 10.1007/s10554-010-9665-5

[40] Reichek N. Myocardial strain: Still a long way to go. Circulation. Cardiovascular Imaging. 2017;**10**(11): e007145. DOI: 10.1161/CIRCIMAGING.117.007145

[41] Collier P, Phelan D, Klein A. A test in context: Myocardial strain measured by speckle-tracking echocardiography. Journal of the American College of Cardiology. 2017;**69**:1043-1056. DOI: 10.1016/j.jacc.2016.12.012

[42] Amzulescu MS, de Craene M, Langet H, Pasquet A, Vancraeynest D, Pouleur AC, et al. Myocardial strain imaging: Review of general principles, validation, and sources of discrepancies. European Heart Journal Cardiovascular Imaging. 2019;**20**:605-619. DOI: 10.1093/ehjci/jez041

[43] Baumgartner H, Falk V, Bax JJ, de Bonis M, Hamm C, Holm PJ, et al. 2017 ESC/EACTS Guidelines for the management of valvular heart disease. European Heart Journal. 2017;**38**:2739-2791. DOI: 10.1093/eurheartj/ehx391

[44] Stokke TM, Hasselberg NE, Smedsrud MK, Sarvari SI, Haugaa KH, Smiseth OA, et al. Geometry as a confounder when assessing ventricular systolic function. Journal of the American College of Cardiology. 2017;**70**:942-954. DOI: 10.1016/j.jacc.2017.06.046

[45] Pagourelias ED, Mirea O, Duchenne J, van Cleemput J, Delforge M, Bogaert J, et al. Echo parameters for differential diagnosis in cardiac amyloidosis. Circulation. Cardiovascular Imaging. 2017;**10**:e005588. DOI: 10.1161/CIRCIMAGING.116.005588

[46] Skulstad H, Edvardsen T, Urheim S, Rabben SI, Stugaard M, Lyseggen E, et al. Postsystolic shortening in ischemic myocardium. Circulation. 2002;**106**:718-724. DOI: 10.1161/01.CIR.0000024102.55150.B6

[47] Ersbøll M, Valeur N, Mogensen UM, Andersen MJ, Møller JE, Velazquez EJ, et al. Prediction of all-cause mortality and heart failure admissions from global left ventricular longitudinal strain in patients with acute myocardial infarction and preserved left ventricular ejection fraction. Journal of the American College of Cardiology. 2013;**61**:2365-2373. DOI: 10.1016/j.jacc.2013.02.061

[48] Niaz T, Hope K, Fremed M, Misra N, Altman C, Glickstein J, et al. Role of a pediatric cardiologist in the COVID-19 pandemic. Pediatric Cardiology. 2021;**42**:19-35. DOI: 10.1007/s00246-020-02476-y

[49] Matsubara D, Kauffman HL, Wang Y, Calderon-Anyosa R, Nadaraj S, Elias MD, et al. Echocardiographic findings in pediatric multisystem inflammatory syndrome associated with COVID-19 in the United States. Journal of the American College of Cardiology. 2020;**76**:1947-1961. DOI: 10.1016/j.jacc.2020.08.056

[50] Leitman M, Vered Z, Tyomkin V, Macogon B, Moravsky G, Peleg E, et al. Speckle tracking imaging in inflammatory heart diseases. International Journal of Cardiovascular Imaging. 2018;**34**(5):787-792. DOI: 10.1007/s10554-017-1284-y

[51] Zamorano JL, Lancellotti P, Rodriguez Muñoz D, Aboyans V, Asteggiano R, Galderisi M, et al. 2016 ESC Position Paper on cancer treatments and cardiovascular toxicity developed under the auspices of the ESC Committee for Practice Guidelines. European Heart Journal. 2016;**37**:2768-2801. DOI: 10.1093/eurheartj/ehw211

[52] Hare JL, Brown JK, Leano R, Jenkins C, Woodward N, Marwick TH. Use of myocardial deformation imaging to detect preclinical myocardial dysfunction before conventional measures in patients undergoing breast cancer treatment with trastuzumab. American Heart Journal. 2009;**158**:294-301. DOI: 10.1016/j.ahj.2009.05.031

[53] Barbier P, Mirea O, Cefalù C, Maltagliati A, Savioli G, Guglielmo M. Reliability and feasibility of longitudinal AFI global and segmental strain compared with 2D left ventricular volumes and ejection fraction: Intra- and inter-operator, test–retest, and inter-cycle reproducibility. European Heart Journal Cardiovascular Imaging. 2015;**16**:642-652. DOI: 10.1093/ehjci/jeu274

[54] Medvedofsky D, Kebed K, Laffin L, Stone J, Addetia K, Lang RM, et al. Reproducibility and experience dependence of echocardiographic indices of left ventricular function: Side-by-side comparison of global longitudinal strain and ejection fraction. Echocardiography. 2017;**34**:365-370. DOI: 10.1111/echo.13446

[55] Knackstedt C, Bekkers SCAM, Schummers G, Schreckenberg M, Muraru D, Badano LP, et al. Fully automated versus standard tracking of left ventricular ejection fraction and longitudinal strain. Journal of the American College of Cardiology. 2015;**66**:1456-1466. DOI: 10.1016/j.jacc.2015.07.052

[56] Camarda JA, Patel A, Carr MR, Young LT. Practice variations in pediatric echocardiography laboratories. Pediatric Cardiology. 2019;**40**:537-545. DOI: 10.1007/s00246-018-2012-7

[57] Yingchoncharoen T, Agarwal S, Popović ZB, Marwick TH. Normal ranges of left ventricular strain: A meta-analysis. Journal of the American Society of Echocardiography. 2013;**26**:185-191. DOI: 10.1016/j.echo.2012.10.008

[58] Ziebell D, Bettermann E, Lipinski J, Border WL, Sachdeva R. Current practice and barriers to implementation of strain imaging in pediatric echocardiography labs: A national survey. Journal of the American Society of Echocardiography. 2021;**34**:316-318. DOI: 10.1016/j.echo.2020.11.011

[59] Correale M, Ieva R, Manuppelli V, Rinaldi A, di Biase M. Controversies in echocardiography: 2D vs 3D vs 4D. Minerva Cardioangiologica. 2009;**57**:443-455

[60] Shirali GS. Three-Dimensional echocardiography in congenital heart disease. Echocardiography. 2012;**29**:242-248. DOI: 10.1111/j.1540-8175.2011.01612.x

[61] Muraru D, Veronesi F, Maddalozzo A, Dequal D, Frajhof L, Rabischoffsky A, et al. 3D printing of normal and pathologic tricuspid valves from transthoracic 3D echocardiography data sets. European Heart Journal Cardiovascular Imaging. 2017;**18**:802-808. DOI: 10.1093/ehjci/jew215

[62] Mahmood F, Owais K, Taylor C, Montealegre-Gallegos M, Manning W, Matyal R, et al. Three-dimensional printing of mitral valve using echocardiographic data. JACC: Cardiovascular Imaging. 2015;**8**:227-229. DOI: 10.1016/j.jcmg.2014.06.020

[63] Mashari A, Montealegre-Gallegos M, Knio Z, Yeh L, Jeganathan J, Matyal R, et al. Making three-dimensional echocardiography more tangible: A workflow for three-dimensional printing with echocardiographic data. Echo Research and Practice. 2016;**3**:R57-R64. DOI: 10.1530/ERP-16-0036

[64] Mowers KL, Fullerton JB, Hicks D, Singh GK, Johnson MC, Anwar S. 3D Echocardiography Provides highly accurate 3D printed models in congenital heart disease. Pediatric Cardiology. 2021;**42**:131-141. DOI: 10.1007/s00246-020-02462-4

[65] Anwar S, Singh GK, Miller J, Sharma M, Manning P, Billadello JJ, et al. 3D Printing is a transformative technology in congenital heart disease. JACC: Basic to Translational Science. 2018;**3**:294-312. DOI: 10.1016/j.jacbts.2017.10.003

[66] Vukicevic M, Mosadegh B, Min JK, Little SH. Cardiac 3D printing and its future directions. JACC: Cardiovascular Imaging. 2017;**10**:171-184. DOI: 10.1016/j.jcmg.2016.12.001

[67] Jeanne Bravo-Valenzuela N, Borges Peixoto A, Carvalho Carrilho M, Letícia Siqueira Pontes A, Cevante Chagas C, Simioni C, et al. Fetal cardiac function by three-dimensional ultrasound using 4D-STIC and VOCAL—An update. Journal of Ultrasonography. 2019;**19**:287-294. DOI: 10.15557/JoU.2019.0043

[68] Gonçalves LF, Lee W, Chaiworapongsa T, Espinoza J, Schoen M, Falkensammer P, et al. Four-dimensional ultrasonography of the fetal heart with spatiotemporal image correlation. American Journal of Obstetrics and Gynecology. 2003;**189**:1792-1802. DOI: 10.1016/S0002-9378(03)00913-X

[69] DeVore GR, Falkensammer P, Sklansky MS, Platt LD. Spatio-temporal image correlation (STIC): New technology for evaluation of the fetal heart. Ultrasound in Obstetrics and Gynecology. 2003;**22**:380-387. DOI: 10.1002/uog.217

[70] DeVore GR, Satou G, Sklansky M. 4D fetal echocardiography—An update. Echocardiography. 2017;**34**:1788-1798. DOI: 10.1111/echo.13708

[71] Qin Y, Zhang Y, Zhou X, Wang Y, Sun W, Chen L, et al. Four-dimensional echocardiography with spatiotemporal image correlation and inversion mode for detection of congenital heart disease. Ultrasound in Medicine & Biology. 2014;**40**:1434-1441. DOI: 10.1016/j.ultrasmedbio.2014.02.008

9

Fetal Echocardiography

Ahmet Cantug Caliskan
Samsun Education and Training Hospital Department of Obstetrics and Gynecology Samsun Turkey

1. Introduction

This is a test using sound waves to show the structure of an unborn baby's heart. An obstetrician may get a limited view of a baby's heart during a routine pregnancy ultrasound. However, a specialist in fetal echocardiography can study a baby's heart in great detail using a fetal echocardiogram.Some pregnant women are at higher risk of giving birth to a baby with a heart defect. They should be considered for referral for a specialized fetal echocardiogram. The ultrasound scanning may be done through the vagina or through the abdomen. There are no known risks to the mother or fetus.

Congenital heart disease is the most common birth defect, occurring at a rate of 8/1,000 births.Because there are many different types of heart defects, ranging from minor to life-threatening problems, examination of the fetal heart before birth has been mandated as a requirement when examining a fetus between 15 and 40 weeks of pregnancy. This has been called the Standard ultrasound evaluation of the heart and has been defined by the American College of Obstetricians and Gynecologists, the American Institute of Ultrasound in Medicine, and the American College of Radiology.In Los Angeles it has been estimated that less than 10% of serious heart defects are detected before birth when the examination is performed by an obstetrician or radiologist who does not have special training evaluating the fetal heart. Fetal Echocardiography is a more comprehensive examination of the fetal heart than the standard examination and includes identification of additional cardiac structures not defined in the standard evaluation. The physician who performs Fetal Echocardiography often uses color Doppler ultrasound and may utilize pulsed Doppler, 3D, and 4D ultrasound; depending upon the circumstances of the examination. Fetal Echocardiography is an important part of Genetic Ultrasound, a new test that identifies over 95% of fetuses with Down syndrome when performed during the second-trimester of pregnancy.

Fetal echocardiography is the primary diagnostic tool used to assess fetal cardiac structure and function.This is a specialized sonogram that is a certainly indicated when there is an increased risk of fetal cardiac abnormalites,and is usually performed at 18-22 weeks gestation.when the risk of a fetal cardiac anomaly is particularly high, an earlier evaluation,at around 13-15 weeks, by either transabdominal or vaginal sonography, may be considered, as many caardiac anomalies are already demonstrable at this stage.this early examination should, however, be corroborated by a repeat evaluation around mid-gestation.

A complete fetal echocardiographic examination should incorporate the following Standard views:a demonstration of the visceral and cardiac situs,a four chamber view,ventriculoarterial connections, and course of the great arteries.Real-time examination of cardiac structures is enhanced by the use of color Doppler.

A baby's heart begins to develop at conception, but is completely formed by eight weeks into the pregnancy. Congenital heart defects happen during this crucial first eight weeks of the baby's development. Specific steps must take place in order for the heart to form correctly.

2. Indications for fetal echocardiography

2.1 Maternal indications fetal indications

- Family history of CHD
- Abnormal obstetrical ultrasound screen
- Metabolic disorders (eg,diabetes, PKU)
- Extracardiac abnormality
- Exposure to teratogens
- Chromosomal abnormality
- Exposure to prostaglandin synthetase inhibitors (eg,ibuprofen, salicylic acid, indomethacin)
- Arrhythmia
- Rubella infection
- Hydrops
- Autoimmune disease (eg,SLE, Sjogren's)
- Increased first trimester nuchal translucency
- Familial inherited disorders (Ellisvan Creveld, Marfan, Noonan's, etc)
- Multiple gestation and suspicion of twin-twin transfusion syndrome
- In vitro fertilization CHD, Congenital heart disease; PKU, phenyl ketonuria; SLE, sytemic lupus erythematosus.

While there are risk factors for congenital heart defects, over 90% of heart malformations have no known cause. For this reason researchers have classified most heart defects as multifactorial, meaning that there is no known explanation for the problem other than the possible interaction between hereditary and environmental factors. For this reason, many physicians have suggested examining all fetuses for heart defects, since most defects arise from pregnancies with no risk factors. The following lists factors associated with an increased risk for congenital heart defects. If any of these are present, the patient should be referred for Fetal Echocardiography at 18 to 24 weeks of gestation. In some cases the patient may desire first-trimester

- Fetal Echocardiography performed between 12 and 14 weeks of gestation.
- Maternal Drug Exposure and Diseases Women with seizure disorders taking anti-convulsants
- Women taking lithium for depression
- Women taking insulin for diabetes
- Women who have phenylketonuria

- Women exposed to Rubella
- Family History of Congenital Heart Disease
- Previous child with CHD, new risk is 1 in 20 to 1 in 100
- Previous two children with CHD, new risk is 1 in 10 to 1 in 20
- Mother has CHD, new risk is as high as 1 in 5 to 1 in 20
- Father has CHD, new risk 1 in 30
- Increased Maternal Risk for Down Syndrome and Other Chromosomal Defects
- Advanced maternal age (>35)
- Abnormal maternal serum screening increasing risk for Downy syndrome or Trisomy 18
- Chromosome abnormalities and CHD
- Down syndrome
- Trisomy 18 and Trisomy 13
- Turner's syndrome
- Cri du chat syndrome
- Wolf-Hirshhorn syndrome
- DiGeorge syndrome (deletion 22q11)
- Other Rare Genetic Diseases
- Marfan syndrome
- Smith-Lemli-Opitz syndrome
- Ellis-van Creveld
- Holt-Oram syndrome
- Noonan syndrome
- Mucopolysaccharidoses
- Goldenhar syndrome (hemifacial microsomia)
- William's syndrome
- VACTERL association (tracheal and esophageal malformations associated with vertebral, anorectal,
- cardiac, renal, radial, and limb abnormalities).
- Ultrasound -Identified Fetal Birth Defects of the Current Pregnancy

When a birth defect is detected during an ultrasound examination, there is a higher risk for an associated defect of the fetal heart. Therefore, a fetal echocardiogram should be performed.

2.2 Cardiovascular anatomy and fetal circulation

After birth the circulation is divided into two separate sides that are not connected. The left side of the heart consists of the pulmonary veins, left atrium, left ventricle, and aorta. The right side of the heart consists of the superior and inferior vena cava, the right atrium, the right ventricle, and the pulmonary artery. These two circulations are independent of each other and do not connect.

However, the fetal circulation is different. The right and left sides of the heart connect at the level of the foramen ovale and the ductus arteriosus. Because of these connections fetuses can develop serious heart defects and live while in the uterus, only to be severely compromised or die because of the circulatory changes that occur following birth. To understand the effect of certain types of heart defects it is therefore important to review fetal circulation.

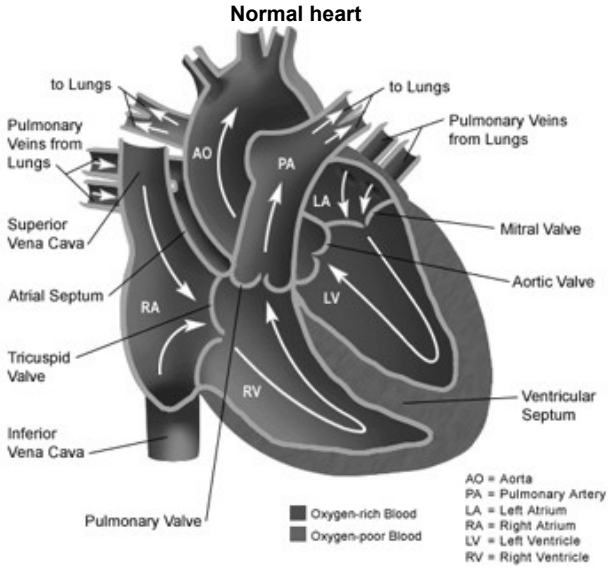

Fig. 1. Right Side of the Heart

1. Blood from the placenta returns to the fetus by the umbilical vein.The umbilical vein enters the fetal abdomen where blood continues through the intra-abdominal portion of this vessel.
2. Once inside the abdomen blood flows through the ductus venosus and is directed into the right atrial chamber. Because this blood has been enriched with oxygen and nutrients that it has picked up from the placenta, it is directed primarily through the foramen ovale into the left atrium. The foramen ovale is a small hole in the wall that separates the right and left atrial chambers. There is some mixing of blood within the right atrium.
3. The majority of blood enters the right atrium from the superior and inferior vena cava, as well as some blood from the ductus venosus (see above). The superior vena cava brings blood back from the head and upper extremities to the heart while blood from the inferior vena cava brings it back to the heart from the remainder of the body.
4. Blood is pumped from the right atrium into the right ventricle.
5. Blood from the right ventricle is pumped through the pulmonary valve into the main pulmonary artery. From here it is distributed to the lungs and to the ductus arteriosus.
6. The ductus arteriosus distributed blood to the entire body (excluding the head and upper extremities) as well as returns blood back to the placenta through the two umbilical arteries.

Left Side of the Heart

1. Blood from the placenta returns to the fetus by the umbilical vein. The umbilical vein enters the fetal abdomen where blood continues through the intra-abdominal portion of this vessel.
2. Once inside the abdomen blood flows through the ductus venosus and is directed into the right atrial chamber.Because this blood has been enriched with oxygen and nutrients that it has picked up from the placenta, it is directed through the foramen ovale into the left atrium.The foramen ovale is a small hole in the wall that separates the right and left atrial chambers
3. Once inside the left atrium the blood mixes with blood returning from the lungs and then enters the left ventricle.
4. Blood from the left ventricle is pumped into the aorta, which distributes blood to the brain and upper extremities.

Ultrasound examination of the fetal heart was first reported in the early 1980's when 2D technology allowed the examiner to identify the four-chambers of the fetal heart.Although the value of prenatal detection of heart defects was appreciated in a theoretical sense, it has only recently been realized as a benefit. The reason for this is that the ability to detect heart defects by the physician and/or sonographer has improved as the result of training and experience COLOR DOPPLER examination of the Heart Color Doppler ultrasound is a technique that enables the physician to identify the direction and speed of blood flow within a vessel or heart chamber. Color Doppler is not part of the Standard Examination of the heart, but is used by a specialist with special training in fetal echocardiography.

The use of color Doppler ultrasound for evaluation of the fetal heart and detection of birth defects was first reported by Dr. DeVore in 1987. Since this first publication over 200 articles have been published in the medical literature describing the use of this technology for evaluating the fetal heart. Color Doppler displays the flow of blood based upon its direction of flow; red-orange towards to top of the transducer, blue away from the transducer.

The transducer is always located at the top of the image. Therefore, when blood flow is towards the transducer it is depicted in red, and away from the transducer in blue. The different hues of red-orange and blue-green indicate the different velocities or speed that blood is flowing. For example, if the color Doppler display is yellow then it is flowing towards the transducer faster than if it is deep red.

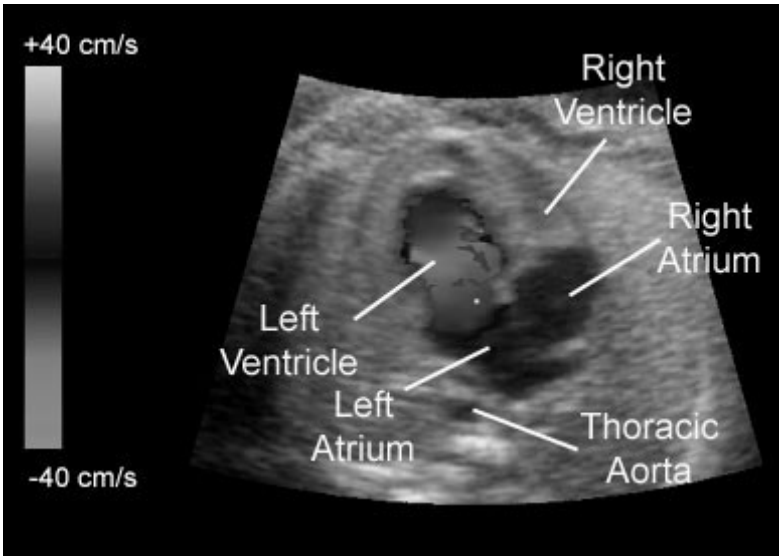

Fig. 2. This illustrates the use of color Doppler to identify the flow of blood into the ventricles.

3. Doppler waveforms analyzed

Measurement of the Doppler waveforms is compared to the age of the fetus. The following graphs illustrate the normal distribution of measurements for the waveforms recorded from the fetal heart.

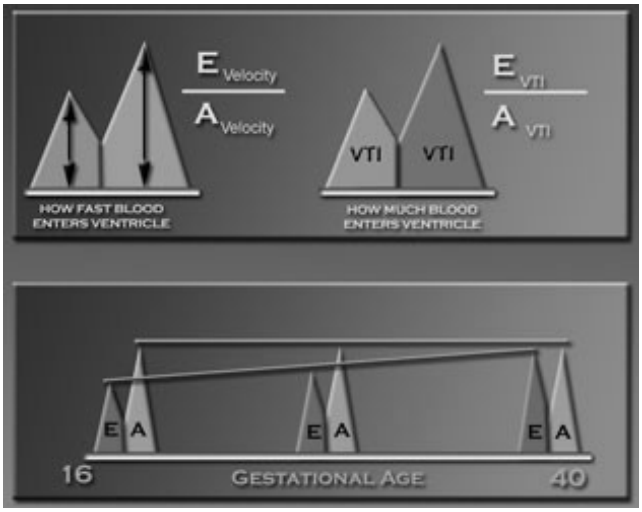

Fig. 3. This illustrates changes in the E and A waves as a function of the age of the fetus. As the fetus ages, the E wave form increases in height, representing an increase in speed as blood enters the ventricular chambers during the early filling phase of diastole. However, the A wave form does not increase in speed as the fetus ages. This suggests that the speed of blood resulting from atrial contraction remains unchanged, irrespective of the age of the fetus.

3.1 E/A ratio

This is a measurement of the compliance or stiffness of the ventricles as blood enters the chamber during diastole. In certain fetal conditions the measurement of this ratio may be altered.

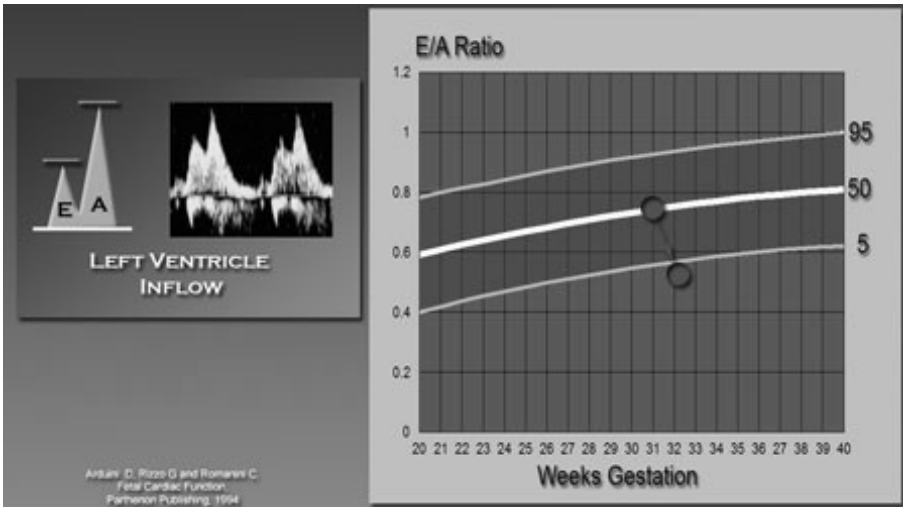

Fig. 4.

3.2 Peak velocity

This measures the speed at which blood is ejected from the ventricles. When the heart is not functioning properly,then the peak velocity may decrease.

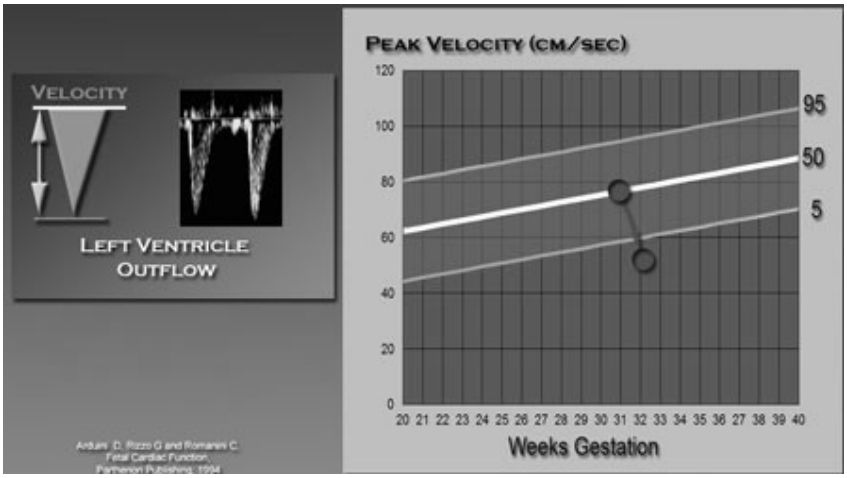

Fig. 5. This illustrates the normal range for the peak velocity of the aorta. If this decreases, this suggests cardiac dysfunction.

3.3 Time-to-peak velocity

This is a measure of how much resistance there is to blood as it is being pumped out of the ventricle. If the value increases, this means there is less resistance than normal. If it decreases, this means that there is more resistance to blood flow. This is often observed in fetuses with abnormal growth in which the fetus is smaller than normal.

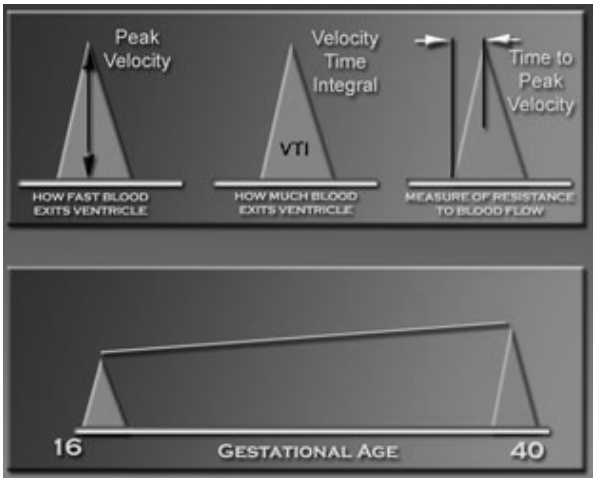

Fig. 6.

3.4 Pulsed doppler ultrasound examination of the heart

Pulsed Doppler ultrasound consists of displaying the blood flow patterns in a waveform. The pulsed Doppler enables the physician to record different flow patterns during the cardiac cycle from specific parts of the heart. From these waveforms measurements can be made to assist the physician in the interpretation of blood flow into and out of the heart.

3.4.1 Pulsed doppler relate to the electrocardiogram

The electrocardiogram, also known as an EKG, is a recording of the electrical activity of the heart during the cardiac cycle. To understand the pulsed Doppler waveform recorded from the heart researchers have compared it to the EKG.

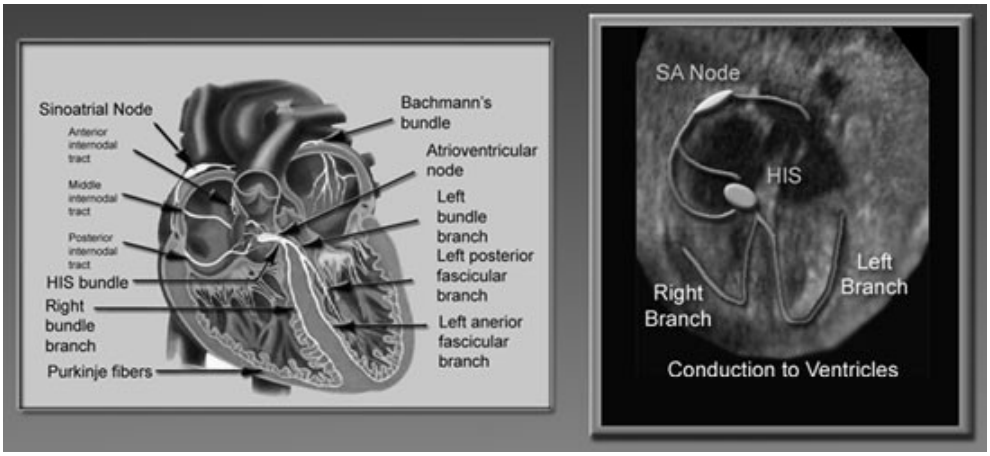

Fig. 7. This illustrates the electrical conduction of the heart.
The electrical signal originates in the SA Node located near the right atrium. It is first sent the atrial walls, resulting in contraction of the atrial chambers. The signal then is transmitted to the AV Node (green) to the ventricles. When this occurs the ventricles contract.

3.4.2 Doppler waveforms different when recorded from the right and left sides of the heart

Yes, the waveforms are different. For example, when the pulsed Doppler is recorded from the left ventricle the diastolic and systolic waveforms can be recorded at the same time. The reason for this is because the mitral and aortic valves are next to each other. However, these valves are not close together for the right ventricle and the waveforms must be recorded separately from different locations within the heart.

This compares the pulsed Doppler waveforms recorded from within the left and right ventricles (inflow) and the pulmonary and aortic outflow tracts (outflow). The waveforms from the inflow tracts are different because the left ventricle displays two waveforms. This is because the mitral and aortic valves are adjacent to each other, resulting in both waveforms being recorded simultaneously.

However, the aortic waveform within the left ventricle represents the flow exiting the left ventricle before it exits through the aortic valve.

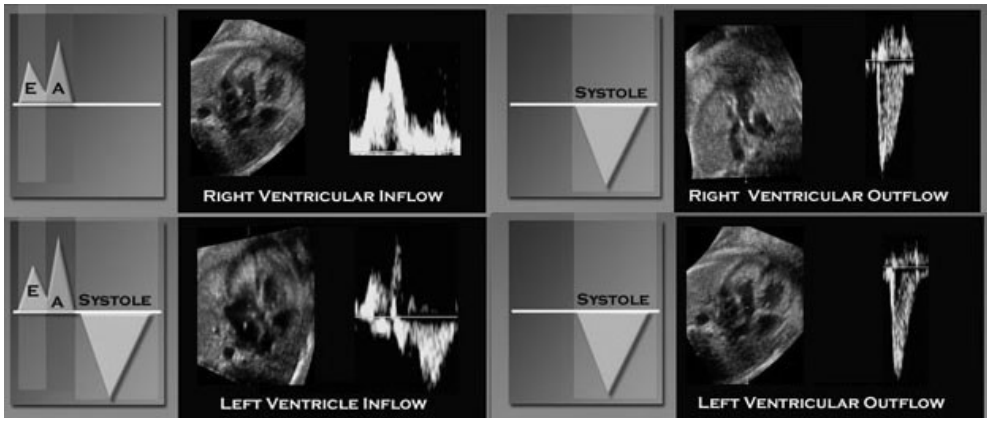

Fig. 8.

3.5 Equipment

Ultrasound systems used for fetal echocardiography should have capabilities for performing 2-dimensional,M-mode, and Doppler imaging.The requirements of fetal echocardiography are more stringent than for an infant or child with congenital or acquired heart disease .This is due to the increased demands for both spatial and temporal resolution.Anatomic surveys require axial resolution of 1mm or less and thiss is particularly important given the small size of critical fetal cardiac structures.Frames rates of 80to 100 Hz are frequentlyneeded to view important events occuring at heart rates in excess of 140 beats per minute.TO meet these requirements,imaging systems need to be optimally configured.In general,system settings are adjusted to minimize persistence and spatial averaging and to increase frame rate.All modalites of Doppler including color, pulse, high pulse repetition frequency, and continuous wave should be available.Tissue Doppler imaging has been recently applied in the assessment of fetal arrhythmania.Harmonic imaging is useful when acoustic penetration is diffucult such as in the presence of maternel obesty.Phased array transducers with fundamental frequencies between 4 and 12MHz are geberally used.Curvilinear ear probes may be helpful given the wider near-field of wiev.High frequency transducers with a narrower footprint commonly used in echocardiography of infants may also be helpful.

3.6 Examination technique

Although the goal is to achieve visualization of each of the essential components,not all will be visualized in every fetus at every examination.Fetal position in the uterus or increased activity may limit the ability to ontain visualization of each of the components.The number of vessels in the umblical cord is counted and Doppler sampling of the umblical artery and umblical vein is performed.After establishing the position of the fetus and the right/left and anterior/posterior orientation, and initial survey of the fetus is used to estimate the gestational age and to establish abdominal situs and cardiac position.The presence or

absence of fluid in the pericardial,pleural, or peritoneal space should be noted.The position of the inferior vena cava and descending aorta at the level of of the diaphragm are established.Multiple scanning positions and sweeps are necessary to adequately image the fetal heart.Suggested views are described below with a brief explanation of how to achieve the view an the structures generally well seen.Reference sources are available, which illustrate these views in detail.The authors recognize that based on operator style, alternative or additional sweeps and views may be utilized to image the various structures of the fetal heart and still accomplish a comprehensive fetal echocardiogram.

3.7 Essential components of the fetal echocardiogram

3.7.1 Feature essential component

- Anatomic overview Fetal number and position in the uterus
- Establish stomach position and abdominal situs
- Establish cardiac position
- Biometric examination Cardiothoracic ratio
- Biparietal diameter
- Femur length
- Cardiac imaging views/sweeps Four-chamber view
- Four-chamber view angled towards great arteries (“Five-chamber” view)
- Long-axis view (left ventricular outflow)
- Long-axis view (right ventricular outflow)
- Short-axis sweep (cephalad angling includes “3 vessel”view
- Caval long-axis view
- Ductal arch view
- Aortic arch view
- Doppler examination Inferior and superior vena cava
- Pulmonary veins
- Hepatic veins
- Ductus venosus
- Foramen ovale
- Atrioventricular valves
- Semilunar valves
- Ductus arteriosus
- Transverse aortic arch
- Umbilical artery
- Umbilical vein
- Measurement data Atrioventricular valve diameter
- Semilunar valve diameter
- Main pulmonary artery
- Ascending aorta
- Branch pulmonary arteries
- Transverse aortic arch
- Ventricular length
- Ventricular short-axis dimensions
- Examination of rhythm and rate M-mode of atrial and ventricular wall motion
- Dopplerexamination of atrial and ventricular flow patterns

Structures viewed in the 4- and 5- chamber view

- Atrial and ventricular size
- Atrial and ventricular septae
- Atrioventricular size and function
- Coronary sinus
- Ventricular function in long axis
- Semilunar valve function (may not, however, be optimal to differentiate aorta from main pulmonary artery)
- Pulmonary veins

Structures viewed in the cardiac short-axis sweep

- Pulmonary venous return
- Inferior vena cava and hepatic veins
- Ventricular short-axis dimensions
- Ventricular-arterial relationship
- Right ventricular outflow tract
- Branch pulmonary arteries and origin
- Caval connections
- Innominate vein
- Ductus arteriosus
- Determination of arch sidedness and branching

Structures viewed in the cardiac long-axis sweep

- Superior and inferior vena cava
- Left ventricular outflow tract
- Ascending aorta
- Great vessel connection and size
- Ductus arteriosus and proximal ductal arch

Structures viewed in the caval long-axis view

- Superior vena cava
- Inferior vena cava and eustachian valve
- Patent foramen ovale
- Right pulmonary artery

Structures viewed in the ductal and aortic arch views

- Main pulmonary artery
- Branch pulmonary arteries
- Patent ductus arteriosus and direction of flow
- Aortic arch dimension (ascending, transverse, isthmus, and descending)
- Direction of flow in the aortic arch

Journal of the American Society of Echocardiography

808 Pediatric Council of the American Society of Echocardiography July 2004

4. Coarctation of aorta

The narrowed segment called coarctation can occur anywhere in the aorta, but is most likely to happen in the segment just after the aortic arch. This narrowing restricts the amount of oxygen-rich (red) blood that can travel to the lower part of the body. Varying degrees of narrowing can occur.

The more severe the narrowing, the more symptomatic a child will be, and the earlier the problem will be noticed. In some cases, coarctation is noted in infancy. In others, however, it may not be noted until school-age or adolescence. Seventy-five percent of children with coarctation of the aorta also have a bicuspid aortic valve - a valve that has two leaflets instead of the usual three. Coarctation of the aorta occurs in about 8 percent to 11 percent of all children with congenital heart disease. Boys have the defect twice as often as girls do.

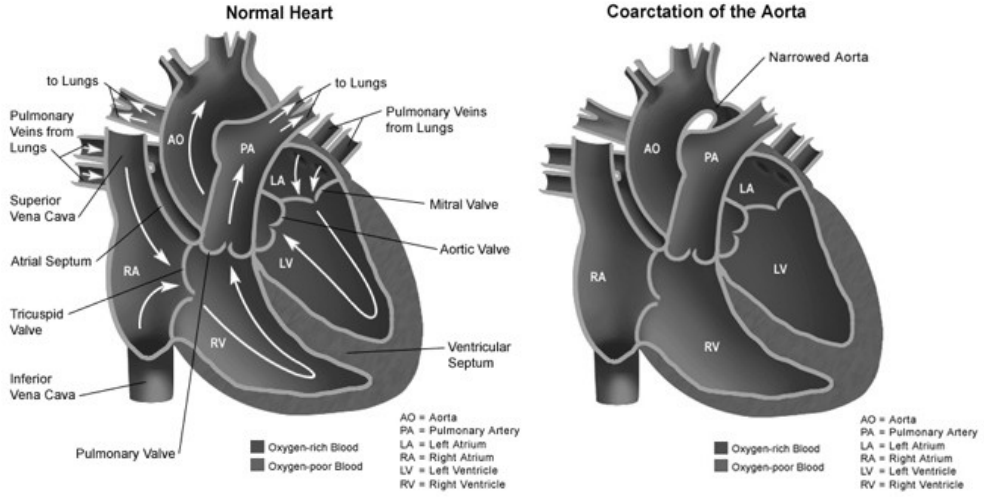

Fig. 9.

5. Hypoplastic left heart syndrome

Hypoplastic left heart syndrome (HLHS) is a combination of several abnormalities of the heart and great blood vessels. It is a congenital (present at birth) syndrome, meaning that the heart defects occur due to abnormal underdevelopment of sections of the fetal heart during the first 8 weeks of pregnancy. In the normal heart, oxygen-poor (blue) blood returns to the right atrium from the body, travels to the right ventricle, then is pumped through the pulmonary artery into the lungs where it receives oxygen. Oxygen-rich (red) blood returns to the left atrium from the lungs, passes into the left ventricle, and then is pumped out to the body through the aorta.

6. Transposition of the great arteries

In transposition of the great arteries, the aorta is connected to the right ventricle, and the pulmonary artery is connected to the left ventricle - the exact opposite of a normal heart's

anatomy. Oxygen-poor (blue) blood returns to the right atrium from the body, passes through the right atrium and ventricle, then goes into the misconnected aorta back to the body. Oxygen-rich (red) blood returns to the left atrium from the lungs, passes through the left atrium and ventricle, then goes into the pulmonary artery and back to the lungs. Two separate circuits are formed - one that circulates oxygen-poor (blue) blood from the body back to the body, and another that recirculates oxygen-rich (red) blood from the lungs back to the lungs.

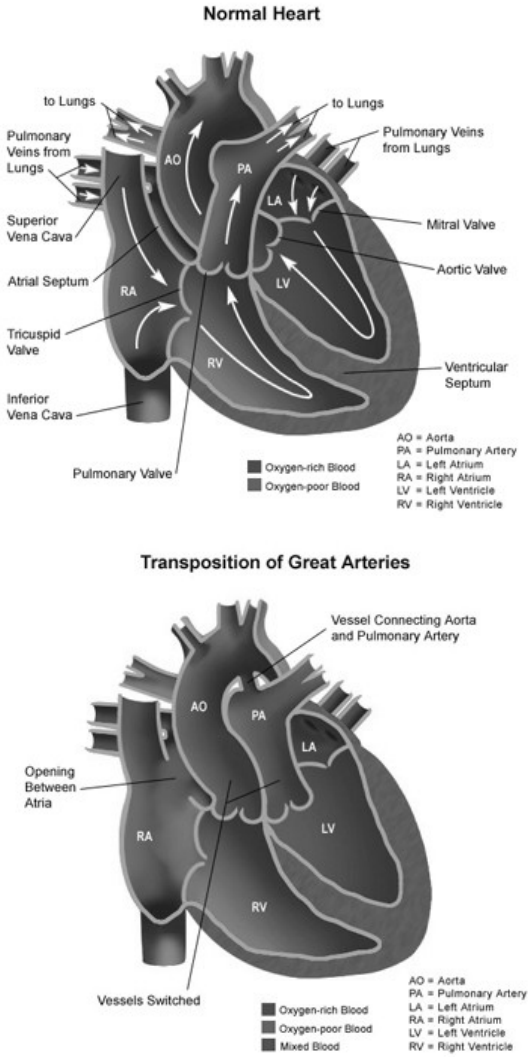

Fig. 10.

7. Pulmonary stenosis and atresia

Pulmonary stenosis and pulmonary atresia with intact ventriculer septum represent 9% and about %2 off all cardiac anomalies,respectively. The most common form of pulmonary stenosis is the valvar type,due to the fusion of the pulmonary leaflets.Hemodynamics are altered proportionally to the degree of the stenosis.The work of the right ventricle is increased,as well as the pressure,leading to hypertrophy of the ventriculer walls.

Pulmonary atresia with intact ventriculer septum in infants is usually associated with a hypoplastic righy ventricle.Prenatal diagnosis of pulmonary atresia with intact ventriculer septum relies on the demonstration off a small pulmonary artery with an atreticpulmonary valve.

8. Ebstein's anomaly

The color Doppler defines the underlying pathology by demonstrating abnormal blood flow back into the right atrium from the right ventricle. The abnormal flow originates from a displaced tricuspid valve which is located lower in the ventricle than it should be. This is called Ebstein's malformation often seen in women who take anti-depressants such as Lithium.

9. Aortic stenosis

In general, the narrowing is found at the level of the aortic valve and a simple stenosis is rarely detected in the four-chamber view. However, a critical aortic stenosis is associated with a dilated and hypokinetic left ventricle with an echogenic endocardium, as a sign of endocardial fibroelastosis. Simple aortic stenosis can be detected only by using color Doppler. Antegrade turbulent flow (aliasing) is a characteristic finding in the five-chamber view. Pulsed Doppler analysis shows high velocities (more than 2 m/s) and a characteristic aliasing pattern. Continuous wave Doppler is therefore necessary to confirm the diagnosis. In critical aortic stenosis, there is antegrade turbulent flow across the aortic valve, but peak systolic velocities can vary from more than 2 m/s to values within the normal range, as an expression of left ventricular dysfunction. Due to the high pressure in the left ventricle, both a mitral regurgitation and a left to- right shunt at the level of the foramen ovale are found. In severe left ventricular dysfunction, a retrograde flow is seen within the aortic arch.

10. Hypoplastic right ventricle

In this condition, the aortic valve is generally atretic or severely stenotic and the left ventricle diminutive and non-contractile. The mitral valve is either atretic or stenotic. Color Doppler demonstrates reduced or absent diastolic filling of the left ventricle . In the four-chamber view, there is unilateral perfusion of the right ventricle. Often, there is mild tricuspid regurgitation. Careful examination of the intra-atrial communication shows an abnormal left-to-right shunt. In hypoplastic left heart syndrome, there is retrograde perfusion of the neck vessels and coronary arteries which can also be used for the differential diagnosis. Using color Doppler, it is then possible to confirm the diagnosis by demonstrating, in the three-vessel view, the retrograde perfusion in the hypoplastic aortic arch.

The color Doppler defines the underlying pathology by demonstrating the flow patterns within the heart.This is the labeled image of the pathology demonstrating several features. When the heart fills with blood (diastole) blood is observed filling only the left ventricle. When the heart begins to contract (systole) blood is observed going across the ventricular septal defect to fill the smaller right ventricle.

The arrows illustrate the ventricular septal defect (VSD). RA=right atrium, LA=left atrium, RV=right ventricle, LV=left ventricle.

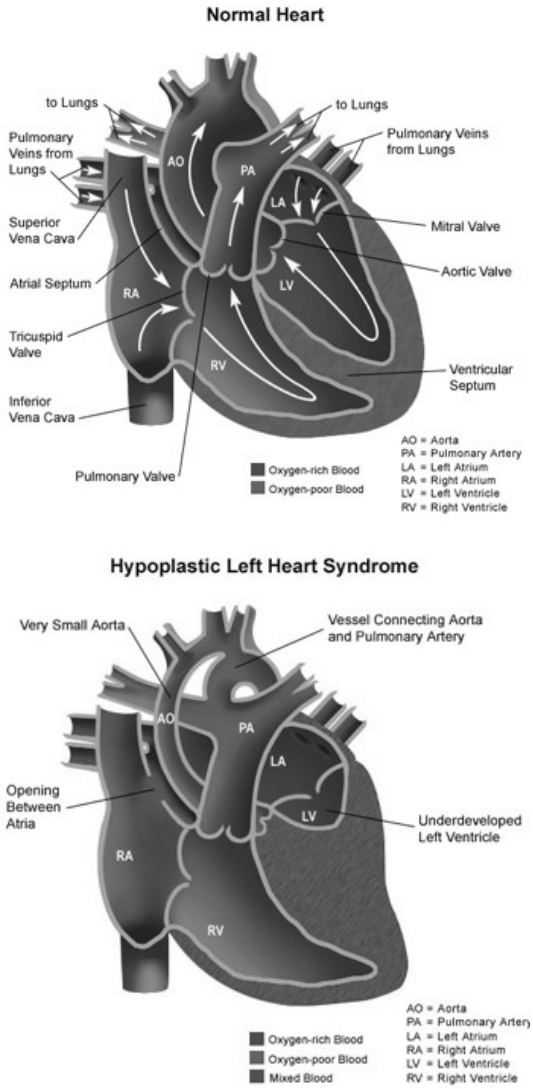

Fig. 11.

11. Tricuspid regurgitation

This image illustrates the four-chamber view using 2D ultrasound on the left and color Doppler on the right. Tricuspid regurgitation cannot be demonstrated using 2D ultrasound. This finding is important because tricuspid regurgitation is associated with an increased risk for Down syndrome when it is observed during the first or second trimeters of pregnancy.

RA=right atrium, LA=left atrium, RV=right ventricle, LV=left ventricle.

The right atrium is enlarged with what appears to be an abnormal triccolor Doppler on the right. Tricuspid regurgitation cannot be demonstrated using 2D ultrasound. This finding is important because tricuspid regurgitation is associated with an increased risk for Down syndrome when it is observed during the first or second trimeters of pregnancy.

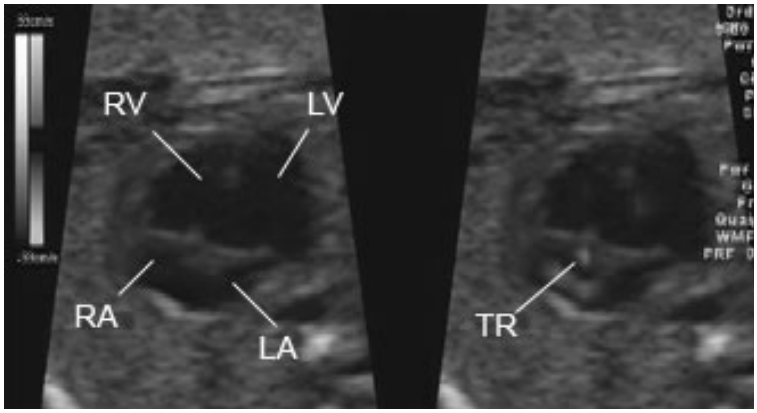

Fig. 12. RA=right atrium, LA=left atrium, RV=right ventricle, LV=left ventricle.

12. Ventricular septal defect

The defect can be either situated in the inlet, in the muscular part or, most commonly, in the perimembranous part of the ventricular septum. The defect can be suspected by two-dimensional ultrasound examination if it is larger than 3 mm. Color Doppler can help to identify small muscular septal defects. Although right and left ventricular pressures are quite equal prenatally, a bidirectional shunt across the defect is present. The best approach to examine a septal defect with color Doppler is the perpendicular insonation of the interventricular septum. In cases of an obstruction of an outflow tract, there is an unidirectional shunt to the contralateral side; in a ventricular septal defect with aortic stenosis, there is a left-to-right shunt.

This is the labeled image of the pathology demonstrating the shunting ventricular septal defect (VSD) easily identified with color Doppler ultrasound RA=right atrium, LA=left atrium, RV=right ventricle, LV=left ventricle.

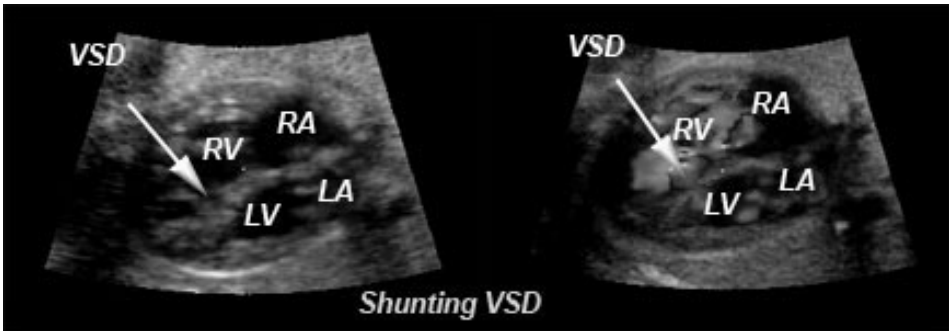

Fig. 13.

13. Other cardiac anomalies and arrhythmias

- Atrioventricular septal defects are a more relevant entity mostly because of the very frequent association with other anomalies such as trisomy 21;diagnosis of this defect is simpler although false-negatives may occur.
- Tricuspid dysplasia and Ebstein's malformation of the tricuspid valva may be complicated by severe tricuspid insufficiency ,cardiomegaly,and hydrops;such combination is most frequently lethal,with very few infants surviving.
- Irreguler paterns of fetal heart rhythms are frequent.short periods of tachycardia,braycardia,and ectopic beats as well are very commonly seen,and in the vast majority of cases have no clinical significanca.A sustained bradycardia of less than 100 bpm, a sustained tachycardia of more than 200 bpm and irregular beats occuring more than 1in 10 should be considered obnormal and require further investigation.The techniques of choice for the diagnosisof fetal dysrhythmias are M-mode and/or spectral Doppler ultrasound.
- premature atrial or ventriculer beats are by far the most frequentfetal arrhythmias.They are benign ,are not associated with an increased risk of cardiac malformations , and tend to disapper throughout gestation.Serial monitoring has been recommended because,thet sometimes can evolve toward fetal tachycardia.
- fetal tachycardias are potentially serious dysrhythmias that may cause fetal hydrops and perinatal death.
- congenital heart block may accur either as a consequence of a cardiac malformation or because of transplacental passage of maternal autoimmune antibodies.

14. Summary

The fetal echocardiogram is a unique ultrasound examination, which differs from the antenatal obstetrical ultrasound and from conventional echocardiogram in the infant,child,or adult.A unique ,high level set of skills and knowledge is required in order to perform this test.Diagnosis of cardiac defect is posibble ;however,a spesific examination is required (fetal echocardiogram)and this usually performed in pregnancies with an increased risk.The sensivity is in range of 80%..Most of the severe cardiac anomalies can be recognized by at least mid-gestation.While performing a standard sonogram from mid-gestation on,it is recommended to obtain a four-chamber view of the heart ;the sensitivity of this approach varies in different studies,but the general consensus is that is an acceptable approach.

15. References

Abramowicz JS, Kossoff G, Marsal K, Ter Haar G. Literature review by the ISUOG bioefects and safety committee. Ultrasound Obstet Gynecol 2002;19:318-9.

Allan L, Hornberger L, Sharland G, editors. Textbook of fetal cardiology. London: Greenwich Medical Media; 2000.

Berning RA, Silverman NH, Villegas M, Sahn DJ, Martin GR, Rice MJ. Reversed shunting across the ductus arteriosus or atrial septum in utero heralds severe congenital heart disease. J Am Coll Cardiol 1996;27:481-6.

Buskens E, Grobbee DE, Frohn-Mulder IME, Stewart PA, Juttmann RE, Wladimiroff JW, et al. Efficacy of routine fetal ultrasound screening for congenital heart disease in normal pregnancy. Circulation 1996;94:67-72.

Carvalho JS, Mavrides E, Shinebourne EA, Campbell S, Thilaganathan B. Improving the effectiveness of routine prenatal screening for major congenital heart defects. Heart 2002;88:387-91.

Deane C, Lees C. Doppler obstetric ultrasound: a graphical display of temporal changes in safety indices. Ultrasound Obstet Gynecol 2000;15:418-23.

Fouron JC, Zarelli M, Drblik SP, Lessard M. Normal flow velocity profile of the fetal aortic isthmus through normal gestation. Am J Cardiol 1994;74:483-6.

Ghi T, Huggon IC, Zosmer N, Nicolaides KH. Incidence of major structural cardiac defects associated with increased nuchal translucency but normal karyotype. Ultrasound Obstet Gynecol 2001;18:610-4.

Glickstein JS, Buyon J, Friedman D. Pulsed Doppler echocardiographic assessment of the fetal PR interval. Am J Cardiol 2000;86:236-9.

Hansen M, Kurinczuk JJ, Bower C, Webb S. The risk of major birth defects after intracytoplasmic sperm injection and in vitro fertilization. N Engl J Med 2002;346:725-30.

International Society of Ultrasound in Obstetrics and Gynecology (ISUOG). Safety statement, 2000. Ultrasound Obstet Gynecol 2000;16:594-6.

Journal of the American Society of Echocardiography Volume 17 Number 7 Pediatric Council of the American Society of Echocardiography.

Kleinman C, Donnerstein R, Jaffe C, DeVore G, Weinstein EM, Lynch DC, et al. Fetal echocardiography. A tool for evaluation of in utero cardiac arrhythmias and monitoring of in utero therapy. Am J Cardiol 1983;51:237-43.

Kurjak A. Are color and pulsed Doppler sonography safe in early pregnancy? J Perinat Med 1999;27:423-30.

Miller MW, Brayman AA, Abramowicz JA. Obstetric ultrasonography: a biophysical consideration of patient safety–the "rules" have changed. Am J Obstet Gynecol 1998;179:241-54. 1. Hoffman JI, Kaplan S. The incidence of congenital heart disease. J Am Coll Cardiol 2002;39:1890-900.

Nelson NL, Filly RA, Goldstein RB, Callen PW. The AIUM/ ACR antepartum obstetrical sonographic guidelines: expecta- Journal of the American Society of Echocardiography Volume 17 Number 7 Pediatric Council of the American Society of Echocardiography indications for detection of anomalies. J Ultrasound Med 1993;4:186-96.

Phillipos EZ, Robertson MA, Still KD. The echocardiographic assessment of the human foramen ovale. J Am Soc Echocardiogr 1994;7:257-63.

Quinones MA, Douglas PS, Foster E, Gorcsan J, Lewos JF, Pearlman AS, et al. ACC/AHA clinical competence statement on echocardiography: a report of the American College of Cardiology/American Heart Association/American College of Physicians-American Society of Internal Medicine task force on clinical competence (committee on echocardiography). J Am Coll Cardiol 2003;41:687-708.

Rein AJ, O'Donnell C, Geva T, Nir A, Perles Z, Hashimoto I, et al. Use of tissue velocity imaging in the diagnosis of fetal cardiac arrhythmias. Circulation 2002;106:1827-33.

Schmidt KG, Silverman NH, Van Hare GF, Hawkins JA, Cloez JL, Rudolph AM. Two-dimensional echocardiographic determination of ventricular volumes in the fetal heart. Circulation 1990;81:325-33.

Sharland GK, Allan LD. Normal fetal cardiac measurements derived by cross-sectional echocardiography. Ultrasound Obstet Gynecol 1992;2:175-81.

Sklansky M, Tang A, Levy D, Grossfeld P, Kashani I, Shaughnessy R, et al. Maternal psychological impact of fetal echocardiography. J Am Soc Echocardiogr 2002;15:159-66. American College of Radiology Standard for the Performance of Antepartum Obstetrical Ultrasound.

Standards for the Performance of the Antepartum Obstetrical Ultrasound Examination. Copyright 1994, by the American Institute of Ultrasound in Medicine.

Stumpflen I, Stumpflen A, Wimmer M, Bernaschek G. Effect of detailed fetal echocardiography as part of routine prenatal ultrasonographic screening on detection of congenital heart disease. Lancet 1996;348:854-7.

Tan J, Silverman NH, Hoffman JIE, Villegas M, Schmidt KG. Cardiac dimensions determined by cross-sectional echocardiography in the normal human fetus from 18 weeks to term. Am J Cardiol 1992;70:1459-67.

Tworetzky W, McElhinney DB, Reddy VM, Brook MM, Hanley FL, Silverman NH. Improved surgical outcome after fetal diagnosis of hypoplastic left heart syndrome. Circulation 2001;103:1269-73.

Verheijen PM, Lisowski LA, Stoutenbeek P, Hitchcock JF, Brenner JI, Cope JA, et al. Prenatal diagnosis of congenital heart disease affects preoperative acidosis in the newborn patient. J Thorac Cardiovasc Surg 2001;121:798.

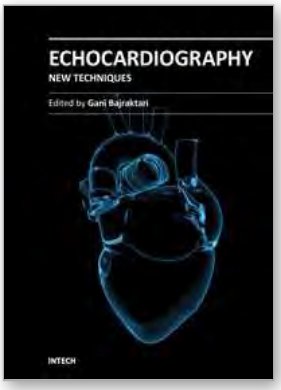

Echocardiography - New Techniques

Edited by Prof. Gani Bajraktari

ISBN 978-953-307-762-8
Hard cover, 218 pages
Publisher InTech
Published online 18, January, 2012
Published in print edition January, 2012

The book "Echocardiography - New Techniques" brings worldwide contributions from highly acclaimed clinical and imaging science investigators, and representatives from academic medical centers. Each chapter is designed and written to be accessible to those with a basic knowledge of echocardiography. Additionally, the chapters are meant to be stimulating and educational to the experts and investigators in the field of echocardiography. This book is aimed primarily at cardiology fellows on their basic echocardiography rotation, fellows in general internal medicine, radiology and emergency medicine, and experts in the arena of echocardiography. Over the last few decades, the rate of technological advancements has developed dramatically, resulting in new techniques and improved echocardiographic imaging. The authors of this book focused on presenting the most advanced techniques useful in today's research and in daily clinical practice. These advanced techniques are utilized in the detection of different cardiac pathologies in patients, in contributing to their clinical decision, as well as follow-up and outcome predictions. In addition to the advanced techniques covered, this book expounds upon several special pathologies with respect to the functions of echocardiography.

How to reference

In order to correctly reference this scholarly work, feel free to copy and paste the following:

Ahmet Cantug Caliskan (2012). Fetal Echocardiography, Echocardiography - New Techniques, Prof. Gani Bajraktari (Ed.), ISBN: 978-953-307-762-8, InTech, Available from: http://www.intechopen.com/books/echocardiography-new-techniques/fetal-echocardiography

INTECH
open science | open minds

InTech Europe
University Campus STeP Ri
Slavka Krautzeka 83/A
51000 Rijeka, Croatia
Phone: +385 (51) 770 447
Fax: +385 (51) 686 166
www.intechopen.com

InTech China
Unit 405, Office Block, Hotel Equatorial Shanghai
No.65, Yan An Road (West), Shanghai, 200040, China
中国上海市延安西路65号上海国际贵都大饭店办公楼405单元
Phone: +86-21-62489820
Fax: +86-21-62489821

Chapter

The Impact of Fetal Echocardiography on the Prognosis of Congenital Heart Disease

Maria Giovanna Russo, Fiorella Fratta, Antonia Giudicepietro, Carmela Morelli, Fortuna Del Gaizo, Laura di Pietto, Marina De Marco, Ludovica Spinelli Barrile and Federica De Fazio

Abstract

Congenital heart disease (CHD) represents the group of the most common malformations detected both prenatally and after birth. Although progress in the management and treatments of CHD, it still remains a significant cause of neonatal morbidity and mortality. However, the recent improvement in the diagnosis and therapy of CHD represents one of the most important successes of cardiac surgery and medical treatment. Accordingly, in the last twenty years, the number of patients with CHD who have reached adulthood has increased significantly and even surpass the number of affected pediatric patients, due to the extraordinary progress in the diagnostic, clinical, and surgical technologies. In particular, the ultrasound study of the fetal heart allows a diagnosis of CHD in the prenatal period, significantly improves perinatal outcomes in infants with critical CHD, and enables a reduction in stillbirth.

Keywords: Congenital heart disease, fetal echocardiography, invasive fetal cardiac intervention, counseling

1. Introduction

Congenital heart disease (CHD) is the most common malformation detected prenatally and at birth. Generally, estimated incidence is approximately 10/1000 of live births and is significantly higher in premature infants and in stillborn [1]. Although remarkable progress has been made in the diagnosis and treatment of this condition, it still remains a significant cause of neonatal morbidity and mortality. Congenital malformations of the heart are a broad spectrum of defects varying from mild lesions that produce only minimal or no symptoms and might be incidentally detected in adult life to severe anomalies that cause premature death. There are many factors that increase the risk of having a child with CHD. The etiology of CHD can be separated into genetic and non-genetic forms. Epidemiological studies have suggested that a

genetic or environmental cause can be identified in approximately 30% of CHD cases [2]. Approximately 17% of CHD occurs in association with a well-defined syndrome such as trisomies 13, 15, 18, 21 and Turner syndrome [3]. Some environmental factors have been identified as responsible for CHD such as congenital rubella infection or teratogenic drugs [2]. However, the majority of cases remain unexplained, probably due to some combination of genetic and environmental factors [4].

The main classification of CHD includes:

- Left-to-right shunt leading to an increased pulmonary flow
- Reduced pulmonary blood flow
- Transposition of the great arteries
- Left and right heart obstruction
- Duct dependent pulmonary or systemic circulation

In this chapter, we will discuss in detail the importance of fetal echocardiography and the fundamental impact of early detection and interventions during fetal life on postnatal outcomes. We will also discuss the importance of adequate counseling in order to allow parents to understand the condition, to support them in the most difficult decision to interrupt or keep pregnancy, to offer extensive information on available therapeutic options, and prevision of data on outcome and quality of life.

2. Fetal echocardiography, impact on the prognosis

Fetal echocardiography is born in the late 80s, when the improvement of ultrasound technology has made possible to focus attention on the characteristics of the fetal heart. Huhta JC, one of the pioneers of this method, raised the question if, without the possibility of treating in utero CHD, is it useful or advisable to make the diagnosis in advance, before birth [5]. It is clearly demonstrated that a team consisting of an expert gynecologist and a pediatric cardiologist can make diagnosis of a number of congenital heart defects in the fetal stage with very high degree of accuracy [6]. The prenatal diagnosis of CHD in the last 30 years has reached a high degree of diagnostic accuracy allowing to identify of almost all forms of CHD during fetal life; this is true in most expert centers since the interpretation of fetal echocardiography requires advanced skills. Accordingly, a suspected cardiac abnormality should then always be referred to a fetal cardiology specialist in a tertiary level center for further evaluation. Prenatal diagnosis rates for CHD increased from 23.0% in 1983–1988 to 47.3% in 1995–2000 [6]. Similarly, termination rates increased from 9.9% (between 1983 and 1989) to 14.7% (between 1989 and 2000) [6]. The spectrum of CHD observed before birth appears similar to the spectrum of CHD postnatally detected [6]. Early diagnosis of CHD during fetal echocardiography can influence the prognosis because it can permit the parents and clinicians to treat the defect. In this chapter, we will address pregnancy and delivery management, issues related to voluntary interruption of pregnancy, and fetal interventions.

3. Pregnancy and delivery management

Prenatal diagnosis has an impact on morbidity and mortality for most severe conditions because it allows an appropriate referral and planning of delivery and immediate assistance in expert centers resulting in improving short-term outcomes. However, its influence on long-term outcomes are still not clarified. In particular, prenatal diagnosis of conditions that constitute a neonatal emergency, such as duct dependent lesions, allows for manage the delivery in a tertiary care center. This strategy improves survival significantly and reduces preoperative morbidity and risk of neurological compromission [7]. CHD patients diagnosed postnatally that were born at non-tertiary centers, without specialist neonatal or cardiac services, presented later and required much higher levels of cardio-respiratory support during transfer from geographically distant locations [8]. Of note, clinical instability in postnatally diagnosed infants with CHD is an established risk factor for morbidity and mortality [8]. Moreover, it has also been proven that prenatally diagnosed infants undergo significantly earlier surgery [8].

4. Voluntary interruption of pregnancy

It has been documented that a parallel increase in pregnancy interruption occurred with fetal CHD diagnosis [9]. Thus, early diagnosis of CHD permits parents to make the difficult choice of eventual interruption of pregnancy. The rates of prenatal diagnosis of CHD were 47,3% in France, 49% in USA, and 52,8% in Australia [10]. In our center, our 21 years' experience is in accord with the one of Khoshnood [6]: the spectrum of prenatally diagnosis CHD is getting similar to the one observed after birth. This is due to the great number of detected cases. Other than hypoplastic left heart syndrome (HLHS), pregnancy termination was exceptional. Early neonatal mortality in patients with severe CHD decreased to less than 1/3 in the period 1995–2000 [6]. The curve of survival shows a slightly worse survival for neonates with the prenatal diagnosis but this is likely to be related to the composition of the population and selection bias since fetal echocardiography is performed only when there is a high index of suspicion for more severe CHD [11].

4.1 Fetal cardiac intervention

Several fetal studies reported that structural heart disease, in particular aortic stenosis, evolves in utero, hindering the growth of the left ventricle [12]. Fetal cardiac intervention (FCI) is a novel and advanced technique that allows in utero treatment of a subset of congenital heart disease. Fetal cardiac intervention with valvuloplasty, is based on the principle that intervention will modify the natural history of the disease process [13]. To prove an eventual favorable impact of FCI, we must first gain a full understanding of the unaltered progression of heart disease in utero. Referral centers that have performed the most procedures have shown that in utero valvuloplasty can be performed successfully, with limited risk to the mother and encouraging outcomes for fetuses, especially in those with aortic stenosis at risk of evolving to HLHS [14].

Fetal intervention is technically feasible only in a small specific subset of congenital heart defects.

The three most commonly performed FCI are [15]:

1. **Fetal aortic stenosis** with risk factors for evolving into hypoplastic left heart syndrome (HLHS).

2. **HLHS** with intact or restrictive atrial septum.

3. **Pulmonary atresia/stenosis with intact ventricular septum,** with concern for worsening right ventricular (RV) hypoplasia.

- **Fetal aortic stenosis**. In Linz center between October 2000 and February 2020, 115 fetal aortic valvuloplasties (FAV) were undertaken in 95 fetuses. All patients but one had at least one technically successful procedure. An overall success rate of 82.4% (14/17 procedures) was reported by Tulzer et al. [16]. Similarly, Pickard et al. reported in a period from 2000 to 2017 that fetal aortic valvuloplasty was technically successful in 84% of 143 fetuses, while fetal demise was observed in 8%. Biventricular circulation was achieved in 50% of the remaining 111 live-born infants with successful fetal aortic valvuloplasty, while only 16% of the 19 patients with unsuccessful valvuloplasty achieved biventricular circulation [17].

- **HLHS with intact or restrictive atrial septum.** The incidence of intact atrial septum in HLHS is approximately 6%, with restrictive atrial septum occurring in up to 22% [18]. Survival for patients with HLHS and intact atrial septum remains poor, with a 1-year survival rate of ~ 30% [19]. The rationale for FCI in HLHS with intact or restrictive atrial septum is to avoid severe neonatal hypoxia and death and to prevent worsening of the lung disease that frequently occurs as a result of chronic in utero pulmonary venous hypertension. Postnatal management involves atrial septostomy, the Rashkind procedure, to open the atrial septum and enhance atrial mixing. Some selected centers performing this type of FCI, have attempted to maintain patency of the atrial septal defect until the time of delivery, with an atrial septal stent. In the largest cohort of patients undergoing FCI on the atrial septum (n = 47) from the International Fetal Cardiac Intervention Registry, technical success was reported in 77% of cases, with 65% success in atrial stent placement [20].

- **Pulmonary atresia/stenosis with an intact ventricular septum.** Even lesions like pulmonary atresia with intact ventricular septum and severe pulmonary stenosis can progress to significant right ventricular dysplasia and evolve to unfavorable univentricular circulation at birth which will require complex and multiple interventions in the follow-up. These fetuses are potential candidates for pulmonary balloon valvuloplasty in utero. Fetal cardiac intervention offers the potential for improved right ventricle and tricuspid valve growth, less damage to the myocardium, potential for biventricular circulation, and improved morbidity and mortality [21].

The International Fetal Cardiac Intervention Registry (IFCIR) has published data from multiple institutions that provide FCI for PA/IVS [22]. In this study, 16 patients enrolled underwent FCI with 11 successful procedures. The procedure success rate was 11/16 (69%). Of the 11 technically successful cases, five (45%) had postnatal biventricular repair [22]. The group at the Children's Hospital Heart Center in Linz has

published a large cohort of patients at a single center [23]. They performed 35 FCI on 25 maternal-fetal pairs for either PA/IVS (n = 15) or critical pulmonary valve stenosis (n = 8). They report either partial or successful FCI in 21/23 maternal-fetal pairs. In the successful intervention group, 15 had a predicted biventricular surgery (70%), three a one and a half ventricle surgery and three an indeterminate outcome. No patients that had a successful FCI were predicted to have a single ventricle outcome [23]. A study performed at Boston Children's Hospital describes their experience [24]. FCI was performed in ten fetuses with PA/IVS. The first four procedures were technically unsuccessful and the following six procedures were successful. Compared with control fetuses (n = 15) with PA/IVS who did not undergo prenatal intervention and had univentricular outcomes after birth, the tricuspid valve annulus, right ventricle length, and PV annulus grew significantly more from midgestation to late gestation in the six fetuses who underwent successful interventions. Nine fetuses were liveborn; one fetus was terminated after an unsuccessful attempt at FCI. All nine patients required postnatal interventions. Of the six successful FCIs, five had a predicted biventricular outcome (83%) and one had a predicted single-ventricle outcome [24].

FCI also includes transplacental drug therapy, such as maternal antiarrhythmic drugs in case of fetal arrhythmias and steroids [25].

4.2 Termination of pregnancy

FCI techniques have made possible to improve the success rates of cardiac interventions in utero, obtaining better postnatal outcomes. However, it is inevitable to consider the consequences of a diagnosis of CHD in the prenatal period, leading to a set of complex emotional states in parents who move away from the concept of "healthy condition" of their future child. Discussion with parents on the long-term prognosis constitutes a fundamental element of adequate counseling. Appropriate counseling is ideally composed of an interdisciplinary team: obstetrician, pediatrician, pediatric cardiologist, and heart surgeon [26]. Counseling to parents following the diagnosis of congenital heart disease should take into account: the severity of CHD, the association with extracardiac malformations, and the presence of an associated genetic syndrome. All of these factors influence the parents' decision regarding pregnancy continuation or interruption.

In recent decades, the study of the heart in the prenatal period through fetal echocardiography, associated with a marked improvement in ultrasound technologies, and a greater competence of the operators, has significantly increased detection of the prenatal CHD. The incidence cardiac anomalies diagnosed at prenatal ultrasound screening differs from that observed at birth, due to intrauterine fetal demise and the recourse to termination of pregnancy (TOP). Indeed, in countries where prenatal evaluation is considered as standard of care, the incidence of CHD births is even lower [27]. As mentioned before, the main advantages of an early diagnosis of cardiac malformation are the possibility of adequate preparation for childbirth and neonatal care and early interventions in utero. However, it is inevitable to consider the consequences of a diagnosis of cardiac malformation have in the prenatal period, leading to a set of complex emotional states in parents who have to move away from the concept of "healthy condition" of their future child and eventually undertake the difficult choice of TOP [6]. Annually in the European Union, it has been estimated that 36000 children are live-born with CHD [28]. Increasing prenatal detection may lead to a reduced birth incidence of severe complex CHD through a high rate of TOP, even if this trend is not universal [29]. In the EUROCAT registry, a total of 31% of prenatally

diagnosed nonchromosomal CHD resulted in TOP [28]. The parent's choice to TOP is conditioned by several factors as listed below [30–32]:

1. ethical and/or religious reasons;

2. current legislation;

3. severity of cardiac malformation;

4. impact of heart disease on quality of life;

5. possibly associated extracardiac malformations;

6. underlying genetic condition;

7. complexity of cardiac surgery;

8. prediction of survival to adulthood and long-term quality of life;

Additional components that influence the couple's decision-making process include the socioeconomic status, the age of the parents, and the overall family context (caregivers) [33]. It is also reported in the literature that the "pressure" regarding the choice to terminate a pregnancy following multidisciplinary counseling is greater when listening to gynecologists than to pediatric cardiologists and cardiac surgeons [34]. A French study reports an interesting analysis of isolated CHD fetuses; concluding that more than half of the choices for termination of pregnancy were based on the "complexity" of heart disease as HLHS, univentricular heart, pulmonary valve atresia, aortic stenosis [6]. It is, therefore, essential to transfer adequate and precise counseling to the couple without limiting the decision-making process. Thus, considering the information that is offered to parents by pediatric cardiologists and cardiac surgeons regarding the diagnosis of hypoplastic left heart syndrome, it is not surprising that the choice for TOP will increase in this condition because this CHD has a poor post-natal outcome with an impact on the quality of life of the newborn, given the multistage palliative surgery and the surgical risks associated with each intervention [35]. After these considerations, we should if fetal echocardiography should be performed ignoring the consequence of such acts [36]. This debate is still ongoing today, asking questions about the impact that prenatal ultrasound diagnosis can have on the future of humanity [37, 38].

4.3 Fetal counseling

Since the prenatal diagnosis of fetal malformation has improved and it's now possible to detect or suspect a fetal malformation from the mid-gestation, it has been necessary to improve the counseling, paying attention to the ethical and psychological aspects related to this issue [39–42]. This is an important issue raised by the large and growing scientific literature on this argument [39–42]. As a consequence of these observations, many authors [43, 44] suggest that is necessary that counseling is performed by a multidisciplinary team comprising the obstetrician, the cardiologist, the surgeon, and the psychologist, in order to provide a fully comprehensive information to the parents. The passage from *paternalistic medicine* to *defensive medicine,* which recognizes

the patient's right to have full information, incites the doctor to tell the truth, even in the case of the inauspicious diagnosis of a life-threatening illness. During counseling, at the communicative level, the challenge is not "*whether to tell the truth, but* rather, *how to tell it".* Since CHD is a significant cause of morbidity and mortality in the newborns, its diagnosis may lead to a huge crisis in the affected families, considering the perceived implications of having an abnormality of such vital an organ. The severity of the crisis depends not only on the nature of the abnormality, but also upon its perceived seriousness and whether the defect is correctable. During the pregnancy, parents idealize the newborn and give him/her qualities, feelings, and capacities that they wish. The birth of a baby with a malformation is a sorrow including the death of the imagined child.

The majority of the diagnosis of fetal congenital heart disease occurs after the 18th week of gestation, when the mother already feels the first fetal movements, and the baby is part of her body [45]. During counseling, parents need to know if there is a possibility of repair and what is the risk of the procedures, and how will be the child's quality of life. Some authors analyzed the mother's desire for more information on prenatal diagnosis of fetal abnormality [46]. Some mothers preferred to have increased information upfront in order to "wrap their head around the disease," while other mothers felt that too much information upfront increased anxiety and would rather "cross that bridge when they came to it."

The explanation should possibly be given with both parents present, allowing each to provide support to the other, considering that the impact may be different on either parent, since each may perceive the abnormality differently.

4.4 Genetic counseling

The etiology of congenital heart disease is currently the focus of intense research.

The ideal genetic counseling for cardiovascular malformations includes a thorough understanding of the anatomy, management, and outcome of the particular defect, identification of other affected family members, and careful pedigree analysis for prediction of familial risks, identification of associated malformations or syndromes, and options for prenatal diagnosis [2]. Preferably, genetic counseling should be provided both by a clinical geneticist with adequate knowledge about cardiac defects and outcomes and by a pediatric cardiologist who has good knowledge and skills in genetic issues.

In the past, genetic counseling for isolated congenital cardiovascular malformations (i.e., without extracardiac malformations or syndromic diagnosis) was transmitted as an advice, with the use of overall recurrence risk for first-degree relatives of 2–5%. These malformations were reputed to be *multifactorial*, but recent studies suggest that specific *genetic* influences may be more important than previously recognized, and that certain malformations are more likely to have a stronger genetic component [47, 48].

A common genetic defect or pathogenetic mechanism may cause several apparently different forms of congenital cardiovascular malformations, as, for example, in case of chromosome 22q deletion, that cause a variety of conotruncal malformations and aortic arch anomalies [49, 50].

5. Conclusions

The prenatal diagnosis of CHD in the last 30 years has reached a high degree of diagnostic accuracy allowing identification of almost all the main forms of CHD

during fetal life, in expert centers. In particular, prenatal diagnosis of conditions that constitute a neonatal emergency, such as duct dependent lesions, allows to manage the delivery in a tertiary care center. This strategy improves survival significantly, and reduces preoperative morbidity, and the risk of neurological compromise. While some CHD may have a successful surgical correction in postnatal life, a small selective subset of these defects can progress during intrauterine life and be susceptible to early interventions in the uterus. Fetal cardiac interventions might prevent in utero worsening from a simple, potentially correctable lesion to a complex cardiac condition in selective patients. FCIs are most commonly and successfully performed in the setting of 1) fetal aortic stenosis with risk for evolving to hypoplastic left heart syndrome, 2) HLHS with intact or restrictive atrial septum 3) pulmonary atresia/stenosis with intact ventricular septum, with specific features associated with risk for worsening right ventricular hypoplasia. FCI also includes transplacental therapy, including maternal antiarrhythmic drugs in case of fetal arrhythmias and steroids. FCI is a procedure that has maternal and/or fetal risks, which must be well explained to parents at the time of counseling, to be sure that they fully understand the possible complications.

Moreover, fetal early diagnosis allows to program earlier clinical management and surgery after birth, improving outcomes. The improvement in the diagnosis and treatment of these conditions, due to extraordinary advances in imaging and cardiac surgical and interventional technologies in the last twenty years, has led to a significant increase in survival rate in patients with CHD, and accordingly, the number of patients with CHD who have reached adulthood has increased significantly and even surpass the number of affected kids.

Author details

© 2022 Maria Giovanna Russo*, Fiorella Fratta, Antonia Giudicepietro, Carmela Morelli, Fortuna Del Gaizo, Laura di Pietto, Marina De Marco, Ludovica Spinelli Barrile and Federica De Fazio Pediatric Cardiology Unit—Luigi Vanvitelli—Campania University Hospital, Monaldi Hospital, Naples, Italy. Originally published in "The Impact of Fetal Echocardiography on the Prognosis of Congenital Heart Disease." IntechOpen under the terms of the Creative Commons Attribution License (http://creativecommons.org/licenses/by/3.0). Available from http://dx.doi.org/10.5772/intechopen.104828

References

[1] Hoffman JI, Kaplan S. The incidence of congenital heart disease. Journal of the American College of Cardiology. 2002;**39**:1890-1900

[2] Pierpont ME, Brueckner M, Chung WK, et al. Genetic basis for congenital heart disease: Revisited: A scientific statement from the american heart association circulation. 2018;**138**:e653-e711

[3] Cowan JR, Ware SM. Genetics and genetic testing in congenital heart disease. Clinics in Perinatology. 2015;**42**:373-393

[4] Jin SC, Homsy J, Zaidi S, Lu Q, Morton S, DePalma SR, et al. Contribution of rare inherited and de novo variants in 2,871 congenital heart disease probands. Nature Genetics. 2017;**49**:1593-1601

[5] Huhta JC. Uses and abuses of fetal echocardiography: A pediatric cardiologist's view. Journal of the American College of Cardiology. 1986;**8**:451-458

[6] Khoshnood B, De Vigan C, Vodovar V, Goujard J, Lhomme A, Bonnet D, et al. Trends in prenatal diagnosis, pregnancy termination, and perinatal mortality of newborns with congenital heart disease in France, 1983-2000: A population-basedevaluation. Pediatrics. 2005;**115**:95-101

[7] Levey A, Glickstein JS, Kleinman C, Levasseur S, Chen J, Gersony W. The impact of prenatal diagnosis of complex congenital heart disease on neonatal outcomes pediatric cardiology. 2010;**31**:587-597

[8] Gupta N, Leven L, Stewart M, Cheung M, Patel N. Transport in infants with congenital heart disease: Benefits of antenatal diagnosis. European Journal of Pediatrics. 2014;**173**:655-660

[9] Bonnet D, Coltri A, Butera G, Fermont L, Bidois J, Kachaner J, et al. Detection of transposition of the great arteries in fetuses reduces neonatal morbidity and mortality. Circulation. 1999;**99**:916-918

[10] Chew C, Halliday JL, Riley MM, Penny DJ. Population-based study of antenatal detection of congenital heart disease by ultrasound examination. Ultrasound in Obstetrics & Gynecology. 2007;**29**:619-624

[11] Israel SW, Roofe LR, Saville BR, Walsh WF. Improvement in antenatal diagnosis of critical congenital heart disease implications for postnatal care and screening. Fetal Diagnostic Therapy. 2011;**30**:180-183

[12] Allan LD. Development of congenital lesions in mid or late gestation. International Journal of Cardiology. 1988;**19**:361e2

[13] Hutha J, Quintero RA, Suh E, Bader RS. Advances in fetal cardiac intervention. Current Opinion in Pediatrics. 2004;**16**:487-493

[14] Tworetzky W, Wilkins-Haug L, Jennings R, Van der Velde M, Marshall A, Marx G, et al. Balloon dilation of severe aortic stenosis in the fetus. Potential for prevention of hypoplastic left heart syndrome: Candidate selection, technique, and results of successful intervention. Circulation. 2004;**110**:2125-2131

[15] Friedman KG, Tworetzky W. Fetal cardiac interventions: Where do we stand?

Archives of Cardiovascular Disease. 2020;**113**:121-128

[16] Tulzer A, Arzt W, Tulzer G. Fetal aortic valvuloplasty may rescue fetuses with critical aortic stenosis and hydrops. Ultrasound in Obstetrics & Gynecology. 2021

[17] Pickard SS, Wong JB, Bucholz E, Newburger JW, Tworetzky W, Lafranchi T, et al. Fetal aortic valvuloplasty for evolving hypoplastic left heart syndrome: A decision analysis. Circulation: Cardiovascular Quality and Outcomes. 2020;**13**:e006127

[18] Rychiket J, Rome J, Collins MH, DeCampli WM, Spray TL. The hypoplastic left heart syndrome with intactatrial septum: Atrial morphology, pulmonary vascular histopathology and outcome. Journal of American College of Cardiology. 1999;**34**(2):554-560

[19] Vlahos AP, Lock J, McElhinney DB, Van der Velde M. Hypoplastic left heart syndrome with intact or highly restrictive atrial septum: Outcome after neonatale transcatheter atrial septostomy. Circulation. 2004;**109**:2326-2330

[20] Jantzen DW. Hypoplastic left heart syndrome with intact or restrictive atrial septum: A report from the international fetal cardiac intervention registry. Circulation. 2017;**136**:1346-1349

[21] Strainic J. Fetal cardiac intervention for right sided heart disease: Pulmonary atresia with intact ventricular septum. Birth Defects Research. 2019

[22] Moon-Grady AJ, Morris SA, Belfort M, et al. International fetal cardiac Intervention Registry: A Worldwide Collaborative Description a Preliminary Outcomes. Journal of American College of Cardiology. 2015;**66**:388-399

[23] Tulzer A, Artz W, Tulzer G. Immediate effects and outcome of *in-utero* pulmonary valvuloplasty in fetuses with pulmonary atresia with intact ventricular septum or critical pulmonary stenosis. Ultrasound in Obstetrics & Gynecology. 2018;**52**:230-237

[24] Tworetzky W, McElhinney DB, Marx G, Benson C, Brusseau R, Morash D, et al. In utero valvuloplasty for pulmonary atresia with hypoplastic right ventricle: Techniques and outcomes. Pediatrics. 2009;**124**:e510-e518

[25] Bravo-Valenzuela N, Alves Rocha L, Marcondes Machado Nardozza L, Araujo JL. Fetal cardiac arrhythmias: Current evidence. Annals of Pediatric Cardiology. 2018;**11**:148-163

[26] Kovacevic A, Elsässer M, Fluhr H, Müller A, Starystach S, Bär S, et al. Counseling for fetal heart disease—Current standards and best practice. Translational Pediatric. 2021;**10**:2225-2234

[27] Rossier MC, Mivelaz Y, Addor MC, Sekarski N, JanMeijboom E, Vial Y. Evaluation of prenataldiagnosis of congenitalheartdisease in a regionalcontrolled case study. Swiss Medical Weekly. 2014;**144**:w14068

[28] Dolk E, Loane M, Garne E. Congenital heart defects in Europe prevalence and perinatal mortality, 2000 to 2005 European Surveillance of Congenital Anomalies (EUROCAT) working group. Circulation. 2011;**123**: 841-849

[29] Bonnet D. Impacts of prenatal diagnosis of congenital heart diseases on outcomes. Translational Pediatrics. 2021;**10**:2241-2249

[30] Perolo A, Prandstraller D, Ghi T, Gargiulo G, Leone O, Bovicelli L, et al.

Diagnosis and management of fetal cardiac anomalies: 10 years of experience at a single institution. Ultrasound in Obstetrics & Gynecology. 2001;**18**:615-618

[31] Montaguti E, Balducci A, Perolo A, Livi A, Contro E, Casadio P, et al. Prenatal diagnosis of congenital heart defects and voluntary termination of pregnancy. American Journal of Obstetrics & Gynecology MFM. 2020;**2**:100207

[32] Evans W, Acherman R, Restrepo H. Prenatal diagnosis of significant congenital heart disease and elective termination of pregnancy in Nevada. The Journal of Maternal-Fetal & Neonatal Medicine. 2021;**23**:1-6

[33] Gowda M, Thiagarajan M, Satheesh S, Mondal N, Gochhait D, Godipelli L. Prenatal grading of fetalcongenitalheartdisease and itsinfluence on decision making during pregnancy and postata period: A prospective study. The Journal of Maternal-Fetal & Neonatal Medicine. 2020;**3**:1-9

[34] Hilton-Kamm D, Sklansky M, Chang R. How not to tell parentsabouttheirchild's new diagnosis of congenitalheartdisease: An Internet survey of 841 parents. Pediatric Cardiology. 2014;**35**:239-252

[35] Allan L, Huggon IC. Counselling following a diagnosis of congenital Heart disease. Prenatal Diagnostic. 2004;**24**:1136-1143

[36] Fouron JC. The changing and complex relationship between paediatric cardiologists and life. Cardiology in the Young. 2000;**10**:551-556

[37] Hutha JC. Uses and abuses of fetal echocardiography:apediatriccardiolog ist'sview. Journal of American College Cardiology. 1986;**8**:451-458

[38] Squarcia U. Fetaldiagnosis of congenital cardiac malformations—a challenge for physicians as well as parents. Cardiology in the Young. 1996;**6**:256-257

[39] Caniano A, Baylis F. Ethical considerations in prenatal surgical consultation. Pediatric Surgery International. 1999;*15*:*303*-309

[40] Flake AW. Prenatal intervention: Ethical considerations for life-threatening and non-life threatening anomalies. Seminars in Pediatric Surgery. 2001;**10**:212-221

[41] Aite L, Trucchi A, Nahom A, Zaccara A, La Sala E, Bagolan P. Antenatal diagnosis of surgically correctable anomalies: Effects of repeated consultations on parental anxiety. Journal of Perinatology. 2003;**23**:*652*-*654*

[42] Di Giusto M, Lazzari R, Giorgetti T, Paesano R, Pachi A. Psychological aspects of therapeutic abortion after early prenatal diagnosis. Clinical and Experimental Obstetrics & Gynecology. 1991;**18**:169-173

[43] Lorenz R, Kuhn M. Multidisciplinary team counselling for fetal anomalies. American Journal of Obstetrics and Gynecology. 1989;**161**:263-266

[44] Dallaire L, Lortie G, Des Rochers M, Clermont R, Vachon C. Parental reaction and adaptability to the prenatal diagnosis of fetal defect or genetic disease leading to pregnancy interruption. Prenatal Diagnosis. 1995;**15**:249-259

[45] Menahem S, Grimwade J. Pregnancy termination following prenatal diagnosis of serious heart disease in the fetus. Early Human Development. 2003;**73**:71-78

[46] Arya B, Glickstein J, Levasseur S, Williams I. Parents of children with

congenital heart disease prefer more information than cardiologists. Congenital Heart Diseases. 2013

[47] Boughman J, Berg KA, Astemborsky J, Clark E, Mc Carter R, Rubin JD, et al. Familial risks of congenital heart defect assessed in a population-based epidemiologic study. American Journal of Medical Genetetics. 1987;**26**:839

[48] Lin AE, Garver KL. Genetic counseling for congenital heart defects. The Journal of Pediatrics. 1988;**113**:1105

[49] Strauss AW, Johnson MC. The genetic basis of pediatric cardiovascular disease. Semina Perinatology. 1996;**20**(564)

[50] Lewin MB, Glass IA, Power P. Genotype-phenotype correlation in congenital heart disease. Current Opinion in Cardiology. 2004;**19**:221

7

Role of Transthoracic Echocardiography in Visualization of the Coronary Arteries and Assessment of Coronary Flow Reserve

Yasser Baghdady, Hussein Hishmat and Heba Farook
Cairo University
Egypt

1. Introduction

Visualization of the epicardial coronary arteries by echocardiography is technically challenging. The physical nature of ultrasound waves prevents them from delineating the coronary tree because of multiple factors. The resolution of tansthoracic echo using a 2.5-3.5MHz probe is only 2mm while the diameter of the epicardial coronary arteries ranges from 1.5 to 4mm. The epicardial coronaries are relatively superficial in the chest, so the lie in near field of the ultrasound waves. The translational and rotational motion of the coronary arteries in the AV grooves poses a challenge in obtaining stable Doppler signals. The relatively low velocity of coronary flow compared to the flow velocity in the ventricles makes color signals hard to discern. Finally, the tomographic nature of the echocardiographic study makes differentiation between adjacent vessels e.g. the LAD and the diagonal branches extremely difficult. Despite these difficulties, the need for a non-invasive bedside tool that could allow inference of the coronary arteries pushed towards more efforts in using echo for that aspect. Using dedicated high-frequency probes made assessment of the left main coronary, the LAD and even the posterior descending branch of the RCA feasible in a large proportion of patients (Hozumi et al., 1998). Transthoracic and transesophageal echo can provide data regarding coronary patency, the presence of coronary stenosis or coronary ectasia (Iliceto S, et al., 1991, Kozakova M, et al., 1997, Lambertz et al., 2000).

2. Coronary flow and Doppler analysis

Normal antegrade coronary flow is predominant diastolic with a small systolic component (Heinz Lambertz et al., 2004). Systolic flow is less important and is a less stable measure as it can be eve retrograde. It may be difficult to record both diastolic and systolic flow in the same cardiac cycle in all patients, because of cardiac motion that displaces the coronary artery from the ultrasound beam in systole. Diastolic flow is antegrade in both epicardial and intramural vessels, whereas systolic flow is antegrade in epicardial but retrograde in intramural vessels, because blood is squeezed backwards by myocardial contraction (Vernon Anderson H et al., 2000). As a result of the two opposite forces, the magnitude of systolic flow velocity may change along the coronary tree and close to the origin of a

perforator there might be a watershed area with stagnation of systolic flow. Therefore, the epicardial anterograde systolic flow is mainly a capacitance, rather than a nutrient flow, and may not reflect myocardial perfusion.

2.1 The parameters that can be assessed by coronary Doppler imaging include

- Diastolic flow velocity
- Systolic flow velocity
- Diastolic Deceleration time
- Coronary flow reserve

The baseline coronary flow velocity may change from one beat to the other of even 5–10 cm/s. Elevated resting flow velocities may occur in tachycardia, anaemia, hyperthyroidism, severe left ventricular hypertrophy etc (Czernin J er al, 1993, Voci P et al., 2004). Coronary vasodilators increase the diameter of the epicardial artery and reduce baseline flow velocity. Analysis of the coronary Doppler waveform can provide useful information about vessel patency and the presence of severe stenosis or moderate stenosis. Noninvasive Doppler has some alleged advantages over IVUS/FFR. Echocardiography avoids contact with the coronary artery, which may be reactive during myocardial infarction. Echo also measuring velocities in regions inaccessible to IVUS such as the septal perforators. The most important limitation of transthoracic Doppler measurement is the difficulty of obtaining accurate adjustment of the Doppler beam parallel to the coronary flow. If the angle between the Doppler beam and the coronary artery is >60°, diastolic flow velocity could be underestimated.

3. Visualization of different coronary artery segments by Echo-Doppler

3.1 Transthoracic echocardiography

In general, assessment of coronary blood flow differs in different coronary arteries. The LAD blood flow can be assessed by using high frequency transducers due to the proximity of this vessel to the chest wall. However, this technique is not suitable for imaging peripheral RCA flow because of the distance between the transducer and the basal inferior cardiac wall (7-10cm). Therefore a lower frequency transducer is required to overcome the problem of inadequate penetration depth of a high frequency transducer. Individual coronary anatomy shows considerable patient to patient variability. Therefore it is not possible to visualize a segment of the right coronary artery in the posterior interventricular grove in every patient (Lethen H et al., 2003, Meimoun P et al., 2004, 2005, Tokai K et al., 2003, Ueno Y et al., 2002, 2003). Recording an accurate systolic-diastolic pulsed wave Doppler signal is often hampered by respiratory movements and lateral as well as vertical motion of the basal inferior cardiac wall during the cardiac cycle. This problem can partially be resolved by obtaining Doppler signals in apnea.

3.2 LMT and proximal segments of the left and right coronary arteries

The proximal portion of the left coronary artery can be visualized from a modified high parasternal short axis view. First obtain the classic parasternal short axis view at the level of

the aortic valve. Then make slight clockwise rotation and anterior tilt of the transducer to visualize the left main trunk as seen in the figure below.

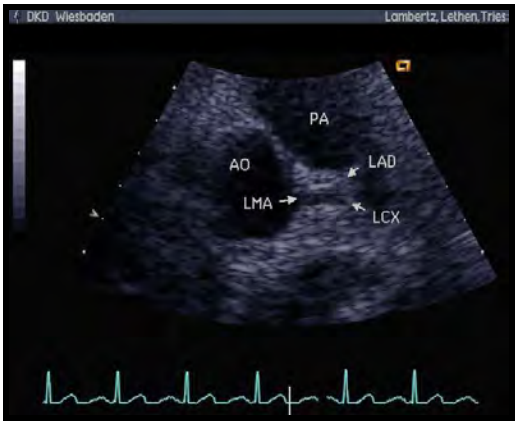

Fig. 1. Parasternal short axis view showing left main stem and its bifurcation into LAD and LCX branches (Heinz Lambertz et al., 2004).

Color Doppler imaging of the coronary flow in the proximal portion of the left coronary artery is technically difficult for two reasons: First, the almost orthogonal alignment of coronary flow to the ultrasound beam and second, the interposition of the right ventricular outflow tract and pulmonary artery. The left main coronary artery can also be imaged from an apical transducer position. From the classical five chamber view, the transducer is carefully angled more anteriorly until the ascending aorta is visualized. With slight tilting and rotation of the transducer, the left and the right coronary arteries can be recorded in one imaging plane: The orifice of the left coronary artery is located approximately three O'clock. The orifice of the RCA can be detected at approximately ten O'clock.

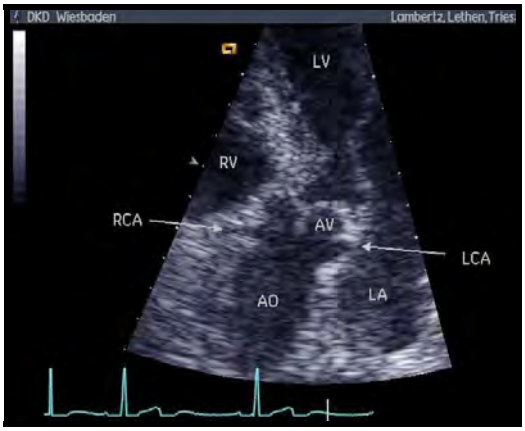

Fig. 2. Modified apical five-chamber view illustrating the origin of the left and right coronary artery from the aortic bulbus (Heinz Lambertz et al., 2004).

3.3 Visualization of the middle segment of the LAD

The middle and distal portion of the left anterior descending artery lies in the anterior ventricular groove close to the anterior chest wall. Due to the proximity of the middle and distal left anterior descending artery to a precordially located transducer, these coronary segments are ideal for transthoracic echocardiographic examination. From the classic parasternal short axis view at the level of the papillary muscles, a lateral displacement of the transducer by 2-3cm allows the visualization of the anterior interventricular groove. With caudal displacement of the transducer of 1-2 intercostal spaces, Color Doppler is used to identify the coronary flow in the anterior groove. Once a predominant diastolic flow signal is detected from a vessel within the anterior interventricular groove, activate the zoom mode while keeping the Doppler box small with adjustment of the velocity range at 12-24cm/s. From the previous view, the transducer is rotated 70 to 90º to obtain the best LAD long axis view. For measurement of the coronary flow velocity, pulsed wave Doppler is used with a sample size of 3mm and care should be taken to avoid an angle exceeding 35 to 45º.

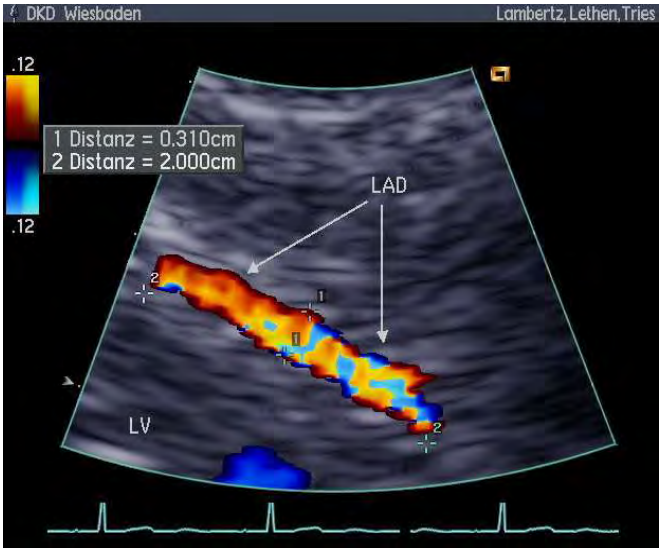

Fig. 3. Modified PLAX view allowing color Doppler assessment of coronary blood flow in the mid segment of the LAD (Heinz Lambertz et al., 2004).

3.4 Visualization of the distal segment of the LAD

The distal part of the left anterior descending artery can be recorded in a modified foreshortened three-chamber view from an apical window. From the conventional apical 2 chamber view the transducer is rotated anti-clockwise to obtain an apical long axis view, showing the left ventricle and left ventricular outflow tract. Using the color Doppler, the distal segment of the LAD, located in the apical part of the interventricular groove can be detected close to the apex of the left ventricle. From this view, the transducer is shifted 1 to 2 intercostal spaces cranially with anterior tilt to visualize the peripheral epicardial segments of the LAD.

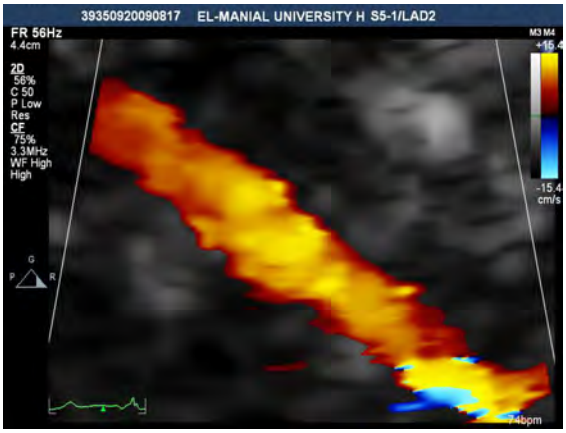

Fig. 4. Modified apical view showing the distal segment of the LAD (H. Farouk, et al., 2010).

3.5 Visualization of the RCA

To visualize the posterior descending branch of the RCA, the left ventricle is first imaged in a conventional apical two-chamber view. From this position, the transducer is slightly rotated anti-clockwise and carefully tilted anteriorly. Using color Doppler, coronary blood flow in the posterior interventricular groove can be identified.

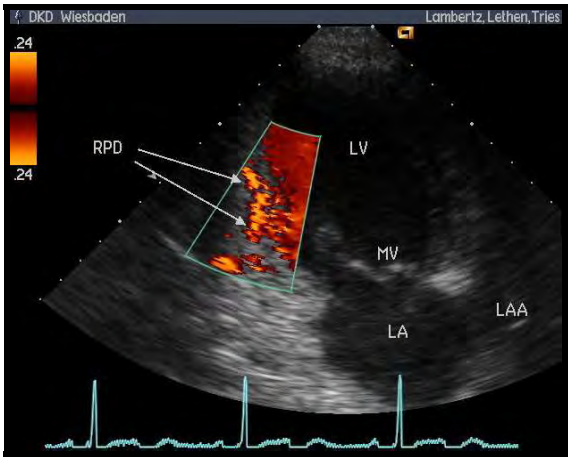

Fig. 5. Modified apical two-chamber view. Color Doppler flow map showing the proximal part of the posterior interventricular branch in the posterior interventricular groove (Heinz Lambertz et al., 2004).

After detection of the characteristic predominant diastolic blood flow in the basal part of the posterior interventricular groove, the sample volume (2.0-3.5mm) is positioned for spectral Doppler analysis of coronary blood flow.

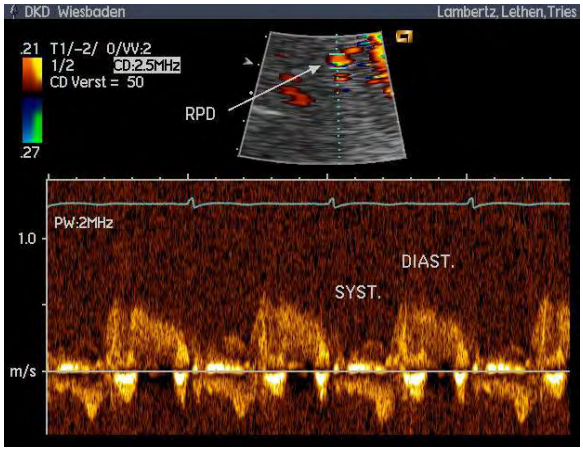

Fig. 6. Characteristic biphasic spectral Doppler recording of coronary blood flow velocity in the distal RCA (Heinz Lambertz et al., 2004).

The modified apical two-chamber view used for assessment of the right coronary artery blood flow allows alignment of the ultrasound beam roughly parallel to the course of the posterior descending artery, thus, unlike assessment of the flow of the left anterior descending artery, provide an adequate registration of the coronary flow velocity.

3.6 Detection of the left circumflex artery by TTE

The proximal third of the LCX can be examined using an apical or parasternal short axis view approach. To assess the distal left circumflex artery, we use the apical 5 chamber view with the transducer is rotated clockwise to direct the imaging plane posteriorly and inferiorly. The direction of the CBF of the circumflex artery is not parallel to the ultrasound beam. Because the success rate in visualizing the flow in the mid and distal circumflex is limited, assessment of the coronary flow reserve is of limited clinical significance in cases of suspected left circumflex artery disease (Heinz Lambertz et al., 2004)

3.7 Detection of the left internal mammary artery

The proximal mammary artery is best visualized from a supraclavicular view using high frequency transducer (8 MHz linear transducer). A patent mammary artery graft is recognized by its typical baseline spectral Doppler flow profile, showing considerably higher diastolic blood flow velocity compared to the other vessels originating in close proximity to the subclavian artery.

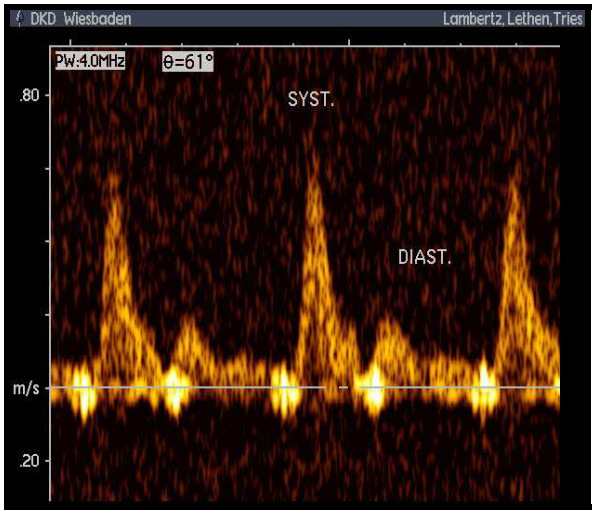

Fig. 7. Pulsed wave Doppler profile of mammary artery. The systolic flow velocity is typically higher than the diastolic (Heinz Lambertz et al., 2004).

3.8 Detection of the septal branches of the LAD by TTE

In immediate proximity of the mid and distal portion of the left anterior descending artery, septal side branches with varying caliber can be seen by color Doppler analysis. Frequently, the vessel course can be followed over a longer distance within the ventricular septum. Diagonal branches or a dominant intermediate branch can't always be clearly differentiated from the left anterior descending artery, as they may have approximately the same diameter and an almost parallel course.

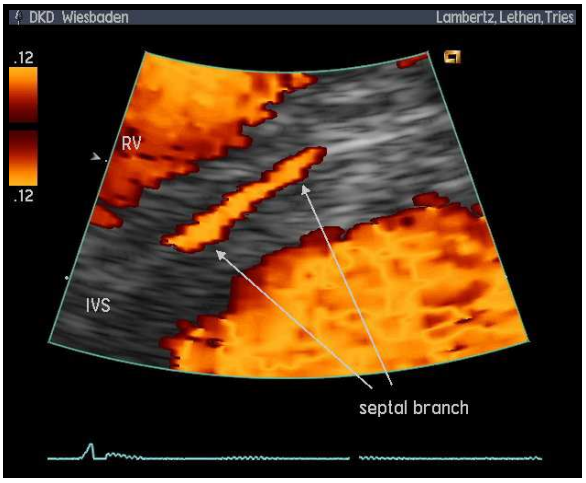

Fig. 8. Parasternal short axis view illustrating a perforator branch in the mid septum (Heinz Lambertz et al., 2004).

3.9 Transesophageal echocardiography

The best way to image the proximal segment of the coronary artery is a transesophageal short axis view at the level of the aortic bulb with a slight anteflexion of the probe. From this view the left main stem and the proximal LAD can be visualized in about 70 to 90% of patients. The success rate in imaging the proximal segment of the left circumflex is even higher (75 to 90%). The best way to visualize the ostuim of the right coronary artery is a sagittal scanning plane showing the ascending aorta in a long axis (Lambertz H et al., 2000). With a slight clockwise rotation of the probe, a short segment of the right coronary artery originating from the aortic bulb can be imaged from the majority of patients.

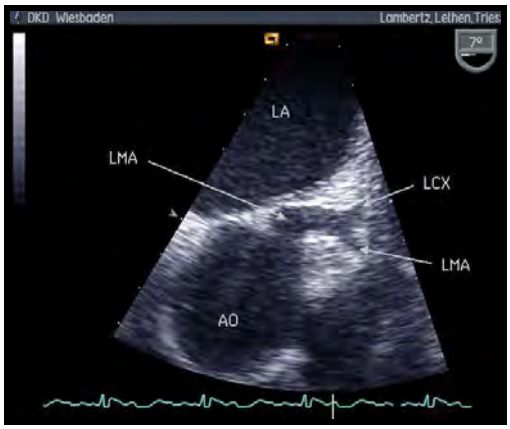

Fig. 9. Transesophageal echocardiography illustrating the left main stem and its bifurcation into LAD and LCX ((Heinz Lambertz et al., 2004).

With a pulsed wave Doppler, sample volume positioned in the proximal portion of the left anterior descending coronary artery, systolic as well as diastolic flow can be recorded (Iliceto S, et al. , 1991)

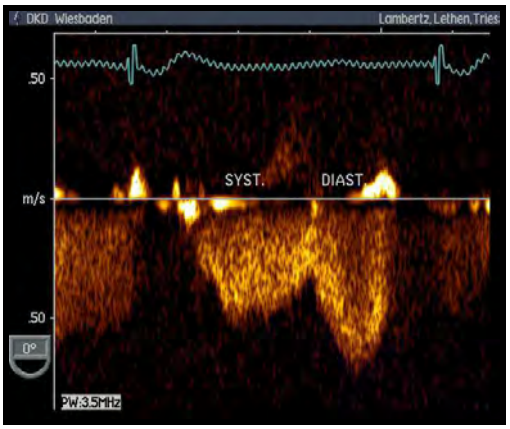

Fig. 10. TEE recording from a normal LAD.CBF occurs systolic-diastolic with the highest velocity during diastole (Heinz Lambertz et al., 2004).

In contrast to the transthoracic approach, TEE imaging allows a reliable Doppler flow analysis in the proximal left anterior descending artery, because the ultrasound beam can be aligned almost parallel to the anatomical course of the vessel. However, due to motion artifacts caused by respiratory excursions and ventricular contraction, adequate recording of the coronary blood flow can be obtained more easily during a short period of apnea.

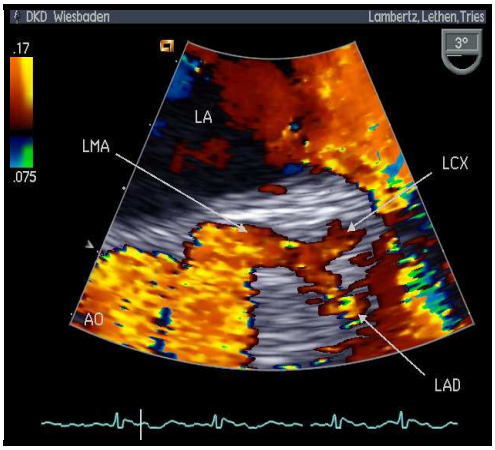

Fig. 11. Color Doppler illustrating normal coronary blood flow within the left main artery and its bifurcation into LAD and LCX (Heinz Lambertz et al., 2004).

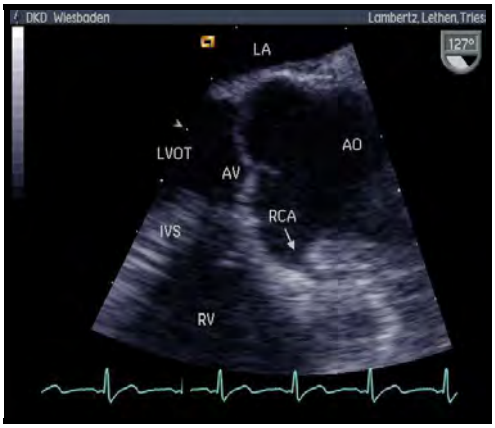

Fig. 12. Orifice of the right coronary artery. The TEE scanning plane is aligned roughly parallel to a long axis of the ascending aorta ((Heinz Lambertz et al., 2004)

Transesophageal echocardiography, with or without contrast, is a low cost method and easily repeatable, which can be used to evaluate coronary circulation in selected patients. However, this approach has less clinical importance in evaluating the hemodynamic relevance of a left anterior descending artery stenosis. This is based on the fact that most of the left anterior descending artery stenoses are located distal to those left anterior descending artery segments that can be visualized by Transesophageal echocardiography.

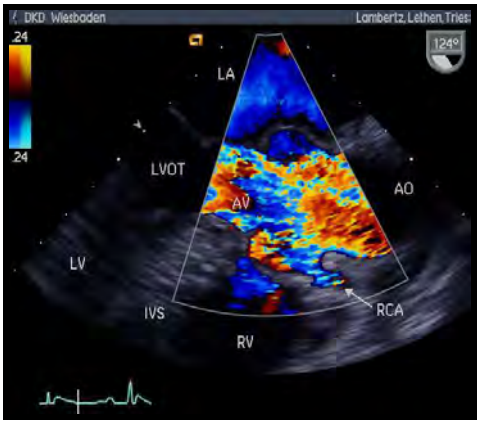

Fig. 13. Visualization of the coronary blood flow in the proximal right coronary artery (Heinz Lambertz et al., 2004).

It has to be taken also into consideration that approximately 20% to 30% of the patients cannot be investigated by Doppler because of respiration, obesity, chest deformity and emphysema, acute changes in cardiac volume, or inadequately stable position of the Doppler signal. Flow in the branches could be erroneously interpreted as the flow in the main trunk. In particular, this could happen for LAD in the two-chamber or in the short axis view, where a long diagonal branch or the first septal perforator might also be visualized.

4. Clinical utilization of echocardiographic coronary imaging

4.1 Coronary artery patency

In the particular situation of acute myocardial infarction, a non-invasive way to visualize the LAD should be of great help to diagnose the success of reperfusion. In this setting, the sensitivity, specificity, positive predictive value, negative predictive value and accuracy of the transthoracic echo Doppler in the noninvasive assessment of the LAD reperfusion with 2.5MHz transducer were 81.6%, 64%, 90.7%, 54% and 78% respectively (H. Farouk et al., 2010). Detection of the distal LAD flow by TTDE was significantly correlated with the reperfusion as assessed by coronary angiography.

Epicardial coronary flow is not always synonymous with cellular myocardial perfusion as seen in the no-reflow phenomenon. Visualization of septal perforator flow can be a more reliable marker of reperfusion. Voci et al (Voci P et al., 2004) considered a myocardial segment to be reperfused when at least two of the predicted four to five perforators could be visualized by transthoracic echo after acute MI. A recanalization score (RS) of 1 to 4 was used—where 1 = LAD closed, no perforators; 2 = LAD open, no perforators; 3 = LAD open, 1 to 2 segments with perforators; 4 = LAD open, 3 to 4 segments with perforators. RS discriminated recovery of ventricular function better than TIMI flow. The RS was the best single multivariate predictor ($p < 0.0001$) of percent changes in wall motion score index and the ejection fraction.

Antti Saraste et al, (Saraste M et al., 2005) found that diastolic deceleration time of the LAD flow velocity correlated with myocardial fluorodeoxyglucose uptake in the LAD territory.

Diastolic deceleration time was markedly longer in patients with viable myocardium than partially viable or non-viable myocardium. A DDT <190ms is always associated with non-viable myocardium. However, this finding was not consistent among different studies.

4.2 Coronary artery occlusion

Coronary flow can be measured by transthoracic coronary Doppler ultrasound in occluded coronary arteries receiving collateral flow. Reverse diastolic flow at rest, reflecting retrograde filling of the artery by collaterals, is a very specific marker of coronary occlusion but it unfortunately has a low sensitivity, since collaterals may perfuse the vessel either retrogradely or anterogradely.

4.3 Severe coronary stenosis

Coronary artery stenosis could be identified with color Doppler as local spot of turbulence. An abnormal maximal-to-prestenotic blood flow velocity ratio greater than 2.0 would signify a critical stenosis. These findings have an overall sensitivity of 82% and specificity of 92%. The sensitivity and specificity were, respectively, 73% and 92% for left anterior descending coronary artery, 63% and 96% for right coronary artery, and 38% and 99% for left circumflex coronary artery stenoses. For left main coronary stenosis, echo showed a 92% sensitivity and 62% specificity to identify IVUS significant (MLA < 6 mm2) left main stenosis if taking a peak diastolic velocity cut off of 112 cm/sec (Gerkens U, et al. , 1989, Samdarshi TE et al.,1990)

4.4 Moderate coronary stenosis

The assessment of moderate-severity coronary stenosis by angiography has limitations related to the "lumenographic "nature of angiography (Topol EJ, et al., 1995). The concept of coronary flow reserve performed by Doppler intracoronary wire during coronary angiography can be also performed by echocardiography. The major advantages of coronary flow assessment by TTDE are that it is completely non-invasive, relatively inexpensive, and gives objective and accurate information on the physiological significance both in epicardial native coronary stenosis as well as in detecting coronary restenosis following coronary percutaneous interventions (Caiati C et al., 1999, 1999, Hozumi T et al., 1998). Another important value of TTDE study of CFVR is the assessment of microvascular coronary circulation.

4.5 Coronary flow reserve

Coronary flow reserve is defined as the maximal increase in coronary blood flow (by using a strong coronary vasodilator) above its basal level for a given perfusion pressure. So, it is a ratio of maximal (stimulated) to baseline (resting) coronary blood flow. The best sampling site of the coronary flow, for assessing the functional significance of a stenosis, is the distal tract of the vessel which could be easily obtained with TDE. Proximal to the stenosis CFR may be normal as there are side branches between the sampling site and the stenosis, which reflects perfusion in normal territories (Voci P et al., 2004). The angle correction is redundant given that CFR is the ratio between hyperemic and baseline flow velocity, and it is not affected by the actual flow velocity. However, the angle has to be kept as small as possible. Blood flow velocity measurements are performed offline by contouring the spectral Doppler signals, using the integrated software package of the ultrasound system. Final values of flow velocity represent

an average of three cardiac cycles. TDE-CFR is defined as hyperemic diastolic mean (or peak) flow velocity divided by baseline flow velocity. It is important to underscore that during administration of the vasodilating agent, the transducer probe is in the same position as baseline, and machine settings including size of sample volume and velocity scale are not changed. The mean time required to complete a CFR test is around 10–15 min.

Adenosine is the most commonly used vasodilator to assess TDE-CFR. It is a potent vasodilator producing maximal coronary vasodilatation within 40-50 seconds. Given its short half life (10s) and rapid onset of action, it allows CFR measurements more rapidly than other vasodilators. Furthermore, Adenosine acts mainly at the level of the microcirculation and does not alter significantly the diameter of the coronary artery. Adenosine is administered intravenously (0.140 mg/kg/min) for 5 minutes (Lapeyre AC III et al., 2004, Sudhir K et al., 1993, Verani MS, 1991, Wilson R et al., 1990). The normal range of CFVR for both men and women is ≥ 2.7. The cut-off value of 2 of CFR for detecting significant epicardial coronary stenosis or to predict ischemia in the underlying territory has been demonstrated in various studies (Kern MJ et al., 1996, Matsumara Y et al., 2003).

The feasibility of TDE-CFR for LAD artery is very high, with more than 90% in experienced hands, and nearly 100% with the use of intravenous contrast agents (Caiati C et al., 1999). The feasibility is less in the PDA artery, between 54 and 86% due to technical limitations (Hozumi T et al., 1998, Lethen H et al., 2003, Ueno Y et al., 2002). The measurements of TDE-CFR, in the LAD as in the PDA arteries, are closely correlated with invasive measurements using a Doppler flow wire. The feasibility of TDE-CFR in the circumflex artery is more challenging given the particular anatomy of this artery and the poor resolution of the lateral wall.

4.6 Kawasaki disease and congenital coronary anomalies

In the pediatric population, visualization of the proximal portions of the left and the right coronaries by transthoracic echo is achievable in almost all cases. Therefore, it is routine to comment on the origin and the course of the proximal left and right coronary arteries in all pediatric studies. The aneurysms of the proximal RCA and proximal LAD in Kawasaki disease provide the diagnosis in infants with febrile illness and the classic rash and can be useful in follow up of this condition (Satomi G et al., 1984, Yoshikawa J et al., 1979). Also, failure of visualization of one of the coronary arteries in children with cardiomyopathy should prompt excluding the diagnosis of anomalous origin of the coronary from the pulmonary artery. Also anomalous origin of the right coronary from the left sinus of valsalva which poses a threat of sudden cardiac death can be readily diagnosed in children by transthoracic echo.

5. Conclusion

Echocardiography can be used to visualize the epicardial coronary arteries directly in a large proportion of patients. The success is greatest in children, ostia of the left and right coronary arteries and in the LAD. However, it is unlikely, at least in the near future, that echo can provide complete anatomical assessment of the coronary tree. X-ray bases modalities, namely angiography and CT are still superior in providing anatomical details. Nevertheless, in some clinical situations, echo can provide very useful data regarding coronary patency, severe stenosis, moderate coronary lesions, the state of the microcirculation and congenital coronary anomalies.

6. References

Caiati C, Montaldo C, Zedda N, Bina A, Iliceto S. A new noninvasive method for coronary flow reserve assessment: contrast-enhanced transthoracic second harmonic echo Doppler. Circulation 1999; 99: 771–778.

Caiati C, Montaldo C, Zedda N, Montisci R, Ruscazio M, Lai G et al. Validation of a non-invasive method (contrast enhanced transthoracic second harmonic echo Doppler) for the evaluation of coronary flow reserve: comparison with intracoronary Doppler flow wire. J Am Coll Cardiol 1999;34:1193 – 200.

Caiati C, Zedda N, Montaldo C, Montisci R, Iliceto S. Contrast-enhanced transthroacic second harmonic echoDoppler with adenosine. A noninvasive, rapid and effective method for coronary flow reserve assessment. JACC 1999; 34:122–130

Czernin J, Muller P, Chan S, Brunken RC, Porenta G, Krivokapitch J et al. Influence of age and hemodynamics on myocardial blood flow and flow reserve. Circulation 1993;88:62 – 9.

Gerkens U, et al. detection of proximal coronary artery stenosis by transesophageal echocardiography. Eur Heart J. 1989; 10:121

Heba F. Saleh, Hussien Heshmat, Y.Baghdady, K. Sorour. Faculty of medicine, Cairo University.

Heinz Lambertz, Hans-Peter Tries, Harald Lethen. Coronary flow reserve: a practical echocardiographic approach. Second edition. 2004.

Hozumi T, Yoshida K, Akasaka T et al. Noninvasive assessment of coronary flow velocity and coronary flow velocity reserve in the left anterior descending coronary artery by Doppler echocardiography: comparison with invasive technique. J Am Coll Cardiol 1998; 32: 1251–1259.

Hozumi T, Yoshida K, Akasaka T et al. Noninvasive assessment of coronary flow velocity and coronary flow velocity reserve in the left anterior descending coronary artery by Doppler echocardiography: comparison with invasive technique. J Am Coll Cardiol 1998; 32: 1251–1259.

Iliceto S. Transesophageal Doppler echocardiography evaluation of coronary flow velocity in baseline conditions and during dipyridamole-induced coronary vasodilation. Circulation 83:61-69, 1991.

Kern MJ, Bach RG, Mechem CJ, et al. Variations in normal coronary vasodilatory reserve stratified by artery, gender, heart transplantation and coronary artery disease. J Am Coll Cardiol. 1996;28:1154-1160.

Kozakova M. Mechanisms of coronary flow impairments in human hypertension. Hypertension 29:551-559, 1997.

Lambertz H, Lethen H. Lehratlas der transősophagealen Echokardiographie, 2000; Thieme Verlag Stuttgart, New York 1-273.

Lapeyre AC III, Goraya TY, Johnston DL, Gibbons RJ. The impact of caffeine on vasodilator stress perfusion studies. J Nucl Cardiol. 2004;11:506–511.

Lethen H, Tries HP, Kersting S, Lambertz H. Validation of noninvasive assessment of coronary flow velocity reserve in the right coronary artery: a comparison of transthoracic echocardiographic results with intracoronary Doppler flow wire measurements. Eur Heart J 2003;24:1567 – 75.

Matsumara Y, Hozumi T, Watanabe H, Fujimoto K, Sugioka K, Takemoto Y et al. Cut-off value of coronary flow velocity reserve by transthoracic Doppler echocardiography for diagnosis of significant left anterior descending artery stenosis in patients with coronary risk factors. Am J Cardiol 2003;92:1389 – 93.

Meimoun P, Benali T, Sayah S, Luycx-Bore A, Boulanger J, Zemir H et al. Evaluation of left anterior descending coronary artery stenosis of intermediate severity using transthoracic coronary flow reserve and dobutamine stress echocardiography. J Am Soc Echocardiogr 2005;12:1233 – 40.

Meimoun P, Sayah S, Maitre B, Luycx-Bore A, Benali T, Beausoleil M et al. Measurement of coronary flow reserve with transthoracic echocardiography: an old concept, a new tool, a lot of applications. Ann Cardiol Angiol 2004;53:325 – 34.

Samdarshi TE et al. Transesophageal color Doppler echocardiography in assessing proximal coronary artery stenosis. J Am Coll Cardiol. 1990; 15:93

Saraste M, Vesalainen RK, Ylitalo A, Saraste A, Koskenvuo JW, Toikka JO, Vaittinen MA, Hartiala JJ, Airaksinen KE: Transthoracic Doppler echocardiography as a noninvasive tool to assess coronary artery stenoses-a comparison with quantitative coronary angiography. J Am Soc Echocardiogr 2005, 18:679-85.

Satomi G, Nakamura K, Narai S, et al. Systematic visualization of coronary arteries by two-dimensional echocardiography in children and infants: evaluation in Kawasaki's disease and coronary arteriovenous fistulas. Am Heart J 107:497-505, 1984.

Sudhir K, MacGregor JS, Barbant SD, Foster E, Fitzgerald PJ, Chaterjee Ket al. Assessment of coronary conductance and resistance vessel reactivity in response to nitroglycerin, ergonovine, and adenosine: in vivo studies with simultaneous intravascular two-dimensional and Doppler ultrasound. J Am Coll Cardiol 1993;21:1261 – 8.

Tokai K, Watanabe H, Hirata K, Otsuka R, Muro T, Yamagishi H et al. Noninvasive assessment of myocardial ischemia in the left ventricular inferior regions by coronary flow reserve measurement using transthoracic Doppler echocardiography. J Am Soc Echocardiogr 2003;16:1252 – 7.

Topol EJ, Nissen SE. Our preoccupation with coronary luminology. The dissociation between clinical and angiographic findings in ischemic heart disease. Circulation 1995; 92: 2333–2342.

Ueno Y, Nakamura Y, Kinoshita M, Fujita T, Sakamoto T, Okamura H. Noninvasive assessment of significant right coronary artery stenosis based on coronary flow velocity reserve in the right coronary artery by transthoracic Doppler echocardiography. Echocardiography 2003;20:495 – 501.

Ueno Y, Nakamura Y, Takashima H, Kinoshita M, Soma A. Noninvasive assessment of coronary flow velocity and coronary flow velocity reserve in the right coronary artery by transthoracic Doppler echocardiography: comparison with intracoronary Doppler guidewire. J Am Soc Echocardiogr 2002;15:1074 – 9.

Verani MS. Adenosine thallium-201 myocardial perfusion scintigraphy. Am Heart J. 1991;122:269–278.

Vernon Anderson H, Stockes MJ, Leon M, Abu-Hawala SA, Stuart Y, Kireeide RL. Coronary artery flow velocity is related to lumen area and regional left ventricular mass. Circulation 2000;102:48 – 54.89.

Voci P, Pizzuto F, Romeo F. Coronary flow: a new asset for the echo lab? Eur Heart J 2004;25:1867–79.

Wilson R, Wyche K, Christensen BV, Zimmer S, Laxson DD. Effects of adenosine on human coronary arterial circulation. Circulation 1990;82: 1595 – 606.

Yoshikawa J, Yanagihara K, Owaki T, et al. Cross-sectional echocardiographic diagnosis of coronary artery aneurysms in patients with mucoucutaneous lymph node syndrome. Circulation 59:133-9, 1979.

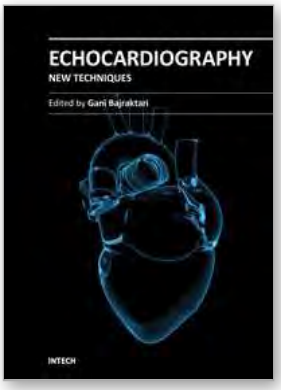

Echocardiography - New Techniques

Edited by Prof. Gani Bajraktari

ISBN 978-953-307-762-8
Hard cover, 218 pages
Publisher InTech
Published online 18, January, 2012
Published in print edition January, 2012

The book "Echocardiography - New Techniques" brings worldwide contributions from highly acclaimed clinical and imaging science investigators, and representatives from academic medical centers. Each chapter is designed and written to be accessible to those with a basic knowledge of echocardiography. Additionally, the chapters are meant to be stimulating and educational to the experts and investigators in the field of echocardiography. This book is aimed primarily at cardiology fellows on their basic echocardiography rotation, fellows in general internal medicine, radiology and emergency medicine, and experts in the arena of echocardiography. Over the last few decades, the rate of technological advancements has developed dramatically, resulting in new techniques and improved echocardiographic imaging. The authors of this book focused on presenting the most advanced techniques useful in today's research and in daily clinical practice. These advanced techniques are utilized in the detection of different cardiac pathologies in patients, in contributing to their clinical decision, as well as follow-up and outcome predictions. In addition to the advanced techniques covered, this book expounds upon several special pathologies with respect to the functions of echocardiography.

InTech Europe
University Campus STeP Ri
Slavka Krautzeka 83/A
51000 Rijeka, Croatia
Phone: +385 (51) 770 447
Fax: +385 (51) 686 166
www.intechopen.com

InTech China
Unit 405, Office Block, Hotel Equatorial Shanghai
No.65, Yan An Road (West), Shanghai, 200040, China
中国上海市延安西路65号上海国际贵都大饭店办公楼405单元
Phone: +86-21-62489820
Fax: +86-21-62489821

8

3D Myocardial Contrast Echocardiography

Katsuomi Iwakura
Division of Cardiology, Sakurabashi Watanabe Hospital
Japan

1. Introduction

Early restoration of coronary perfusion is the most important objective in the management of ST-segment elevation myocardial infarction (STEMI), and primary percutaneous coronary intervention (PCI) is established as the most effective strategy for it. Advances in interventional techniques and pharmacological therapy have made it possible to achieve Thrombolysis in Myocardial Infarction (TIMI) grade 3 flow in as many as 95% of patients undergoing primary PCI. Nevertheless, optimal myocardial perfusion is not achieved in approximately 15% of patients despite of successful opening of infarct-related artery. The inadequate myocardial perfusion, or "no-reflow" phenomenon, may be caused by microvascular damage after myocardial ischemia, distal coronary emboli resulting from thrombus, platelets and atheroma, in situ thrombosis, vasospasm, or cell necrosis and regional inflammatory responses induced by reperfusion. The no-reflow phenomenon is associated with worse functional and clinical outcomes after STEMI. It was linked to larger infarction size, lower ejection fraction, ventricular arrhythmias(Aiello *et al.*,1995), early congestive heart failure(Ito *et al.*,1996), and even cardiac rupture(Morishima *et al.*,1995). It may have an adverse effect on left ventricular (LV) remodeling(Gerber *et al.*,2000). Therefore, detection of no-reflow early after primary `PCI is important for the risk stratification of patients with STEMI. Several invasive and non-invasive imaging modalities have been developed to detect no-reflow. We had focused on one of these modalities, myocardial contrast echocardiography (MCE), and used it in several clinical studies to investigate the pathogenesis of the no-reflow. In this article, we investigated the ability of newly developed, real-time 3D MCE to assess the microvascular dysfunction in patients with AMI.

2. Imaging modalities for assessment of the no-reflow phenomenon

No-reflow can be assessed during PCI with Thrombolysis In Myocardial Infarction (TIMI) flow grade(TIMI Study Group,1985), with TIMI-myocardial perfusion grade(van 't Hof *et al.*,1998) (TMPG), or with coronary flow velocity pattern assessed by Doppler guidewire(Iwakura *et al.*,1996). It can be better quantified by noninvasive imaging techniques, such as myocardial contrast echocardiography (MCE), cardiac CT, and contrast-enhanced cardiac magnetic resonance (CMR).

2.1 CMR and contrast-enhanced CT

CMR using gadolinium can diagnose the no-reflow as: 1) lack of gadolinium enhancement during first pass (microvascular obstruction); and 2) lack of gadolinium enhancement within a

necrotic region, identified by late gadolinium hyperenhancement (Albert *et al.*,2006) (Ingkanisorn *et al.*,2004). There is a good correlation between gadolinium enhancement during first pass and TMPG, thus suggesting that these two parameters might reflect the microvascular integrity within the infarct zone (Porto *et al.*,2007). There is a significant correlation between area of microvascular obstruction and that of hyperenhancement on CMR (Lund *et al.*,2004). Presence of substantial microvascular obstruction on CMR also predicts LV remodeling (Gerber *et al.*,2000) (Hombach *et al.*,2005) and major adverse cardiac events (Hombach *et al.*,2005). Contrast enhanced multi-detector CT also delineates infarct zone as hyperenhancement area. Transmural hyperenhancement was observed immediately after successful PCI, and its area was correlated with non-viable area assessed by dobutamine stress echocardiography (Habis *et al.*,2007). Thus, hyperenhancement observed early after PCI on contrast enhanced CT could be associated with the no-reflow phenomenon.

2.2 Myocardial contrast echocardiography (MCE)

MCE uses ultrasonic contrast agent containing microbubbles which are strong scatters in an ultrasonic field and send compression and rarefaction waves back to the scanner. MCE has been proven useful in evaluating patients with AMI receiving reperfusion therapy. Ito et al. examined myocardial microvascular perfusion with MCE in patients with AMI, and found that some patients showed a lack of contrast enhancement (no-reflow) after successful PCI(Ito *et al.*,1992). Their finding is the first clinical report of the no-reflow phenomenon in patients with AMI. They demonstrated patients with substantial no-reflow have poor functional and clinical outcomes after AMI (Ito *et al.*,1996). They performed MCE using intracoronary injection of fragile microbubbles through catheter. The no-reflow phenomenon was also observed by MCE with intravenous administration of stable microbubbles, which is capable of passing through pulmonary circulation and into coronary microcirculation (Porter *et al.*,1998). These studies indicated that no-reflow phenomenon is observed in 25-40% of patients receiving successful primary PCI resulting into TIMI-3 flow grade. The substantial myocardial contrast defect on MCE predicts poor recovery of contractile function (Ito *et al.*,1992)(Balcells *et al.*,2003) and is associated with both death and recurrent infarction on the later stage (Dwivedi *et al.*,2007). Multicenter studies have recently demonstrated that the extent of microvascular damage, assessed on day 1 after reperfusion therapy in AMI, is the most powerful independent predictor of development of LV remodeling (Galiuto *et al.*,2008).

Accumulating study results proved the usefulness of MCE as a clinical tool for evaluating myocardial perfusion, though no contrast agent is approved for this indication currently. MCE has its pros and cons comparing to other imaging modalities such as CMR (Table 1).

	CMR	**MCE**
Contrast Agent	Gadomium	Microbubbles
Resolution	High Spatial Resolution	High Temporal Resolution
Image quality	Good in almost all cases	Sometimes inappropriate
Reproducibility	Excellent	Moderate
Acquisition	About 30 minutes	Real-time
Image mode	2D/3D	2D
Measurement	Area/Volume	Area
Operation	In MRI lab	Bedside / in cath-lab

Table 1. Characteritics of CMR and MCE

MCE is a very easy method not requiring a large apparatus, and it can be performed not only in the echo-lab but also in bed side or in the cath-lab. MCE is a suitable imaging modality for assessing myocardial perfusion soon after PCI. On the other hand, interpretation of MCE depends on the quality of obtained images and it could be difficult to obtain reliable images in some cases. Quantification of contrast enhancement on MCE is possible but is still difficult and requires complicated techniques. Even the subjective evaluation of myocardial perfusion is difficult in some cases because of attenuation, lung and rib shadowing, apical bubble distraction by ultrasound.

2.3 Potential of real-time 3D-MCE

3D-image reconstruction is the other advantage of CMR over MCE. Precise assessment of myocardial perfusion in a whole LV can be achieved by 3D-imaging. 2D-MCE observes myocardial opacification only on very limited slices, and assessment of contrast defect could be insufficient. Most of myocardial wall thickening is determined by contractile function of the subendocardial layer (Hashimoto *et al.*,2003), and recovery of contractility after AMI mostly depends on the viability of the subendocardial layer (Garot *et al.*,2000). Ischemic myocardial injury progress from endocardial- to epicardial layers (wavefront phenomenon), and subendocardium is the most vulnerable layer to ischemic insults (Grattan *et al.*,1986). Assessment of subendocardial perfusion is important for prediction of contratile function after AMI. 2D-MCE has only limited ability to visualize subendocardial perfusion.

3D- echocardiography visualizes the whole LV, and it is superior to 2D-echocardiography in assessment of regional wall motion abnormalities (Corsi *et al.*,2005). It also visualizes endocardial surface structure within a beating heart (Inoue *et al.*,2006). In the next chapter, we investigated whether real-time 3D-MCE could assess subendocardial perfusion in patients with AMI undergoing primary PCI , and compared its perfusion patterns to those obtained with 2D-MCE (Iwakura *et al.*,2007). We also compared the ability of these two modalities to assess infarct size and to predict functional recovery.

3. Assessment of subendocardial perfusion by real-time 3D-MCE

3.1 Study population and protocol

Between October 2004 and December 2005, consecutive 68 patients with AMI underwent primary PCI within 24 hours after symptom onset, and subsequently underwent intracoronary 2D- and 3D-MCE study. The diagnosis of AMI was based on the chest pain prolonged ≥ 30 minutes, ST segment elevation of ≥ 2 mm in at least two contiguous electrocardiograph leads, and greater than 3 fold increase in serum creatine kinase (CK) levels. Seven patients were excluded because of poor echocardiograph images, including 2 patients in whom 2D-MCE was adequate but 3D-MCE was suboptimal. We excluded 14 patients who did not undergo follow-up left ventriculography (LVG) study. Therefore, the final study population consisted of 47 patients.

After the admission, we performed echocardiography examination with SONOS 7500 (Philips Medical Systems), and defined the risk area as myocardial segments showing dyskinesia, akinesia or severe hypokinesia. After aspirin (243 mg) and intravenous heparin

(100 U/kg) administration, we performed coronary angiography (CAG) using the right femoral approach. We determined the culprit lesion and performed primary PCI to achieve the residual diameter stenosis < 25 %. After the PCI procedure, we assessed TMPG on CAG from the view chosen to minimize superimposition of non-infarcted territories(Gibson *et al.*,2000).

A mean of 15 minutes after the last PCI procedure, we performed 2D-MCE with SONOS 7500 using a S4 transducer. We made microbubbles of a mean size of 12 μm by sonicating iodinated contrast medium, Ioxagate (Hexabrix-320, Tanabe), using an ultrasonic homogenizer with a sterilized tip (Figure 1). We injected 2 mL of sonicated medium into the right coronary artery in patients with inferior wall AMI and into the left coronary artery in those with anterior or posterior wall AMI. We recorded 2D-echocardiogram from the apical two- or four-chamber view. Then, we performed real time 3D-MCE using Live 3D system without ECG gating. We observed 3D images from apical 2- or 4-chamber view with an X4 matrix array transducer on second harmonic mode. We adjusted time-gain compensation and lateral gain control carefully to obtain clear view of endocardial surface. Then, we injected microbubbles into culprit coronary artery again, and recorded a 3D-MCE image for 20 heartbeats. All MCE images were digitally stored for the further analysis.

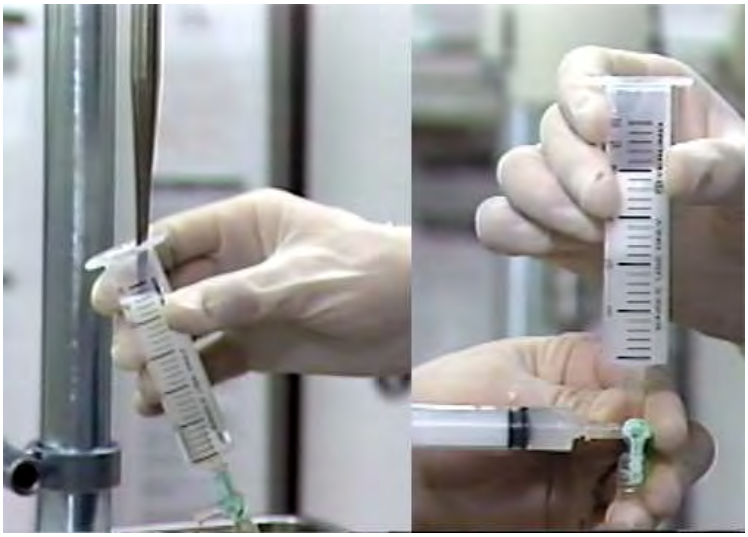

Fig. 1. Sonification of contrast medium to make microbubbles for MCE

We performed LVG in 42 patients (89.4%) following MCE study, and measured left ventricular end-diastolic and end-systolic volume index (LVEDVI and LVESVI, mL/m^2) and LV ejection fraction (LVEF, %) by the biapical Simpson's rule. Regional wall motion (RWM, SD/chord) within the culprit artery territory was analyzed using the centerline method. Follow-up coronary angiography and LVG were performed in all patients at a mean of 4.6±2.7 months later.

An experienced echocardiographer analyzed 2D-MCE images to determine myocardial perfusion within the risk area. We used the apical long-axis view or apical 4-chamber view

for the patients with anterior wall AMI and posterior wall AMI and the apical 2-chamber view for the patients with inferior wall AMI. We divided LV wall into myocardial segments based on 16-segment model endorsed by American Society of Echocardiography(Cerqueira *et al.*,2002), and scored myocardial opacification in each segment as 1 (homogenous opacification), 0.5 (patchy opacification or opacification only in epicardium), or 0 (no opacification)(Ragosta *et al.*,1994). We calculated the averaged contrast score by dividing the sum of contrast scores in the segments within risk area by the number of these segments. We graded myocardial perfusion in each patient as good- (the averaged score = 1), poor- (0.5 ≤ score <1.0) and no-reflow (score <0.5).

A sonographer blinded to 2D-MCE data assessed subendocardial contrast opacification on end-systolic 3D-MCE images. For assessing the risk area and myocardial perfusion, we used the echo windows to include the whole risk area within 3D echocardiograph image. We observed myocardial opacification from LV cavity side. The "shade" mode was activated to reduce the effect of opacification from the epicardial layers. If necessary, some parts of the LV were cropped to obtain clear image of endocardial surface (Figure 2). Risk area was defined as myocardium showing no contraction of endocardial surface. We divided whole LV into myocardial segments corresponding to those of 16-segment model in 2D-echocardiogram(Kapetanakis *et al.*,2005), and scored endocardial opacification within each segment as 1 (enhancement as good as that within nearby normal segment), 0.5 (enhancement was observed but not as strong as that within the normal area), or 0 (no clear enhancement). We calculated the averaged endocardial contrast score in the segments within the risk area. We graded myocardial opacification in endocardium (MOE) into 3 groups; good- (the averaged score = 1), poor- (0.5 ≤ score <1.0) and no-MOE (score <0.5).

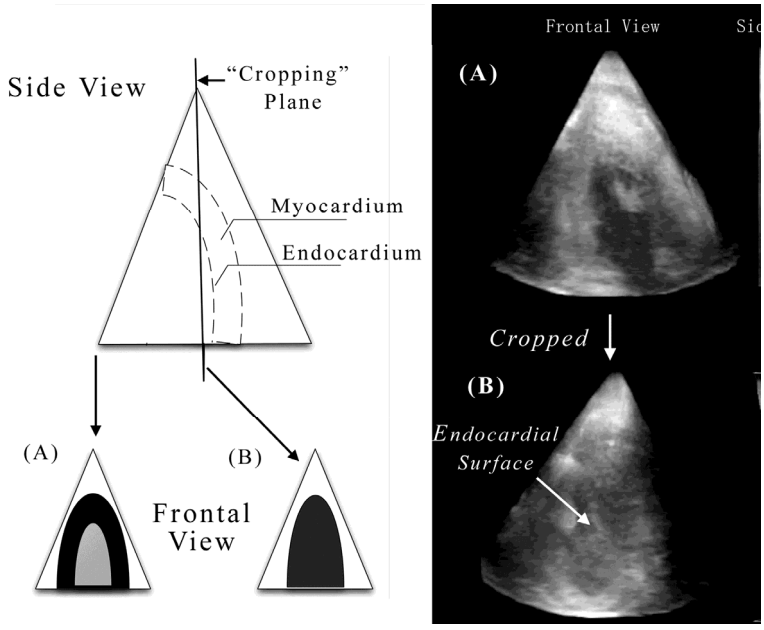

Fig. 2. Cropping of 3D-MCE images to reveal endocardial surface

All data are expressed as mean ± SD. We made comparisons by one-way ANOVA for continuous variables, and significance of difference was calculated with Tukey's HSD test for factor analysis. Categorical variables were compared with the Fisher's exact test. The differences in the changes of RWM from the initial- to the follow-up LVG study among the groups were analyzed with multivariate analysis of variance (MANOVA). Differences were considered significant at $P < 0.05$ (two-sided).

3.2 Patient characteristics

The mean age of the 47 study patients was 61±11 years (range 40 to 81 years), and 38 patients (80.9%) were male. The culprit artery was the left anterior descending artery in 28 patients, the left circumflex artery in 6 patients and the right coronary artery in 13 patients. Multivessel disease was observed in 12 patients. The mean time from the symptom onset to coronary reperfusion was 12.3 ± 14.2 hours. The peak CK and CK-MB level was 3069±2490 IU/L and 235±185 IU/L, respectively.

3.3 Representative cases of 3D-MCE

Figures 3 shows 2D- and 3D-MCE images in a patient with inferior wall AMI. 2D-MCE (upper left) showed good-reflow within the risk area (between arrows). On 3D-echocardiograph before injection, endocardial surface of area at risk was revealed through cropping (lower left). After microbubble injection, contrast enhancement was observed within the risk area, and we judged this case as good-MOE. Peak CK and CK-MB of this case were 1977 IU/L and 118 IU/L, respectively.

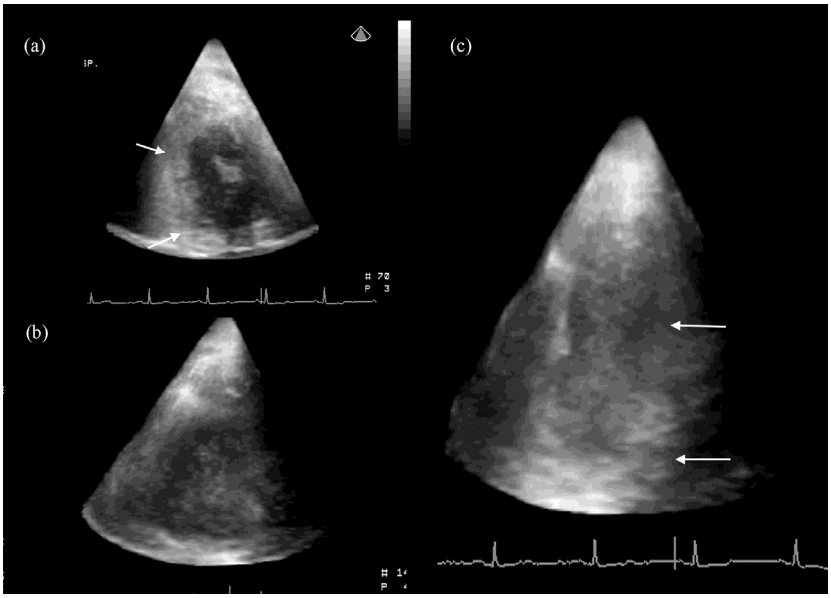

Fig. 3. A representative case showing good-reflow on 2D-MCE (a) and good-MOE on 3D-MCE (c).

Figure 4 showed MCE images in a patient with posterior wall AMI. 2D-MCE (upper left) showed good-reflow within the risk area (between arrows). 3D-MCE (right) showed almost no endocardial contrast enhancement (no-MOE) within the risk area (between arrows). A good contrast enhancement was observed in the normal myocardium around the risk are (Compare it to the 3D-image before contrast injection, on lower left). Peak CK and CK-MB of this case were 4758 IU/L and 414 IU/L, respectively.

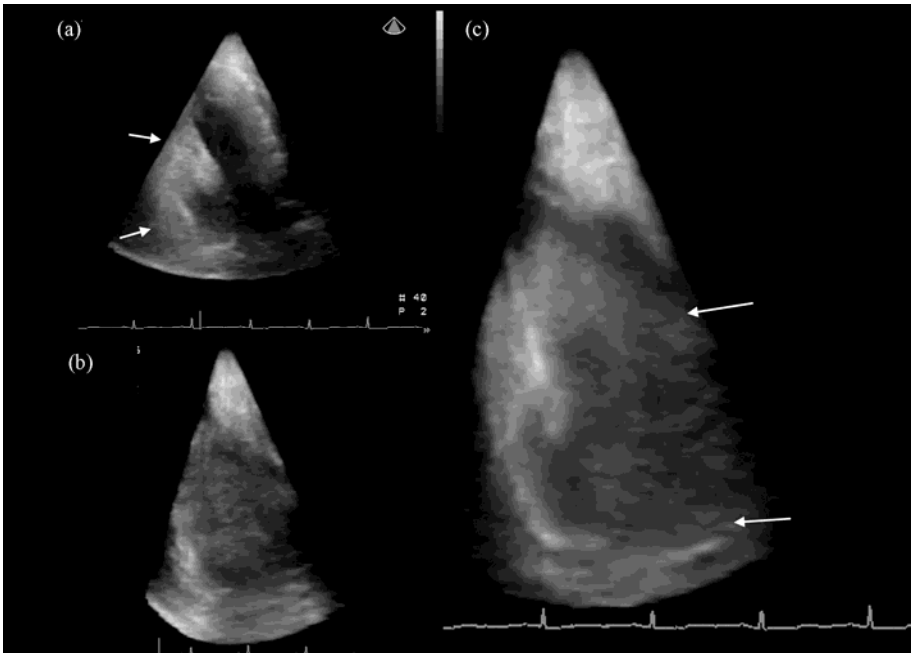

Fig. 4. A case with posterior AMI showing good-reflow on 2D-MCE (a) but no-MOE on 3D-MCE (c).

Figure 5 showed interesting images obtained in other case with anterior wall AMI. Good opacification was observed on endocardial surface of septum on 3D-MCE at 790msec after injection of microbubbles (b). Then, a jet of contrast medium was observed to flow out directly from the apical myocardium (arrow) at 2220 msec (c) and 2990 msec (d) after injection ((e) and (f) are zoomed images of (c) and (d)). These images demonstrated that endocardial hemorrhage occurred immediately after AMI. Possibly rupture of subendocardial hematoma occurred in this case (Iwakura, 2011).

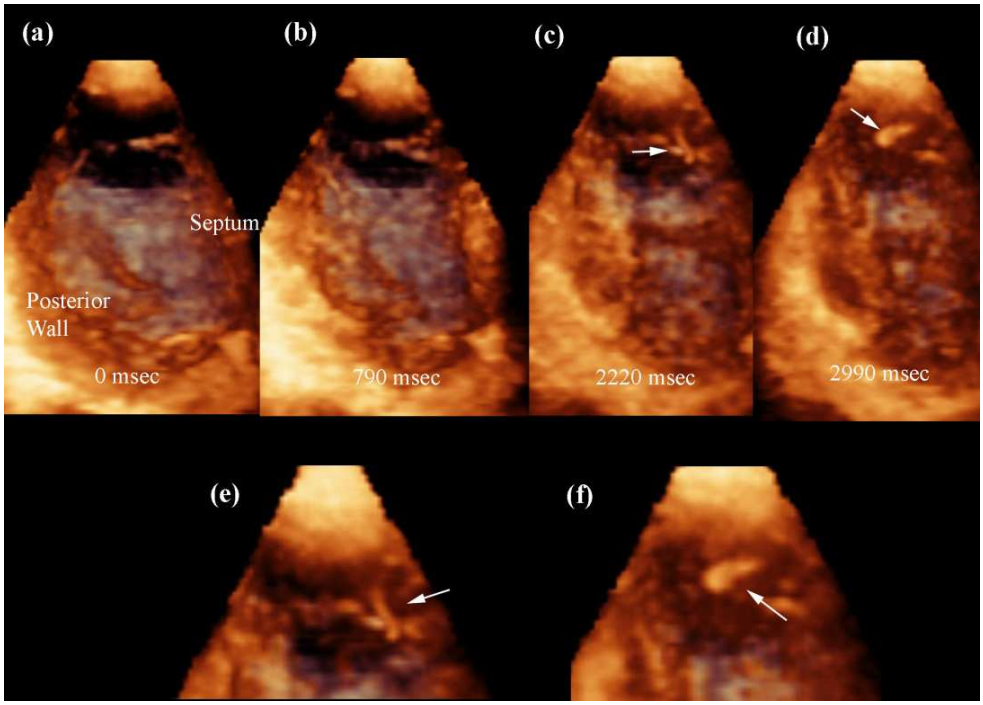

Fig. 5. Endocardial hemorrhage observed immediately after primary PCI.

3.4 Assessment of endocardial perfusion with 3D-MCE.

2D-MCE showed good-reflow in 31 out of 47 study patients (66.0%), poor-reflow in 9 patients (19.1%) and no-reflow in 7 patients (14.9%). Patient characteristics of each group were illustrated in Table 2. The incidence of anterior wall AMI was significantly higher in the no- and poor-reflow than the good-reflow (p=.01). The additional ST elevation after reperfusion was more frequently observed in the no-reflow (p=.04). There were significant differences in the incidence of the multivessel disease (p=.02) and the collateral grade (p=.03) among three subsets (Table 2).

	2D-MCE				3D-MCE			
	Good-reflow	Poor-reflow	No-reflow	P	Good-MO	Poor-MOE	No-MOE	P
Number of Patients	31	9	7		17	16	14	
Age, y	62±11	60±10	55±11	.30	63±12	63±9	55±10	.08
Gender, male/female	24/7	9/0	5/2	.25	15/2	13/3	10/4	.50
Peak CK, IU/L	2516±2186	3195±2209	5240±3040	.03	1166±1081	2796±1700	5583±2345	<.0001
Peak CK-MB, IU/L	204±185	259±166	349±177	.16	100±100	261±189	383±144	<.0001
Diabetes Mellitus, n (%)	12 (38.8)	4 (44.4)	3 (42.9)	.94	6 (35.3)	7 (43.8)	6 (42.9)	.86
Hypertension, n (%)	19 (61.3)	5 (55.6)	5 (71.4)	.81	10 (58.8)	11 (68.8)	8 (57.1)	.77
Hyperlipidemia, n (%)	16 (51.6)	6 (66.7)	2 (28.6)	.32	12 (70.6)	5 (31.3)	7 (50.0)	.08
Smoking, n (%)	22 (71.0)	8 (88.9)	6 (85.7)	.44	12 (70.6)	12 (75.0)	12 (85.7)	.60
Onset to reperfusion , h	13.0±13.1	15.1±20.9	5.9±4.9	.41	11.2±13.4	18.7±17.9	5.8±4.3	.04
Stent implantation, n (%)	29 (93.4)	9 (100)	5 (71.4)	.10	16 (94.1)	15 (93.8)	12 (85.7)	.65
Thrombectomy, n (%)	21 (67.7)	7 (77.8)	6 (85.7)	.58	12 (70.6)	11 (68.8)	11 (78.6)	.82
Anterior wall MI, n (%)	17 (54.8)	6 (66.7)	5 (71.4)	.64	11 (64.7)	7 (43.8)	10 (71.4)	.26
Multivessel disease, n	8 (25.8)	3 (33.3)	1 (14.3)	.68	4 (23.5)	5 (31.2)	3 (21.4)	.80
ST re-elevation, n (%)	11 (35.5)	1 (11.1)	5 (71.4)	.04	2 (11.8)	7 (43.8)	8 (57.1)	.02

Table 2. Clinical parameters of the study patients.

Good-MOE was observed on 3D-MCE only in 17 patients (36.2%). Poor-MOE was observed in 16 patients (34.0%) and no-MOE in 14 patients (29.8%). Among the 31 patients with good-reflow on 2D-MCE, only 14 patients (45.2 %) showed good-MOE, and 4 patients (12.9%) showed no-MOE. In contrast, all 7 patients with no-reflow on 2D-MCE showed no-MOE on 3D-MCE (Table 3).

	3D-MCE			
2D-MCE	Good-MOE, n	Poor-MOE, n	No-MOE, n	Total, n
Good-reflow, n	14	13	3	31
Poor-reflow, n	3	3	3	9
No-reflow, n	0	0	7	7
Total, n	17	16	14	47

Table 3. Distribution of myocardial perfusion grade on 2D- and 3D-MCE

Among the 31 patients with good-reflow, only 19 patients (61.3%) showed TMPG-3, and 6 patients showed TMPG-0/1 on CAG after PCI. On the other hand, 16 out of 17 patients (94.1%) with good-MOE showed TMPG-3.

3.5 Prediction of infarct size with 2D- and 3D-MCE

Among the 3 groups classified with 2D-MCE, the no-reflow had the highest peak-CK value (5240±3040 IU/L), followed by the poor-reflow (3195±2209 IU/L) and the good-reflow (2516±2186 IU/L). The differences in peak CK among three subsets were significant (p=.03), and the no-reflow had significantly higher peak CK than the good-reflow. However, the differences in peak CK between the poor-reflow and the good- or the no-reflow did not reach statistical significance (Figure 6). There were no significant differences in CK-MB values among the three subsets (p=0.16).

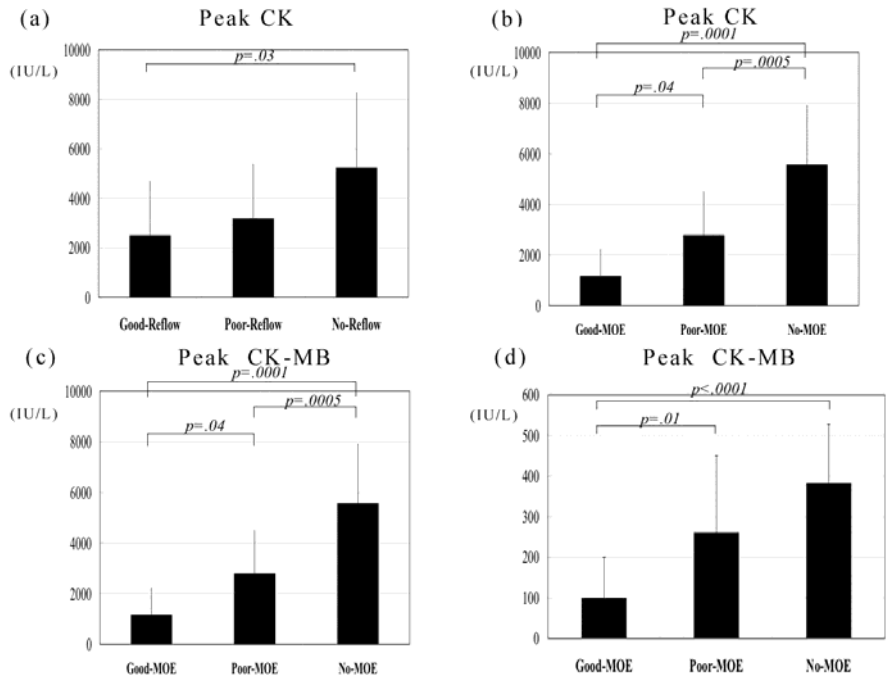

Fig. 6. Peak CK/CK-MB and myocardial perfusion grade on 2D/3D-MCE

The no-MOE on 3D-MCE also had the highest peak CK value (5583±2345 IU/L), followed by the poor-MOE (2796±1700 IU/L) and by the good –MOE (1166±1080 IU/L). The differences in peak CK were significant not only among 3 groups (p<.0001) but also in each pair of groups (Figure 6). Moreover, there were significant differences in CK-MB among 3 groups (p<.0001). The good-MOE had significantly lower CK-MB then the poor- (p=.01) or the no-MOE (p<.0001) (Figure 6). These results indicated that myocardial perfusion grade by 3D-MCE predicted infarct size more distinctively than that by 2D-MCE does.

3.6 Prediction of LV functional and morphological outcomes with 2D- and 3D-MCE

At baseline study, there was no significant difference in RWM among 3 groups based on 2D-MCE. The good-MOE had the highest RWM among 3 groups based on 3D-MCE at

baseline study (good-/poor-/no-MOE = -2.28±0.91/-3.03±0.67/-2.99±0.71, p=0.02). A mean of 4.6±2.7 months later, RWM of the no-reflow (-2.84±0.83) was lower than that of the good-reflow (-1.37±1.11, p=.004). However, RWM was not statistically different between the poor-reflow (-1.73±0.71) and the good-reflow or the no-reflow (Figure 7). On the other hand, there were significant differences in RWM in each pair of the 3 groups defined by 3D-MCE (Figure 7).

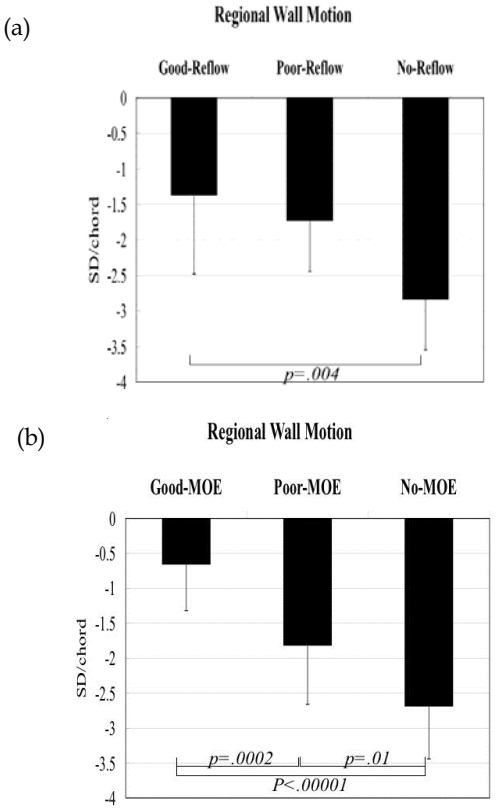

Fig. 7. RWM on the chronic stage and myocardial perfusion grade on 2D/3D-MCE

Among the 42 patients in whom initial ventriculography study was performed, the improvement of RWM from baseline to follow-up study was the highest in the good-MOE, followed by the poor-MOE and the no-MOE (1.59±0.98 vs. 1.19±0.71 vs. 0.31±0.84, p=.001). Although RWM improvement was also the highest in the good-reflow, but it showed significant overlap among 3 groups, and no significant differences were observed among them (p=0.10). These results implied that myocardial perfusion pattern assessed with 3D-MCE predicts the functional recovery more definitively than that with 2D-MCE.

There were no differences in LVEDVI and LVESVI at baseline study among 3 groups based on 2D-MCE, and there were no significant differences in LVEDVI and LVESVI among 3 groups at

follow-up study. The no-reflow had significantly lower ejection fraction than the good-reflow at baseline study. At the follow-up study, the good-reflow showed higher LVEF than the no-reflow, but LVEF of the poor-reflow showed significant overlap with those of other two subsets (Figure 8). At baseline, LVEDVI was comparable among 3 groups defined by 3D-MCE. The good-MOE had smaller LVESVI than the no-MOE and better LVEF than other two groups on initial LVG. At the follow-up study, the no-MOE had larger LVEDVI than the good-MOE, and larger LVESVI and LVEF fraction than two other groups (Figure 8).

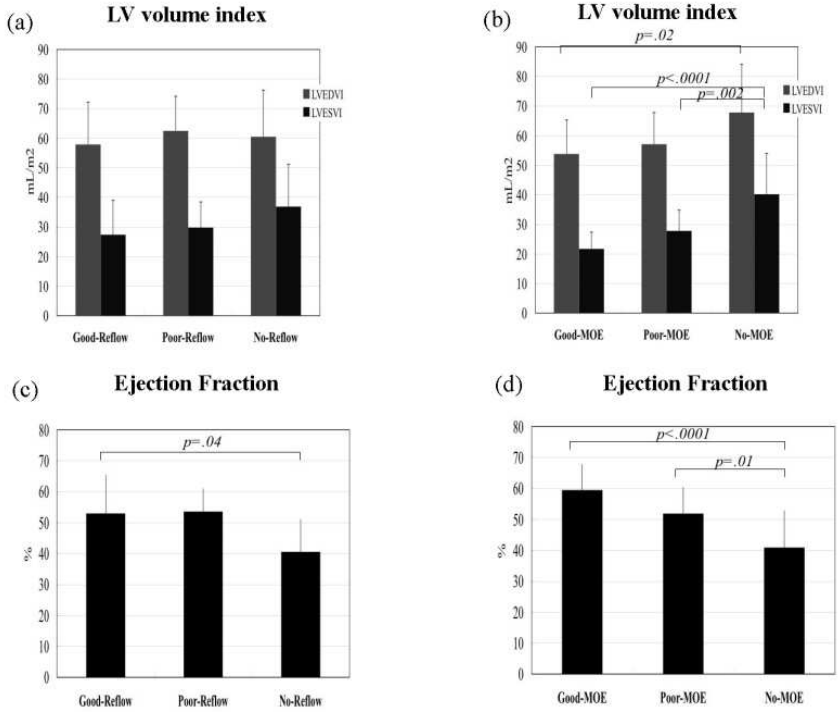

Fig. 8. LV volume index and LVEF on the chronic stage

4. 3D-MCE as a novel method for assessment of subendocardial perfusion

The present study demonstrated that subendocardial perfusion after coronary recanalization was well visualized with 3D-MCE in patients with AMI. Assessment of subendocardial perfusion with 3D-MCE predicted infarct size and discriminated patients with poor functional outcome more precisely than 2D-MCE. We used intracoronary injection of microbubbles for 3D-MCE rather than intravenous injection because intravenous injection of contrast agent would make LV filled with microbubbles, which make endocardial surface invisible.

4.1 Comparison between 2D- and 3D-MCE for detection of the no-reflow

While the no-reflow assessed by 2D-MCE is associated with poor functional recovery after AMI, the microvascular integrity does not always go along with functional recovery on the

chronic stage(Galiuto *et al.*,1998). TMPG-3 on coronary angiogram is generally achieved only in less than 30% of the patients with AMI after primary PCI(Gibson *et al.*,2000)(Costantini *et al.*,2004), while good reflow is observed on 2D-MCE in about 70% of the patients(Ito *et al.*,1992)(Galiuto *et al.*,1998)(Porter *et al.*,1998). TMPG grade was far better correlated with MOE on 3D-MCE than with perfusion pattern on 2D-MCE in the present study. Thus, 2D-MCE might overestimate myocardial reperfusion and predict functional recovery excessively(Bolognese *et al.*,1996).

Myocardial perfusion patterns assessed by 3D-MCE were not necessarily coincident with those with 2D-MCE. The frequency of good-MOE on 3D-MCE was significantly lower than that of good reflow on 2D-MCE (36.2% vs. 66.0%) in the present study. Although 2D-MCE might detect subendocardial perfusion defect in some cases(Ragosta *et al.*,1994), it basically could not well assess transmural differences in myocardial perfusion(Kaul *et al.*,1992). 3D-MCE observes contrast opacification on the endocardial surface directly from the view point of LV cavity, and could assess subendocardial perfusion more precisely than 2D-MCE. Nevertheless, direct observation of subendocardial opacification has some limitations for precise subendocardial perfusion. Contrast signal from the mid-layers might contaminate the subendocardial opacification, even with adjustment of recording conditions to reduce such interference. We used sonicated contrast medium for intracoronary MCE, which contains various sized microbubbles(Ito *et al.*,1992). Large bubbles work as scatters rather than reflectors of ultrasound, and ultrasound scatter would produce false ultrasound signals in the neighboring myocardium. This interference has the potential for inhibiting the discrimination between endocardium and epicardium on 3D-MCE(Kaul *et al.*,1992).

While 2D-MCE observed myocardial perfusion only in a slice of the risk area, 3D-MCE observed spatial distribution of perfusion more widely. If the echo-plane on 2D-MCE is not placed at the center area of the infarct zone, we would observe myocardial perfusion at the marginal zone. Microvascular injury in the peripheral zone is not as severe as in the center area, and myocardial perfusion could be overestimated. The 3D-MCE image in Figure 4 showed high contrast enhancement area around the central risk area. This could be hyperemic response occurring at the marginal area. Presence of hyperemia might make 2D-MCE overestimate myocardial perfusion.

4.2 Limitation of the study

In the present study, we used real-time 3D echocardiography (Live-3D) instead of full-volume imaging. Real-time 3D acquisition is limited to an angle of about 30° - 50° degrees, and provides only a partial view of LV. To cover the complete LV, acquisition of wide-angle ('full-volume') volumetric data sets using ECG gating is required. 3D-contrast echocardiography, using intravenous contrast agents, assesses LV volumes more precisely than 2D-contrast echocardiography or 3D-echocardiography in patients with a history of myocardial infarction(Jenkins *et al.*,2009). LV volumes measured with 3D-contrast echocardiography is compatible with those measured on CMR. However, 3D-contrast echocardiography was used to delineate endocardial border clearly (LV opacification), and myocardial perfusion was not assessed in these studies. Full-volume 3D-MCE will not only assess myocardial perfusion within a complete LV, but will be able to measure myocardial volume showing microvascular dysfunction. At the time of the present study, the image-analysis software for SONOS 7500 was not suitable for observation of contrast enhancement

in a full-volume image, let alone measurement of the volume of microvascular dysfunction. New software should be developed to analyze a full-volume 3D-MCE image quantitatively.

Despite of the limitation described above, real-time 3D-MCE has some advantages over full-volume imaging, including direct and easy observation of changes in endocardial structures. In one of the present study patients, we observed eruption of contrast medium from endocardial surface immediately after intracoronary injection of microbubbles. We considered this phenomenon as indicating rupture of subendocardial hematoma. In an experimental model, intramural hemorrhage is not observed early after coronary reperfusion on intracoronary 2D-MCE (Shishido *et al.*,1997). The contrast defect spread significantly with time after reperfusion in the cases developing intramural hemorrhage, but enhancement immediately after reperfusion was compatible between those with and without hemorrhage (Shishido *et al.*,1997). 2D-MCE might fail to detect small hemorrhage limited to the subendocardial layer, while 3D-MCE could detect it by direct observation of endocardial surface. Thus, real time 3D-MCE is a promising method not only to observe on endocardial perfusion but also to observe pathological events occurring endocardial surface.

The present real time 3D-MCE technique has other limitations. The spatial resolution of 3D-echocardiograhy is still inferior to that of 2D-echocardiography, which might lead to the poorer 3D-MCE image quality. We evaluated perfusion pattern and MOE only visually, because the present system does not have the objective method to measure myocardial opacification on 3D-images. The quantitative measures using replenishment curves which is available in 2D-MCE (Wei *et al.*,1998) still could not be performed in 3D-MCE. We hope that the technical progress would soon resolve these technical issues.

5. Conclusion

Newly developed, real time 3D-MCE was a feasible method to assess endocardial perfusion in patients with AMI. 3D-MCE assessed infarct size and predicted functional outcomes after AMI better than 2D-MCE did. It also observed endocardial hemorrhage occurred after PCI in one of the study patients. Thus, 3D-MCE is a promising method for assessment of microvascular function and of endocardial structural changes immediately after primary PCI for AMI.

6. References

Aiello, E.A., Jabr, R.I. & Cole, W.C. (1995) Arrhythmia and delayed recovery of cardiac action potential during reperfusion after ischemia. role of oxygen radical-induced no-reflow phenomenon. *Circ. Res.*, Vol.77, No.1, (Jul, 1995), pp. 153-162, ISBN0009-7330

Ito, H., Maruyama, A., Iwakura, K., Takiuchi, S., Masuyama, T., Hori, M., Higashino, Y., Fujii, K. & Minamino, T. (1996) Clinical implications of the 'no reflow' phenomenon. a predictor of complications and left ventricular remodeling in reperfused anterior wall myocardial infarction. *Circulation*, Vol.93, No.2, (Jan, 1996), pp. 223-228, ISBN0009-7322

Morishima, I., Sone, T., Mokuno, S., Taga, S., Shimauchi, A., Oki, Y., Kondo, J., Tsuboi, H. & Sassa, H. (1995) Clinical significance of no-reflow phenomenon observed on angiography after successful treatment of acute myocardial infarction with

percutaneous transluminal coronary angioplasty. *Am. Heart J.*, Vol.130, No.2, (Aug, 1995), pp. 239-243, ISBN0002-8703

Gerber, B.L., Rochitte, C.E., Melin, J.A., McVeigh, E.R., Bluemke, D.A., Wu, K.C., Becker, L.C. & Lima, J.A. (2000) Microvascular obstruction and left ventricular remodeling early after acute myocardial infarction. *Circulation*, Vol.101, No.23, (Jun, 2000), pp. 2734-2741, ISBN1524-4539

TIMI Study Group (1985) The thrombolysis in myocardial infarction (TIMI) trial. phase i findings.. *N. Engl. J. Med.*, Vol.312, No.14, (Apr, 1985), pp. 932-936, ISBN0028-4793

van 't Hof, A.W., Liem, A., Suryapranata, H., Hoorntje, J.C., de Boer, M.J. & Zijlstra, F. (1998) Angiographic assessment of myocardial reperfusion in patients treated with primary angioplasty for acute myocardial infarction: myocardial blush grade. zwolle myocardial infarction study group. *Circulation*, Vol.97, No.23, (Jun, 1998), pp. 2302-2306, ISBN0009-7322

Iwakura, K., Ito, H., Takiuchi, S., Taniyama, Y., Nakatsuchi, Y., Negoro, S., Higashino, Y., Okamura, A., Masuyama, T., Hori, M., Fujii, K. & Minamino, T. (1996) Alternation in the coronary blood flow velocity pattern in patients with no reflow and reperfused acute myocardial infarction. *Circulation*, Vol.94, No.6, (Sep, 1996), pp. 1269-1275, ISBN0009-7322

Albert, T.S.E., Kim, R.J. & Judd, R.M. (2006) Assessment of no-reflow regions using cardiac mri. *Basic Res. Cardiol.*, Vol.101, No.5, (Sep, 2006), pp. 383-390, ISBN0300-8428

Ingkanisorn, W.P., Rhoads, K.L., Aletras, A.H., Kellman, P. & Arai, A.E. (2004) Gadolinium delayed enhancement cardiovascular magnetic resonance correlates with clinical measures of myocardial infarction. *J. Am. Coll. Cardiol.*, Vol.43, No.12, (Jun, 2004), pp. 2253-2259, ISBN0735-1097

Porto, I., Burzotta, F., Brancati, M., Trani, C., Lombardo, A., Romagnoli, E., Niccoli, G., Natale, L., Bonomo, L. & Crea, F. (2007) Relation of myocardial blush grade to microvascular perfusion and myocardial infarct size after primary or rescue percutaneous coronary intervention. *Am. J. Cardiol.*, Vol.99, No.12, (Jun, 2007), pp. 1671-1673, ISBN0002-9149

Lund, G.K., Stork, A., Saeed, M., Bansmann, M.P., Gerken, J.H., Müller, V., Mester, J., Higgins, C.B., Adam, G. & Meinertz, T. (2004) Acute myocardial infarction: evaluation with first-pass enhancement and delayed enhancement mr imaging compared with 201tl spect imaging. *Radiology*, Vol.232, No.1, (Jul, 2004), pp. 49-57, ISBN0033-8419

Hombach, V., Grebe, O., Merkle, N., Waldenmaier, S., Höher, M., Kochs, M., Wöhrle, J. & Kestler, H.A. (2005) Sequelae of acute myocardial infarction regarding cardiac structure and function and their prognostic significance as assessed by magnetic resonance imaging. *Eur. Heart J.*, Vol.26, No.6, (Mar, 2005), pp. 549-557, ISBN0195-668X

Habis, M., Capderou, A., Ghostine, S., Daoud, B., Caussin, C., Riou, J., Brenot, P., Angel, C.Y., Lancelin, B. & Paul, J. (2007) Acute myocardial infarction early viability assessment by 64-slice computed tomography immediately after coronary angiography: comparison with low-dose dobutamine echocardiography. *J. Am. Coll. Cardiol.*, Vol.49, No.11, (Mar, 2007), pp. 1178-1185, ISBN1558-3597

Ito, H., Tomooka, T., Sakai, N., Yu, H., Higashino, Y., Fujii, K., Masuyama, T., Kitabatake, A. & Minamino, T. (1992) Lack of myocardial perfusion immediately after successful

thrombolysis. a predictor of poor recovery of left ventricular function in anterior myocardial infarction. *Circulation*, Vol.85, No.5, (May, 1992), pp. 1699-1705, ISBN0009-7322

Porter, T.R., Li, S., Oster, R. & Deligonul, U. (1998) The clinical implications of no reflow demonstrated with intravenous perfluorocarbon containing microbubbles following restoration of thrombolysis in myocardial infarction (TIMI) 3 flow in patients with acute myocardial infarction. *Am. J. Cardiol.*, Vol.82, No.10, (Nov, 1998), pp. 1173-1177, ISBN0002-9149

Balcells, E., Powers, E.R., Lepper, W., Belcik, T., Wei, K., Ragosta, M., Samady, H. & Lindner, J.R. (2003) Detection of myocardial viability by contrast echocardiography in acute infarction predicts recovery of resting function and contractile reserve. *J. Am. Coll. Cardiol.*, Vol.41, No.5, (Mar, 2003), pp. 827-833, ISBN0735-1097

Dwivedi, G., Janardhanan, R., Hayat, S.A., Swinburn, J.M. & Senior, R. (2007) Prognostic value of myocardial viability detected by myocardial contrast echocardiography early after acute myocardial infarction. *J. Am. Coll. Cardiol.*, Vol.50, No.4, (Jul, 2007), pp. 327-334, ISBN1558-3597

Galiuto, L., Garramone, B., Scarà, A., Rebuzzi, A.G., Crea, F., La Torre, G., Funaro, S., Madonna, M., Fedele, F., Agati, L. (2008) The extent of microvascular damage during myocardial contrast echocardiography is superior to other known indexes of post-infarct reperfusion in predicting left ventricular remodeling: results of the multicenter amici study. *J. Am. Coll. Cardiol.*, Vol.51, No.5, (Feb, 2008), pp. 552-559, ISBN1558-3597

Hashimoto, I., Li, X., Hejmadi Bhat, A., Jones, M., Zetts, A.D. & Sahn, D.J. (2003) Myocardial strain rate is a superior method for evaluation of left ventricular subendocardial function compared with tissue doppler imaging. *J. Am. Coll. Cardiol.*, Vol.42, No.9, (Nov, 2003), pp. 1574-1583, ISBN0735-1097

Garot, J., Bluemke, D.A., Osman, N.F., Rochitte, C.E., Zerhouni, E.A., Prince, J.L. & Lima, J.A. (2000) Transmural contractile reserve after reperfused myocardial infarction in dogs. *J. Am. Coll. Cardiol.*, Vol.36, No.7, (Dec, 2000), pp. 2339-2346, ISBN0735-1097

Grattan, M.T., Hanley, F.L., Stevens, M.B. & Hoffman, J.I. (1986) Transmural coronary flow reserve patterns in dogs. *Am. J. Physiol.*, Vol.250, No.2 Pt 2, (Feb, 1986), p. H276-83, ISBN0002-9513

Corsi, C., Lang, R.M., Veronesi, F., Weinert, L., Caiani, E.G., MacEneaney, P., Lamberti, C. & Mor-Avi, V. (2005) Volumetric quantification of global and regional left ventricular function from real-time three-dimensional echocardiographic images. *Circulation*, Vol.112, No.8, (Aug, 2005), pp. 1161-1170, ISBN1524-4539

Inoue, K., Ito, H., Iwakura, K., Kawano, S., Okamura, A., Kurotobi, T., Date, M., Otsu, K., Hori, M. & Fujii, K. (2006) Usefulness of high-resolution real-time three-dimensional echocardiography to visualize the left ventricular endocardial surface in myocardial infarction. *Am. J. Cardiol.*, Vol.97, No.11, (Jun, 2006), pp. 1578-1581, ISBN0002-9149

Iwakura, K., Ito, H., Okamura, A., Kurotobi, T., Koyama, Y., Date, M., Inoue, K., Nagai, H., Imai, M., Arita, Y., Toyoshima, Y., Ozawa, M. & Fujii, K. (2007) Comparison of two- versus three-dimensional myocardial contrast echocardiography for assessing subendocardial perfusion abnormality after percutaneous coronary intervention in

patients with acute myocardial infarction. *Am. J. Cardiol.*, Vol.100, No.10, (Nov, 2007), pp. 1502-1510, ISBN0002-9149

Gibson, C.M., Cannon, C.P., Murphy, S.A., Ryan, K.A., Mesley, R., Marble, S.J., McCabe, C.H., Van De Werf, F. & Braunwald, E. (2000) Relationship of timi myocardial perfusion grade to mortality after administration of thrombolytic drugs. *Circulation*, Vol.101, No.2, (Jan, 2000), pp. 125-130, ISBN1524-4539

Iwakura, K (2011) . Visualization of Myocardial Hemorrhage with Real Time Three-Dimensional Myocardial Contrast Echocardiography in Patients with Acute Myocardial Infarction. *J Echocardiogr*, *in press*

[Cerqueira2002] Standardized myocardial segmentation and nomenclature for tomographic imaging of the heart: a statement for healthcare professionals from the cardiac imaging committee of the council on clinical cardiology of the american heart association. . 2002.

Ragosta, M., Camarano, G., Kaul, S., Powers, E.R., Sarembock, I.J. & Gimple, L.W. (1994) Microvascular integrity indicates myocellular viability in patients with recent myocardial infarction. new insights using myocardial contrast echocardiography. *Circulation*, Vol.89, No.6, (Jun, 1994), pp. 2562-2569, ISBN0009-7322

Kapetanakis, S., Kearney, M.T., Siva, A., Gall, N., Cooklin, M. & Monaghan, M.J. (2005) Real-time three-dimensional echocardiography: a novel technique to quantify global left ventricular mechanical dyssynchrony. *Circulation*, Vol.112, No.7, (Aug, 2005), pp. 992-1000, ISBN1524-4539

Galiuto, L. & Iliceto, S. (1998) Myocardial contrast echocardiography in the evaluation of viable myocardium after acute myocardial infarction. *Am. J. Cardiol.*, Vol.81, No.12A, (Jun, 1998), p. 29G-32G, ISBN0002-9149

Costantini, C.O., Stone, G.W., Mehran, R., Aymong, E., Grines, C.L., Cox, D.A., Stuckey, T., Turco, M., Gersh, B.J., Tcheng, J.E., Garcia, E., Griffin, J.J., Guagliumi, G., Leon, M.B. & Lansky, A.J. (2004) Frequency, correlates, and clinical implications of myocardial perfusion after primary angioplasty and stenting, with and without glycoprotein iib/iiia inhibition, in acute myocardial infarction. *J. Am. Coll. Cardiol.*, Vol.44, No.2, (Jul, 2004), pp. 305-312, ISBN0735-1097

Bolognese, L., Antoniucci, D., Rovai, D., Buonamici, P., Cerisano, G., Santoro, G.M., Marini, C., L'Abbate, A. & Fazzini, P.F. (1996) Myocardial contrast echocardiography versus dobutamine echocardiography for predicting functional recovery after acute myocardial infarction treated with primary coronary angioplasty. *J. Am. Coll. Cardiol.*, Vol.28, No.7, (Dec, 1996), pp. 1677-1683, ISBN0735-1097

Kaul, S., Jayaweera, A.R., Glasheen, W.P., Villanueva, F.S., Gutgesell, H.P. & Spotnitz, W.D. (1992) Myocardial contrast echocardiography and the transmural distribution of flow: a critical appraisal during myocardial ischemia not associated with infarction. *J. Am. Coll. Cardiol.*, Vol.20, No.4, (Oct, 1992), pp. 1005-1016, ISBN0735-1097

Jenkins, C., Moir, S., Chan, J., Rakhit, D., Haluska, B. & Marwick, T.H. (2009) Left ventricular volume measurement with echocardiography: a comparison of left ventricular opacification, three-dimensional echocardiography, or both with magnetic resonance imaging. *Eur. Heart J.*, Vol.30, No.1, (Jan, 2009), pp. 98-106, ISBN1522-9645

Shishido, T., Beppu, S., Matsuda, H., Yutani, C. & Miyatake, K. (1997) Extension of hemorrhage after reperfusion of occluded coronary artery: contrast echocardiographic assessment in dogs. *J. Am. Coll. Cardiol.*, Vol.30, No.2, (Aug, 1997), pp. 585-591, ISBN0735-1097

Wei, K., Jayaweera, A.R., Firoozan, S., Linka, A., Skyba, D.M. & Kaul, S. (1998) Quantification of myocardial blood flow with ultrasound-induced destruction of microbubbles administered as a constant venous infusion. *Circulation*, Vol.97, No.5, (Feb, 1998), pp. 473-483, ISBN0009-7322

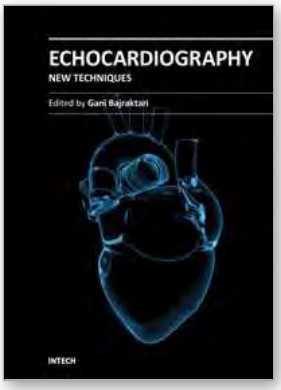

Echocardiography - New Techniques

Edited by Prof. Gani Bajraktari

ISBN 978-953-307-762-8
Hard cover, 218 pages
Publisher InTech
Published online 18, January, 2012
Published in print edition January, 2012

The book "Echocardiography - New Techniques" brings worldwide contributions from highly acclaimed clinical and imaging science investigators, and representatives from academic medical centers. Each chapter is designed and written to be accessible to those with a basic knowledge of echocardiography. Additionally, the chapters are meant to be stimulating and educational to the experts and investigators in the field of echocardiography. This book is aimed primarily at cardiology fellows on their basic echocardiography rotation, fellows in general internal medicine, radiology and emergency medicine, and experts in the arena of echocardiography. Over the last few decades, the rate of technological advancements has developed dramatically, resulting in new techniques and improved echocardiographic imaging. The authors of this book focused on presenting the most advanced techniques useful in today's research and in daily clinical practice. These advanced techniques are utilized in the detection of different cardiac pathologies in patients, in contributing to their clinical decision, as well as follow-up and outcome predictions. In addition to the advanced techniques covered, this book expounds upon several special pathologies with respect to the functions of echocardiography.

INTECH
open science | open minds

InTech Europe
University Campus STeP Ri
Slavka Krautzeka 83/A
51000 Rijeka, Croatia
Phone: +385 (51) 770 447
Fax: +385 (51) 686 166
www.intechopen.com

InTech China
Unit 405, Office Block, Hotel Equatorial Shanghai
No.65, Yan An Road (West), Shanghai, 200040, China
中国上海市延安西路65号上海国际贵都大饭店办公楼405单元
Phone: +86-21-62489820
Fax: +86-21-62489821

10

Cardiac Tumors

Maryam Moshkani Farahani
Department of Echocardiography, Faculty of Medicine,
Baqiyatallah University of Medical Sciences,
Molla Sadra Avenue, Tehran
Iran

1. Introduction

Cardiac tumors are among important group of cardiovascular diseases. Early diagnosis is necessary for the best management of the tumors. There are several imaging modalities available for cardiac tumors for diagnosis including echocardiography (transthoracic echocardiography, transesophageal echocardiography, 3 dimensional echocardiography) magnetic resonance imaging (MRI) and CT scan. However, echocardiography remains the best available noninvasive tool for the diagnosis of cardiac masses, while CT and MRI provide more information about the texture and extension of tumor.

Echocardiography provides useful information about the size, texture, location, extension of tumors, hemodynamic effects on heart such as stenosis.

Cardiac tumors can be found incidentally such as myxoma or left atrial thrombus in a patient with mitral stenosis. There is also different clinical presentation for cardiac masses such as constitutional symptoms, embolic events, fever etc.

Two groups of tumors can involve the heart: primary and secondary tumors. Primary tumors are rare with a prevalence of 0.001 to 0.03 percent in autopsies (1).The majority of primary tumors are benign such as myxoma, the most common form of primary tumors, responsible for half of these tumors (2). One fourth of cardiac tumors are malignant, and sarcomas with primary cardiac lymphomas are the most common malignant primary cardiac tumors (3).

Malignant primary cardiac tumors include: angiosarcoma, rhabdomyosarcoma, osteosarcoma, myxosarcoma, fibrosarcoma and synovial sarcoma. Various sarcomas and lymphomas are the most common primary malignant cardiac tumors (4, 5).

Metastatic tumors are 20 to 40 times more common than primary malignant ones with prevalence of 6% in post-mortem autopsies in malignant diseases (6). The most common tumors that metastasize to heart are from lung, breast, kidney, and liver; and among tumor variety, lymphoma, melanoma and osteogenic sarcoma (2).

Malignant tumors can metastasize to heart via hematogenous spread from inferior vena cava such as renal and hepatic tumors or via metastatic formation by systemic tumors such

as malignant melanoma, lymphomas, leukaemias and sarcomas. Lymphatics and direct invasion from adjacent organs such as lung and breast cancers or mediastinal lymphomas is another way of spread (7, 6).

2. Benign primary cardiac tumors

2.1 Myxoma

Three quarters of all primary cardiac tumors are benign and half of them are myxomas. These tumors occur mostly in third decade or later. Myxomas can occur as an isolated tumor in left atrium (the most common site of this tumor)[figure 1] or as familial form (Carney syndrome) which is associated with other manifestations. Most frequently it occurs in left atrium, then in right atrium, right ventricle and left ventricle; it can infrequently involve the valves. It is mostly attached to fossa ovalis via its stalk.

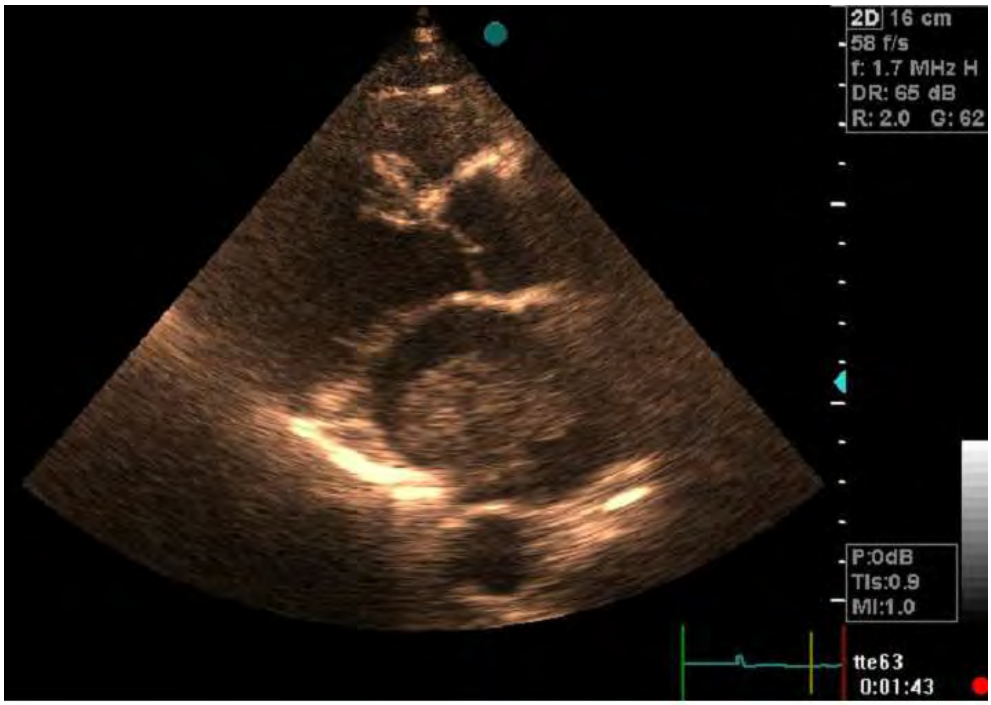

Fig. 1. Parasternal long axis view. A 38 year old man with history of dyspnea. Echocardiography revealed left atrial mass. He underwent cardiac surgery and pathology showed myxoma.

Myxoma has different clinical presentations. These include constitutional symptoms such as fever, weight loss, embolic events and symptoms of valvular obstruction such as the symptoms of mitral valve stenosis (figure 2).

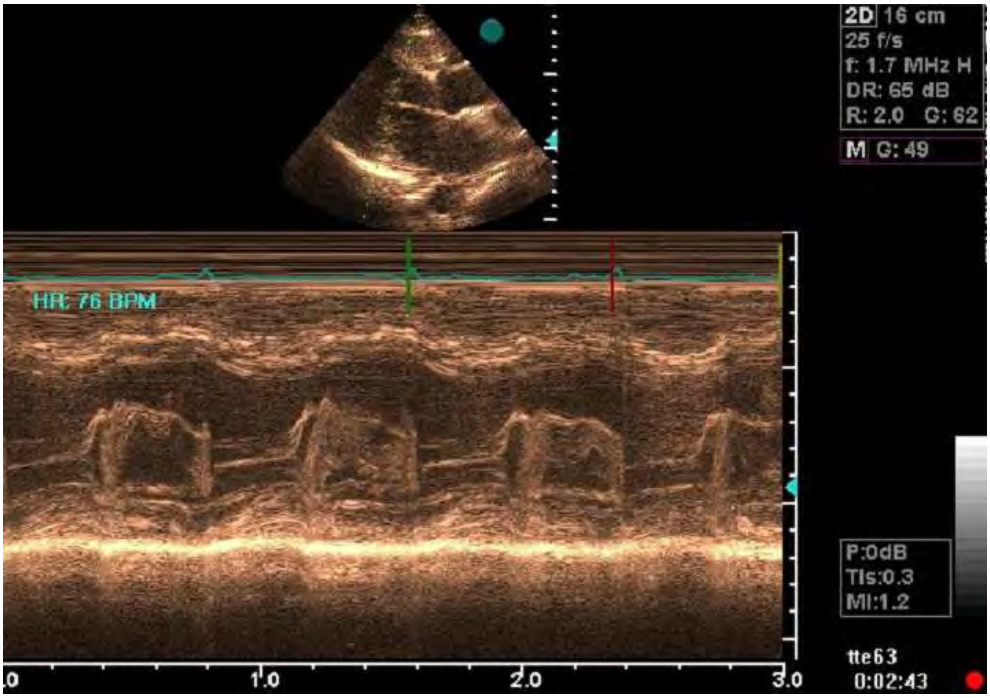

Fig. 2. A 38 year old man with history of dyspnea. Myxoma can protrude through mitral valve and in M-mode mitral stenosis can be visualized as seen in this Echocardiograph.

It has also different shapes as rounded or polypoid with narrow stalk and attachment to interatrial septum or fossa ovalis. The mass is mostly homogenous; however, small scattered area of calcification may be seen. Mobile particles of this tumor describe and predict its tendency for embolic events (8).

Echocardiography provides useful information about the location, size, extension and texture of this tumor, and one should be careful not to miss the multiple myxomas that could be found in other chambers.

Definite treatment for myxoma is total excision of the mass. Follow up echocardiography to rule out recurrence is recommended.

2.2 Papillary fibroelastoma

Papillary fibroelastoma is a rare, primary benign cardiac tumor that is most frequently found in the cardiac valves (9). It is the third primary cardiac tumor after myxoma and lipoma. These tumors are mostly found incidentally on post mortem. However, because of high tendency for systemic emboli, prompt diagnosis and management is necessary. Other rare presentations such as sudden death have been reported (10-12).

Papillary fibroelastoma represents 7.9% of benign primary cardiac tumor in adults (9). Approximately 90% of primary fibroelastomas arise from valves on ventricular side of pulmonary and aortic valve and atrial side of mitral and tricuspid valve (13-14). Aortic or mitral valves are mostly affected (15-16). The tricuspid valve is most affected in children; however, mitral and aortic valves are mostly affected in adults (17). Echocardiography remains the main tool for detection of this tumor. Because of involvement of cardiac valves other diagnosis such as infective endocarditis, degenerative changes and 0Lamble's excrescences should be kept in mind. Typical echocardiographic features include round, oval or irregular appearance, with a homogenous texture with small stalk (18). Surgical removal is indicated for large mobile tumors.

2.3 Rhabdomyoma

It is the most frequent cardiac tumor of childhood (about 60% of cardiac tumors) which is frequently found by fetal echocardiography (8). This tumor occurs in both ventricles equally with intramural involvement; however, atrioventricular valves involvement is also seen. This tumor may regress spontaneously.

2.4 Lipoma

It is a benign cardiac tumor that is asymptomatic in many patients (3). CT scan or MRI can easily define the tissue characteristic of fat and make an accurate diagnosis.

2.5 Hemangioma

It is a benign vascular tumor which occurs equally in left and right ventricles, and in right atrium. When tumor is resectable, total excision is recommended. Other benign cardiac tumors include cardiac paraganglioma (8) and fibroma.

3. Malignant primary cardiac tumors

Sarcomas are the most common primary malignant tumors and consist of 95% of cases. Any part of heart can be affected and rapid progression of disease is the usual clinical course of this tumor (8).

3.1 Angiosarcoma

Angiosarcoma is the most common primary malignant cardiac tumor (7). Men are involved more than female with a ratio of 2:1. Its usual location is right atrium and interatrial septum with involvement of pericardium and pericardial effusion [figure 3] (8). Other forms of sarcoma can occur in the left side of the heart and resemble the presentation of myxoma. It has a poor prognosis.

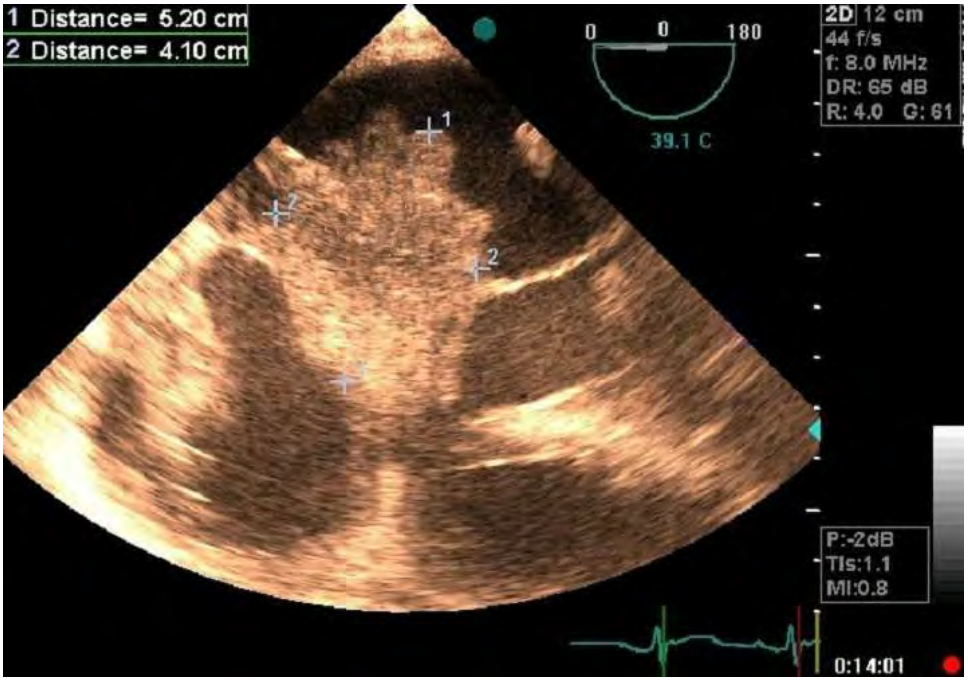

Fig. 3. Large tumor in right atrium with invasion toward interatrial septum and left atrium with pericardial effusion. In a 27 year old man who presented with progressive dyspnea.

4. Metastatic cardiac tumors

Metastatic tumors are 20 to 40 times more common than primary malignant ones with prevalence of 6% in post-mortem autopsies in malignant diseases (6).

4.1 Malignant melanoma

For the first time the term "melanotic heart" was introduced by William Norris in 1820 (7). However, many cases of malignant melanoma have been described in scientific literature.

Malignant melanoma frequently (50-71%) metastasizes to the heart (19). It seems to have the highest rate of metastases to heart. When a patient presents with cardiac metastases of melanoma, the disease has already spread throughout the body and is rarely curable (20). Single metastasis is rare. Metastases could be found in right side or left side; however, bilateral metastasis is frequently seen (21). The way of tumor spread toward heart is mostly hematogenous as seen in lymphoma and leukemia.

Previously, histologic diagnosis of malignant melanoma was made postmortem; however, with early detection of metastases due to availability of new imaging modalities, definite antemortem diagnosis and pathologic examination is frequently possible. Tissue specimen can be obtained by echocardiography guided transvenous biopsy or by resection of mass (22).

The symptoms are nonspecific such as chronic pericarditis, congestive heart failure, pericardial effusion, tamponade, conduction disturbances or defects, arrhythmias such as ventricular or supraventricular heart rhythm disturbances (23,24), syncope, embolism events such as transient ischemic attack and hemodynamic changes secondary to valve dysfunction.

Malignant melanoma has the highest rate of metastases to heart; however, due to improvement in treatment for this disease, longer survival than previous is now possible (25) and with newer imaging modalities early detection of metastases is possible and the physician should be alert of the risk of metastases. Transesophageal echocardiography has higher sensitivity than transthoracic echocardiography and cardiac magnetic resonance imaging with its ability to define the mediastinal involvement could also be used. According to tumor characteristics, its burden, location and size, palliative surgery or complete resection or adjuvant systemic therapy is recommended.

5. Summary

Echocardiography both transthoracic echocardiography (TTE), transesophageal echocardiography (TEE), is the commonly available noninvasive method for the diagnosis of cardiac masses. Tumor size, location and texture, and its extension to adjacent organs, its attachment to cardiac structures, presence or absence of pericardial effusion, interference with valve function, any obstruction and tumor mobility could be evaluated by echocardiography. In patients with poor echo window, TEE gives superior results, however, in some patients for better evaluation of cardiac tumor and its extension, other imaging modalities such as MRI is needed. Extra cardiac structures could be visualized better in TTE then TEE which is important for surgeons for choosing the most suitable plan for surgery(7).

6. Acknowledgement

Special thanks to doctor Hyderi for his valuable comments.

7. References

[1] Reynen K. Frequency of primary tumors of the heart. Am J Cardiol 1996;77: 107.
[2] Reynen K. Cardiac myxomas. N Engl J Med 1995; 333: 1610–1617.

[3] Libby P, Bonow R, Mann DL, Zipes DP. Braunwald's Heart Disease: A Textbook of Cardiovascular Medicine, 8th edition
[4] Roberts WC, Glancy DL, DeVita VT. Heart in malignant lymphoma. A study of 196 autopsy cases. Am J Cardiol 1968;22: 85–107
[5] Silverman J, Olwin JS, Graettinger JS. Cardiac myxomas with systemic embolization review of the literature and report of a case. Circulation 1962; 26: 99–10
[6] Hoffmann U, Globits S, Frank H, Cardiac and paracardiac masses Current opinion on diagnostic evaluation by magnetic resonance imaging . Eur Heart J (1998) 19, 553–563.
[7] McAllister Jr HA, Fenoglio Jr JJ. Tumors of the cardiovascular system. Atlas of tumor pathology, 2nd series. Fascicle 15 Washington, D. C. Armed Forces Institute of Pathology, 1978:1–20.
[8] Otto CM. The Practice of Clinical Echocardiography. 3rd edition. 2008, pp. 1108-1131.
[9] Edwards FH, Hale D, Cohen A, et al: Primary cardiac valve tumors. Ann Thoracic Surg 1991; 52:1127-31.
[10] Klarich KW, Enriquez Sarano M, Gura GM, Edwards WD, Tajik AJ, Seward JB. Papillary fibroelastoma:Echocardiographic Characteristics for diagnosis and pathologic correlation Am Coll Cardiol 1997;30:784-790.
[11] Mugge A, Daniel WG, Haverich A, et al: Diagnosis of non-infective cardiac mss lesions by two-dimensional echocardiography. Comparison of the transthoracic and transesophageal approaches. Circulation 1991; 83:70-78.
[12] Winkler M, Higgins CB: Suspected intracardiac masses: Evaluation with MR imaging. Radiol 1987; 165:117-122.
[13] Sun JP, Ashe CR, Yang XS, Cheng GG, Scalia GM, Massed AG, Griffin BP, Ratlift NB, Stewart WJ, Thomas JD. Clinical and echocardiographic characteristics of papillary fibroelastoma : a retrospective and prospective study in 162 patients. Circulation 2001;103:2687-93.
[14] Lichtenstein HL, Lee JC, Stewart S. Papillary tumor of the heart:incidental finding at surgery. Hum pathol 1979;10:473-5.
[15] Mc Alister HA, Fenoglio JJ. Tumors of the cardiovascular system. In: Atrak of tumor pathology second series fascicle 15. Washington DC Armed Forces Institute of pathology, 1978; 20-25.
[16] Roberts WC, Papillary Fibroelastoma of the heart. Am J Cardiol 1997; 80:973-975.
[17] Hicks KA, Kovach JA, Frishberg DP, Wiley TM, Gurezak PB, Vernalis MN. Echocardiographic evaluation of papillary fibroelastoma: a case report and review of the literature. Am J Soc Echocardiogr 1996;9:353-60
[18] Almagro UA, Perry LS, Choi H, Pinator K. Papillary fibroelastoma of the heart. Report of six cases. Arch Pathol Lab Med. 1982;106:318-321
[19] latt EC, Heiz DR, Cardiac Metastases. Cancer 1990;65:1456-9
[20] Chen RH, Gaos CM, Frazier OH. Complete resection of a right atrial intracavitary metastatic melanoma. Annals thoracic surgery 1996;61:1255-7
[21] Reynen K, Köckeritz U, Strasser R. H. Metastases to the heart Annals of Oncology 2004;15:375–381.
[22] Rubin DC, Ziskind AA, Hawke MW, Plotnick GD. Transesophageal echocardiographically guided percutaneous biopsy of a right atrial mass. Am Heart J 1994;127:935-6.

[23] Lin TK, Stech JM, Eckert WG, Liu JJ et al. Pericardial angiosarcomata simulating pericardial effusion by echography. Chest 1978; 73: 881–3.
[24] Coghlan JG, Paul VE, Mitchell AG. Cardiac involvement by lymphoma. Diagnostic difficulties. Eur Heart J 1989; 10:765–8
[25] Samiei N, Moshkani Farahani M, Sadeghipour A, Mozaffari K, Maleki M. Intracardiac metastasis of malignant melanoma. European Journal of Echocardiography (2008) 9, 393–394.

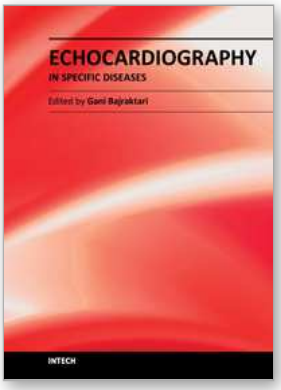

Echocardiography - In Specific Diseases

Edited by Prof. Gani Bajraktari

ISBN 978-953-307-977-6
Hard cover, 160 pages
Publisher InTech
Published online 18, January, 2012
Published in print edition January, 2012

The book "Echocardiography - In Specific Diseases" brings together contributions from well- known researchers from around the world, some of them specialized in imaging science in their clinical orientation, but also representatives from academic medical centers. Each chapter is structured and written to be accessible to those with a basic knowledge of echocardiography but also to be stimulating and informative to experts and researchers in the field of echocardiography. This book is primarily aimed at cardiology fellows during their basic echocardiography rotation, fellows of internal medicine, radiology and emergency medicine, but also experts in echocardiography. During the past few decades technological advancements in echocardiography have been developing rapidly, leading to improved echocardiographic imaging using new techniques. The authors of this book tried to explain the role of echocardiography in several special pathologies, which the readers may find in different chapters of the book.

How to reference

In order to correctly reference this scholarly work, feel free to copy and paste the following:

Maryam Moshkani Farahani (2012). Cardiac Tumors, Echocardiography - In Specific Diseases, Prof. Gani Bajraktari (Ed.), ISBN: 978-953-307-977-6, InTech, Available from: http://www.intechopen.com/books/echocardiography-in-specific-diseases/cardiac-tumors

INTECH
open science | open minds

InTech Europe
University Campus STeP Ri
Slavka Krautzeka 83/A
51000 Rijeka, Croatia
Phone: +385 (51) 770 447
Fax: +385 (51) 686 166
www.intechopen.com

InTech China
Unit 405, Office Block, Hotel Equatorial Shanghai
No.65, Yan An Road (West), Shanghai, 200040, China
中国上海市延安西路65号上海国际贵都大饭店办公楼405单元
Phone: +86-21-62489820
Fax: +86-21-62489821

Chapter 1

Introductory Chapter: Practical Approach to the Use of Intracardiac Echocardiography in Invasive Electrophysiology Procedures

Umashankar Lakshmanadoss

Additional information is available at the end of the chapter

http://dx.doi.org/10.5772/65243

1. Introduction

Use of intracardiac echocardiography (ICE) has been significantly increased with the advent of invasive electrophysiology and interventional procedures. In this day and age, we as a clinician are focused more on efficient and safe procedures for the patient. Intracardiac echocardiography plays a major role in doing these interventional procedures in a safe and efficient way. In addition to this, the use of ICE significantly reduced the need for fluoroscopy and hence reduced the occupational hazards of radiation and lead aprons for the physicians. It changed the way of doing these interventional procedures and one could easily say that this is one of the paradigm shift for us. In this chapter, I intend to review the basics of intracardiac echocardiography and also describe the various views and applications of intracardiac echocardiography in invasive electrophysiological procedures.

Several types of ice catheters are available in the market currently. They could be broadly divided into two different modalities. One catheter is a mechanical non-steerable catheter, which utilizes a rotating element to create a video 360° imaging claim perpendicular to the long axis of the catheter (UltraICE® Boston Scientific). This is 9 Fr catheter using 9 MHz. The second group of the catheter is a 64 element phased array 4-way steerable catheter. AcuNav® catheter (Biosense – Webster) is one of the commonly available phased out a catheter with the frequency range of 5.5–10 MHz. This is available in 8 and 10 Fr sizes. The system uses gray scale and has the facility for performing color Doppler, tissue Doppler and 3-D localization with Cartosound®. The images from this catheter result in a 90° sector image in the form of pie. ClearICE® catheter (St. Jude Medical) is another form of 64 elements phased array site looking highly steerable catheter with two sets of electrodes for integration of 3-D localization

with NavX®. In addition to the gray scale and tissue Doppler, this can also do synchronization mapping which speckles tracking. In our electrophysiology laboratory, we commonly use the phased array 8 or 10 Fr AcuNav® catheter. For the purpose of this chapter, one the images from phased array system is included.

2. What are all the moments possible with the ICE catheter?

There are totally eight movements possible with this steerable catheter. With these eight movements, an experienced operator should be able to navigate through the important structures of the heart.

1. Clockwise: rotation of the catheter away from the operator
2. Counterclockwise: rotation of the catheter towards the operator
3. Anterior flexion: catheter bends forward
4. Posterior flexion: catheter bends backward
5. Right tilt: catheter bends towards the right side
6. Left tilt: catheter bends towards the left side
7. Push: catheter is advanced in further
8. Pull: catheter is withdrawn

3. How to advance the ICE catheter into the heart?

In our laboratory, the imaging catheter is mostly advanced, either from the right or left femoral vein into the right atrium. This could be performed without the use of fluoroscopy. After getting a venous access, the ICE catheter is advanced through the sheath into the femoral vein. Once the catheter is out of the venous access sheath, one should be able to visualize the lumen of the venous system. We typically advance the catheter making sure that there is a sufficient lumen seen at the tip of the catheter. To negotiate the side branches and tortuous veins, we use the knob of the ice catheter to do the various possible movements as described above. While advancing the catheter, one could clearly visualize the structures including liver. Once we reached right atrium, we typically leave the catheter to get the home you as described below. Fluoroscopy guidance should be used by less experienced operators as the catheter tip is not soft.

http://dx.doi.org/10.5772/65243

4. What settings does one need to have to optimize the ice images?

It is also important to understand the basics and physical principles of echocardiography to optimize the images obtained.

1. Frequency: the frequency range of the ice catheter is 5.5–10 MHz. High frequency lengthens the near field and hence has higher resolution. However, the depth of the penetration is reduced and thereby limiting its usefulness. A frequency setting of 7.5 MHz is a good starting point for most of the electrophysiological procedures. If we need to examine one particular area with a higher resolution, then the operator could use higher frequency mode. For example, lower frequencies (5.5 MHz) may be required to visualize distant structures such as the inferior and lateral wall of the left ventricle in the dilated heart. Similarly, higher frequencies (8.5–10.0 MHz) may be required to visualize a near field structure with a high resolution as in the case of outflow tract tachycardia.
2. Depth: depth of the imaging sector could be either increased or decreased to include the area of interest. For the purpose of transseptal access and imaging of the right-sided pulmonary veins from the right atrium, and the setting of 60–80 mm would be sufficient. For imaging, the left-sided pulmonary veins and left atrial appendage from the right atrium at the setting of 80–100 mm would be optimal. If the operator wants to evaluate the pericardium for the purpose of pericardial effusion, a depth setting of 100–120 mm could be sufficient. For the purpose of imaging right ventricle and left ventricle from the right atrium, a wide range of depth setting of 100–120 mm could be used depending on the size of the ventricles.
3. Gain: gain is the amplitude of the received signal. When the gain is increased, we are amplifying the received signal, and hence the image becomes brighter. However, an excessive increase in grain and noise to the image and hence lateral resolution is not great. Hence, to enhance lateral resolution, the minimum amount of system gain should be used.
4. Focus: usually, it is not needed to adjust focus. Most of the imaging sectors have the focal zone set to a region that is 2/3 of the total. If the how to evaluate the near-field structure is with more detailed analysis (visualizing right atrium lead thrombus from the right atrium)], then we have to adjust the focus.
5. Dynamic range: dynamic range refers to the range of ultrasound intensities that can be displayed; it is one of the methods of controlling the contrast of the image. The higher the dynamic range, the better the contrast resolution. During ablation, if there is any doubt of the thickness of the structures, one could reduce the dynamic range and see if the thickness of the structures is increased or not. This could be very helpful to assess the catheter contact with a left atrial appendage, left the atrial ridge and other endocavitary structures.
6. Mechanical index: during an ablation procedure, ablationist would be interested in looking for the bubbles from the tissue which could be an impending sign of steam pop. If the mechanical index is very high, these microbubbles could be destructed with the subsequent admission of high intensive signals. Hence, the mechanical index should be kept as intermediate if one wants to see the microbubbles.

7. Tissue Doppler: tissue Doppler could be used to find the area of scar or fibrosis. This could be of vital importance in ventricular tachycardia ablation.

8. Color Doppler and continuous wave Doppler: this could be used in evaluating pulmonary veins and valves.

5. What are all the structures one could view using ICE catheter?

Right atrium:

Superior vena cava

Eustachian valve

Crista terminalis

Right atrium appendage

Tricuspid valve

Ostium of the coronary sinus

Cavotricuspid isthmus

Right ventricle:

Right ventricular inflow

Tricuspid valve attachments

Papillary muscle

Moderator band

Right ventricular inferior wall, apex, and lateral wall

Para Hisian region

Right ventricular outflow tract

Pulmonic valve

Left atrium:

Inter atrial septum

Left-sided pulmonary veins

Right-sided pulmonary veins

Left atrial appendage

http://dx.doi.org/10.5772/65243

Left atrial posterior wall

Mitral annulus

Coronary sinus

Left ventricle:

Left ventricular inflow

Anterolateral and posteromedial papillary muscle

Left ventricle apex

Left ventricular outflow tract

Aortic valve

Aorta

Miscellaneous:

Pericardial effusion

Thrombus or mass attached to the intracardiac leads

Adequate contact of the catheter with the tissue

Echogenicity of the tissue during ablation

Left atrial appendage closure device

Atrial septal defect closure device

Esophagus

6. How does one use the ICE catheter in atrial fibrillation ablation?

While advancing the ice catheter from the femoral vein, one could visualize the liver. At this time, the catheter is slightly advanced into the mid-right atrium. When the catheter in this position, we could visualize most of the right atrium, tricuspid valve, and right ventricle. This is referred to "home position". The catheter is left over here in an unlocked are a neutral position. This whole meal allows the assessment of the tricuspid valve structure, function and estimation of pulmonary artery systolic pressure using tricuspid regurgitation. This view also gives a better sense about right atrium and the right ventricle leads. Whenever the operator feels that he is lost secondary to the unfamiliar imaging plane, he just needs to put on the catheter to the home view by removing all catheter deflections and gently rotating the ice catheter in the clockwise and counterclockwise rotation until the tricuspid valve is visualized (**Figure 1**).

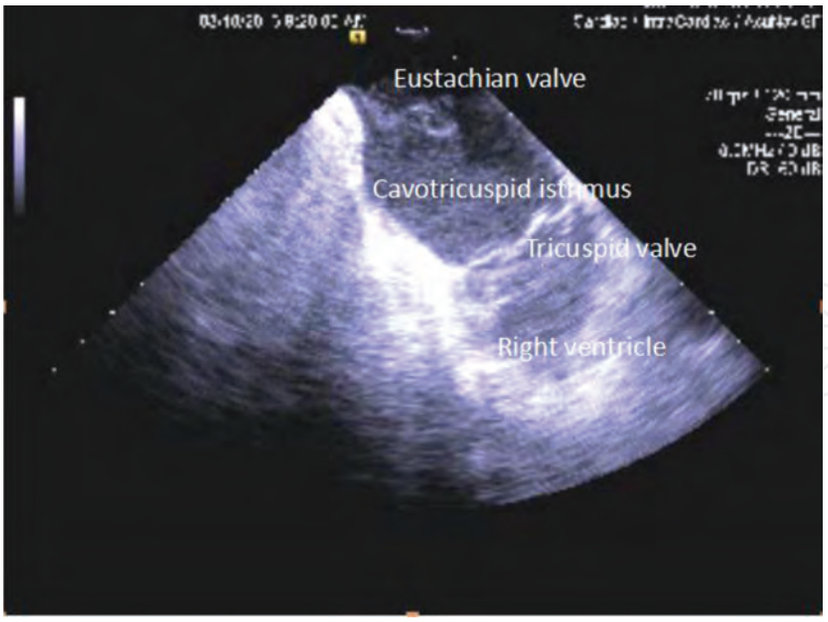

Figure 1. Home position.

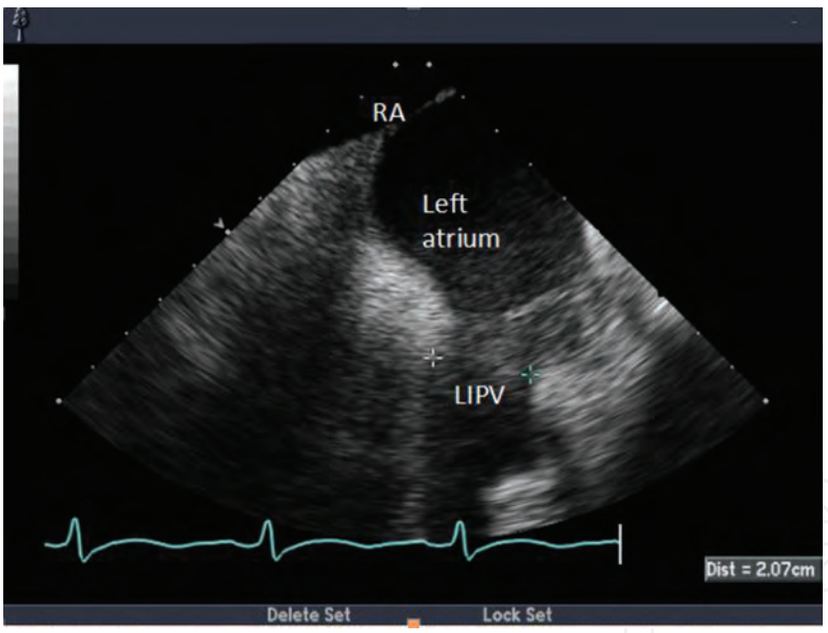

Figure 2. Left atrium and pulmonary veins.

From the home position, with the mild clockwise rotation, we can direct imaging plane posteriorly and left the ward. Initially, we can see the aortic valve, right ventricle inflow and right ventricle outflow just below the aortic valve. From this view, for the clockwise rotation of the catheter with about 45°, we can see the long axis of the aortic root. Here, we can analyze any atheroma of the aorta. This could be of vital importance when the operator is planning for a retrograde aortic approach. The aortic valve is also visualized well in this view. This is a good

http://dx.doi.org/10.5772/65243

view to look for any regurgitation through the aortic valve. Just behind the aortic valve, one may be able to see the pulmonary artery and pulmonic valve. A continued clockwise rotation from this view will direct the image plane more posteriorly. This view is a good view to visualize left atrial appendage, mitral annulus and ostium of the coronary sinus. Many operators use this view to interrogating left atrial appendage for any thrombus. This view can also be used to help in cannulation of the coronary sinus in the case of any technical difficulties (**Figures 2** and **3**).

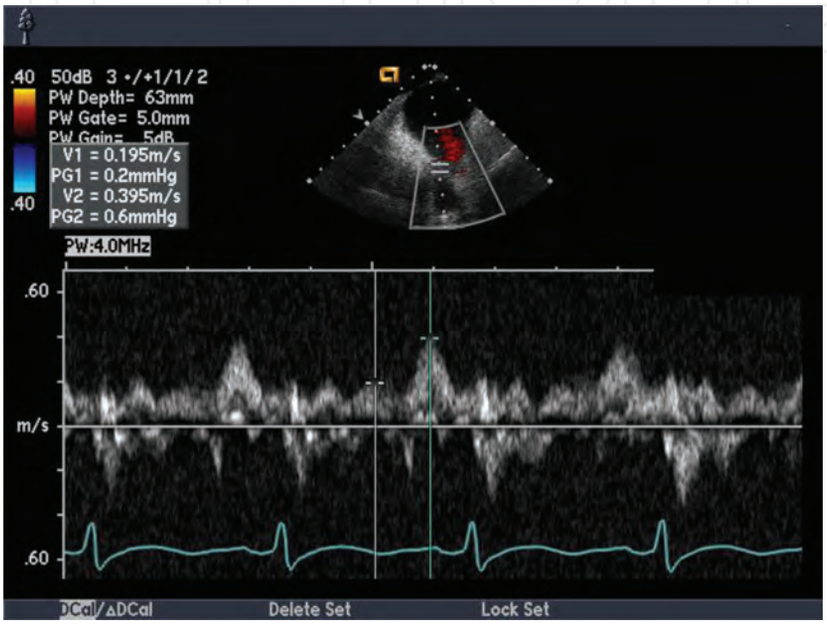

Figure 3. Continuous wave Doppler of the pulmonary veins.

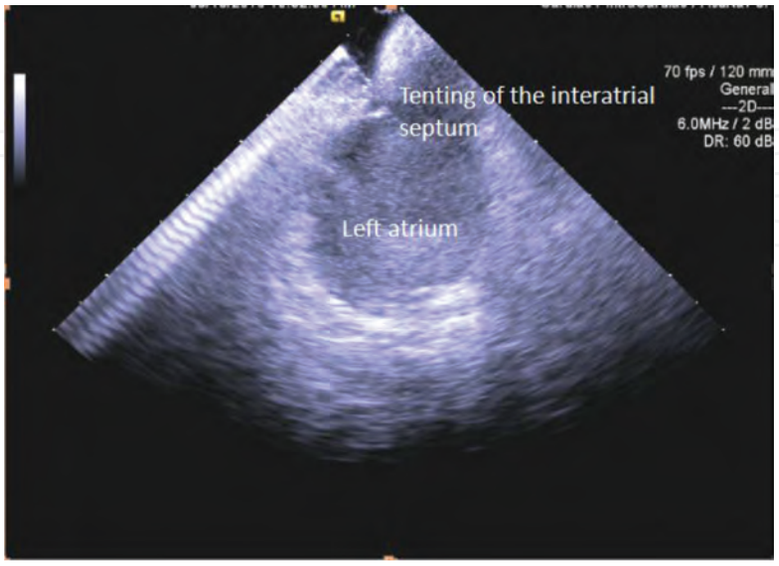

Figure 4. Tenting of the interatrial septum.

From this view, the catheter is slightly rotated clockwise. In this plane, one could visualize both left-sided pulmonary veins. The left superior pulmonary vein is usually visualized earlier and further clockwise rotation from that angle will bring left inferior pulmonary vein into visualization. This is a good view to measure the dimensions of the pulmonary vein, color Doppler of the pulmonary vein and continuous wave Doppler to evaluate the velocity of the pulmonary vein. During atrial fibrillation ablation, this view could be used to avoid ablation deep into the veins (**Figure 4**).

For the clockwise rotation of the ice catheter from this view will typically show the posterior wall of the left atrium. In this view, one could visualize esophagus and descend aorta. Esophageal temperature probe catheter can be visualized in the esophagus from the right atrium using this view. During ablation of the posterior wall of the right atrium, it would be easy to visualize the echogenicity of the lesion and proximity to the esophagus. Continued clockwise rotation of the ice catheter from this view will bring the right-sided pulmonary veins closer to the imaging surface of the ice catheter. The right-sided pulmonary veins will be visualized in a short axis. Using color Doppler, we could identify the pulmonary vein flow. Further advancement of the catheter into the right atrium and continued clockwise rotation from this level will bring up the right superior pulmonary vein in a better imaging plane. We will be able to see both right-sided pulmonary veins and pulmonary artery at this level. Usually, the right superior pulmonary vein is one of the most difficult veins to visualize. Sometimes the addition of a slight posterior tilt and right or left steering can further optimize this image to visualize the right superior pulmonary vein. Further clockwise rotation from this view will bring the catheter to the home view.

From the home position, ice catheter is advanced with a little bit of posterior flexion and rightward tilt. At this view, one could visualize the junction of the superior vena cava with right atrium. This view is commonly used to advance the guidewire into the superior vena cava before transseptal puncture. From here, the ice catheter is pulled down a little bit with continued posterior and right tilt. Now, they can clearly visualize interatrial septum including limbus and fossa ovalis. Typically, the operator advances the transseptal access needle in this view. One will be able to identify the tenting of the interatrial septum and further advancement of the transseptal needle into the left atrium. Slight clockwise rotation over here will help the operator to visualize and estimate the distance between the transseptal access site and posterior left atrial wall, thereby avoiding perforation into the left atrial posterior wall during transseptal access. Similarly, the distance between the transseptal access and left lateral wall can also be assessed in the previous imaging plane and hence avoiding left atrial perforation during transseptal access.

7. How does one use ICE catheter in ventricular tachycardia ablation?

From the home view, the catheter is tilted anteriorly. Now, we can visualize the posterior tricuspid leaflet and inferior wall of the right ventricle. The catheter is further advanced through the tricuspid valve into the right ventricle with continuous monitoring of the ICE

http://dx.doi.org/10.5772/65243

imaging. Once the catheter is just below the aortic valve in this view, further anterior tilt will make the catheter flex towards the inferior part of the right ventricle. This view is a good view to visualize the long axis of the posteromedial papillary muscle. From here, the anterior tilt is gently released in the catheter is further advanced towards the right ventricular apical region. Here, the catheter is brought to a neutral position with no tension on the knob. From here, clockwise rotation of the catheter will help us in visualizing the interventricular septum. This is also a good view of the epicardial axis as the right ventricular apical region is well visualized over here. With continuous clocking from here, we could visualize the posteromedial papillary muscle, and further clocking will bring the popular anterolateral muscle. The left ventricle cavity will be well visualized. Further clocking will also bring aortomitral continuity into the picture. Further advancement of the catheter into the right ventricle outflow tract with continued clockwise rotation will bring left ventricular outflow tract into the picture in a short axis view. We will be able to see all the three cusps of the aortic valve. Here noncoronary cusp will be adjacent to the inter-atrial septum; right coro-

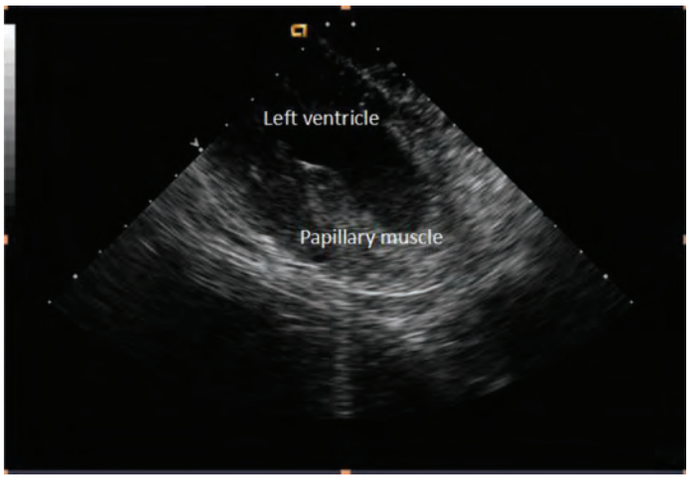

Figure 5. Left ventricle.

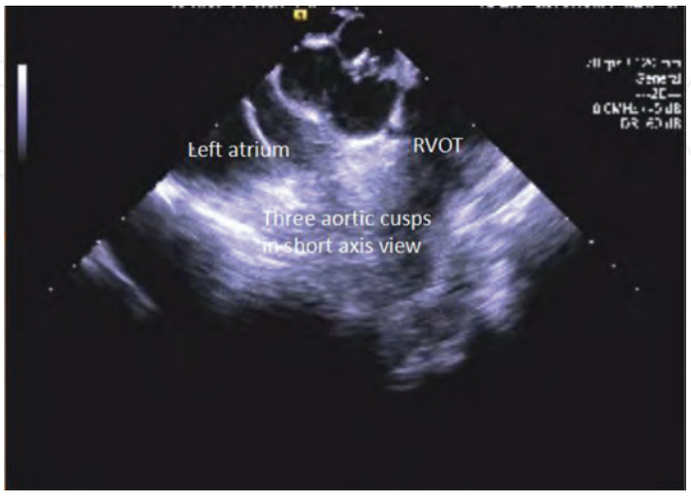

Figure 6. Aortic cusps.

nary cusp will be adjacent to the right ventricular outflow tract and left coronary cusp will be adjacent to the left ventricular outflow tract. In this view, one can also visualize left atrial appendage. In between the left coronary cusp on the left atrial appendage, we may be able to see left main coronary artery or left anterior descending artery. Further clockwise rotation over here will bring the aortic valve and ascending aorta in long axis (**Figures 5** and **6**).

8. How does one use ICE catheter to avoid complications during electrophysiological procedures?

Ice catheter can be used to monitor the catheter contact with the tissue. This helps us to make sure that they are ablating the right structure. It also helps us to maintain a better stability during respiration or with cardiac motion. With the help of the near field lesion visualization, one could avoid over ablating a region. Steam pops can happen during ablation secondary to high temperatures in the tissue. Impending signs of steam pop like increased echogenicity and microbubbles can be seen using ice catheter and hence avoiding imminent complications including perforation. Ice catheters also help us in negotiating through the valves safely without getting entangled in the valve apparatus. During ablation, continuous monitoring of the pericardial space can identify an early pericardial effusion thereby avoiding a less optimal outcome for the patient.

9. Conclusion

Imaging using intracardiac echocardiography has led to significant improvement in the safety and efficacy of the complex local physiological procedures. In addition to this, less dependence on the fluoroscopy also produces the occupational hazards for the physicians and the patients.

Author details

©2016 Umashankar Lakshmanados, Louisiana State University Health Science Center, Shreveport, USA. Originally published in "Introductory Chapter: Practical Approach to the Use of Intracardiac Echocardiography in Invasive Electrophysiology Procedures" IntechOpen Available from http://dx.doi.org/10.5772/65243

Chapter 5

Speckle-Tracking Imaging, Principles and Clinical Applications: A Review for Clinical Cardiologists

Iacopo Fabiani, Nicola Riccardo Pugliese, Veronica Santini, Lorenzo Conte and Vitantonio Di Bello

Additional information is available at the end of the chapter

http://dx.doi.org/10.5772/64261

Abstract

Evaluation of myocardial mechanics, although complex, has now entered the clinical arena, thanks to the introduction of bedside imaging techniques, such as speckle-tracking echocardiography.

Overcoming the limitations of previous techniques, such as tissue Doppler Imaging (TDI), bi-dimensional (2D) and, only recently, three-dimensional (3D) speckle tracking, allows a fast, reproducible, and semi-automated description of myocardial deformation parameters, including strain, strain rate, velocity, displacement, torsion, and timing of contraction/relaxation. From research tool, speckle tracking has become a great help for clinicians, validated with respect to more complex, time-consuming, and expensive techniques.

Nowadays, further development in technology and image processing draws the attention of the cardiology community. This review intends to describe the fundamental aspects of the imaging technique, together with some recent innovations and clinical applications in this field.

Keywords: cardiac mechanics, deformation, strain, strain rate, speckle tracking

1. Introduction

Speckle-tracking imaging (STI) is a non-invasive ultrasound technique that allows an objective and quantitative evaluation of global and regional myocardial function, independently from the angle of insonation and partly from cardiac translational movements [1–4].

Technique	Advantage	Disadvantage
STI	• Analysis in 2D	• Temporal resolution
	• Tissue movement relative to adjacent segments	• Poor image quality
	• Angle independency	• Myocardial curvature
	• Spatial resolution	• Lower frame rates in tachycardia
	• Low noise	
	• Automated tracking system	
	• Lower interobserver variability	
TDI	• Adequate image quality	• Interobserver variability
	• Temporal resolution	• Time-consuming
		• Technically demanding
		• Low signal-noise ratio
		• Poor spatial resolution
		• Angle dependency
		• One dimension
		• Displacement in relation to transducer

2D, bi-dimensional; STI, speckle-tracking imaging; TDI, tissue Doppler imaging

Table 1. Advantage and disadvantage of different techniques for myocardial deformation analysis.

Echocardiographic estimation of segmental left ventricular contractility is routinely accomplished through visual interpretation of endocardial motion and myocardial thickening. This method is subjective and requires a relatively experienced observer. Quantitative analysis based on tracing of the endocardial border may also be hampered by endocardial "dropout" and trabeculations.

Tissue Doppler imaging (TDI) has been previously used in deriving myocardial velocities and assessing fundamental parameters of myocardial deformation (strain and strain rate) [5]. Myocardial tissue velocities represent the net effect of the contractile and elastic properties of the area under investigation and the motion caused by traction and tethering from other regions. In contrast, strain is a dimensionless index reflecting the total deformation of the ventricular myocardium during a cardiac cycle, as a percentage of its initial length. Strain rate is the rate of deformation or stretch. Strain techniques are, in principle, the optimal modalities for the assessment of regional myocardial function. The major limitation of TDI has been its angle dependency [5], requiring alignment of the ultrasound beam parallel

http://dx.doi.org/10.5772/64261

to the direction of tissue movement. Thus, deformation study was substantially limited to the analysis of the tissue moving toward or away from the probe (**Table 1**).

STI is based on bi-dimensional (2D) echocardiographic technology, not limited by Doppler analysis [6–8]. Segments of myocardial tissue show a pattern of gray values in the ultrasound. This pattern, resulting from the spatial distribution of gray values, is commonly referred to as speckle pattern, characterizes the underlying myocardial tissue acoustically and is unique for each myocardial segment. Speckle tracking allows the measure of all in-plane components of the velocity vector, in all pixels [9]. More recently, the addition of the third dimension (3D) has partly expanded the scope of this technology.

2. Human myocardium

Human myocardium is made up of multiple layers [10–12]. According to the helical model described by Torrent-Guasp, a single myocardial muscle band folding upon itself creates varying orientations of fibers throughout the myocardium, with two principal loops, basal (transverse) and apical (oblique). Myocardium finally consists of three separate layers: transversely oriented circular fibers that wrap (around both ventricles), the inner oblique layer (clockwise rotation), and the outer oblique layer (counterclockwise rotation). Briefly, the myofiber geometry of the LV changes gradually from a right-handed helix in the subendocardium to a left-handed helix in the subepicardium.

The mechanics of the LV is complex, but three principal components contribute to systole: inward motion, longitudinal motion (base moving toward the apex), and differential rotation of the apex and base (twisting). Diastolic mechanics is the opposite of systolic motion. LV torsion (or twist) has an important role in cardiac systo-diastolic mechanics. During the cardiac cycle, there is a systolic twist and an early diastolic untwist around left ventricular long axis, due to opposite apical and basal rotations. Systolic apical rotation is counterclockwise and basal rotation is clockwise [13]. LV rotation is a sensitive indicator of changes in regional and global LV function.

2.1. Cardiac mechanics and limits of conventional indices

Cardiac function is the result of force development (inotropism: opening of the cardiac valves) and deformation (shortening of the myocytes: volume ejection) and can be evaluated globally (pump performance) or regionally [14]. Correct evaluation of systolic function should focus on the intrinsic properties of the fibers and myocytes that represent the real actors behind heart function as well as a pathologic process. The deformation of a myocardial segment during the cardiac cycle is a complex phenomenon and consists of normal deformation (longitudinal shortening/lengthening, radial thickening/thinning, and circumferential shortening/lengthening) and shear deformation (base-apex twisting, epi-endo circumferential shear, and epi-endo longitudinal shear). There is a clear gradient from base to apex in both velocity and displacement (stationary of the apex within the thorax while the base is moving toward it). In contrast, deformation is more or less homogenous throughout the (normal) myocardial wall.

It is important to understand the relation between intrinsic function (contractility) and the resulting motion/deformation. A myocardial segment develops a force but it is also subject to the forces developed by near segments. The intrinsic contractile force of the myocardium (inotropism) is the most important determinant of myocardial performance, but any segment of myocardium is part of a ventricle, with external forces acting up on it (mostly in the opposite direction of the contractile force) and resulting from local wall stress, caused by the intracavitary pressure (related to local geometry of the ventricle) and the interaction with neighboring contracting segments ("pulling" the segment itself). The relationship between acting forces and the resultant deformation is influenced by regional elasticity, which by itself is not a constant; due to the structure of the tissue, the more the myocardium is stretched, the more difficult it becomes to stretch it even further.

Regional myocardial deformation is thus the result of:

Active forces:

- Intrinsic contractility (influenced by tissue perfusion and electrical activation).

Passive forces:

- Intracavitary pressure (afterload/preload; ventricular geometry);
- Segment interaction.

Tissue elasticity:

- Myofibrillar architecture;
- Collagen amount (fibrosis).

Despite this pathophysiological insight, echocardiography is still mainly based on global and indirect indices such as ejection fraction, a volume-based parameter that does not reflect contractility, being based on geometric assumptions. For example, "supranormal" values of ejection fraction (EF) are often found in hypertrophied or volume-overloaded ventricles, thus not reflecting real changes in contractility. EF is also load dependent and, per se, is only a global index, without regional implications and not taking into account segmental interactions, which do not contribute to pump function. Moreover, indices for global functional assessment reflect mainly radial function, ignoring longitudinal function, which is usually altered long before changes occur in radial indices.

2.2. The concept of myocardial deformation

When two neighboring points of the myocardium move at different velocities, myocardium changes its shape (deforming). Otherwise, myocardium is moving but not deforming. When the velocity of the tissue is known, several other parameters can be derived.

Displacement is the integral of the velocity over time (Eq. (1)).

http://dx.doi.org/10.5772/64261

$$d = \int_{T_0}^{T} v(t)dt \tag{1}$$

Strain and strain rate are measures of changes in shape, that is, deformation.

For mono-dimensional deformations, that is, shortening or lengthening, the simplest measurement is conventional or Lagrangian strain (Eq. (2)).

$$\varepsilon(t) = \frac{L(t) - L_0}{L_0} \tag{2}$$

The Greek letter epsilon (ε) is commonly used as a symbol for conventional strain. The strain value is dimensionless and can be presented as a fractional number or as a percentage. For Lagrangian strain, a single reference length (L_0) is defined, against which all subsequent deformation ($L(t)$) will be measured. Strain is positive if L is major than L_0 (an object has lengthened) and negative if L is smaller than L_0 (shortening). If L equals L_0, the strain is thus zero.

Natural strain (ε') is defined as [15]:

$$\varepsilon' = \ln(\frac{L}{L_0}) \tag{3}$$

Natural strain employs a reference length that changes as the object deforms. It therefore describes the instantaneous length change and it is independent of reference times. Compared to that of conventional strain, the natural strain amplitude is smaller for positive strains and larger for negative strains. This concept applies in principle to all three one-dimensional (longitudinal, circumferential, and radial) displacement and strain components.

In two or three dimensions, we should also consider shear strain, i.e., measurement of deformation in angle. It is also mandatory to specify directions and magnitudes of maximal and minimal strain.

The strain rate is the temporal derivative of the strain (Eq. (4)).

$$\varepsilon' = \frac{d\varepsilon}{dt} \tag{4}$$

Whereas strain indicates the amount of deformation, strain rate indicates the rate of the deformation. The spatial gradient in myocardial velocities represents the rate of myocardial deformation, that is, the strain rate. The unit of the strain rate is normally 1/s or s^{-1}. Strain rate is more uniformly distributed along the different regions of the LV, whereas myocardial velocity decreases from base toward apical parts of the LV. Strain can subsequently be derived

by temporal integration of the strain rate curve. Indeed, if the rate of deformation is known at each time instance during the cardiac cycle, the total amount of deformation can easily be calculated. A positive strain rate means that the length of the object is increasing, whereas a negative strain rate means that the length is decreasing. If the length is constant, the strain rate is zero. Therefore, whereas strain is a measurement of deformation relative to a reference state, strain rate is an instantaneous measurement. When the strain rate has been calculated for each time point during the deformation, the strain can be found as the temporal integral of the strain rate (Eq. (5)).

$$\varepsilon' = \int_{T_0}^{T} \varepsilon'(t)dt \tag{5}$$

2D strain comprises four measurements: two natural strains and two shear strains [6].

A 3D model allows the evaluation of three natural strain and six shear strain measurements along *x*, *y*, and *z* or azimuthal axes.

2.3. Fundamentals of speckle tracking

"Speckles" are small groups of myocardial pixels created by the interaction of ultrasonic beams and the myocardium, with specific gray scale characteristics. A speckle is commonly defined as the spatial distribution of gray values in the ultrasound image. The result of a speckle-tracking procedure (followed by regularization process) is an estimate of the in-plane velocity vector in all pixels in each of the frames of the ultrasound data set (dynamic velocity vector field). The spatial distribution of the gray values within the ultrasound image is due to constructive and destructive interference of reflections from the individual scatterers within the myocardium. Reflections occur at transitions between different types of tissues or at specific sites, and are much smaller than the wavelength. Constructive interference generates a high-amplitude signal, destructive a low-amplitude one. The exact scatter positions determine the speckle characteristics. Speckle-tracking technology offers the ability to identify and track the same speckle throughout the cardiac cycle [4].

In the ultrasound image, we see the speckle pattern occurring at a position further away from the transducer. To correctly detect speckles, the motion of the tissue should be slower than the motion of the ultrasound beam (image lines). Sound waves propagate through tissues at an average velocity of 1530 m/s, while myocardial tissue moves at velocities in the order of centimeters per second: the basic condition is thus clearly met [16].

There are different algorithms used by different vendors in tracking these speckles. Some speckle-tracking methods are based on so-called block matching, where a region in the image is selected (the kernel) and is followed in the next image frame by subsequently trying out different positions and by determining the similarity between the kernel and the pattern observed in that position. The position where the similarity between the kernel ("fingerprint") and the observed pattern is maximal is assumed to be the new position of the speckle pattern

http://dx.doi.org/10.5772/64261

[16]. Another common approach is based on conservation of gray value, that is, it is assumed that gray values do not change over time. Radio frequency (RF) speckle—used in block-matching method—is a high-frequency signal, so that small between-frame motion can be detected, whereas its corresponding gray-scale speckle—used in gray-scale tracking—is derived from lower-frequency signals, being less sensitive to small displacements. Importantly, speckle tracking of gray-scale images does not necessarily perform well on high frame-rate data [16]. Then, RF-based methods allow to obtain a higher spatial, temporal, and velocity resolution because they use a signal with a higher-frequency content; at the same time, these methods are more sensitive to decorrelation and noise, requiring more severe regularization, which in turn might limit their resolution. Because both RF and gray-scale approaches offer advantages, a hybrid method was recently proposed.

So far, it is possible to evaluate the direction of movement, the speed of movement, and the distance of such movement at any point in the myocardium, independently from the transducer, relative to adjacent segments. The semi-automated nature of speckle-tracking echocardiography guarantees good intra-observer and inter-observer reproducibility [4].

Given that the velocity vector field is known for all pixels within the image, the axes are known with minimal user interaction. The radial, longitudinal, or circumferential velocity profiles throughout the cardiac cycle can be reconstructed, independent of the angle between the ultrasound image line and the direction of motion as in the conventional Doppler imaging [16]. The process of correcting the initial velocity vector estimates by applying additional boundary conditions based on a priori knowledge about the characteristics of the velocity field is called regularization. Regularization can consist of median filtering, weighted smoothing, elastic model, and myocardial boundaries definition.

Velocity vector imaging is partly analogous to 2D STI as it too tracks the speckles using 2D echocardiography, but utilizes additional physiological information to more robustly track the speckle kernels [17]. Each vector is an expression of direction and the magnitude of the velocity. The qualitative evaluation of the velocity is determined by comparing vectors along the tracked contour. Longitudinal strain is the percentage decrease in the length of the myocardium during systole (movement of the base toward the apex). It is expressed as a percent negative value (decrease in length in systole) [18]. Longitudinal strain may be calculated as an endocardial strain, midline strain, epicardial strain, or averaged over the entire cardiac wall. There is currently insufficient evidence to favor one way over another. Radial strain refers to the thickening of the myocardial wall during inward motion of the ventricle, measured in the short-axis views. The value is traditionally defined as percent positive (thickening in systole). Circumferential strain represents the change in the length along the circular perimeter, by definition percent negative in systole. Strain parameters can be individualized for each myocardial segment or can be expressed as global strain (averaging of all segments). Strain rate (evaluated globally or for each segment) represents rate of longitudinal, radial, or circumferential deformation in time. It has a marked systolic negative peak (S) with two positive peak in early (E) and late diastole (A).

Relevant strain values along strain curves are, but are not limited to:

- End-systolic strain: the value at end-systole;
- Peak systolic strain: the peak value during systole;
- Positive peak systolic strain;
- Peak strain: the peak value during the entire heart cycle. The peak strain may coincide with the systolic or end-systolic peak, or may appear after aortic valve closure (AVC) (it may be described as "post-systolic strain") [19].

Modern software allows display of results in bull's eye (polar map) similar to single-photon emission computed tomography (SPECT). This is more familiar to cardiologists as it depicts single myocardial segments with relative values of strain, strain rate, and time to peak strain/strain rate (synchronicity). A more unfamiliar method to display results in a monoplane view is the so-called curved anatomic M-mode (CAMM) which depicts timely variation of single parameters evaluated for a specific segment of interests from base to the apex and from septal to lateral wall. This offers a unique opportunity for timing and recognizing precise phases of a cardiac cycle (relaxation) and for the evaluation of AVC. End-systole coincides with AVC and can be visualized in the parasternal or apical long-axis view or by detecting the closure click on the spectral tracing of the pulsed-wave Doppler of aortic valve flow [19].

Rotation is the measure of the rotational movement of the myocardium in relation to an imaginary long-axis line from apex to base drawn through the middle of LV cavity 4]. Clockwise rotation is defined as negative, while counterclockwise rotation has a positive value. Twist is the algebraic difference in rotation between the apex and the base. Torsion is the twist normalized for the length of the LV cavity (degrees per centimeter). LV rotation or twisting motion has an important role in LV systolic and diastolic function. Normal values for LV rotation and twist angle have shown high variability (technique used, location of the region of interest, age, and loading hemodynamics of the ventricle). The increase in LV twist angle with age observed in literature can be explained by less opposed apical rotation, resulting from a gradual decrease in subendocardial function with aging. Worsening of diastolic relaxation and reduced diastolic suction is, however, associated with an early reduced and delayed diastolic untwisting.

Myocardial strain and Strain Rate (SR) are sensitive parameters for the quantification of diastolic function. Diastolic SR signals can be recorded during isovolumic relaxation, during early filling, and in late diastole. The hemodynamic determinants of protodiastolic strain rate include LV relaxation, regional diastolic stiffness, systolic function, end-systolic wall stress, and filling pressures. In addition, protodiastolic strain rate can assess interstitial fibrosis and can be used to identify viable myocardium after stunning and infarction. Measurement of diastolic strain and strain rate may be useful for research applications but is presently not recommended for routine clinical use.

The detection of myocardial fibrosis and viability depends on the evaluation of myocardial characteristics and shape during the cardiac cycle. Fibrotic tissue may be focal (as occurs in patients with myocardial infarction [MI]) or diffuse (systemic or metabolic disturbances). Fibrosis is actually accurately identified using myocardial late enhancement or T-weighted

http://dx.doi.org/10.5772/64261

mapping with cardiac magnetic resonance imaging (MRI), but speckle tracking (especially systolic and protodiastolic strain rate) has a good correlation with tissue fibrosis, evaluated via cardiac magnetic resonance or biopsy.

All these parameters can be measured not only for the LV but also for the right ventricle (RV) and left and right atria (LA and RA, respectively), but have not been fully validated and, still together, commercial applications to process these chambers do not exist.

Timing peak strain is pivotal in defining dyssynchrony as well as for the evaluation of ischemia (post-systolic thickening or shortening).

2.4. Image acquisition

Gated images are obtained during end-expiratory breath holding with stable electrocardiographic traces, avoiding foreshortening of the ventricle and proper visualization of endocardial border. Images acquired should be of high quality. Optimal frame rate should be 60–110 frames per second (FPS). The operator should keep the sector width and depth minimal to focus on the structure of interest. Usually, three consecutive cardiac cycles are obtained and the values averaged for the final processing. Low FPS limits tracking efficacy, while higher FPS "smooths" speckle pattern and the final quality of the analysis. Apical four-chamber, two-chamber, and three-chamber views are necessary for estimation of LV strain and strain rates by 2D STI. This finally offers global longitudinal strain (GLS) value, that is, the average of longitudinal strain for all segments in all views. Parasternal short-axis views (basal, papillary muscles, and apex) are necessary for radial and circumferential strains (finally averaged in global radial and circumferential strain) and strain rates as well as for rotation, twist, and torsion analysis. The ways myocardial segments are divided widely vary among vendors, but in general, a 16–18-segment LV model is used. Myocardium is divided into six segments: basal septal, mid septal, apical septal, apical lateral, mid lateral, and basal lateral. For the timing determination of cardiac events, mitral inflow and LV outflow velocities are recorded using pulsed-Doppler echocardiography and the aortic and mitral valve closure/opening (AVC/O and MVC/O, respectively) times are obtained, as well as visually (AVC in apical long-axis view) or semi-automatically (evaluation of CAMM). The recordings are analyzed offline using semi-automated computer software for estimation of strain and strain rate by 2D STI. A region of interest (ROI) has to be outlined manually, tracing the endocardium. The epicardium is automatically traced by the system, but the wall thickness can be manually adjusted.

The ROI is defined at end-diastole by [19]:

- Endocardial border;
- Epicardial border;
- Myocardial midline.

Each of these contours can be user defined or generated automatically.

Topographic definitions of the myocardial ROI in apical views are [19]:

- "Left/right base";
- "Midbase";
- "Apex";
- "Left/right ROIs."

Vendors have incorporated tools to help users identify tracking reliability. Various methods are utilized. Some vendors have introduced protocols that identify segments where tracking is suboptimal and is excluded from the final results. In addition, some vendors provide accuracy indices to guide the user in tracking performance estimates.

Longitudinal strain is more robust and reproducible than other parameters. The values tend to be partly different for different walls and segments. There is a gradient of longitudinal strain values from base to apex (higher values for apical segments) as well as from endo to epicardium (higher values of strain in the subendocardial region). **Table 2** depicts the recently published data on normal values for different strains of LV, while **Table 3** depicts the principal advantages and pitfalls of different strain imaging techniques [20].

Longitudinal Strain	**Circumferential Strain**	**Radial Strain**
Apical septal	Anterior	Anterior
21 ± 4	24 ± 6	39 ± 16
Mid septal	Lateral	Lateral
19 ± 4	22 ± 7	37 ± 18
Basal septal	Posterior	Posterior
17 ± 4	21 ± 7	37 ± 17
Apical lateral	Inferior	Inferior
21 ± 7	22 ± 6	37 ± 17
Mid lateral	Septal	Septal
19 ± 6	24 ± 6	37 ± 19
Basal lateral	Anteroseptal	Anterospetal
19 ± 6	26 ± 11	39 ± 15

Table 2. Mean percentage left ventricular strain values for strain in healthy adults.

A recent meta-analysis identified normal values for strain as (GLS) -19.7% (95% CI, −20.4 to −18.9%), global circumferential strain (GCS) −23.3% (95% CI, −24.6 to −22.1%), global radial strain (GRS) 47.3% (95% CI, 43.6–51.0%). Age, gender, body mass index, systolic blood pressure, frame rate, and equipment vendor were considered the variables most likely to influence GLS. In a general linear model, only mean blood pressure was independently associated with higher values of strain. The differences in each strain component are probably actually linked to technical motives: the superiority of longitudinal strain is linked to the

http://dx.doi.org/10.5772/64261

reliability of measurements in the axial plane respective to azimuthal one; the variability of radial strain may reflect the limited amount of tissue to track in the short-axis view of the non-hypertrophied heart; the ROI, which is user defined, may affect the strain amplitude [21]. 2D strain parameters have been validated against tagged MRI studies and sonomicrometry studies [22–24]. 2D strain data correlate well with TDI-derived ones, although with higher strength and reproducibility [2].

	TDI	2D STI	3D STI
Feasibility	++	++	+
Reproducibility	++	++	+++
Temporal resolution (strain curves)	+++	+	–
Spatial resolution (strain curves)	++	+	+
Angle independency	–	+	++
Validation: simulated	+	+	+
Validation: in vitro	+(+)	+(+)	+
Validation: in vivo	++	++	++
Validation: other techniques in clinical scenario	++	+++	+
Defined normal values	+++	+++	–
Time sparing	–	++	++
Standardized software	–	+/-	–

2D, bi-dimensional; 3D, three-dimensional; STI, speckle-tracking imaging; TDI, tissue Doppler imaging.

Table 3. Tissue Doppler imaging, bi-dimensional and three-dimensional speckle-tracking imaging.

2.5. 3D strain

With developments in ultrasound transducer technology and both hardware and software computing, systems capable of acquiring real-time volumetric LV data are now widely available. Reasonable spatial and temporal resolution of 3D data sets can now be achieved. The ability to estimate true 3D myocardial motion and deformation using various STI approaches may provide cardiologists with a better view of regional myocardial mechanics, which may be important for diagnosis, prognosis, and therapy. These 3D approaches can measure all strain components in all LV segments from a single acquisition [25–27]. Furthermore, they are angle independent, do not suffer from strain estimation errors associated with out-of-plane motion, and may in theory allow more precise calculations of LV twist and assessment of shear strain components [28–31]. This tool is promising for the evaluation of deformation parameters, although only preliminary data are available. A single apical full-volume acquisition is performed, according to standard modalities, with an FPS between 18 and 25 (3D temporal resolution is lower than that obtained with 2D images) [32]. This avoids multiple acquisitions making readily and instantaneously available evaluation of strain

parameters and torsion. The operator is able to limit foreshortening and properly identify walls and segments [33, 34]. 3D strain offers a combined assessment of longitudinal and circumferential strain [35]. To evaluate transmural (radial) deformation, due to image quality and tracking limitation, a derivative parameter, area strain, has been introduced. However, it is important to note that full volume is the result of a stitching process, which can limit tracking of speckles. Frame rate and lateral resolution can also limit good tracking.

2.6. Recent advances and consensus: need for standardization

Recognizing the critical need for standardization in strain imaging, in particular in order to derive a common standard for GLS, the most affordable parameter, in 2010, the European Association of Echocardiography and the American Society of Echocardiography (ASE) invited technical representatives from all interested vendors to participate in a concerted effort to reduce intervendor variability of strain measurement [36, 37]. In order to obtain a perfectly defined strain, synthetic ultrasound images simulated from mathematically modeled ventricles (phantoms) were developed. Jan D'hooge and colleagues from the University of Leuven generated cine loops mimicking normal, hypertrophied, and dysfunctional ventricles (**Figures 1**–**3**), and provided them to the vendors: after several attempts, results were similar for the principal vendors.

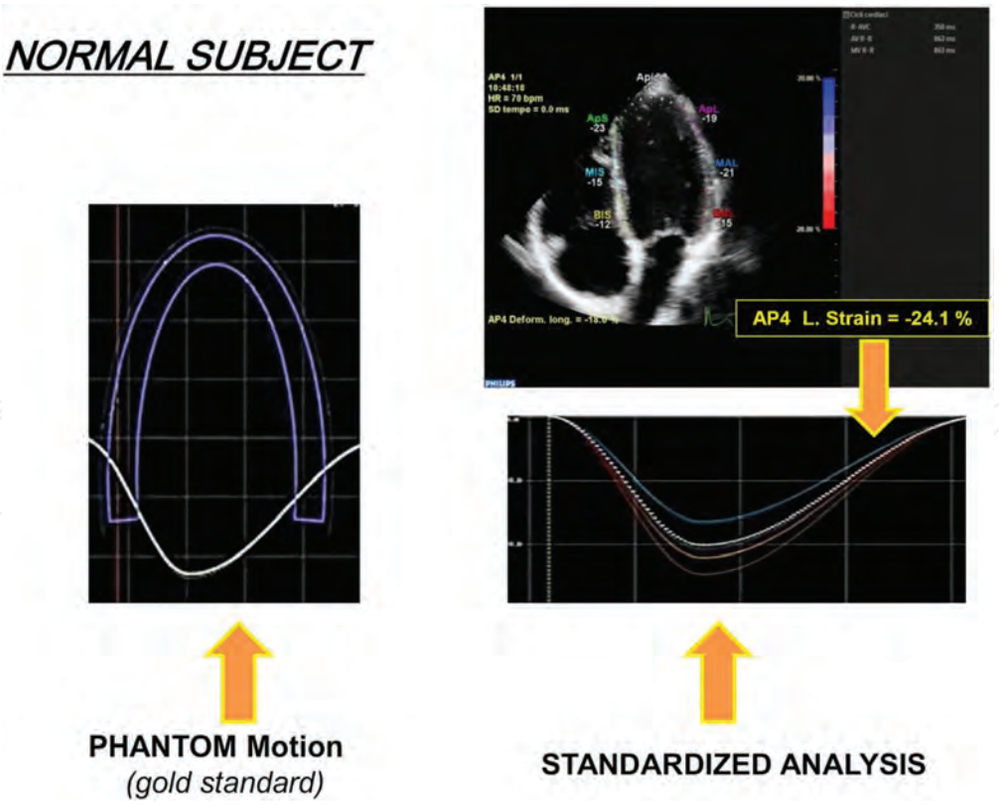

Figure 1. Global longitudinal strain calculation from phantom model (normal). AP4: apical four-chamber view; L. Strain: longitudinal strain.

http://dx.doi.org/10.5772/64261

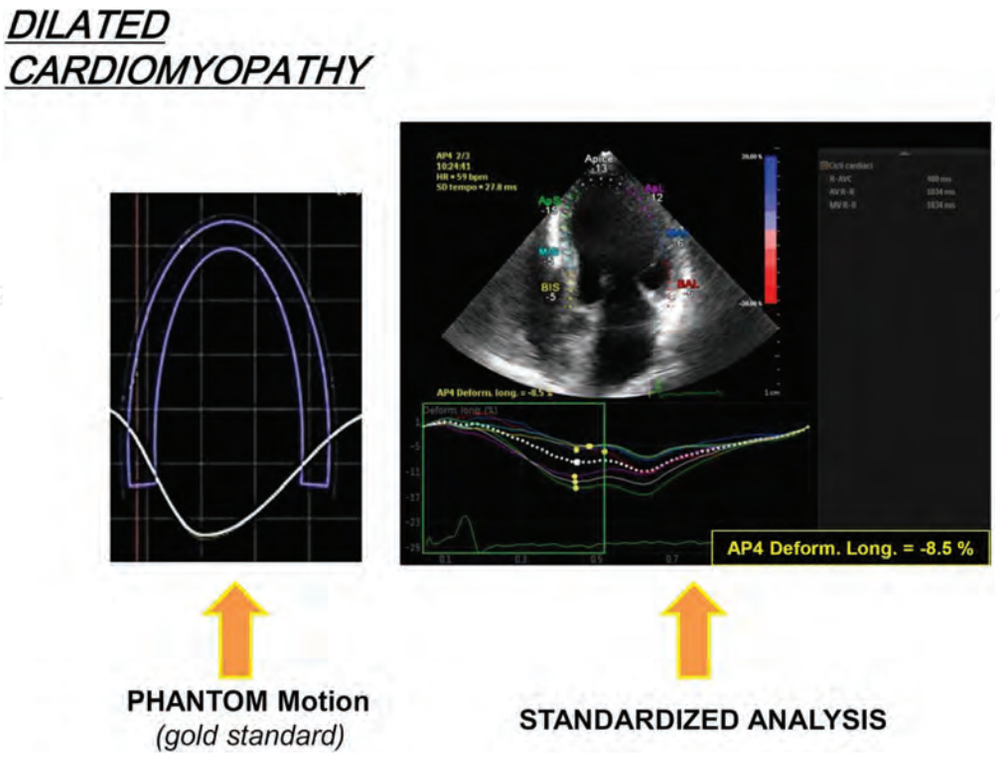

Figure 2. Global longitudinal strain from phantom model (dilated cardiomyopathy). AP4: apical four-chamber view; Deform. Long.: longitudinal deformation.

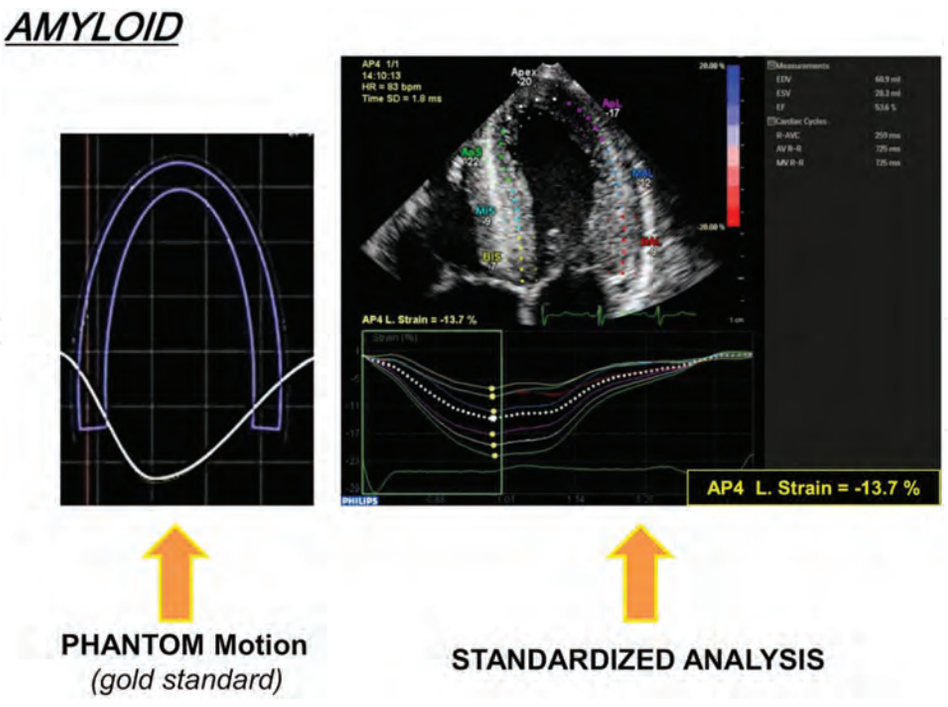

Figure 3. Global longitudinal strain from phantom model (amyloid). AP4: apical four-chamber view; L. Strain: longitudinal strain.

Moreover, a great effort has been made to standardize, speedup, and automatize (less subjective approach) GLS calculation, in order to offer immediate results to clinicians (bedside) and avoid errors in calculations (heart rate variability).

2.7. Clinical applications

2D STI has a wide field of clinical applications. We focus on main and novel fields of application (see also '**Table 4**') [38–48].

Field of Application	Explanation
Myocardial ischemia	Reduction in strain by 2D STI more objective than WMSI. Longitudinal, radial, and circumferential strain reduction in ischemia.
Myocardial infarction	Differentiation of transmural from subendocardial infarction. Remodeling.
Myocardial viability	Objective evaluation during stress echo. Differentiation of active contraction from passive tethering.
Heart failure with normal LVEF (HFnEF)	Twisting/untwisting.
Cardiac resynchronization therapy (CRT)	Longitudinal strain from TDI velocity with 2D STI radial strain. Longitudinal strain delay index. Radial strain and survival.
Takotsubo cardiomyopathy	Impaired longitudinal strain.
Restrictive cardiomyopathy	Impaired longitudinal deformation and twist.
Constrictive pericarditis	Impaired LV circumferential deformation and torsion.
Cardiotoxicity	Chemotherapy.
Detection of subclinical myocardial disease	Systemic hypertension, diabetes mellitus, systemic sclerosis, amyloidosis, and Duchenne's muscular dystrophy.
Valvular heart disease	Decreased radial, circumferential, and longitudinal strain in patients with severe aortic stenosis despite normal EF. Septal strain and mitral regurgitation.
Congenital heart disease	Right ventricular longitudinal strain and strain rate.

2D, bi-dimensional; 3D, three-dimensional; EF, ejection fraction; HFnEF, heart failure with normal ejection fraction; LV, left ventricle; STI, speckle-tracking imaging; TDI, tissue Doppler imaging; WMSI, wall motion score index.

Table 4. Principal clinical applications of speckle-tracking echocardiography.

Moreover, a recent meta-analysis presented the incremental value respective to EF retained by GLS [49]. It is essential to understand that technology development has today made available a fast, objective (automatized), and standardized definition of GLS, with final representation of bull's-eye plot of longitudinal strain value making it appealing, easily recognizable, and aligned with standardized segmentation of LV wall (**Figures 4** and **5**).

http://dx.doi.org/10.5772/64261

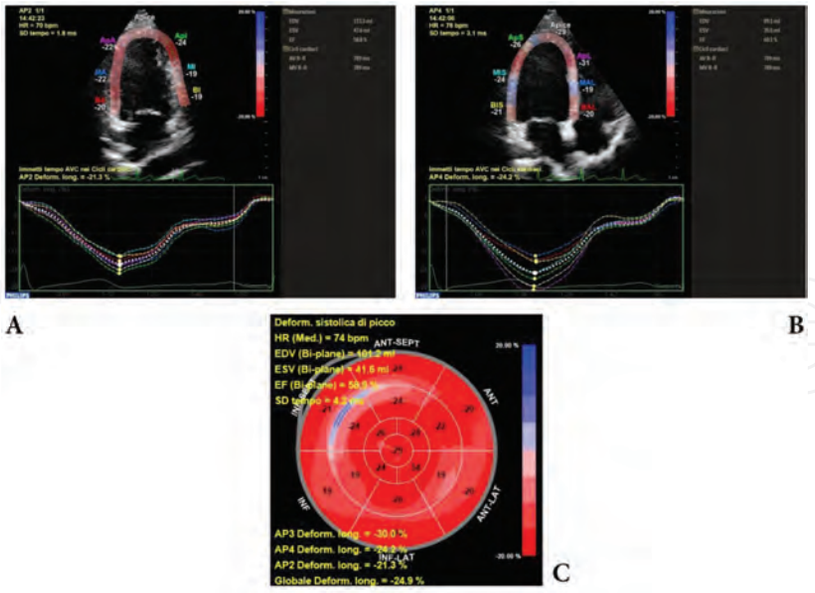

Figure 4. Global longitudinal strain calculation: on top showing tracking in four- (**B**) and two- (**A**) chamber view with strain curves; final bull's-eye plot (**C**) showing global results and superimposed regional values (Normal subject). AP2: apical two-chamber view; AP3: apical three-chamber view; AP4: apical four-chamber view; Deform. Long.: longitudinal deformation; EDV (bi-plane): end-diastolic volume (bi-plane); ESV (bi-plane): end-systolic volume (bi-plane); EF (bi-plane): ejection fraction (bi-plane); global Deform. Long. (GLS): global longitudinal strain; HR: heart rate.

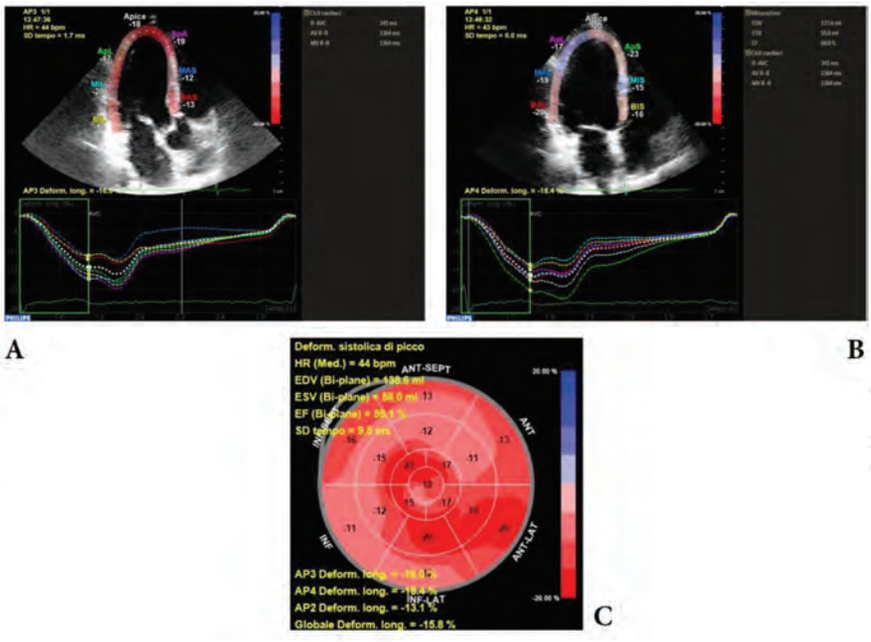

Figure 5. Global longitudinal strain calculation: on top showing tracking in three- (**A**) and four- (**B**) chamber view with strain curves; final bull's-eye plot (**C**) showing global results and superimposed regional values (dysfunctioning patient). AP2: apical two-chamber view; AP3: apical three-chamber view; AP4: apical four-chamber view; Deform. Long.: longitudinal deformation; EDV (bi-plane): end-diastolic volume (bi-plane); ESV (bi-plane): end-systolic volume (bi-plane); EF (bi-plane): ejection fraction (bi-plane); global Deform. Long. (GLS): global longitudinal strain; HR: heart rate.

2.7.1. Ischemic cardiomyopathy

In coronary artery disease, an assessment of myocardial ischemia other than simple visual wall motion score estimation (high inter-observer variability) has been invoked from a long time. Regional velocities (TDI) as well as peak systolic strain rate and systolic strain (TDI and STI) reduce linearly with a reduction in regional perfusion, time-delay prolongation to treatment, and the presence of fibrosis [14, 50, 51]. Subendocardial longitudinal fibers are the most vulnerable ones, resulting in an early deterioration of longitudinal strain, followed by radial and circumferential strains. Anyway, it's rather improper to consider a "radial function," because there are no myocardial fibers going in the radial direction. Actually, wall thickening measured by radial strain is a function of wall shortening, as the heart muscle is incompressible. At the same time, circumferential strain does not reflect circumferential fiber contraction because circumferential shortening is mainly due to the inward movement of mid-wall circumference as the wall thickens (inwards—as described by the eggshell model) [52–54]. Briefly, there would have been circumferential shortening even without circumferential fibers. These aspects, together with less standardized values than GLS, make GRS and GCS considerably reliable.

Dobutamine stress echocardiography is an important area of interest because in normal tissues an increased deformation occurs (continuously increasing strain/strain rate) as long as filling is not reduced by increased heart rate. On the contrary, acutely ischemic tissue during stress test shows less deformation and post-systolic deformation (PSD, thickening/shortening with radial/longitudinal strain, respectively), that is, the continued contraction of the myocardium after AVC. PSD is a common finding in myocardial ischemia. All these alterations are proportional to the severity of ischemia and persist in the experimental setting for up to 2 h after the ischemic insult resolution, with a peculiar time decay [55–57]. A noteworthy fact is that the stunned myocardium is characterized by decreased systolic deformation and PSD at rest, but almost normal systolic deformation and disappearance of PSD with dobutamine [50]. This behavior could be secondary to the heterogeneous contractile properties of the myocardium, probably linked to myofibrillar edema reducing the effective force myocardium can develop [58]. Furthermore, interstitial myocardial edema results in a sudden and temporary increase in end-diastolic wall thickness (this behavior is observed also in infarcted segments at the moment of reperfusion) [59, 60]. In chronic infarction, dobutamine is associated with low or no deformation increase, depending on the fibrosis extension (from subendocardial to transmurality involvement) [50].

2.7.2. Volume overload

Deformation is also closely related to ventricular geometry. Dilation is the end stage of most of the cardiomyopathies and heart valve diseases because for a given volume, the object with the smallest surface area is the sphere. This means that the same deformation (determined by the contractile force) can generate a larger stroke volume in a dilated heart. Similarly, in a dilated heart the same amount of stroke volume can be generated with less contractility and less deformation, that we can directly evaluate with strain(-rate) [14]. Remodeling in the long term will lead to irreversible damage to the heart muscle and finally ventricular dysfunction,

http://dx.doi.org/10.5772/64261

but there is no specific diagnostic method to detect subclinical changes in systolic function. STI and TDI might potentially be useful in detecting subclinical changes in cardiac function [60].

Mitral regurgitation (MR) is a typical volume overload condition. Primary MR leads to cardiac remodeling, increased left ventricular filling pressure, pulmonary arterial hypertension, and myocardial dysfunction. Conventional 2D, M-mode, and Doppler examination play a critical role in the initial and longitudinal assessment; anyway, most variables are load dependent and both afterload and preload are altered during the disease course. TDI and STI provide new parameters to assess regional and global myocardial performance and may help in identifying asymptomatic patients and choosing the optimal time for surgical correction. It is worthy to note that patients with severe primary degenerative MR may have near-normal left ventricle ejection fractions (LVEFs) because of disproportionately higher compensation in GLS. Moreover, the higher the GLS, the higher the risk of substantial reduction in LVEF (>10%) during the immediate postoperative period [61]. On the contrary, in patients tested at 6 months after surgery, when LV reverse remodeling has already settled, LVEF reductions >10% were associated with lower baseline strains [62]. Chronic ischemic MR instead is not a valvular disease per se but is rather a "ventricular disease." In particular, inferior MI has been recognized as the most frequent cause of ischemic MR because of the geometric distortion in the papillary muscle-bearing segments [63]. Therefore, the site of MI might be a more important determinant of MR degree in LV dysfunction than the extent of post-MI LV remodeling. Under normal conditions, the basal rotation, which is determined mainly by inferior and posterior myocardial segments [64], shortens the distance between the mitral valve and the head of the papillary muscles, contributing to MVC and counterbalancing the tethering forces. When local remodeling occurs, as in patients with inferior-posterior MIs, the basal strain and basal rotation are significantly lower and fail to shorten the distance between the papillary muscles and the mitral valve. Interestingly, Zito et al. demonstrated that basal rotation but not basal strain was an independent predictor of the severity of MR [65].

2.7.3. Pressure overload

Considering pressure overload pathology, aortic stenosis (AS) is the most common valve lesion causing chronic pressure overload on the LV. The development of symptoms in AS heralds a malignant phase of the condition and prompt aortic valve replacement results in a clear reduction in mortality [66]. In contrast, the management of patients with severe AS in the absence of symptoms remains one of the most controversial and debated areas in modern cardiology [67, 68].

The increased afterload leads to left ventricular hypertrophy and the basal septal is the first to show changes, due to increased wall stress according to the Laplace law [69]. It first shows a decrease in strain(-rate) and the development of PSD is observed, as well as the development of localized hypertrophy (septal bulge) [70]. Recently, GLS has been shown to be an independent predictor of outcomes in patients with severe asymptomatic AS, incremental to other echocardiographic markers [71]. Not to forget, the role of exercise testing in asymptomatic AS is well established, and recommended by guidelines in equivocal cases [72].

2.7.4. Mechanical dyssynchrony

Searching for the presence of mechanical dyssynchrony to identify potentially recruitable function, rather than looking only for electrocardiogram (ECG) manifestations of ventricular conduction delay, could increase the rate of cardiac resynchronization therapy (CRT) responders [73]. Mitigation of intraventricular dyssynchrony is currently thought to be the primary mechanism of improved myocardial performance with CRT. Anyway, many patients eligible for CRT have dilated ventricles with complex motion, especially if infarcted areas are present. Moreover, in dilated hearts local motion is importantly influenced by other myocardial segments and even by right ventricular motion [74]. That's why to this day, M-mode, 2D e TDI analyses have expressed modest sensitivity and specificity in measuring dyssynchrony and improving patient selection for CRT [73].

STI-based methods, mostly assessing the time difference between maximal values form different myocardial segments (e.g. septal to posterior wall motion delay [75], septal rebound stretch [76], wasted work ratio) [77, 78], are promising, but they must be validated in multicenter randomized trials.

2.7.5. Diabetic cardiomyopathy

Another field of interest is represented by diabetes mellitus because studies showed that myocardial damage occurred in at least 30% diabetic patients when LV diameter and LVEF were normal [79]. Diabetic myocardial diastolic dysfunction seems to precede systolic dysfunction, but this might be explained by the insensitivity of techniques for detecting LV systolic function. In many but small studies, longitudinal dysfunction (segmental GLS) occurred in early stages of diabetes, while LV torsion increased compensatively [80–84].

2.7.6. Cancer therapeutics-related cardiac dysfunction

Cardiotoxicity from cancer therapy has become a leading cause of morbidity and mortality in survivors [85, 86]. A careful consideration of potential cardiotoxicity during therapy and a focus on early detection and intervention are developing. Echocardiography is the cornerstone in the cardiac imaging evaluation of patients in preparation for, during, and after cancer therapy because of its wide availability, repeatability, versatility, lack of radiation exposure, and safety. The most commonly used parameter for monitoring LV function with echocardiography is LVEF. In addition, the calculation of LVEF should be combined with assessment of the wall motion score index [87]. Anyway, 2D echocardiography appears to be reliable in the detection of differences close to 10% in LVEF [88]. Because this is the same magnitude of change used to adjudicate cancer therapeutics-related cardiac dysfunction, the sensitivity of LVEF has been questioned. Moreover, detecting a decreased LVEF after anthracyclines may be too late for treatment [89], suggesting that more sensitive parameters of LV dysfunction could be helpful. The prognostic value of early measurement of systolic deformation indices (above all ΔGLS) measured in the prediction of subsequent LV systolic function has been evaluated in several studies, both in animals [90] and in humans [91–94].

2.7.7. Left atrium

Speckle tracking was recently applied to study the myocardial mechanics of a thin-walled structure such as the LA [95–98]. For the analysis, apical views are obtained using conventional 2D gray-scale echocardiography, during a breath-hold, with a stable electrocardiographic recording. The frame rate is set between 60 and 80 frames/s, and recordings are processed using acoustic-tracking software. The LA mechanical indices are calculated by averaging values observed in all LA segments (global strain) with a 15-segment or a 12-segment model. The software generates longitudinal strain and strain rate curves for each atrial segment. The radial deformation cannot be calculated because the LA wall is thin and the spatial resolution is limited [99].

2.7.8. Right ventricle

A recent methodological study has reported the feasibility, the reference values, and the reproducibility of right ventricular longitudinal strain measured by STI in normal patients and in patients with RV dysfunction [100]. The technique is similar as for LV: global strain is the average of six single segments (ROI) traced semi-automatically and processed by software packages (today, a dedicated software for RV does not exist). The evaluation of right ventricular function with STI, considering the important limitations of other parameters and methods, could offer more detailed information about regional and global RV mechanics with important clinical implications for non-invasive evaluation of RV systolic function (subclinical RV dysfunction). Further prospective studies are necessary to define its role in the management of patients.

3. Limitations

Rotation, deformation, and out-of-plane motion can cause speckle patterns to change between acquisitions (decorrelation). Loss of tracking can be limited acquiring at a proper frame rate. Image artifacts should be avoided. In general, high-quality acquisition is a prerequisite for optimal speckle-tracking results [16].

Among limitations of the method, we should include:

- Lack of reproducibility: even if much less compared with TDI, every STI study should include an intra- and interobserver variability testing [101];
- Intervendor variability: lack of standardization results in changes in reference values [102];
- Oversimplification due to software processing algorithms: automatic tracking of epicardial border (assumption of uniform thickness of myocardium); averaging of parameters within a segment; drifting;
- 2D imaging limitations: image quality; artifacts; image dropout; frame rate (low frame: no tracking, as at high heart frequencies; high frame: limited lateral resolution); lateral resolu-

tion and depth; depth dependence of transverse tracking; out-of-plane motion in short axis limiting tracking of the same ROI; noise.

Evaluation of radial strain poses important technical challenges compared to longitudinal one.

This is due to:

- Measurements in the axial plane are more reliable than those that depend on lateral and elevation (or azimuthal) resolution;
- Limited amount of tissue to track in the short-axis view of the non-hypertrophied heart;
- Placement of the ROI is user defined;
- Intervendors' differences.

4. Conclusions

Speckle tracking is actually a reality in echocardiography. Simple protocols of acquisition and novel processing packages have made available deformation analysis in daily clinical arena.

Overcoming many of the previous limitations, thanks to technological development, including 3D introduction and STI, offers to the cardiologists the potential benefit of a solid, fast, easy, and reproducible quantization of myocardial mechanics [37].

Author details

©2016 Iacopo Fabiani[1*], Nicola Riccardo Pugliese[2], Veronica Santini[1], Lorenzo Conte[1] and Vitantonio Di Bello[1.] .

1 Dept. Section Universitary Cardio-Angiology, Surgical, Medical, Molecular and Critical Area Pathology Department, Pisa Univeristy, Pisa, Italy

2 Operative Unit Cardio-Vascular Disease Univ., Surgical, Medical, Molecular and Critical Area Pathology Department, Pisa Univeristy, Pisa, Italy

References

[1] Perk G, Tunick PA, Kronzon I. Non-Doppler two-dimensional strain imaging by echocardiography – from technical considerations to clinical applications. J Am Soc Echocardiogr. 2007;20:234–243. DOI: 10.1016/j.echo.2006.08.023

[2] Dandel M, Lehmkuhl H, Knosalla C, Suramelashvili N, Hetzer R. Strain and strain rate imaging by echocardiography – basic concepts and clinical applicability. Curr Cardiol Rev. 2009;5:133–148. DOI: 10.2174/157340309788166642

[3] Blessberger H, Binder T. NON-invasive imaging: two dimensional speckle tracking echocardiography: basic principles. Heart. 2010;96:716–722. DOI: 10.1136/hrt.2007.141002

[4] Blessberger H, Binder T. Two dimensional speckle tracking echocardiography: clinical applications. Heart. 2010;96:2032–2040. DOI: 10.1136/hrt.2010.199885

[5] Storaa C, Aberg P, Lind B, Brodin LA. Effect of angular error on tissue Doppler velocities and strain. Echocardiography. 2003;20:581–587. DOI: 10.1046/j.1540-8175.2003.01135

[6] Dandel M, Hetzer R. Echocardiographic strain and strain rate imaging – clinical applications. Int J Cardiol. 2009;132:11–24. DOI: 10.1016/j.ijcard.2008.06.091

[7] Dokainish H, Sengupta R, Pillai M, Bobek J, Lakkis N. Usefulness of new diastolic strain and strain rate indexes for the estimation of left ventricular filling pressure. Am J Cardiol. 2008;101:1504–1509. DOI: 10.1016/j.amjcard.2008.01.037

[8] Gorcsan J, 3rd, Tanaka H. Echocardiographic assessment of myocardial strain. J Am Coll Cardiol. 2011;58:1401–1413. DOI: 10.1016/j.jacc.2011.06.038

[9] Mor-Avi V, Lang RM, Badano LP, Belohlavek M, Cardim NM, Derumeaux G, et al. Current and evolving echocardiographic techniques for the quantitative evaluation of cardiac mechanics: ASE/EAE consensus statement on methodology and indications endorsed by the Japanese Society of Echocardiography. Euro J Echocardiogr. 2011;12:167–205. DOI: 10.1093/ejechocard/jer021

[10] Streeter DD, Jr., Spotnitz HM, Patel DP, Ross J, Jr., Sonnenblick EH. Fiber orientation in the canine left ventricle during diastole and systole. Circ Res. 1969;24:339–347. DOI: 10.1371/journal.pone.0132360

[11] Greenbaum RA, Ho SY, Gibson DG, Becker AE, Anderson RH. Left ventricular fibre architecture in man. Br Heart J. 1981;45:248–263. DOI: 10.1136/hrt.45.3.248

[12] Torrent-Guasp F, Buckberg GD, Clemente C, Cox JL, Coghlan HC, Gharib M. The structure and function of the helical heart and its buttress wrapping. I. The normal macroscopic structure of the heart. Semin Thorac Cardiovasc Surg. 2001;13:301–319. DOI: none

[13] Sun JP. Ventricular Torsion. In: Marwick TH, Yu CM, Sun JP. Myocardial Imaging Tissue Doppler and Speckle Tracking. Wiley-Blackwell; Hoboken, New Jersey, 2007. pp. 273–277. DOI: 10.1002/9780470692448.ch23

[14] Bijnens BH, Cikes M, Claus P, Sutherland GR. Velocity and deformation imaging for the assessment of myocardial dysfunction. Eur J Echocardiogr. 2009;10:216–226. DOI: 10.1093/ejechocard/jen323

[15] Heimdal A. Technical Principles of Tissue Velocity and Strain Imaging Methods. In: Marwick TH, Yu CM, Sun JP. Myocardial Imaging Tissue Doppler and Speckle Tracking. Wiley-Blackwell; Hoboken, New Jersey, 2007. pp. 3–16. DOI: 10.1002/9780470692448.ch1

[16] D'hooge J. Principles and Different Techniques for Speckle Tracking. In: Marwick TH, Yu CM, Sun JP. Myocardial Imaging Tissue Doppler and Speckle Tracking. Wiley-Blackwell; Hoboken, New Jersey, 2007. pp. 17–25. DOI: 10.1002/9780470692448.ch2

[17] Vannan MA, Pedrizzetti G, Li P, Gurudevan S, Houle H, Main J, et al. Effect of cardiac resynchronization therapy on longitudinal and circumferential left ventricular mechanics by velocity vector imaging: description and initial clinical application of a novel method using high-frame rate B-mode echocardiographic images. Echocardiography. 2005;22:826–830. DOI: 10.1111/j.1540-8175.2005.00172.x

[18] Biswas M, Sudhakar S, Nanda NC, Buckberg G, Pradhan M, Roomi AU, Gorissen W, Houle H. Two- and three-dimensional speckle tracking echocardiography: clinical aplications and future directions. Echocardiography. 2013;30:88–105. DOI: 10.1111/echo.12079

[19] Voigt JU, Pedrizzetti G, Lysyansky P, Marwick TH, Houle H, Baumann R et al. Definitions for a common standard for 2D speckle tracking echocardiography: consensus document of the EACVI/ASE/industry task force to standardize deformation imaging. J Am Soc Echocardiogr. 2015;28(2):183–193. DOI: 10.1016/j.echo.2014.11.003

[20] Hurlburt HM, Aurigemma GP, Hill JC, Narayanan A, Gaasch WH, Vinch CS, et al. Direct ultrasound measurement of longitudinal, circumferential, and radial strain using 2-dimensional strain imaging in normal adults. Echocardiography. 2007;24:723–731. DOI: 10.1111/j.1540-8175.2007.00460.x

[21] Yingchoncharoen T, Agarwal S, Popovic ZB, Marwick TH. Normal ranges of left ventricular strain: a meta-analysis. J Am Soc Echocardiogr. 2013;26:185–191. DOI: 10.1016/j.echo.2012.10.008

[22] Nguyen JS, Lakkis NM, Bobek J, Goswami R, Dokainish H. Systolic and diastolic myocardial mechanics in patients with cardiac disease and preserved ejection fraction: impact of left ventricular filling pressure. J Am Soc Echocardiogr. 2010;23:1273–1280. DOI: 10.1016/j.echo.2010.09.008

[23] Amundsen BH, Helle-Valle T, Edvardsen T, Torp H, Crosby J, Lyseggen E, et al. Noninvasive myocardial strain measurement by speckle tracking echocardiography: validation against sonomicrometry and tagged magnetic resonance imaging. J Am Coll Cardiol. 2006;47:789–793. DOI: 10.1016/j.jacc.2005.10.040

[24] Cho GY, Chan J, Leano R, Strudwick M, Marwick TH. Comparison of two-dimensional speckle and tissue velocity based strain and validation with harmonic phase magnetic resonance imaging. Am J Cardiol. 2006;97:1661–1666. DOI: 10.1016/j.amjcard.2005.12.063

[25] Papademetris X, Sinusas AJ, Dione DP, Duncan JS. Estimation of 3D left ventricular deformation from echocardiography. Med Image Anal. 2001;5:17–28. DOI: 10.1016/S1361-8415(00)00022-0

[26] Elen A, Choi HF, Loeckx D, Gao H, Claus P, Suetens P, et al. Three-dimensional cardiac strain estimation using spatio-temporal elastic registration of ultrasound images: a feasibility study. IEEE Trans Med Imaging. 2008;27:1580–1591. DOI: 10.1109/TMI.2008.2004420

[27] Crosby J, Amundsen BH, Hergum T, Remme EW, Langeland S, Torp H. 3-D speckle tracking for assessment of regional left ventricular function. Ultrasound Med Biol. 2009;35:458–471. DOI: 10.1016/j.ultrasmedbio.2008.09.011

[28] Hayat D, Kloeckner M, Nahum J, Ecochard-Dugelay E, Dubois-Rande JL, Jean-Francois D, et al. Comparison of real-time three-dimensional speckle tracking to magnetic resonance imaging in patients with coronary heart disease. Am J Cardiol. 2012;109:180–186. DOI: 10.1016/j.amjcard.2011.08.030

[29] Abate E, Hoogslag GE, Antoni ML, Nucifora G, Delgado V, Holman ER, et al. Value of three-dimensional speckle-tracking longitudinal strain for predicting improvement of left ventricular function after acute myocardial infarction. Am J Cardiol. 2012;110:961–967. DOI: 10.1016/j.amjcard.2012.05.023

[30] Kleijn SA, Aly MF, Terwee CB, van Rossum AC, Kamp O. Three-dimensional speckle tracking echocardiography for automatic assessment of global and regional left ventricular function based on area strain. J Am Soc Echocardiogr. 2011;24:314–321. DOI: 10.1016/j.echo.2011.01.014

[31] Kleijn SA, Aly MF, Knol DL, Terwee CB, Jansma EP, Abd El-Hady YA, et al. A meta-analysis of left ventricular dyssynchrony assessment and prediction of response to cardiac resynchronization therapy by three-dimensional echocardiography. Eur Heart J Cardiovasc Imaging. 2012;13:763–775. DOI: 10.1093/ehjci/jes041

[32] Yodwut C, Weinert L, Klas B, Lang RM, Mor-Avi V. Effects of frame rate on three-dimensional speckle-tracking-based measurements of myocardial deformation. J Am Soc Echocardiogr. 2012;25:978–985. DOI: 10.1016/j.echo.2012.06.001

[33] Urbano-Moral JA, Patel AR, Maron MS, Arias-Godinez JA, Pandian NG. Three-dimensional speckle-tracking echocardiography: methodological aspects and clinical potential. Echocardiography. 2012;29:997–1010. DOI: 10.1111/j.1540-8175.2012.01773.x

[34] Urbano-Moral JA, Rowin EJ, Maron MS, Crean A, Pandian NG. Investigation of global and regional myocardial mechanics with 3-dimensional speckle tracking echocardiography and relations to hypertrophy and fibrosis in hypertrophic cardiomyopathy. Circ Cardiovasc Imaging. 2014;7:11–19. DOI: 10.1161/CIRCIMAGING.113.000842

[35] Perez de Isla L, Millan M, Lennie V, Quezada M, Guinea J, Macaya C, et al. Area strain: normal values for a new parameter in healthy people. Rev Esp Cardiol. 2011;64:1194–1197. DOI: 10.1016/j.recesp.2011.03.021

[36] Thomas JD, Badano LP. EACVI-ASE-industry initiative to standardize deformation imaging: a brief update from the co-chairs. Eur Heart J Cardiovasc Imaging. 2013;14:1039–1040. DOI: 10.1093/ehjci/jet184

[37] Voigt JU, Pedrizzetti G, Lysyansky P, Marwick TH, Houle H, Baumann R, et al. Definitions for a common standard for 2D speckle tracking echocardiography: consensus document of the EACVI/ASE/Industry Task Force to standardize deformation imaging. Eur Heart J Cardiovasc Imaging. 2015;16:1–11. DOI: 10.1093/ehjci/jeu184

[38] Heggemann F, Weiss C, Hamm K, Kaden J, Suselbeck T, Papavassiliu T, et al. Global and regional myocardial function quantification by two-dimensional strain in Takotsubo cardiomyopathy. Eur J Echocardiogr. 2009;10:760–764. DOI: 10.1093/ejechocard/jep062

[39] Shimoni S, Gendelman G, Ayzenberg O, Smirin N, Lysyansky P, Edri O, et al. Differential effects of coronary artery stenosis on myocardial function: the value of myocardial strain analysis for the detection of coronary artery disease. J Am Soc Echocardiogr. 2011;24:748–757. DOI: 10.1016/j.echo.2011.03.007

[40] Becker M, Hoffmann R, Kuhl HP, Grawe H, Katoh M, Kramann R, et al. Analysis of myocardial deformation based on ultrasonic pixel tracking to determine transmurality in chronic myocardial infarction. Eur Heart J. 006;27:2560–2566. DOI: 10.1093/eurheartj/ehl288

[41] Chan J, Hanekom L, Wong C, Leano R, Cho GY, Marwick TH. Differentiation of subendocardial and transmural infarction using two-dimensional strain rate imaging to assess short-axis and long-axis myocardial function. J Am Coll Cardiol. 2006;48:2026–2033. DOI: 10.1016/j.jacc.2006.07.050

[42] Tan YT, Wenzelburger F, Lee E, Heatlie G, Leyva F, Patel K, et al. The pathophysiology of heart failure with normal ejection fraction: exercise echocardiography reveals complex abnormalities of both systolic and diastolic ventricular function involving torsion, untwist, and longitudinal motion. J Am Coll Cardiol. 2009;54:36–46. DOI: 10.1016/j.jacc.2009.03.037

[43] Gorcsan J, 3rd, Tanabe M, Bleeker GB, Suffoletto MS, Thomas NC, Saba S, et al. Combined longitudinal and radial dyssynchrony predicts ventricular response after resynchronization therapy. J Am Coll Cardiol. 2007;50:1476–1483. DOI: 10.1016/j.jacc.2007.06.043

[44] Delgado V, van Bommel RJ, Bertini M, Borleffs CJ, Marsan NA, Arnold CT, et al. Relative merits of left ventricular dyssynchrony, left ventricular lead position, and myocardial scar to predict long-term survival of ischemic heart failure patients undergoing cardiac

resynchronization therapy. Circulation. 2011;123:70–78. DOI: 10.1161/CIRCULATIONAHA.110.945345

[45] Bellavia D, Abraham TP, Pellikka PA, Al-Zahrani GB, Dispenzieri A, Oh JK, et al. Detection of left ventricular systolic dysfunction in cardiac amyloidosis with strain rate echocardiography. J Am Soc Echocardiogr. 2007;20:1194–1202. DOI: 10.1016/j.echo.2007.02.025

[46] Delgado V, Tops LF, van Bommel RJ, van der Kley F, Marsan NA, Klautz RJ, et al. Strain analysis in patients with severe aortic stenosis and preserved left ventricular ejection fraction undergoing surgical valve replacement. Eur Heart J. 2009;30:3037–3047. DOI: 10.1093/eurheartj/ehp351

[47] De Isla LP, De Agustin A, Rodrigo JL, Almeria C, del Carmen Manzano M, Rodriguez E, et al. Chronic mitral regurgitation: a pilot study to assess preoperative left ventricular contractile function using speckle-tracking echocardiography. J Am Soc Echocardiogr. 2009;22:831–838. DOI: 10.1016/j.echo.2009.04.016

[48] Sengupta PP, Krishnamoorthy VK, Abhayaratna WP, Korinek J, Belohlavek M, Sundt TM, 3rd, et al. Disparate patterns of left ventricular mechanics differentiate constrictive pericarditis from restrictive cardiomyopathy. JACC Cardiovasc Imaging. 2008;1:29–38. DOI: 10.1016/j.jcmg.2007.10.006

[49] Kalam K, Otahal P, Marwick TH. Prognostic implications of global LV dysfunction: a systematic review and meta-analysis of global longitudinal strain and ejection fraction. Heart. 2014;100:1673–1680. DOI: 10.1136/heartjnl-2014-305538

[50] Bijnens B, Claus P, Weidemann F, Strotmann J, Sutherland GR. Investigating cardiac function using motion and deformation analysis in the setting of coronary artery disease. Circulation. 2007;116:2453–2464. DOI: 10.1161/CIRCULATIONAHA.106.684357

[51] Turschner O, D'Hooge J, Dommke C, Claus P, Verbeken E, De Scheerder I, et al. The sequential changes in myocardial thickness and thickening which occur during acute transmural infarction, infarct reperfusion and the resultant expression of reperfusion injury. Eur Heart J. 2004;25:794–803. DOI: 10.1016/j.ehj.2004.01.006

[52] Carlhall CJ, Lindstrom L, Wranne B, Nylander E. Atrioventricular plane displacement correlates closely to circulatory dimensions but not to ejection fraction in normal young subjects. Clin Physiol. 2001;21:621–628. DOI: 10.1046/j.1365-2281.2001.00356.x

[53] Zaky A, Nasser WK, Feigenbaum H. A study of mitral valve action recorded by reflected ultrasound and its application in the diagnosis of mitral stenosis. Circulation. 1968;37:789–799. DOI: 10.1161/01.CIR.37.5.789

[54] Roberson DA, Cui W. Tissue Doppler imaging measurement of left ventricular systolic function in children: mitral annular displacement index is superior to peak velocity. J Am Soc Echocardiogr. 2009;22:376–382. DOI: 10.1016/j.echo.2009.01.008

[55] Voigt JU, Exner B, Schmiedehausen K, Huchzermeyer C, Reulbach U, Nixdorff U, et al. Strain-rate imaging during dobutamine stress echocardiography provides objective evidence of inducible ischemia. Circulation. 2003;107:2120–2126. DOI: 10.1161/01.CIR.0000065249.69988.AA

[56] Weidemann F, Dommke C, Bijnens B, Claus P, D'Hooge J, Mertens P, et al. Defining the transmurality of a chronic myocardial infarction by ultrasonic strain-rate imaging: implications for identifying intramural viability: an experimental study. Circulation. 2003;107:883–888. DOI: 10.1161/01.CIR.0000050146.66577.4B

[57] Asanuma T, Uranishi A, Masuda K, Ishikura F, Beppu S, Nakatani S. Assessment of myocardial ischemic memory using persistence of post-systolic thickening after recovery from ischemia. JACC Cardiovasc Imaging. 2009;2:1253–1261. DOI: 10.1016/j.jcmg.2009.07.008

[58] Bragadeesh T, Jayaweera AR, Pascotto M, Micari A, Le DE, Kramer CM, et al. Post-ischaemic myocardial dysfunction (stunning) results from myofibrillar oedema. Heart. 2008;94:166–171. DOI: 10.1136/hrt.2006.102434

[59] Merli E, Sutherland GR, Bijnens B, Fischer A, Chaparro M, Karu T, et al. Usefulness of changes in left ventricular wall thickness to predict full or partial pressure reperfusion in ST-elevation acute myocardial infarction. Am J Cardiol. 2008;102:249–256. DOI: 10.1016/j.amjcard.2008.03.047

[60] Marciniak A, Claus P, Sutherland GR, Marciniak M, Karu T, Baltabaeva A, et al. Changes in systolic left ventricular function in isolated mitral regurgitation. A strain rate imaging study. Eur Heart J. 2007;28:2627–2636. DOI: 10.1093/eurheartj/ehm072

[61] Pandis D, Sengupta PP, Castillo JG, Caracciolo G, Fischer GW, Narula J, et al. Assessment of longitudinal myocardial mechanics in patients with degenerative mitral valve regurgitation predicts postoperative worsening of left ventricular systolic function. J Am Soc Echocardiogr. 2014;27:627–638. DOI: 10.1016/j.echo.2014.02.008

[62] Florescu M, Benea DC, Rimbas RC, Cerin G, Diena M, Lanzzillo G, et al. Myocardial systolic velocities and deformation assessed by speckle tracking for early detection of left ventricular dysfunction in asymptomatic patients with severe primary mitral regurgitation. Echocardiography. 2012;29:326–333. DOI: 10.1111/j.1540-8175.2011.01563.x

[63] Kumanohoso T, Otsuji Y, Yoshifuku S, Matsukida K, Koriyama C, Kisanuki A, et al. Mechanism of higher incidence of ischemic mitral regurgitation in patients with inferior myocardial infarction: quantitative analysis of left ventricular and mitral valve geometry in 103 patients with prior myocardial infarction. J Thorac Cardiovasc Surg. 2003;125:135–143. DOI: 10.1067/mva.2003.78

[64] Gustafsson U, Lindqvist P, Morner S, Waldenstrom A. Assessment of regional rotation patterns improves the understanding of the systolic and diastolic left ventricular

function: an echocardiographic speckle-tracking study in healthy individuals. Eur J Echocardiogr. 2009;10:56–61. DOI: 10.1093/ejechocard/jen141

[65] Zito C, Cusma-Piccione M, Oreto L, Tripepi S, Mohammed M, Di Bella G, et al. In patients with post-infarction left ventricular dysfunction, how does impaired basal rotation affect chronic ischemic mitral regurgitation? J Am Soc Echocardiogr. 2013;26:1118–1129. DOI: 10.1016/j.echo.2013.04.017

[66] Singh A, Steadman CD, McCann GP. Advances in the understanding of the pathophysiology and management of aortic stenosis: role of novel imaging techniques. Can J Cardiol. 2014;30:994–1003. DOI: 10.1016/j.cjca.2014.03.008

[67] Shah PK. Should severe aortic stenosis be operated on before symptom onset? Severe aortic stenosis should not be operated on before symptom onset. Circulation. 2012;126:118–125. DOI: 10.1161/CIRCULATIONAHA.111.079368

[68] Carabello BA. Should severe aortic stenosis be operated on before symptom onset? Aortic valve replacement should be operated on before symptom onset. Circulation. 2012;126:112–117. DOI: 0.1161/CIRCULATIONAHA.111.079350

[69] Carabello BA. The relationship of left ventricular geometry and hypertrophy to left ventricular function in valvular heart disease. J Heart Valve Dis. 1995;4 Suppl 2:S132–138; discussion S138–139. DOI: none

[70] Baltabaeva A, Marciniak M, Bijnens B, Moggridge J, He FJ, Antonios TF, et al. Regional left ventricular deformation and geometry analysis provides insights in myocardial remodelling in mild to moderate hypertension. Eur J Echocardiogr. 2008;9:501–508. DOI: 10.1016/j.euje.2007.08.004

[71] Yingchoncharoen T, Gibby C, Rodriguez LL, Grimm RA, Marwick TH. Association of myocardial deformation with outcome in asymptomatic aortic stenosis with normal ejection fraction. Circ Cardiovasc Imaging. 2012;5:719–725. DOI: 10.1161/CIRCIMAGING.112.977348

[72] Nishimura RA, Otto CM, Bonow RO, Carabello BA, Erwin JP, 3rd, Guyton RA, et al. 2014 AHA/ACC guideline for the management of patients with valvular heart disease: executive summary: a report of the American College of Cardiology/American Heart Association Task Force on practice guidelines. Circulation. 2014;129:2440–2492. DOI: 10.1161/CIR.0000000000000029

[73] Hawkins NM, Petrie MC, Burgess MI, McMurray JJ. Selecting patients for cardiac resynchronization therapy: the fallacy of echocardiographic dyssynchrony. J Am Coll Cardiol. 2009;53:1944–1959. DOI: 10.1016/j.jacc.2008.11.062

[74] Marciniak M, Bijnens B, Baltabaeva A, Marciniak A, Parsai C, Claus P, et al. Interventricular interaction as a possible mechanism for the presence of a biphasic systolic velocity profile in normal left ventricular free walls. Heart. 2008;94:1058–1064. DOI: 10.1136/hrt.2007.126938

[75] Suffoletto MS, Dohi K, Cannesson M, Saba S, Gorcsan J, 3rd. Novel speckle-tracking radial strain from routine black-and-white echocardiographic images to quantify dyssynchrony and predict response to cardiac resynchronization therapy. Circulation. 2006;113:960–968. DOI: 10.1161/CIRCULATIONAHA.105.571455

[76] Carasso S, Rakowski H, Witte KK, Smith P, Carasso D, Garceau P, et al. Left ventricular strain patterns in dilated cardiomyopathy predict response to cardiac resynchronization therapy: timing is not everything. J Am Soc Echocardiogr. 2009;22:242–250. DOI: 10.1016/j.echo.2008.12.003

[77] Russell K, Eriksen M, Aaberge L, Wilhelmsen N, Skulstad H, Remme EW, et al. A novel clinical method for quantification of regional left ventricular pressure-strain loop area: a non-invasive index of myocardial work. Eur Heart J. 2012;33:724–733. DOI: 10.1093/eurheartj/ehs016

[78] Russell K, Eriksen M, Aaberge L, Wilhelmsen N, Skulstad H, Gjesdal O, et al. Assessment of wasted myocardial work: a novel method to quantify energy loss due to uncoordinated left ventricular contractions. Am J Physiol Heart Circ Physiol. 2013;305:H996–1003. DOI: 10.1152/ajpheart.00191.2013

[79] Galderisi M. Diastolic dysfunction and diabetic cardiomyopathy: evaluation by Doppler echocardiography. J Am Coll Cardiol. 2006;48:1548–1551. DOI: 10.1016/j.jacc.2006.07.033

[80] Guo R, Wang K, Song W, Cong T, Shang ZJ, Sun YH, et al. Myocardial dysfunction in early diabetes patients with microalbuminuria: a 2-dimensional speckle tracking strain study. Cell Biochem Biophys. 2014;70:573–578. DOI: 10.1007/s12013-014-9958-8

[81] Shim CY, Park S, Choi EY, Kang SM, Cha BS, Ha JW, et al. Is albuminuria an indicator of myocardial dysfunction in diabetic patients without overt heart disease? A study with Doppler strain and strain rate imaging. Metabolism. 2008;57:448–452. DOI: 10.1016/j.metabol.2007.11.003

[82] Ernande L, Rietzschel ER, Bergerot C, De Buyzere ML, Schnell F, Groisne L, et al. Impaired myocardial radial function in asymptomatic patients with type 2 diabetes mellitus: a speckle-tracking imaging study. J Am Soc Echocardiogr. 2010;23:1266–1272. DOI: 10.1016/j.echo.2010.09.007

[83] Ernande L, Bergerot C, Rietzschel ER, De Buyzere ML, Thibault H, Pignonblanc PG, et al. Diastolic dysfunction in patients with type 2 diabetes mellitus: is it really the first marker of diabetic cardiomyopathy? J Am Soc Echocardiogr. 2011;24:1268–1275 e1261. DOI: 10.1016/j.echo.2011.07.017

[84] Karagoz A, Bezgin T, Kutluturk I, Kulahcioglu S, Tanboga IH, Guler A, et al. Subclinical left ventricular systolic dysfunction in diabetic patients and its association with retinopathy: a 2D speckle tracking echocardiography study. Herz. 2014. DOI: 10.1007/s00059-014-4138-6

[85] Hooning MJ, Botma A, Aleman BM, Baaijens MH, Bartelink H, Klijn JG, et al. Long-term risk of cardiovascular disease in 10-year survivors of breast cancer. J Natl Cancer Inst. 2007;99:365–375. DOI: 10.1093/jnci/djk064

[86] Doyle JJ, Neugut AI, Jacobson JS, Grann VR, Hershman DL. Chemotherapy and cardiotoxicity in older breast cancer patients: a population-based study. J Clin Oncol. 2005;23:8597–8605. DOI: 10.1200/JCO.2005.02.5841

[87] Lang RM, Bierig M, Devereux RB, Flachskampf FA, Foster E, Pellikka PA, et al. Recommendations for chamber quantification: a report from the American Society of Echocardiography's Guidelines and Standards Committee and the Chamber Quantification Writing Group, developed in conjunction with the European Association of Echocardiography, a branch of the European Society of Cardiology. J Am Soc Echocardiogr. 2005;18:1440–1463. DOI: 10.1016/j.echo.2005.10.005

[88] Thavendiranathan P, Grant AD, Negishi T, Plana JC, Popovic ZB, Marwick TH. Reproducibility of echocardiographic techniques for sequential assessment of left ventricular ejection fraction and volumes: application to patients undergoing cancer chemotherapy. J Am Coll Cardiol. 2013;61:77–84. DOI: 10.1016/j.jacc.2012.09.035

[89] Cardinale D, Colombo A, Lamantia G, Colombo N, Civelli M, De Giacomi G, et al. Anthracycline-induced cardiomyopathy: clinical relevance and response to pharmacologic therapy. J Am Coll Cardiol. 2010;55:213–220. DOI: 10.1016/j.jacc.2009.03.095

[90] Neilan TG, Jassal DS, Perez-Sanz TM, Raher MJ, Pradhan AD, Buys ES, et al. Tissue Doppler imaging predicts left ventricular dysfunction and mortality in a murine model of cardiac injury. Eur Heart J. 2006;27:1868–1875. DOI: 10.1093/eurheartj/ehl013

[91] Sawaya H, Sebag IA, Plana JC, Januzzi JL, Ky B, Cohen V, et al. Early detection and prediction of cardiotoxicity in chemotherapy-treated patients. Am J Cardiol. 2011;107:1375–1380. DOI: 10.1016/j.amjcard.2011.01.006

[92] Fallah-Rad N, Walker JR, Wassef A, Lytwyn M, Bohonis S, Fang T, et al. The utility of cardiac biomarkers, tissue velocity and strain imaging, and cardiac magnetic resonance imaging in predicting early left ventricular dysfunction in patients with human epidermal growth factor receptor II-positive breast cancer treated with adjuvant trastuzumab therapy. J Am Coll Cardiol. 2011;57:2263–2270. DOI: 10.1016/j.jacc.2010.11.063

[93] Poterucha JT, Kutty S, Lindquist RK, Li L, Eidem BW. Changes in left ventricular longitudinal strain with anthracycline chemotherapy in adolescents precede subsequent decreased left ventricular ejection fraction. J Am Soc Echocardiogr. 2012;25:733–740. DOI: 10.1016/j.echo.2012.04.007

[94] Sawaya H, Sebag IA, Plana JC, Januzzi JL, Ky B, Tan TC, et al. Assessment of echocardiography and biomarkers for the extended prediction of cardiotoxicity in patients treated with anthracyclines, taxanes, and trastuzumab. Circ Cardiovasc Imaging. 2012;5:596–603. DOI: 10.1161/CIRCIMAGING.112.973321

[95] Sirbu C, Herbots L, D'Hooge J, Claus P, Marciniak A, Langeland T, et al. Feasibility of strain and strain rate imaging for the assessment of regional left atrial deformation: a study in normal subjects. Eur J Echocardiogr. 2006;7:199–208. DOI: 10.1016/j.euje.2005.06.001

[96] Cameli M, Lisi M, Focardi M, Reccia R, Natali BM, Sparla S, et al. Left atrial deformation analysis by speckle tracking echocardiography for prediction of cardiovascular outcomes. Am J Cardiol. 2012;110:264–269. DOI: 10.1016/j.amjcard.2012.03.022

[97] Vianna-Pinton R, Moreno CA, Baxter CM, Lee KS, Tsang TS, Appleton CP. Two-dimensional speckle-tracking echocardiography of the left atrium: feasibility and regional contraction and relaxation differences in normal subjects. J Am Soc Echocardiogr. 2009;22:299–305. DOI: 10.1016/j.echo.2008.12.017

[98] Okamatsu K, Takeuchi M, Nakai H, Nishikage T, Salgo IS, Husson S, et al. Effects of aging on left atrial function assessed by two-dimensional speckle tracking echocardiography. J Am Soc Echocardiogr. 2009;22:70–75. DOI: 10.1016/j.echo.2008.11.006

[99] D'Hooge J, Heimdal A, Jamal F, Kukulski T, Bijnens B, Rademakers F, et al. Regional strain and strain rate measurements by cardiac ultrasound: principles, implementation and limitations. Eur J Echocardiogr. 2000;1:154–170. DOI: 10.1053/euje.2000.0031

[100] Meris A, Faletra F, Conca C, Klersy C, Regoli F, Klimusina J, et al. Timing and magnitude of regional right ventricular function: a speckle tracking-derived strain study of normal subjects and patients with right ventricular dysfunction. J Am Soc Echocardiogr. 2010;23:823–831. DOI: 10.1016/j.echo.2010.05.009

[101] Kleijn SA, Aly MF, Terwee CB, van Rossum AC, Kamp O. Reliability of left ventricular volumes and function measurements using three-dimensional speckle tracking echocardiography. Eur Heart J Cardiovasc Imaging. 2012;13:159–168. DOI: 10.1093/ejechocard/jer174

[102] Gayat E, Ahmad H, Weinert L, Lang RM, Mor-Avi V. Reproducibility and inter-vendor variability of left ventricular deformation measurements by three-dimensional speckle-tracking echocardiography. J Am Soc Echocardiogr. 2011;24:878–885. DOI: 10.1016/j.echo.2011.04.016

Chapter 6

Cardiac Imaging in Hypertrophic Cardiomyopathy

Dai-Yin Lu and Ming-Chong Hsiung

Additional information is available at the end of the chapter

http://dx.doi.org/10.5772/64364

Abstract

Hypertrophic cardiomyopathy (HCM) is a relatively common inherited cardiomyopathy, which is occasionally challenging to differentiate from hypertensive heart disease and athlete hearts on the basis of morphologic or functional abnormalities alone. Imaging studies provide solutions for most clinical needs, from diagnosis, anatomical and functional assessment, family screening, risk stratification, to monitoring of treatment response. Generally, transthoracic echocardiography is used as first-line imaging tool to establish the diagnosis. A multimodality imaging approach (cardiac magnetic resonance, cardiac computed tomography, and cardiac nuclear imaging) is also encouraged in the assessment of these patients. The choice of imaging tool should be based on a broad perspective and expert knowledge of what each technique has to offer, including its specific advantages and disadvantages. In this chapter, we discuss the utility and pitfalls of established imaging modalities and discuss the evolving role of novel echocardiographic imaging modalities.

Keywords: cardiac computed tomography, cardiovascular magnetic resonance, echocardiography, hypertrophic cardiomyopathy, nuclear imaging

1. Introduction

1.1. Definition and prevalence

Hypertrophic cardiomyopathy (HCM) is the most common inherited cardiac disease presented with exercise intolerance, heart failure, cardiac arrhythmias and sudden cardiac death [1]. Across different ethnicities, the prevalence is approximately 0.2% [2]. This estimated frequency in the general population appears to exceed the relatively low visit of HCM in cardiology practices, implying that the most affected individuals remain undiagnosed, probably in most cases without symptoms or shortened life expectancy [3]. The clinical

diagnosis of HCM is based on the demonstration of asymmetric left ventricular hypertrophy (LVH) with maximal wall thickness ≥15 mm, in the absence of other cardiac or systemic cause that would produce such magnitude of hypertrophy.

1.2. Natural history and clinical course

The natural history is generally benign in vast majority of patients, with a life span close to general population [4]. However, hemodynamic-related symptoms secondary to dynamic left ventricular outflow tract (LVOT) obstruction as well as myopathy-related complications may happen. Although symptoms may occur at any age, they are more common between young adult and middle age. Development of symptoms at older age is generally associated with less severe forms of the disease.

Although HCM presents primarily with ventricular septal hypertrophy, a key recognizable feature has been dynamic LVOT obstruction and HCM has been regarded as a predominantly obstructive disease [5]. Left ventricular outflow tract (LVOT) obstruction may be noted at rest or during physiological exercise in 50–70% of the HCM patients [6]. LVOT obstruction at rest, defined as ≥30 mmHg, is a strong, independent predictor for progression of heart failure and death [7, 8]. Accordingly, current AHA/ACC/ESC guidelines classify HCM patients based on their LVOT gradients into obstructive (resting and provoked gradients ≥30 mmHg); latent obstructive (resting <30 and provoked ≥30 mmHg); non-obstructive (resting and provoked gradients <30 mmHg) [3, 4].

HCM also represents the most frequent cause of sudden cardiac death (SCD), one of the most serious complications, in young athletes in countries without systematic sport screening programs. Dynamic LVOT obstruction and disarrayed myocardial fiber impair diastolic function of left ventricle, followed by enlargement of left atrium and heart failure with preserved ejection fraction (EF). Atrial fibrillation (AF) is also a clinical presentation secondary to left atrial enlargement, which may later cause cardioembolic events and the following disability in the middle and older age groups.

2. The role of imaging in HCM

Multimodality imaging—echocardiography, cardiac magnetic resonance, cardiac computed tomography, and cardiac nuclear imaging—provide comprehensive information. Patients with HCM usually require long-term follow-up. It is suggested that transthoracic echocardiography be performed every 1–2 years and cardiac magnetic resonance at least once after the diagnosis is made, yet the strategy needs to be individualized (**Table 1**).

2.1. Role of echocardiography in evaluation of HCM (Table 2) [9]

2.1.1. Anatomical evaluation

HCM presents primarily with LVH, which progresses with time (**Figure 1**). The presentation is rare when in childhood, and the growth of LVH becomes more obvious during adolescence.

http://dx.doi.org/10.5772/64364

Other systemic causes of LVH (obesity, athlete heart, systemic hypertension, aortic stenosis, or infiltrative disease) should be ruled out first before the diagnosis is confirmed. The pattern of hypertrophy and LV volume can be analyzed by echocardiography. Ventricular volumes are generally normal or slightly lower, and the biplane Simpson's method has been applied to the measurement of LV volumes and EF [10]. Three-dimensional (3D) echocardiography has also been shown to provide more accurate means of quantification, [11] yet the references for HCM are limited.

	Indications	Strengths	Limitations
Echocardiography	• First line imaging tool in screening and follow-up	• Real time • Repeatable • Demonstrate dynamic change • Provide hemodynamic information	• Imaging quality depends on patient's acoustic window • Interpretation operator dependent
Cardiac magnetic resonance (CMR)	• Anatomic evaluation • Fibrosis assessment • Differential diagnosis	• Good spatial resolution • Fibrosis assessment	• No real-time information • Contrast needed • Not applicable for every patient (with metallic device or pacemaker)
Cardiac nuclear imaging (CNI)	• Perfusion assessment • Metabolism	• Information of microvascular disease	• Radiation • Low spatial resolution

Table 1. Imaging tools in HCM.

Screening	
LV	Presence of hypertrophy and its distribution; report should include measurements f LV dimensions and wall thickness (septal, posterior, and maximum)
	Ejection fraction
	Diastolic function (comments n LV relaxation and filling pressures)
	Dynamic obstruction at rest and with Valsalva maneuver; report should identify the site of obstruction and the gradient
MV	Mitral valve and papillary muscle evaluation, including the direction, mechanism, and severity of mitral regurgitation; if needed, TEE should be performed to satisfactorily answer these questions
RV	RV hypertrophy and whether RV dynamic obstruction is present
PA	Pulmonary artery systolic pressure
LA	LA volume indexed to body surface area
Guidance	TEE is recommended to guide surgical myectomy, and TTE or TEE for alcohol septal ablation

LA = left atrium; LV = left ventricle; MV = mitral valve; PA = pulmonary artery; RV = right ventricle; TEE = transesophageal echocardiography (Adapted with permission from Nagueh et al. [9]).

Table 2. Echocardiogrophic evaluations of patients with HCM.

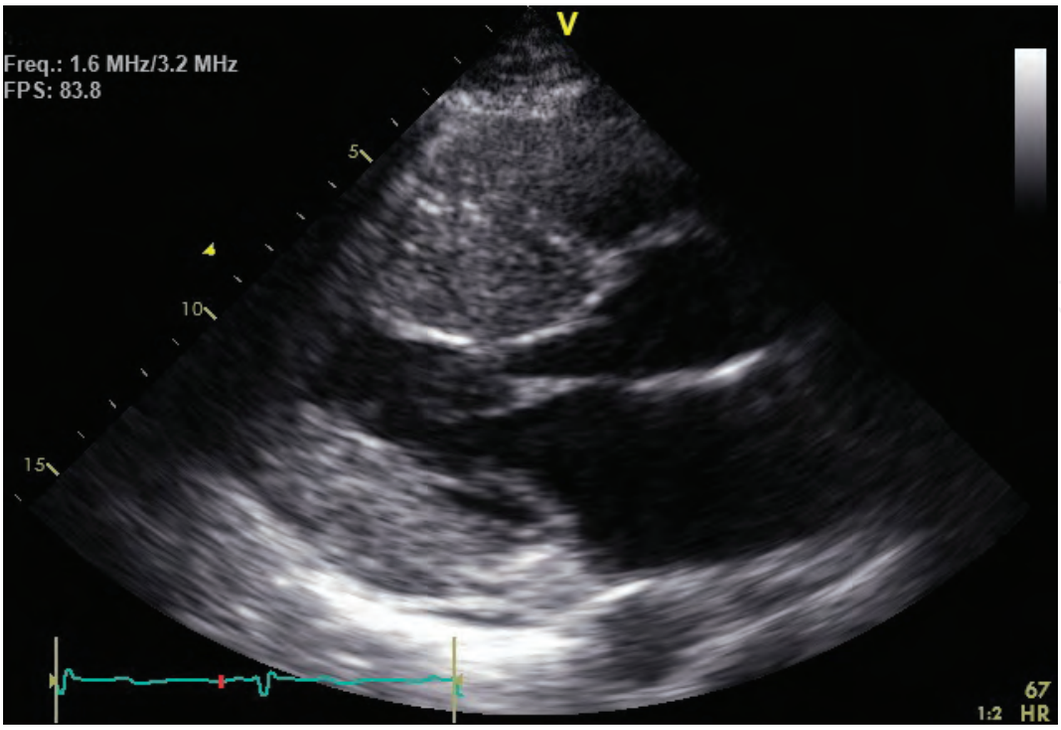

Figure 1. Left ventricular thickness, evaluated at septum and free wall level, is considered abnormal when ≥ 15 mm, and defined asymmetrical in presence of a septal to free wall thickness ratio between 1.3 and 1.5.

2.1.2. Hemodynamic evaluation

A key recognizable feature has been dynamic LVOT obstruction, and HCM has been regarded as a predominantly obstructive disease [5]. Patients with LVOT obstruction, defined by the presence of a peak gradient higher than 30 mmHg at rest or after provocative maneuvers (Valsalva, standing, and exercise) is a strong, independent predictor for progression of heart failure and death [7, 8] (**Figure 2**). Structural abnormalities of the mitral valve apparatus in HCM include hypertrophy of the papillary muscles, resulting in anterior displacement of papillary muscles, and mitral valve elongation [12, 13]. Systolic anterior motion (SAM) is defined as the systolic motion of the mitral leaflet, mainly anterior leaflet, or chordae into LVOT, resulting in outlet narrowing and flow disturbance. SAM also impairs the mitral leaflet coaptation, followed by regurgitation (**Figure 3**). The anterior leaflet motion is greater than that of the posterior leaflet during SAM and an interleaflet gap occurs, resulting in a typically posteriorly directed jet of mitral regurgitation. The anterior leaflet has a greater surface area and hence greater redundancy and mobility. If a concentric regurgitation jet is found in HCM patients, concomitant mitral valvulopathy should be carefully evaluated.

2.1.3. Assessment of LV systolic function

The ejection fraction of left ventricle in HCM patients is generally normal or even increased. However, patients with significant hypertrophy may have small LV end-diastolic volumes and the following lower stroke volumes despite a normal LVEF. LV systolic dysfunction is usually

http://dx.doi.org/10.5772/64364

defined as LVEF < 50%. When present, the prognosis is markedly worse. In addition to 2D imaging, Doppler echocardiography has been used to assess subclinical LV systolic dysfunction. Tissue Doppler imaging measures the velocity of myocardial motion. A lower systolic (Sa) or reduced early diastolic (Ea or e') velocities can occur before overt hypertrophy develops [14].

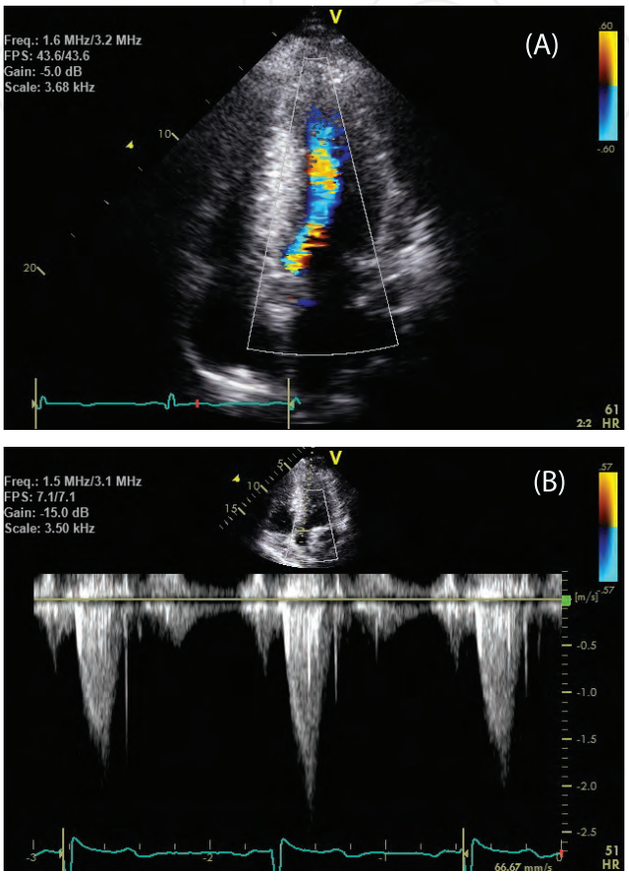

Figure 2. (A) Asymmetric septal hypertrophy may cause narrowing of the left ventricular outflow tract, resulting in turbulent flow. (B) Doppler analysis across the LVOT in dynamic obstructive HCM results in a characteristic signal with a late-peaking dagger-shaped appearance.

2.1.4. Assessment of LV diastolic function

Reduction in ventricular compliance and increased stiffness due to myocardial fibrosis coupled with a reduction of chamber volume and suction play a role in the pathophysiology of diastolic dysfunction in patients with HCM. LV and left atrial (LA) filling abnormalities have been reported in patients with HCM, irrespective of the presence and extent of LV hypertrophy. Tissue Doppler echocardiography indicates impaired myocardial relaxation regardless of symptoms or severity of LVOT obstruction [15]. Although tissue Doppler echocardiography has been successfully used to estimate filling pressures in a variety of cardiac disorders [16, 17], it is not as reliable in patients with hypertrophic cardiomyopathy as in patients with left ventricular systolic dysfunction [18]. In a study consisting

of 35 patients, LV filling pressures can be estimated with reasonable accuracy in HCM patients by measuring mitral early diastolic inflow/flow propagation velocity or ratio of early diastolic mitral flow velocity to the early diastolic mitral septal annulus motion velocity (E/e′) [19]. Whereas a later report with symptomatic HCM patients concluded Doppler echocardiographic estimates of left ventricular filling pressure with the use of transmitral flow and mitral annular velocities correlated modestly with direct measurement of left atrial pressure [20]. Despite of this inconsistency in filling pressure estimation, tissue Doppler imaging remains a useful tool for risk stratification of patients with HCM [21]. A higher septal E/e′ predicts patients with HCM who are at risk of sustained ventricular tachycardia (VT), implantable cardioverter defibrillator (ICD) discharge, cardiac arrest or sudden cardiac death [22, 23].

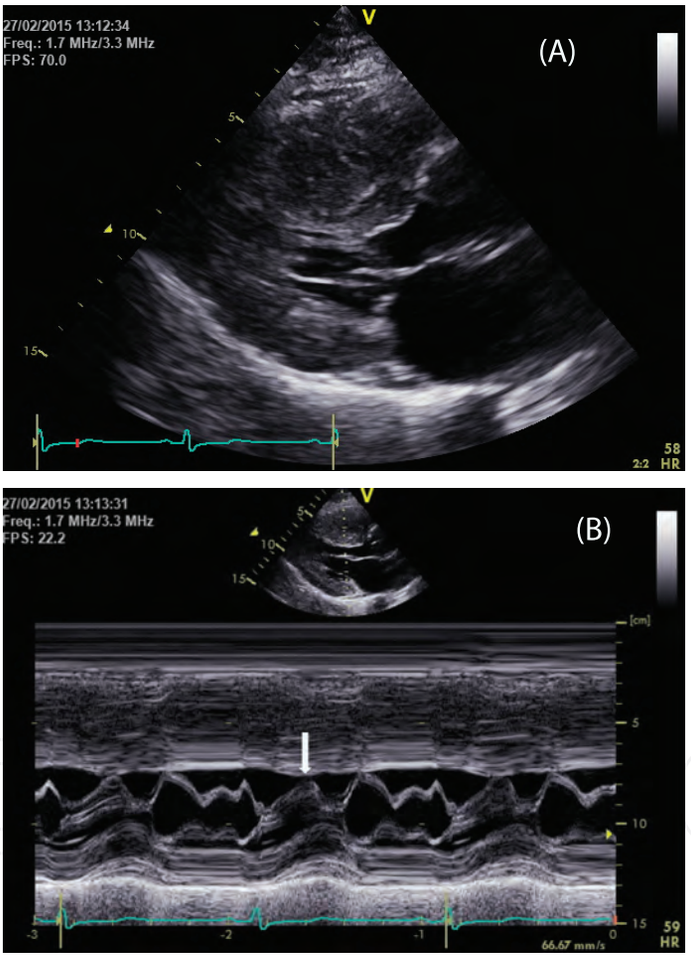

Figure 3. Systolic anterior motion (SAM) of anterior mitral leaflet at mid to late systolic phase (A) parasternal long axis view, 2D; (B) parasternal long axis view, M-mode.

LA volume is mainly secondary to diastolic dysfunction, mitral regurgitation and atrial myopathy. LA enlargement is generally assessed by 2D or M-mode linear dimensions. However, it is important to recognize that linear dimensions, particularly anteroposterior measurements of the LA, may not measure true LA size, as LA remodeling frequently happens

asymmetrically [24]. Increased LA volume is an independent indicator of functional capacity [25] and an LA volume index of >34 ml/m^2 has been shown to be predictive of a more severe LVH, diastolic dysfunction, and adverse cardiovascular outcomes [26].

2.2. Role of deformation imaging in HCM

2.2.1. TDI-derived strain

Although tissue Doppler velocity was considered as a technique for evaluation of regional myocardial performance, the utility is limited in distinguishing myocardial contractility from passive motion. Such restriction later leads to the development of strain imaging. Strain is a measure of tissue deformation and is defined as the change in length normalized to the original length. The rate at which this change occurs is called strain rate (SR). In contrast to tissue Doppler velocity, which examines myocardial motion relative to the transducer, strain measures myocardial motion relative to the adjacent myocardium [27]. When the left ventricle contracts, the myocardium shortens in longitudinal and circumferential direction (negative value in strain) and thickens in the radial direction (positive value in strain) (**Figure 4**) [28]. Strain rate (SR) represents the local rate of myocardial deformation (**Figure 5**) [29]. Weidemann et al. (30) firstly described the use of TDI-derived strain for the evaluation of HCM in a case report of a child with non-obstructive HCM. Tissue Doppler velocities were found to be normal in all the septal segments interrogated. However, systolic longitudinal strain SR was significantly decreased in the mid septal region with no significant changes in the basal regions when compared with healthy children [30]. Later reports also confirmed similar findings in adults with HCM [31, 32].

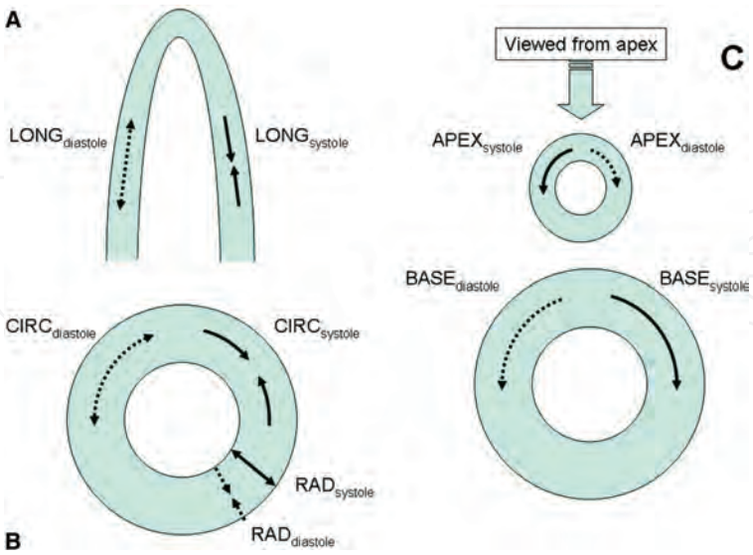

Figure 4. Graphic representation of the principal myocardial deformations: longitudinal (A), radial and circumferential (B), and torsion (C). The direction of deformation in systole is shown as solid lines and that in diastole is shown as dashed lines. LONG indicates longitudinal; RAD, radial; and CIRC, circumferential. (Reprinted with permission from Abraham et al. [28]).

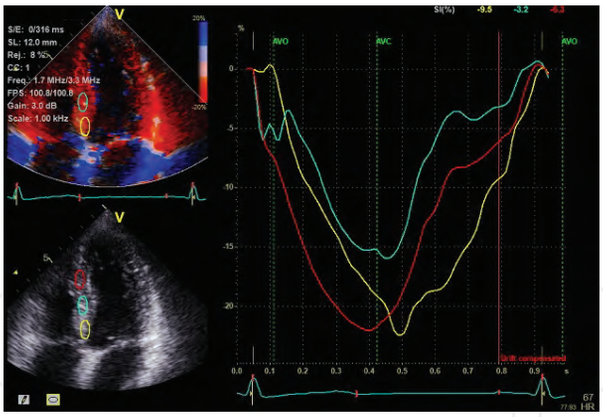

Figure 5. Strain analysis from tissue Doppler imaging from three representative regions of interest (ROIs) in LV septal wall.

2.2.2. 2D strain or speckle tracking imaging

The interaction of ultrasound with the myocardium produces unique acoustic patterns, also known as "speckles." These speckles can be tracked over time and speckle displacement can be used to calculate the tissue velocity and strain [33]. This method is not based on the Doppler principle and relatively angle independent [34]. Deformation is calculated with frame-by-frame speckle displacement, yielding angle independent parameters of myocardial contraction, and gives longitudinal, transverse strain and strain rate in long-axis images (**Figure 6**). Similarly, radial and circumferential strain or strain rate may be analyzed by the short-axis images. In a study for patients with familial non-obstructive HCM, average longitudinal was reduced in affected individuals compared with healthy controls, despite apparently normal systolic function. In addition, no significant difference in the values obtained by TDI versus 2D strain echocardiography was observed [35]. A recent study of patients with HCM and preserved systolic function demonstrated attenuated longitudinal strain, increased circumferential strain, and normal overall systolic LV twist or torsion [36].

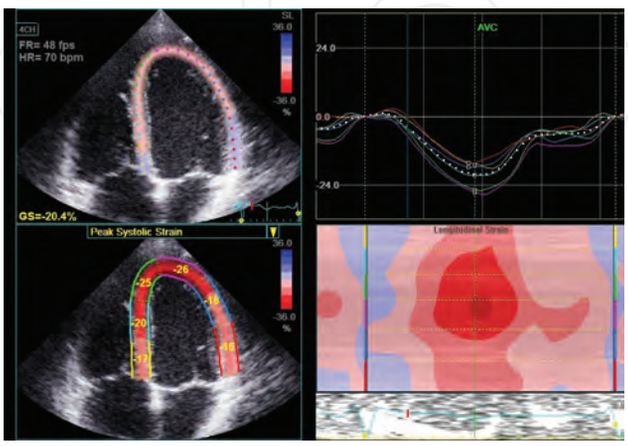

Figure 6. Strain analysis from two-dimensional speckle tracking from apical four chamber view.

2.3. Application of interventional echocardiography in HCM

2.3.1. Alcohol septal ablation (ASA)

2D echo is useful in search of suitable patients for ASA. During the procedure under transthoracic echocardiographic guidance, injection of echo contrast into a septal perforator branch of the left anterior descending artery helps determine whether the selected branch to occlude supplies the appropriate myocardium where SAM contacts interventricular septum (**Figure 7**) [37]. For patients with suboptimal transthoracic echo window, transesophageal echo imaging may be another option.

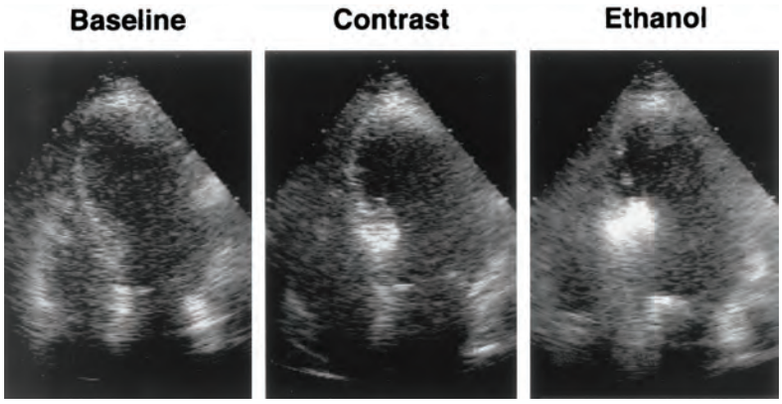

Figure 7. Myocardial contrast echocardiography of the hypertrophied septum after injection of sonicated albumin (Contrast) and ethanol (Reprinted wth permission from Nagueh et al. [37]).

2.3.2. Surgical myectomy and mitral surgery

It is important to have a real-time imaging analysis in the peri-procedural assessment of HCM patients undergoing myectomy, with or without mitral surgery. Intraoperative Transesophageal echocardiography (TEE) plays a key role in surgery, assessing mechanisms of LVOTO, mechanism of MR, extension of myocardial region that need to be removed and other possible intra-operative complications.

2.4. Other imaging modality

*2.4.1. Cardiac magnetic resonance (**Table 3**) [38]*

2.4.1.1. Anatomical evaluation

Cardiac magnetic resonance (CMR) should be considered in the initial evaluation of all patients with HCM when clinic resources are available [4]. It provides comprehensive evaluation of both the ventricle, including assessment of wall thickness [39–41] and the chamber volumes, with high quality of spatial and temporal resolution (**Figure 8**) [38]. CMR may be more sensitive than echocardiography in detecting LVH [40]. The extension of LVH can be defined using CMR

as focal (1–2 hypertrophic segments), intermediate (3–7 segments), and diffuse (8–16 hypertrophic segments). CMR can also give more precise measurement in maximal diastolic wall thickness [42].

Left ventricle volumes, mass and ejection fraction
Location, type, distribution of hypertrophy, maximal wall thickness and diastolic wall thickness to volume ratio
Degree of asymmetry
LVOT or mid-cavity obstruction
LGE: presence or absence; pattern and extension
Evidence of MR
Description of mitral valve apparatus (leaflets, chordae, papillary muscles) and its relation to obstruction or MR

LGE = late gadolinium enhancement; LVOT = left ventricular outlet tract; MR = mitral regurgitation. (Adapted with permission from Cardim et al. [38].)

Table 3. CMR evaluations of patients with HCM.

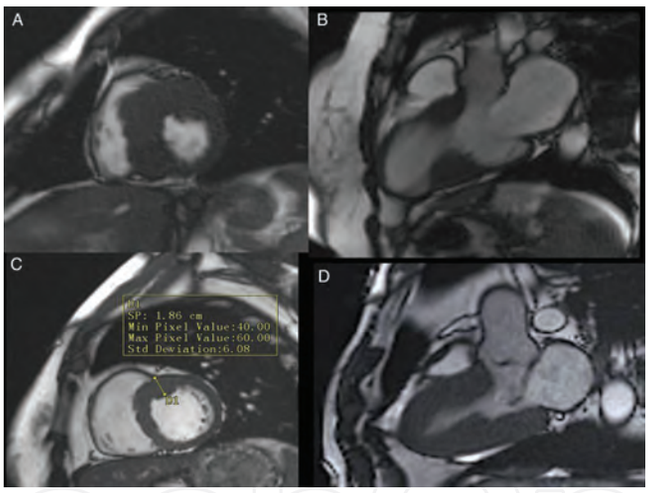

Figure 8. Cardiac MR in HCM patients. Cine CMR-SSFP in different HCM patients. (A) Basal short-axis view, asymmetric LVH with lateral wall sparing. (B) Three-chamber view, mid-ventricular hypertrophy of the medial segments of the posterior wall and anterior interventricular septum. (C) short-axis view, LVH localized in the anteroseptal wall (18 mm), undetected by echocardiography. (D) Three-chamber view, systolic phase. (Reprinted with permission from Cardim et al. [38]).

2.4.1.2. Tissue characterization

CMR is the most important technique in tissue characterization. The principle of late gadolinium enhancement (LGE) in CMR is based on those tissues, with an expanded extracellular space that provides a larger distribution volume for the conventional CMR contrast agents, which occupy extravascular and extracellular space. Within 30 minutes, differences between the tissue with normal and expanded extracellular volumes are large and LGE imaging is

http://dx.doi.org/10.5772/64364

acquired (**Figure 9**) [43]. Current LGE protocols provide a very high spatial resolution (≤1 mm) and also provide a very high contrast to noise ratio, allowing to delineate small amounts of myocardial fibrosis. In HCM patients, there is frequent [44] and progressive [45] fibrosis. Two major patterns of LGE distribution are demonstrated: Intramural LGE was seen within the hypertrophied segments, which are thought to be reflective of replacement fibrosis [46]. RV insertion points LGE corresponds to interstitial fibrosis and myocyte disarray [47].

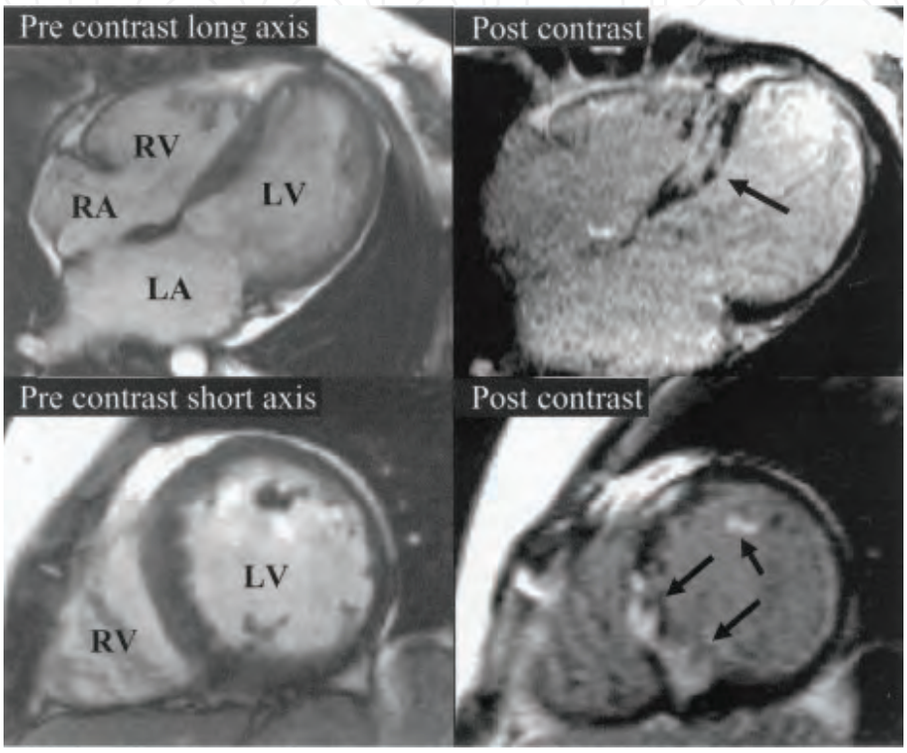

Figure 9. Pre- and post-contrast CMR images demonstrating enhancement. The pre-contrast images are the diastolic frames of fast imaging with steady-state precession cine loops. In the post-contrast images, normal myocardium appears dark. There is a large area of septal enhancement, with additional papillary muscle enhancement and subendocardial enhancement of the lateral wall. The total extent of enhancement was 25% of the left ventricular mass. (Reprinted with permission from Moon et al. [43]).

2.4.2. Cardiac nuclear imaging

Single photon-emission computed tomography (SPECT) myocardial perfusion imaging with Thallium-201 and Tc-99 m labelled tracers often demonstrate reversible (suggestive of ischemia) and fixed defects (scar), even when there is no obvious epicardial coronary artery disease [48]. The positive predictive value for SPECT study in HCM is relatively low for epicardial coronary artery disease compared to a high negative predictive value. Ischemic and scarring have been demonstrated a predictor of worse outcome, including adverse remodeling, systolic dysfunction and sudden cardiac death [49]. In obstructive HCM patients, improvement of perfusion may be observed when the obstruction is relieved after myectomy (**Figure 10**) [38, 50].

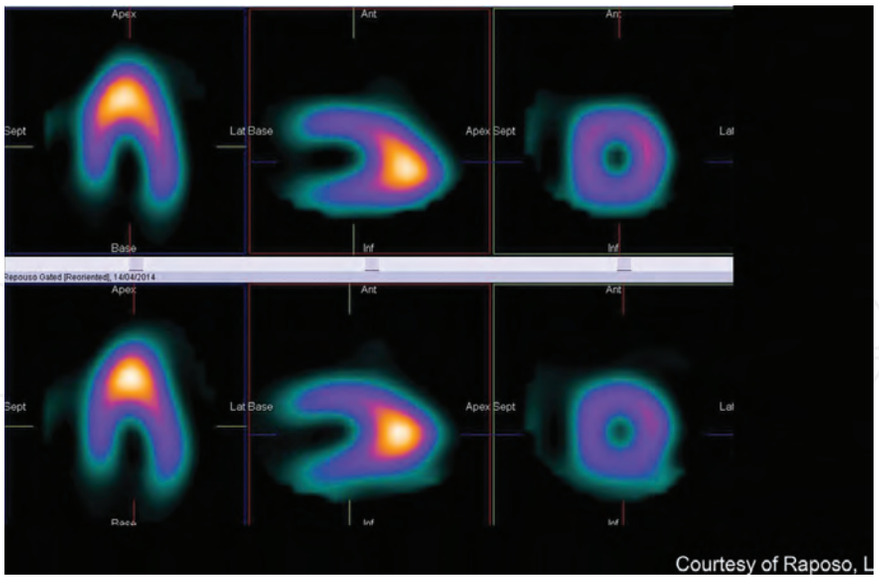

Figure 10. Functional imaging of ischemia with single photon-emission computed tomography (SPECT) with Tc-99m-Sestamibi in a 34-year-old male patient with HCM with history of chest pain in the absence of epicardial coronary artery disease). Stress (upper row) and rest (lower row). A fixed, non-reversible defect (scar) in the basal segments of the LV was found, with a non-coronary artery distribution. The apical perfusion is normal. However, this pattern may be a false perfusion defect due to increased hypertrophic mid-ventricular and apical uptake of the radiotracer. (Reprinted with permission from Cardim et al. [38]).

Using N-13-labelled ammonia and O-15-labelled water, proton emission tomography (PET) imaging detects absolute myocardial blood flow in patients with HCM. In contrast to SPECT, PET allows the direct quantification of myocardial blood flow (**Figure 11**) [38]. PET imaging

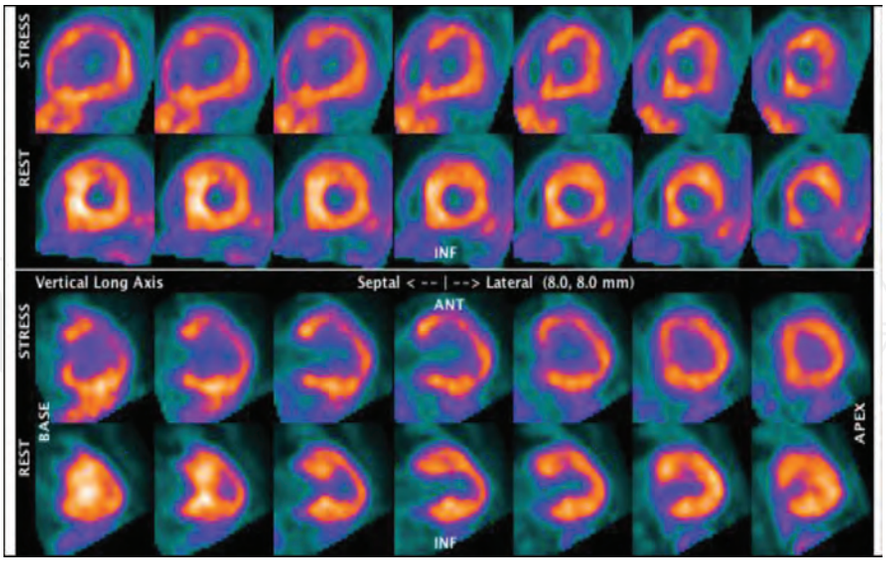

Figure 11. Functional imaging of ischemia with nuclear proton emission tomography (PET). Stress dipyridamole (upper row) and rest (lower row) $^{13}NH_3$ perfusion images in an 14-year-old girl diagnosed with HCM with interventricular septum (IVS) 29 mm. Stress: LV dilation and subendocardial hypoperfusion (IVS and antero-lateral wall). Rest: increased IVS $^{13}NH_3$ uptake is seen, indicative of IVS hypertrophy. (Reprinted with permission from Cardim et al. [38]).

is the most reliable noninvasive quantitative method for assessing myocardial ischemia in HCM [51].

3. Summary

Echocardiography remains the first-line imaging tool in the assessment of HCM patients, while the role of cardiac MR and nuclear imaging is getting more and more important, providing specific clinical information, which echocardiography is unable to give. The assessment of fibrosis, tissue characterization, and myocardial function, represents imaging future priorities of HCM imaging.

Author details

1 Division of Cardiology, Department of Medicine, Taipei Veterans General Hospital, Taipei, Taiwan

2 Department of Medicine, National Yang-Ming University, Taipei, Taiwan
3 Division of Cardiology, Heart Center, Chen-Hsin General Hospital, Taipei, Taiwan

References

[1] Maron BJ, Ommen SR, Semsarian C, Spirito P, Olivotto I, Maron MS. Hypertrophic cardiomyopathy: present and future, with translation into contemporary cardiovascular medicine. Journal of the American College of Cardiology. 2014;64(1):83–99.

[2] Maron BJ, McKenna WJ, Danielson GK, Kappenberger LJ, Kuhn HJ, Seidman CE, et al. American College of Cardiology/European Society of Cardiology clinical expert consensus document on hypertrophic cardiomyopathy. A report of the American College of Cardiology Foundation Task Force on Clinical Expert Consensus Documents and the European Society of Cardiology Committee for Practice Guidelines. Journal of the American College of Cardiology. 2003;42(9):1687–713.

[3] Gersh BJ, Maron BJ, Bonow RO, Dearani JA, Fifer MA, Link MS, et al. 2011 ACCF/AHA Guideline for the Diagnosis and Treatment of Hypertrophic Cardiomyopathy: a report of the American College of Cardiology Foundation/American Heart Association Task Force on Practice Guidelines. Developed in collaboration with the American Associa-

tion for Thoracic Surgery, American Society of Echocardiography, American Society of Nuclear Cardiology, Heart Failure Society of America, Heart Rhythm Society, Society for Cardiovascular Angiography and Interventions, and Society of Thoracic Surgeons. Journal of the American College of Cardiology. 2011;58(25):e212–60.

[4] Elliott PM, Anastasakis A, Borger MA, Borggrefe M, Cecchi F, et al. 2014 ESC Guidelines on diagnosis and management of hypertrophic cardiomyopathy: the Task Force for the Diagnosis and Management of Hypertrophic Cardiomyopathy of the European Society of Cardiology (ESC). European Heart Journal. 2014;35(39):2733–79.

[5] Maron BJ, Maron MS, Wigle ED, Braunwald E. The 50-year history, controversy, and clinical implications of left ventricular outflow tract obstruction in hypertrophic cardiomyopathy from idiopathic hypertrophic subaortic stenosis to hypertrophic cardiomyopathy: from idiopathic hypertrophic subaortic stenosis to hypertrophic cardiomyopathy. Journal of the American College of Cardiology. 2009;54(3):191–200.

[6] Maron MS, Olivotto I, Zenovich AG, Link MS, Pandian NG, Kuvin JT, et al. Hypertrophic cardiomyopathy is predominantly a disease of left ventricular outflow tract obstruction. Circulation. 2006;114(21):2232–9.

[7] Maron MS, Olivotto I, Betocchi S, Casey SA, Lesser JR, Losi MA, et al. Effect of left ventricular outflow tract obstruction on clinical outcome in hypertrophic cardiomyopathy. The New England Journal of Medicine. 2003;348(4):295–303.

[8] Elliott PM, Gimeno JR, Tome MT, Shah J, Ward D, Thaman R, et al. Left ventricular outflow tract obstruction and sudden death risk in patients with hypertrophic cardiomyopathy. European Heart Journal. 2006;27(16):1933–41.

[9] Nagueh SF, Bierig SM, Budoff MJ, Desai M, Dilsizian V, Eidem B, et al. American Society of Echocardiography clinical recommendations for multimodality cardiovascular imaging of patients with hypertrophic cardiomyopathy: Endorsed by the American Society of Nuclear Cardiology, Society for Cardiovascular Magnetic Resonance, and Society of Cardiovascular Computed Tomography. Journal of the American Society of Echocardiography: Official Publication of the American Society of Echocardiography. 2011;24(5):473–98.

[10] Lang RM, Bierig M, Devereux RB, Flachskampf FA, Foster E, Pellikka PA, et al. Recommendations for chamber quantification: a report from the American Society of Echocardiography's Guidelines and Standards Committee and the Chamber Quantification Writing Group, developed in conjunction with the European Association of Echocardiography, a branch of the European Society of Cardiology. Journal of the American Society of Echocardiography: Official Publication of the American Society of Echocardiography. 2005;18(12):1440–63.

[11] Caselli S, Pelliccia A, Maron M, Santini D, Puccio D, Marcantonio A, et al. Differentiation of hypertrophic cardiomyopathy from other forms of left ventricular hypertrophy

by means of three-dimensional echocardiography. The American Journal of Cardiology. 2008;102(5):616–20.

[12] Grigg LE, Wigle ED, Williams WG, Daniel LB, Rakowski H. Transesophageal Doppler echocardiography in obstructive hypertrophic cardiomyopathy: clarification of pathophysiology and importance in intraoperative decision making. Journal of the American College of Cardiology. 1992;20(1):42–52.

[13] Klues HG, Maron BJ, Dollar AL, Roberts WC. Diversity of structural mitral valve alterations in hypertrophic cardiomyopathy. Circulation. 1992;85(5):1651–60.

[14] Nagueh SF, Bachinski LL, Meyer D, Hill R, Zoghbi WA, Tam JW, et al. Tissue Doppler imaging consistently detects myocardial abnormalities in patients with hypertrophic cardiomyopathy and provides a novel means for an early diagnosis before and independently of hypertrophy. Circulation. 2001;104(2):128–30.

[15] Maron BJ, Spirito P, Green KJ, Wesley YE, Bonow RO, Arce J. Noninvasive assessment of left ventricular diastolic function by pulsed Doppler echocardiography in patients with hypertrophic cardiomyopathy. Journal of the American College of Cardiology. 1987;10(4):733–42.

[16] Nagueh SF, Middleton KJ, Kopelen HA, Zoghbi WA, Quinones MA. Doppler tissue imaging: a noninvasive technique for evaluation of left ventricular relaxation and estimation of filling pressures. Journal of the American College of Cardiology. 1997;30(6):1527–33.

[17] Yamamoto K, Nishimura RA, Chaliki HP, Appleton CP, Holmes DR, Jr., Redfield MM. Determination of left ventricular filling pressure by Doppler echocardiography in patients with coronary artery disease: critical role of left ventricular systolic function. Journal of the American College of Cardiology. 1997;30(7):1819–26.

[18] Nishimura RA, Appleton CP, Redfield MM, Ilstrup DM, Holmes DR, Jr., Tajik AJ. Noninvasive doppler echocardiographic evaluation of left ventricular filling pressures in patients with cardiomyopathies: a simultaneous Doppler echocardiographic and cardiac catheterization study. Journal of the American College of Cardiology. 1996;28(5):1226–33.

[19] Nagueh SF, Lakkis NM, Middleton KJ, Spencer WH, 3rd, Zoghbi WA, Quinones MA. Doppler estimation of left ventricular filling pressures in patients with hypertrophic cardiomyopathy. Circulation. 1999;99(2):254–61.

[20] Geske JB, Sorajja P, Nishimura RA, Ommen SR. Evaluation of left ventricular filling pressures by Doppler echocardiography in patients with hypertrophic cardiomyopathy: correlation with direct left atrial pressure measurement at cardiac catheterization. Circulation. 2007;116(23):2702–8.

[21] Kitaoka H, Kubo T, Okawa M, Takenaka N, Sakamoto C, Baba Y, et al. Tissue doppler imaging and plasma BNP levels to assess the prognosis in patients with hypertrophic

cardiomyopathy. Journal of the American Society of Echocardiography: Official Publication of the American Society of Echocardiography. 2011;24(9):1020–5.

[22] Efthimiadis GK, Giannakoulas G, Parcharidou DG, Karvounis HI, Mochlas ST, Styliadis IH, et al. Clinical significance of tissue Doppler imaging in patients with hypertrophic cardiomyopathy. Circulation Journal: Official Journal of the Japanese Circulation Society. 2007;71(6):897–903.

[23] Kitaoka H, Kubo T, Hayashi K, Yamasaki N, Matsumura Y, Furuno T, et al. Tissue Doppler imaging and prognosis in asymptomatic or mildly symptomatic patients with hypertrophic cardiomyopathy. European Heart Journal Cardiovascular Imaging. 2013;14(6):544–9.

[24] Lester SJ, Ryan EW, Schiller NB, Foster E. Best method in clinical practice and in research studies to determine left atrial size. The American Journal of Cardiology. 1999;84(7): 829–32.

[25] Sachdev V, Shizukuda Y, Brenneman CL, Birdsall CW, Waclawiw MA, Arai AE, et al. Left atrial volumetric remodeling is predictive of functional capacity in nonobstructive hypertrophic cardiomyopathy. American Heart Journal. 2005;149(4):730–6.

[26] Yang H, Woo A, Monakier D, Jamorski M, Fedwick K, Wigle ED, et al. Enlarged left atrial volume in hypertrophic cardiomyopathy: a marker for disease severity. Journal of the American Society of Echocardiography: Official Publication of the American Society of Echocardiography. 2005;18(10):1074–82.

[27] Marwick TH. Measurement of strain and strain rate by echocardiography: ready for prime time? Journal of the American College of Cardiology. 2006;47(7):1313–27.

[28] Abraham TP, Dimaano VL, Liang HY. Role of tissue Doppler and strain echocardiography in current clinical practice. Circulation. 2007;116(22):2597–609.

[29] Gilman G, Khandheria BK, Hagen ME, Abraham TP, Seward JB, Belohlavek M. Strain rate and strain: a step-by-step approach to image and data acquisition. Journal of the American Society of Echocardiography: Official Publication of the American Society of Echocardiography. 2004;17(9):1011–20.

[30] Weidemann F, Mertens L, Gewillig M, Sutherland GR. Quantitation of localized abnormal deformation in asymmetric nonobstructive hypertrophic cardiomyopathy: a velocity, strain rate, and strain Doppler myocardial imaging study. Pediatric Cardiology. 2001;22(6):534–7.

[31] Yang H, Sun JP, Lever HM, Popovic ZB, Drinko JK, Greenberg NL, et al. Use of strain imaging in detecting segmental dysfunction in patients with hypertrophic cardiomyopathy. Journal of the American Society of Echocardiography: Official Publication of the American Society of Echocardiography. 2003;16(3):233–9.

[32] Sengupta PP, Mehta V, Arora R, Mohan JC, Khandheria BK. Quantification of regional nonuniformity and paradoxical intramural mechanics in hypertrophic cardiomyop-

athy by high frame rate ultrasound myocardial strain mapping. Journal of the American Society of Echocardiography: Official Publication of the American Society of Echocardiography. 2005;18(7):737–42.

[33] Leitman M, Lysyansky P, Sidenko S, Shir V, Peleg E, Binenbaum M, et al. Two-dimensional strain-a novel software for real-time quantitative echocardiographic assessment of myocardial function. Journal of the American Society of Echocardiography: Official Publication of the American Society of Echocardiography. 2004;17(10):1021–9.

[34] Amundsen BH, Helle-Valle T, Edvardsen T, Torp H, Crosby J, Lyseggen E, et al. Noninvasive myocardial strain measurement by speckle tracking echocardiography: validation against sonomicrometry and tagged magnetic resonance imaging. Journal of the American College of Cardiology. 2006;47(4):789–93.

[35] Serri K, Reant P, Lafitte M, Berhouet M, Le Bouffos V, Roudaut R, et al. Global and regional myocardial function quantification by two-dimensional strain: application in hypertrophic cardiomyopathy. Journal of the American College of Cardiology. 2006;47(6):1175–81.

[36] Carasso S, Yang H, Woo A, Vannan MA, Jamorski M, Wigle ED, et al. Systolic myocardial mechanics in hypertrophic cardiomyopathy: novel concepts and implications for clinical status. Journal of the American Society of Echocardiography: Official Publication of the American Society of Echocardiography. 2008;21(6):675–83.

[37] Nagueh SF, Lakkis NM, He ZX, Middleton KJ, Killip D, Zoghbi WA, et al. Role of myocardial contrast echocardiography during nonsurgical septal reduction therapy for hypertrophic obstructive cardiomyopathy. Journal of the American College of Cardiology. 1998;32(1):225–9.

[38] Cardim N, Galderisi M, Edvardsen T, Plein S, Popescu BA, D'Andrea A, et al. Role of multimodality cardiac imaging in the management of patients with hypertrophic cardiomyopathy: an expert consensus of the European Association of Cardiovascular Imaging Endorsed by the Saudi Heart Association. European Heart Journal Cardiovascular Imaging. 2015;16(3):280.

[39] Maron MS, Appelbaum E, Harrigan CJ, Buros J, Gibson CM, Hanna C, et al. Clinical profile and significance of delayed enhancement in hypertrophic cardiomyopathy. Circulation Heart Failure. 2008;1(3):184–91.

[40] Rickers C, Wilke NM, Jerosch-Herold M, Casey SA, Panse P, Panse N, et al. Utility of cardiac magnetic resonance imaging in the diagnosis of hypertrophic cardiomyopathy. Circulation. 2005;112(6):855–61.

[41] Maron BJ, Haas TS, Lesser JR. Images in cardiovascular medicine. Diagnostic utility of cardiac magnetic resonance imaging in monozygotic twins with hypertrophic cardiomyopathy and identical pattern of left ventricular hypertrophy. Circulation. 2007;115(24):e627-8.

[42] Moon JC, Fisher NG, McKenna WJ, Pennell DJ. Detection of apical hypertrophic cardiomyopathy by cardiovascular magnetic resonance in patients with non-diagnostic echocardiography. Heart. 2004;90(6):645–9.

[43] Moon JC, McKenna WJ, McCrohon JA, Elliott PM, Smith GC, Pennell DJ. Toward clinical risk assessment in hypertrophic cardiomyopathy with gadolinium cardiovascular magnetic resonance. Journal of the American College of Cardiology. 2003;41(9): 1561–7.

[44] Petersen SE, Jerosch-Herold M, Hudsmith LE, Robson MD, Francis JM, Doll HA, et al. Evidence for microvascular dysfunction in hypertrophic cardiomyopathy: new insights from multiparametric magnetic resonance imaging. Circulation. 2007;115(18):2418–25.

[45] Todiere G, Aquaro GD, Piaggi P, Formisano F, Barison A, Masci PG, et al. Progression of myocardial fibrosis assessed with cardiac magnetic resonance in hypertrophic cardiomyopathy. Journal of the American College of Cardiology. 2012;60(10):922–9.

[46] Moravsky G, Ofek E, Rakowski H, Butany J, Williams L, Ralph-Edwards A, et al. Myocardial fibrosis in hypertrophic cardiomyopathy: accurate reflection of histopathological findings by CMR. JACC Cardiovascular Imaging. 2013;6(5):587–96.

[47] Moon JC, Reed E, Sheppard MN, Elkington AG, Ho SY, Burke M, et al. The histologic basis of late gadolinium enhancement cardiovascular magnetic resonance in hypertrophic cardiomyopathy. Journal of the American College of Cardiology. 2004;43(12):2260–4.

[48] O'Gara PT, Bonow RO, Maron BJ, Damske BA, Van Lingen A, Bacharach SL, et al. Myocardial perfusion abnormalities in patients with hypertrophic cardiomyopathy: assessment with thallium-201 emission computed tomography. Circulation. 1987;76(6): 1214–23.

[49] Dilsizian V, Bonow RO, Epstein SE, Fananapazir L. Myocardial ischemia detected by thallium scintigraphy is frequently related to cardiac arrest and syncope in young patients with hypertrophic cardiomyopathy. Journal of the American College of Cardiology. 1993;22(3):796–804.

[50] Cannon RO, 3rd, Dilsizian V, O'Gara PT, Udelson JE, Tucker E, Panza JA, et al. Impact of surgical relief of outflow obstruction on thallium perfusion abnormalities in hypertrophic cardiomyopathy. Circulation. 1992;85(3):1039–45.

[51] Maron MS, Olivotto I, Maron BJ, Prasad SK, Cecchi F, Udelson JE, et al. The case for myocardial ischemia in hypertrophic cardiomyopathy. Journal of the American College of Cardiology. 2009;54(9):866–75.

Chapter 8

The Role of Echocardiography in the Management of Patients Undergoing a Ventricular Assist Device Implantation and/or Transplantation

Tomoko Kato, Takashi Nishimura, Shunei Kyo,
Kenji Kuwaki, Hiroyuki Dada and Atsushi Amano

Additional information is available at the end of the chapter

http://dx.doi.org/10.5772/65095

Abstract

Heart transplantation (HTx) is a curative treatment for patients with advanced heart failure (HF); however, since transplant opportunities are severely limited due to donor shortage, the left ventricular assist device (LVAD) has become a standard therapy for patients awaiting HTx. The role of echocardiography as a primary imaging modality to monitor the allograft function in transplant recipients as well as to optimize LVAD settings in LVAD recipients has been expanding. The purpose of this review is to highlight the clinical role of echocardiography in the management of patients undergoing LVAD implantation and/or HTx. In particular, we overview (1) how to detect LVAD malfunction and device-associated complication in LVAD recipients and (2) echocardiographic assessments of cardiac allograft rejection in transplant recipients.

Keywords: heart failure, transplant, rejection, ventricular assist device, echocardiography

1. Introduction

Heart transplantation (HTx) provides considerable survival benefits for patients with end-stage heart failure, but it is available for only a small fraction of such patients all over the world due to donor shortage [1]. Therefore, many heart transplant candidates require long-term support by a left ventricular assist device (LVAD) while they await transplantation [1, 2]. More recently, mechanical circulatory support has evolved into a standard therapy for

patients with advanced heart failure, not only as a bridge to cardiac transplantation but also as a destination therapy or a bridge to myocardial recovery [3].

Echocardiography is a primary imaging modality in the assessment of cardiac structure and function in patients with advanced HF. In addition, echocardiography can be performed at the patient's bedside, and results are immediately available. In this review, we highlight the effectiveness of echocardiography in the management of patients undergoing LVAD implantation and/or HTx.

2. Echocardiography in LVAD recipients

A growing number of heart transplant candidates require long-term support by an LVAD while they await cardiac transplantation. Further, LVAD therapy has become a standard therapy for patients with advanced HF, not only as a bridge to cardiac transplantation but also as a destination therapy or a bridge to myocardial recovery. Here, we focused on the usefulness of echocardiography in patients undergoing LVAD implantation.

2.1. Preoperative assessment

It is important to assess the LVAD eligibility and rule out any contraindications against LVAD surgery prior to an operation. Several structural issues that can be surgically corrected at the time of LVAD implantation should be carefully evaluated prior to the LVAD surgery. The presence of clots, especially at the apex, should be carefully assessed because it will increase the risk of inflow cannula obstructions and/or perioperative stroke. Intracardiac shunts, including patent foramen ovale, should also be carefully assessed before and during surgery. Intracardiac shunts must be closed at the time of LVAD surgery. Further, coexisting valvular heart disease should be assessed prior to the LVAD procedure. Concomitant valvular surgery can be performed at the time of LVAD implantation; however, although such an additional approach can provide possible benefits, data regarding its long-term effect are limited, and the indications are still controversial. Another important issue to be carefully evaluated preoperatively includes right ventricular (RV) function because right ventricular failure (RVF) after LVAD placement is associated with increased morbidity and mortality.

2.1.1. Preoperative valvular assessment

Regarding tricuspid regurgitation (TR), several previous papers have revealed that tricuspid annular dilatation is highly associated with post-LVAD right ventricular failure [4]. Kukucka M et al. reviewed 122 patients without significant TR at the time of VAD implant and found that a tricuspid annulus diameter >43 mm was an independent predictor of survival after LVAD (**Figure 1**). On the other hand, whether the TR should be surgically managed at the time of LVAD surgery is controversial. Dunlay et al. performed a literature search of randomized controlled trials and observational studies (including 3249 patients) that compared the outcome of concomitant tricuspid valve surgery at the time of LVAD with that of LVAD alone [5]. They found that the addition of valvular surgery at the time of the LVAD procedure

http://dx.doi.org/10.5772/65095

prolonged cardiopulmonary bypass times by an average of 31 minutes, but no differences were found between the groups for acute renal failure, early mortality, or the need for a right ventricular assist device. Having said that, a recent paper from Columbia University suggested that concomitant tricuspid valve procedures at the time of LVAD surgery can be performed safely and protect against worsening tricuspid regurgitation during the first two years of support [6]. In either case, the severity of TR and annular size need to be assessed preoperatively. Surgeons should also bear in mind that preexisting severe TR, especially with annular size >43 mm, is at higher risk of adverse events after surgery.

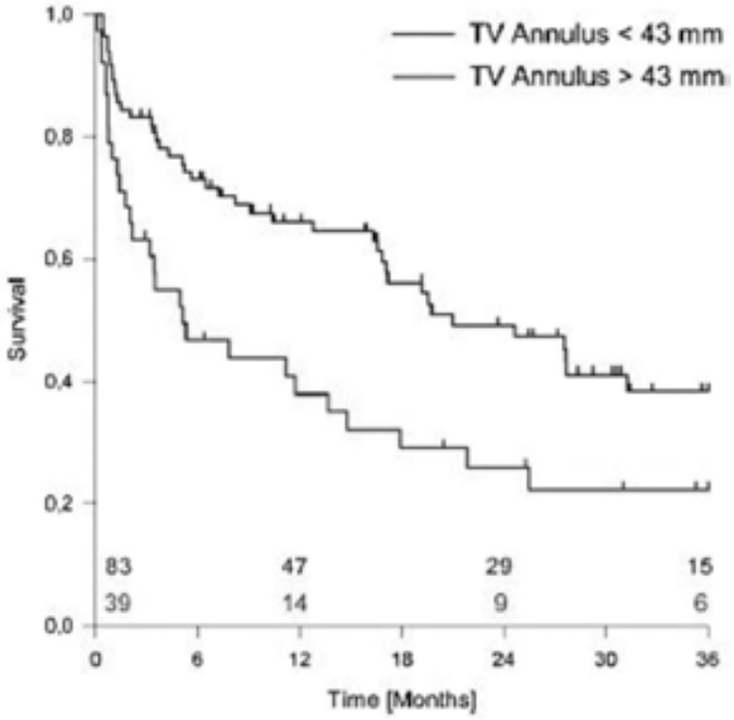

Figure 1. The impact on tricuspid valve annulus dilation on post-LVAD survival (quoted from Ref. [4]). Kaplan-Meier survival curves of patients with tricuspid valve (TV) annulus diameter <43 mm (blue) and >43 mm (red). Censored patients are represented by vertical marks. Numbers of patients at risk at 0, 12, 24, and 36 months of follow-up are presented above the x-axis (log-rank test, p = 0.007).

Aortic insufficiency (AI) occurs in up to 50% of patients within 1 year after continuous flow LVAD implantation. Although de novo AI can be commonly seen postoperatively, the presence of more than mild AI as well as any structural abnormality, as detected by transthoracic echocardiography (TTE), should be reported to the LVAD surgery team. In cases with poor TTE images, the results derived from intraoperative transesophageal echocardiography (TEE) should be carefully discussed. The valvular morphology, valvular calcification, possible fusion, and myxomatous changes should also be reported to the surgeons. The recently published comprehensive review of AI post-LVAD by Cowger et al. suggested the importance of intraoperative TEE to detect unmasked AI [7]. During the initiation of continuous flow LVAD support, as LV filling pressures drop with early unloading, the gradient between the aortic root and the LV increases, potentially exposing significant AI that was previously unrecog-

nized. Because AI severity can be associated with an increase in pump speeds, we can quantitatively assess AI severity at different pump speeds to consider the necessity of concomitant aortic valve surgery in an operating room. This review summarized the risk and benefits of aortic valve surgery at the time of LVAD (**Table 1**).

Strategy	Pros	Cons
Partial closure with a single central stitch (Park's stitch)	• Simple and effective when the leaflet tissue has adequate tensile strength to hold sutures • Permit blood ejection through the aortic valve	• Questionable durability • Risk of progression to aortic stenosis • Need for AVR in the event of myocardial recovery leading to LVAD explant
Modified Park's stitch—additional pledgeted mattress suture between the central stitch and each commissure	• Relatively simple and can be effective, even if leaflets are thin • Permits blood ejection through the aortic valve but could be reduced compared to single central stitch	• Questionable durability • Risk of progression to aortic stenosis • Need for AVR in the event of myocardial recovery leading to LVAD explant
Complete closure of the ventriculo-aortic juncture with a circular patch	• Simple with relatively fast repair time • Long-term durability	• No blood ejection through the aortic valve • Risk of thrombus formation • Risk of death in the case of pump stoppage or failure
Replacement of incompetent aortic valve with bioprosthetic valve	• Maintenance of valve opening in the postoperative period • Testing for cardiac recovery • Tolerance to exercise	• Increase CPB and cross-clamp time • Risk of leaflet fusion • Risk of valvular and subvalvular thrombus formation due to fresh suture lines combined with decreased flow across the new valve

Table 1. Pros and cons of surgical management strategies of the native aortic valve (quoted from Ref. [7]).

Mitral valve insufficiency has fewer effects on postoperative outcome compared with aortic and tricuspid valve insufficiency. Indeed, a significant number of patients who had severe mitral regurgitation due to annulus dilatation and tethered pupillary muscle preoperatively showed a remarkable decrease in mitral regurgitation flow under LVAD support [8]. Although mitral valve surgery at the time of LVAD implant to correct severe mitral regurgitation does not affect postoperative mortality or cause other adverse events, the procedure can be considered in cases undergoing an LVAD procedure as a bridge to recovery. In addition, concomitant mitral valve repair can decrease pulmonary vascular resistance [9]. Kitada et al. investigated preoperative echocardiographic features associated with persistent mitral regurgitation after LVAD implantation (**Figure 2**) [10]. They found that the posterior displacement of the coapta-

http://dx.doi.org/10.5772/65095

tion point of a mitral leaflet (30 vs. 24 mm), papillary muscle distance (49 vs. 43 mm), and tethering area (353 vs. 299 mm^2) before surgery were greater in patients who had persistent moderate to severe mitral regurgitation post-LVAD than those in patients who did not have significant MR postoperatively. A multivariate analysis showed that the posterior displacement was the only independent predictor for persistent MR.

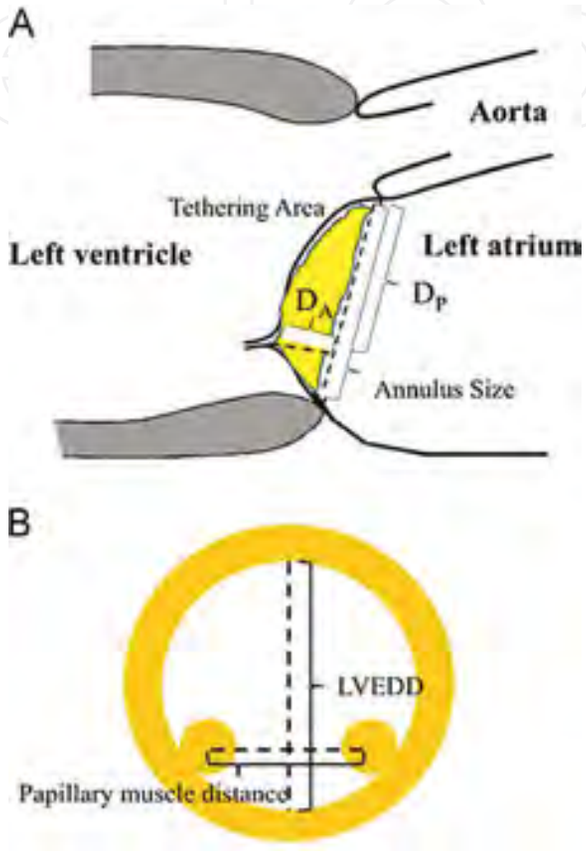

Figure 2. The measurements of echocardiographic parameters to quantify the mitral leaflet configurations in 2D echocardiography (quoted from Ref. [10]). DA, apical displacement; DP, posterior displacement; LVEDD, left ventricular end diastolic dimension.

2.1.2. Preoperative and perioperative right ventricular assessment

Right ventricular failure (RVF) remains a major cause of morbidity and mortality following LVAD surgery. The incidence of RVF post-LVAD is 10–30% despite the recent improvements in device technology and postoperative patient management. Under LVAD support, right ventricular (RV) preload increases as a result of increased circulatory volume, whereas RV afterload is expected to decrease, secondary to improvement in pulmonary vascular resistance [11]. A sepal wall shift induced by LVAD alters the RV structure, which may worsen RV contractile and relaxation abnormalities. Therefore, when considering RV systolic and diastolic reserve before and also after surgery, it is important to identify which patients may need RV-specific mechanical and medical support post-LVAD [12].

Study	Patients	RVF definition and rate	Multivariable predictors	Echocardiographic RV parameters considered
Michigan RV failure risk score (2008)[a]	197 LVADs 28 CF-LVAD 94% BTT	Need for RVAD/ inotropes RVF rate: 35%	Preoperative vasopressors (4 pts) AST ≥80 IU/L (2 pts) Bilirubin ≥2.0 mg/dL (2.5 pts) Creatinine ≥2.3 mg/dL (3 pts)	RV systolic function (visual semiquantitative) TR (visual semiquantitative)
Penn RVAD risk score[b] (2008)	266 LVADs 6 CF-LVAD BTT vs. DT not reported	Need for RVAD RVF rate: 37%	Cardiac index ≤2.2 L/min/m^2 RVSWI ≤0.25 mm Hg × L/m^2 Severe RV dysfunction Creatinine ≥1.9 mg/dL Prior cardiac surgery Systolic BP ≤96 mm Hg	RV systolic function (visual semiquantitative)
Utah RV risk score[c] (2010)	175 LVADs 25 CF-LVAD 58% BTT, 42% DT	Need for RVAD/ inotropes/ inhaled NO RVF rate: 44%	DT indication (3.5 pts) IABP (4 pts) PVR (1–4 pts) Inotrope dependency (2.5 pts) Obesity (2 pts) ACEI or ARB use (−2.5 pts) β-blocker use (2 pts)	Right atrial area
Kormos[d] (2010)	484 LVADs All CF-LVAD BTT 100%	Need for RVAD/ inotropes RVF rate: 20.2%	CVP/PCWP >0.63 (OR, 2.3) Need for preoperative ventilator support (OR, 5.5)BUN >39 mg/dL (OR, 2.1)	None
Pittsburgh Decision Tree[e] (2012)	183 LVADs 40 CF-LVAD BTT vs. DT not reported	Need for RVAD RVF rate: 15%	Age, heart rate, transpulmonary gradient; right atrial pressure; INR, white blood cell count, ALT, number of inotropic agents	None
CRITT[f] (2013)	167 LVADs, all CF-LVAD 51 BiVADsBTT vs. DT not reported	Need for BiVAD RVF rate: 23%	CVP >15 mm Hg (C) Severe RV dysfunction (R) Preoperative intubation (I) Severe TR (T) Heart rate >100 (tachycardia [T])	RV systolic function (visual semiquantitative) Severe TR (visual semiquantitative)

ACEI, angiotensin-converting enzyme inhibitor; ALT, alanine aminotransferase; ARB, angiotensin receptor blocker; AST, aspartate aminotransferase; BiVAD, biventricular assist device; BP, blood pressure; BTT, bridge to transplantation; BUN, blood urea nitrogen; CF, continuous flow; CRITT, central venous pressure-RV dysfunction-preoperative intubation-severe tricuspid regurgitation-tachycardia; CVP, central venous pressure; DT, destination therapy; IABP; intra-aortic balloon pump; INR, international normalized ratio; ITT, intention to treat; LVAD, left ventricular assist device; NO, nitric oxide; OR, odds ratio; PCWP, pulmonary capillary wedge pressure; PVR, pulmonary vascular resistance; RV, right ventricle; RVAD, right ventricular assist device; RVF, right ventricular failure; RVSWI, right ventricular stroke work index; and TR, tricuspid regurgitation.
The data were obtained from the following papers: (a) Matthews JC, et al. J Am Coll Cardiol. 2008;51:2163–2172; (b) Fitzpatrick JR III, et al. J Heart Lung Transplant. 2008;27:1286–1292; (c) Drakos SG, et al. Am J Cardiol. 2010;105:1030–1035; (d) Kormos RL, et al; HeartMate II Clinical Investigators. J Thorac Cardiovasc Surg. 2010;139:1316–1324; (e) Wang Y, et al. J Heart Lung Transplant. 2012;31:140–149; (f) Atluri P, et al. Ann Thorac Surg. 2013;96:857–863.

Table 2. Clinical risk prediction scores for right ventricular failure in left ventricular assist device recipients (quoted from Ref. [13]).

http://dx.doi.org/10.5772/65095

Table 2 summarizes the clinical risk prediction scores that have been cited in the recently published review literature [13]. In addition to these risk scores, serial echocardiographic assessments are helpful in evaluating RV functional reserve prior to surgery. Previously reported echocardiographic parameters associated with the risk for developing RVF after LVAD implantation have included tricuspid annular dilation (>43 mm) [4], tricuspid annular motion (8 vs. 15 mm) [14], and RV-to-LV end-diastolic diameter ratio (>0.72) [15]. However, it is sometimes technically difficult to obtain ideal RV images that allow quantitative assessments of patients with advanced heart failure, particularly if the patients are severely congested, intubated, and/or have a markedly enlarged left ventricle (LV) that obscures the right ventricle (RV) [16]. Kato et al. focused only on left-sided 2D echo parameters that can predict RVF post-LVAD. They showed that patients with relatively small LV size, preserved LV contraction, and a dilated left atrium were at higher risk for RVF after LVAD surgery (**Figure 3**) [16]. In addition to the conventional echo parameters, Grant et al. reported that the incremental role of RV strain to predict RVF [17]. More recently, Kato et al. reported that serial echocardiograms using tissue Doppler imaging (TDI) and speckle tracking echocardiography (STE) before and soon after (within 72 hours) LVAD surgery may aid in identifying the need to initiate targeted RVF-specific therapy [12]. In this study, RV stiffness (as reflected by TDI-derived E/E′) and decreased RV contractility (as reflected by TDI-derived S′ and RV longitudinal strain) before and soon after LVAD surgery were found to be useful parameters to include in the perioperative management of LVAD patients (**Figure 4**).

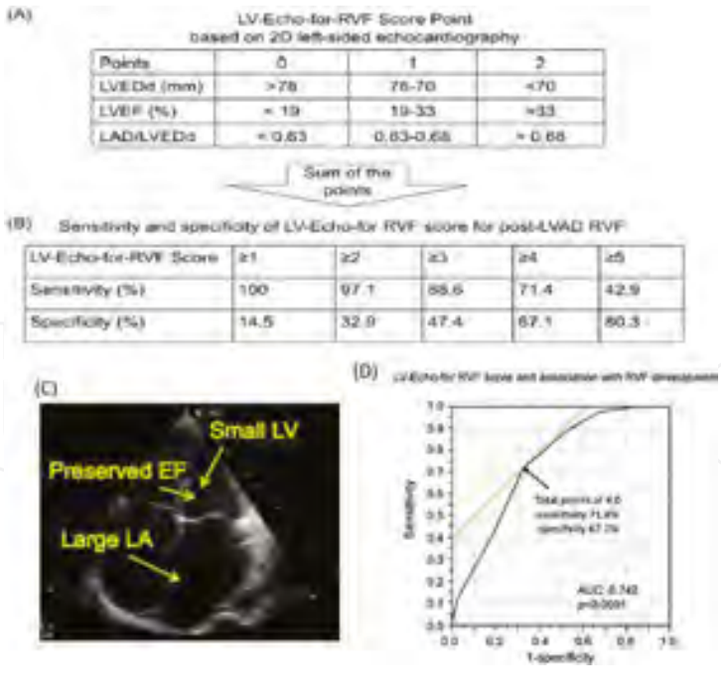

Figure 3. Left ventricular echocardiographic right ventricular failure score (LV-for-Echo-RVF) based on two-dimensional echocardiographic left-sided heart parameters (quoted from Ref. [16]). (A) Points associated with value of each variable. (B) Sensitivity and specificity of sum of points associated with right ventricular failure development after left ventricular assist device placement. (C) Representative 2D echo images in patients developing RVF post-LVAD. (D) Receiver operating characteristics curve for LV echocardiographic RVF score. AUC, area under the curve.

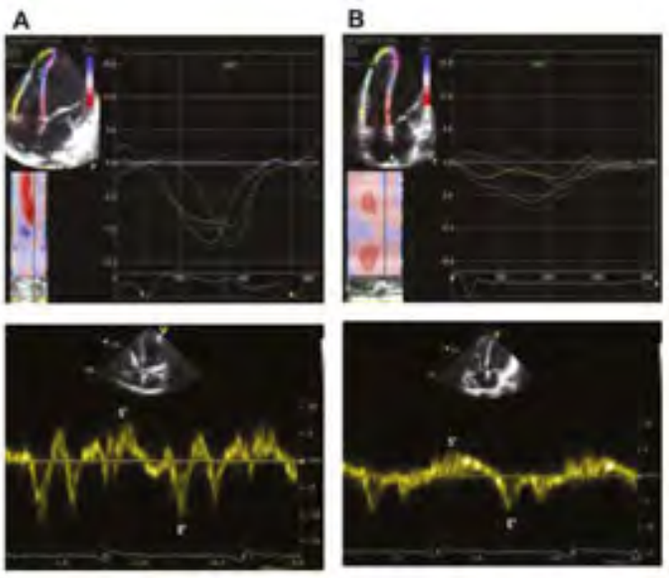

Figure 4. Representative global RV longitudinal strain and TDI obtained before surgery from a patient without RVF after LVAD and from a patient with RVF after LVAD (quoted from Ref. [18]). (A) The right ventricular (RV) global longitudinal strain; tissue Doppler image (TDI)-derived S′ and E′ for patient A was −14.3%, 7.8 cm/s and −10.8 cm/s, respectively. (B) These parameters were −6.2%, 4.6 cm/s and −5.3 cm/s, respectively. LVAD, left ventricular assist device; RVF, right ventricular failure.

2.2. Perioperative assessment

Other than the speed adjustment to avoid RV failure due to excessive RV preload by LVAD support, several important points should be evaluated by intraoperative TEE. First, de-airing of the heart chamber should be confirmed. Careful observation of trapped air at the site of anastomosis sites and around the LVAD inflow/outflow cannula is required [18]. Second, adjusting LV speed to maintain appropriate LV unloading without a septal shift under TEE guidance is required. The positioning of the inflow cannula at the apex should be monitored by TEE as well. Third, as mentioned above, the existence of valvular diseases and intracardiac shunts, which can be corrected simultaneously at the time of LVAD implantation, should be communicated to the surgeons. Finally, pericardial effusion and its amount should also be carefully observed by TEE. Cardiac tamponade can occur relatively often because patients under LVAD support require sufficient anticoagulation soon after surgery to prevent clot formation at the cannula and inside the device.

2.3. Postoperative assessment

Table 3 illustrates the checklist that will help sonographers/echocardiologists to perform an LVAD echo. In general, we can simply summarize the purposes of echo in LVAD recipients as follows: (1) to carefully monitor device malfunction, (2) to adjust appropriate LVAD setting/speed (appropriate peripheral perfusion and RV preload), and (3) to evaluate myocardial recovery and to seek optimal timing for LVAD weaning.

The points to be evaluated by TEE on a periodic basis are as follows: the location and thrombus at the inflow cannula; LV cavity diameters; septal position; RV function; valvular regurgitation, especially about the aortic valve opening/intervals and regurgitation.

View	Points to be checked
Parasternal views	• LV dimensions (ensure they are taken on axis)
	• AV opening (long acquisitions, use long and short axis, and M-mode)
	• Mitral regurgitation (tethering is the hallmark of functional regurgitation, and the degree may change according to LVAD rpm)
	• Consider evaluating cardiac output through RV out flow
Apical views	• Evaluate LV and RV function
	• Evaluate inlet cannula flow (position and suctioning)
	• Rule out thrombus in LV, RV, LA, and RA (use contrast as needed)
	• Evaluate aortic regurgitation
Image the inlet cannula	• Use multiple views including nonstandard
	• Rule out thrombus or other cause of obstruction (use contrast as needed)
	• Positioning (against LV wall)

Table 3. Echo LVAD checklist.

2.3.1. General postoperative assessment in LVAD recipients

Recommendations for device speed adjustment include the target measures of mean arterial pressure above 65 mmHg, maintaining the position of interventricular septum and shape, and intermittent aortic valve opening, under the condition of no more than mild mitral regurgitation to ensure appropriate unloading of the LV. Optimization of speed settings is extremely important to prevent several of the key complications associated with chronic LVAD support. The importance of ensuring the middle septal position for optimal RV function has been well established [19, 20].

Serially monitoring the timing and its interval of aortic valve opening in all LVAD recipients are necessary. Also, adjusting the LVAD speed to maintain the aortic valve opening is important to prevent the development of aortic valve regurgitation. At least 10 cardiac cycles should be recorded to evaluate the aortic valve opening. Because the interval of aortic valve opening, LV diameter, and grade of MR entirely depend on the degree of LV unloading, the LVAD setting together with the echo report needs to be recorded (**Figure 5**). Aortic regurgitation is sometimes seen with atypical timing (**Figure 6**) or continuously, both during the diastolic and systolic phases [21].

Cardiac output using RV outflow-derived Doppler estimation can be calculated as follows: cardiac output = stroke volume × heart rate, stroke volume = $\pi \times (\text{RV outflow diameter}/2)^2 \times$

time velocity integral at RV outflow. In patients who have at least an intermittent aortic valve opening, RV cardiac output minus LV outflow-derived cardiac output is equivalent to the estimated pump flow.

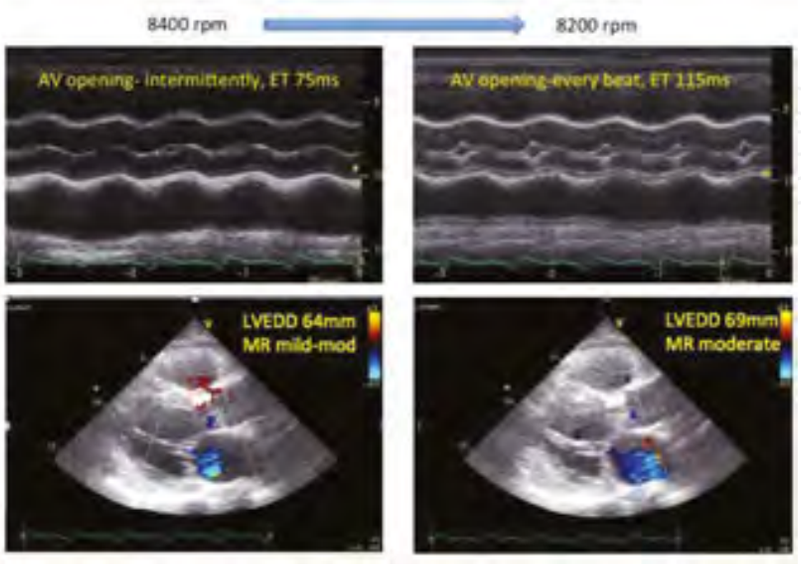

Figure 5. Representative images in a LVAD recipient with different LVAD speeds. This patient received HeartMate II (Thoratec Corp) implantation. Under 8400 rpm, the aortic valve opened intermittently, and the ejection time was only 75 ms. When we set the speed down to 8200, the aortic valve opened every beat, but due to less unloading, the LV diameter increased and the amount of mitral regurgitation also increased.

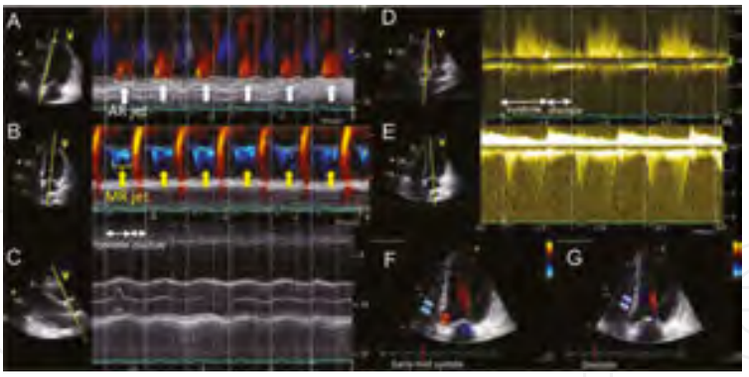

Figure 6. Aortic regurgitation during systolic phase accompanied by mitral regurgitation in patients with a continuous-flow left ventricular assist device (quoted from Ref. [22]). Echo images obtained from a patient undergoing LVAD implantation who showed systolic-phase aortic regurgitation (AR). The timing of the regurgitation jet started at the mid-systolic phase and ended at the early diastolic phase (A). The AR occurred slightly after the onset of mitral regurgitation (MR) (B), and both MR and AR timings were consistent with the systolic phase. No remarkable AR jet was documented during the diastolic phase. The AV was mostly closed throughout the cycles, which opens once every 8–10 beats (C). The mean pressure gradients of the trans-AV and trans-mitral valve based on the continuous wave Doppler measurements of AR (D) and MR flow (E) were 3.7 and 24.3 mmHg, respectively. The morphology of AV annulus changes through the cycles irrespective of the AV opening, with the AV annulus abnormally distorted and dilated during early mid-systole (F), whereas the septum wall as well as the AV annulus edge slightly pushed toward the LV during diastole (G).

http://dx.doi.org/10.5772/65095

Serial assessments of pulmonary artery pressure by Doppler-derived TR pressure gradients are also important. In general, LVAD support can successfully unload LV, which results in the correction of pulmonary hypertension due to left-sided heart failure. However, some patients have showed residual pulmonary vascular resistance post-LVAD; therefore, echo-guided optimal medical therapy, including the necessity of pulmonary dilators such as PDE5 inhibitors (sildenafil®, etc.), is required.

2.3.2. Detection of LVAD malfunction

The careful observation of the inflow cannula is critically important. By using multiple views, including nonstandard ones, the thrombus or other causes of obstruction should be ruled out. The direction of the inflow cannula should also be reported. The direction may sometimes change after the surgery and direct toward the lateral wall, which may cause suctioning or inadequate LVAD support. Contrast echocardiography can provide additional information. Detecting the outflow cannula obstruction by echocardiography is difficult, but practitioners should try to find a good echo window and investigate any abnormality, including kinking (**Figure 7**) [22, 23].

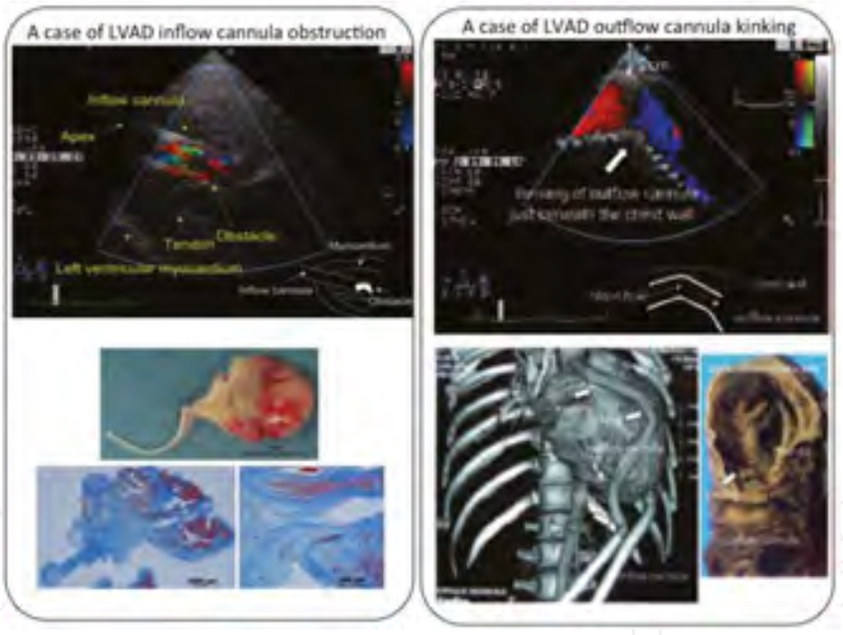

Figure 7. Cases of LVAD malfunction detected by echocardiography (quoted from Refs. [23, 24]). Left: A 29-year-old male developed low output syndrome 5 months after LVAD implantation. Echocardiography revealed pendulating obstacles at the inflow cannula of the LVAD. The obstacle was removed surgically, which histologically turned out to be myocardium with fibrous tissue and thrombi. Right: A 53-year-old man undergoing LVAD implantation developed low output syndrome. Echocardiography indicated distortion of the outflow cannula of the LVAD. A 3D CT also showed the kinking of the cannula. The autopsy revealed thrombus at the kinking site.

The protocol for a ramp study was established by Uriel N [20]. It is useful in optimizing LVAD settings and in diagnosing device malfunctions. Ramp test echocardiography can be performed at the time of discharge for speed optimization and/or if device malfunction is

suspected (**Figure 8**) [24]. The patient's left ventricular size, the frequency of the aortic valve opening, valvular insufficiency, blood pressure, and continuous flow-LVAD parameters should be recorded according to the increments of the device speed. Serial assessments of ramp tests are also helpful to detect LVAD clots [24].

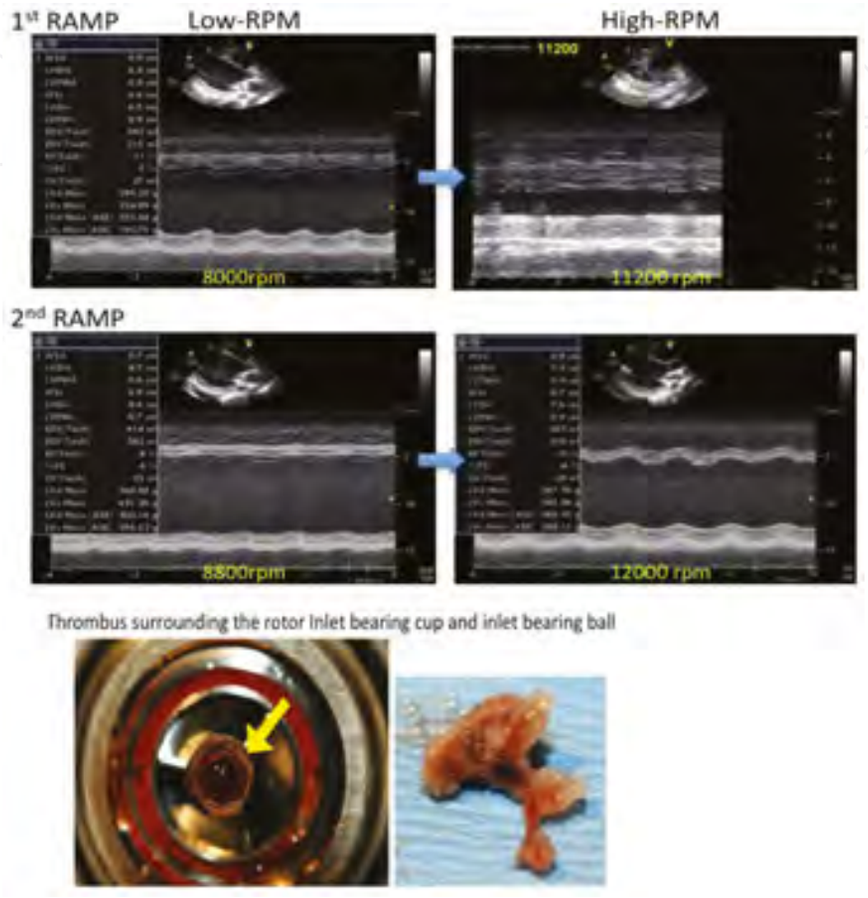

Figure 8. A representative case with device thrombosis was detected by a ramp echocardiography device (quoted from Ref. [24]). A case of a 29-year-old woman undergoing HeartMate II LVAD implantation; serial ramp studies were used to diagnose intradevice thrombus after device implantation. The first ramp study on postoperative day (POD) 26 revealed an adequate reduction in ventricular size according to the increase in LVAD. The patient was discharged home and received routine anticoagulation maintenance therapy. However, a second ramp test was performed on POD 56 due to increased lactase dehydrogenase and brain natriuretic peptide levels and showed a marked increase in the LV chamber size without an adequate response to the LVAD speed changes. Given the suspicion for partial pump thrombosis, the patient was immediately hospitalized and received intravenous heparin infusion. The patient eventually underwent cardiac transplant successfully, and the partial clot was found inside of the pump (lower panel).

2.3.3. Assessment of native cardiac function

It is important to assess native LV function, especially in patients receiving LVAD as a bridge to recovery. We cannot assess LV function without turning off the LVAD because it drastically affects preload and afterload; therefore, we need to reduce the LVAD speed under adequate anticoagulation during weaning test echocardiography. Strain assessment has been reported

http://dx.doi.org/10.5772/65095

to be more sensitive in evaluating the myocardial systolic and diastolic reserve, and 2D speckle tracing echocardiography for the assessment of myocardial recovery in LVAD recipients may be useful [25].

3. Echocardiography in transplant recipients

3.1. Donor heart evaluation

Evaluating a donor heart as accurately as possible at the time of procurement provides essential information to a recipient team leading the delicate posttransplant management of the heart [26]. If an organ procurement team has a cardiologist or sonographer who knows which patient is going to receive the heart, the team can gather detailed information by bedside echocardiography on the donor in light of the potential recipient's conditions at the organ procurement.

Measuring the heart size of the donor from bedside echocardiography at the time of organ procurement can provide useful information for judging the appropriateness of proceeding with the heart transplant in the case of a donor-recipient size mismatch. The wall thickness of the donor heart may also be useful information for optimizing the medical therapy after transplantation, as well as for deciding whether or not to use the organ. Information regarding the presence or absence of a septal defect would be of help to surgeons planning the additional procedure of septal closure at the time of transplantation. Information about the coronary flow in the left anterior descending artery of the donor heart, especially in cases with coronary risk factors, is useful for judging the availability of the heart, as well as for considering issues related to posttransplant medical management. Finally, information about preexisting localized wall motion abnormalities from bedside echocardiography is useful for speculating on the possibility of rejection or other reasons for wall motion abnormality after transplant surgery.

According to such information, the team can make a final decision whether or not to harvest the heart. For example, the donor heart may be relatively small for the potential recipient. If a donor heart with a lower limit of normal systolic function shows decreased coronary flow and localized right heart wall motion abnormality, the heart should be declined in cases where the potential recipients have moderately high pulmonary vascular resistance. Such recipients need to receive a donor heart with good right ventricular function.

3.2. A noninvasive rejection diagnosis

Advances in immunosuppressive therapy have resulted in a marked decrease in the incidence of acute allograft rejection in heart transplant recipients; however, acute rejection still remains an important determinant factor for long-term morbidity and mortality. Acute rejection can result in not only the immediate risk of graft loss or heart failure but also of subsequent allograft vasculopathy [27]. Therefore, early diagnosis of rejection and consequent timely treatment are crucial for the early and long-term care in heart transplant recipients. Detection of allograft rejection based on the findings derived from endomyocardial biopsy (EMB) is still a gold

standard; however, EMB is invasive, cost and time consuming, and may have a possibility of sampling error and interobserver variability. Although many noninvasive modalities, including radionuclide imaging, MRI, and gene expression profiling, have been investigated for their potential to detect rejection, none of them have been found to be sufficient for replacing EMB. Echocardiography has been routinely used in the management of cardiac transplant recipients. Indeed, it is an easily applicable, repeatable, and powerful noninvasive tool in the management of posttransplant recipients [28].

Variables	Characteristics and pitfalls
LVEF ↓ LV %FS ↓	• Occurs in the late phase of the rejection process • Mild/moderate rejection cannot be detected
LV wall thickness ↑ LV mass ↑	• May be related to inflammatory cell infiltration • Myocardial edema/preoperative ischemia also cause increase in LV wall thickness; so difficult to interpret during early postoperative periods
Mitral E/A ratio ↑ Mitral DcT ↓ IVRT ↓	• Abnormal filling pattern/restrictive physiology is associated with rejection • Relatively pre/after-load dependent • Doppler angle dependent • Heart rate dependent (not appropriate for patients with tachycardia)
TEI Index* (MPI) ↑	• Can evaluate global ventricular performance (both systolic and diastolic) • Derived from Doppler-derived time intervals • HR independent
Pericardial effusion↑	• May be related to the inflammatory process of rejection, but can have many causes, especially during the early postoperative phase

A, late diastolic mitral inflow velocity; DcT, deceleration time; E, early diastolic mitral inflow velocity; EF, ejection fraction; FS, fractional shortening; LV, left ventricle, left ventricular; IVRT, isovolumic relaxation time; IMP, myocardial performance index. *MPI = (isovolumic contraction time – IVRT)/ejection time.

Table 4. Conventional echocardiographic variables associated with rejections (quoted from Ref. [29]).

3.2.1. Conventional echocardiography

Table 4 summarizes the conventional echocardiographic parameters associated with acute cellular rejection [28]. Conventional echocardiography soon after the surgery can provide information about global systolic and diastolic functions, wall motion abnormality, and the hemodynamics of the transplanted hearts. Any apparent abnormal findings such as remarkable systolic and/or diastolic impairment may acute or hyperacute rejection, including antibody-mediated rejection, although primary graft failure, donor-related graft dysfunction, and any perioperative accidents should also be considered. The ability of conventional echo parameters to detect rejection is still limited to severe clinically detectable rejection. However,

http://dx.doi.org/10.5772/65095

the findings are still useful for assessing responsiveness to treatment. In general, patients with rejection develop restrictive physiology accompanied by various degrees of systolic dysfunction. Valantine HA et al. reported that a 15% decrease in mitral deceleration time or isovolumic relaxation time (IVRT) is associated with biopsy proven rejection [29]. More recently, Sun et al. reported that a combination of IVRT less than 90 ms, a mitral E/A ratio more than 1.7, and other clinical parameters is independently associated with rejection [30]. However, because transplant recipients usually have higher resting heart rates than the nontransplant population due to denervation, their mitral E and A waves can be fused. Indeed, it is difficult to obtain clear Doppler waves from transplant recipients. They frequently have extended adhesion of the transplanted heart to the chest cavity, which hinders the acquisition of an appropriate Doppler angle. The TEI index or myocardial performance index (MPI), which is a parameter of a Doppler-derived combination of systolic and diastolic time intervals, is a useful parameter in patients with E-A fusion and high heart rate; therefore, the MPI has the potential to detect rejection more accurately than traditional Doppler indices [31]. Representative conventional 2D echo images associated with and without rejection are shown in **Figure 9**.

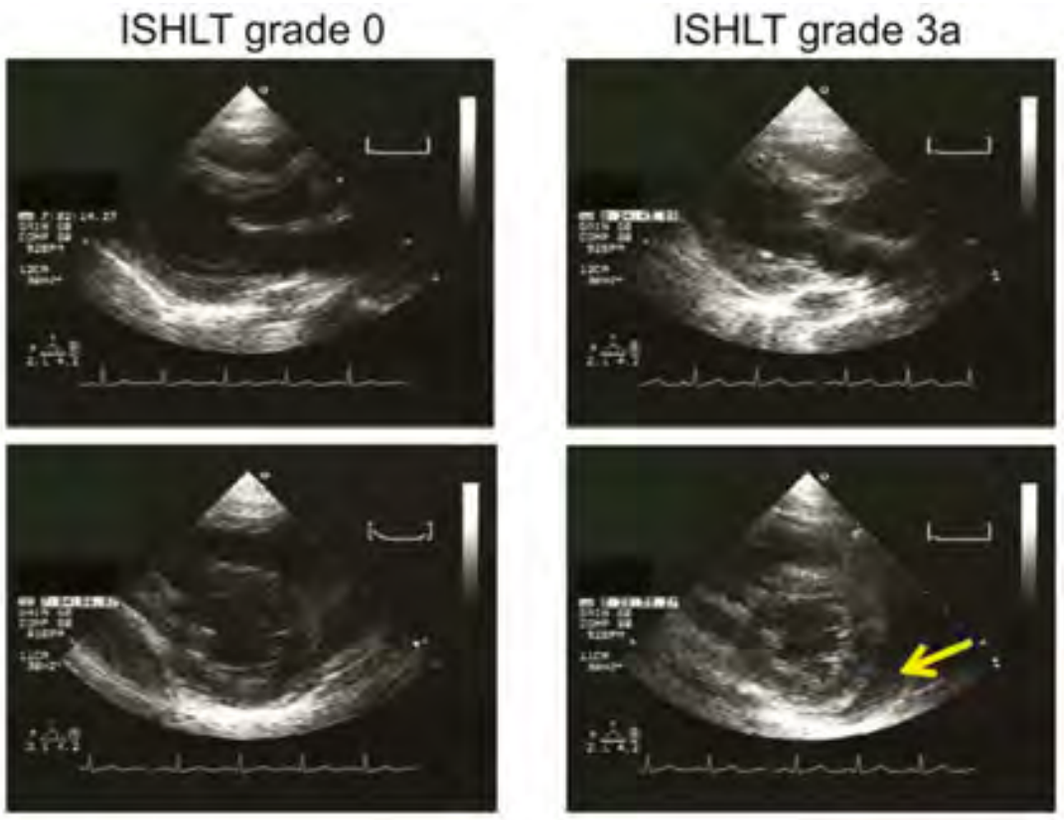

Figure 9. Representative 2D echocardiography in a patient with and without cellular rejection. Representative conventional 2D echocardiograms obtained from a 26-year-old female transplant recipient at the time when her EMB showed conventional ISHLT grade 0 (left) and ISHLT grade 3a rejection (right). The posterior wall thickness of LV and the LV mass index without rejection (left) were 9 mm and 88 g/m^2, respectively. The same parameters associated with rejection (right) were 13 mm and 112 g/m^2. The arrow in the right lower panel indicates a pericardial effusion. EMB, endomyocardial biopsies; ISHLT, International Society for Heart and Lung Transplantation; LV, left ventricular and left ventricle.

Variables	Characteristics and pitfalls
TDI derived E′ ↓ A′ ↓ E/E′ ↑	• Reflecting increased LV filling pressure/relaxation abnormalities • Angle dependent
TDI-derived longitudinal systolic strain ↓ TDI-derived radial systolic strain ↓	• Reflecting both systolic and diastolic abnormalities • Possibility of reflecting heterogeneous myocardial abnormalities • Ability to detect subclinical rejection • Angle dependent • Frame rate limitations
TDI-derived diastolic strain rate ↓	• Reflecting relaxation abnormalities • Ability to detect subclinical rejection • Angle dependent • Frame rate limitations
2D-STE-derived LV torsion ↓	• Reflecting relaxation abnormalities • Ability to detect subclinical rejection • Angle independent • Values can be calculated offline using stored 2D images
2D-STE-derived global radial systolic strain ↓	• Reflecting both systolic and diastolic abnormalities • Possibility of reflecting heterogeneous myocardial abnormalities • Ability to detect subclinical rejection • Angle independent • Values can be calculated offline using stored 2D images
2D-STE-derived systolic and diastolic global strain rate ↓	• May be more sensitive for the early detection of rejection than systolic and early diastolic global strains • Angle independent • Values can be calculated offline using stored 2D images

A′, late diastolic mitral annular velocity, E′, early diastolic mitral annular tissue velocity. * LV torsion = (apical end-systolic rotation) – (basal end-systolic rotation).

Table 5. Tissue-Doppler imaging and 2D-speckle-tracking echocardiography-derived variables associated with rejections (quoted from Ref. [29]).

3.2.2. Tissue Doppler imaging and speckle tracking echocardiography

Tissue Doppler imaging (TDI) enables the measurements of systolic and diastolic velocities within the myocardium. Several studies have evaluated the usefulness of TDI-derived mitral annular velocities to detect allograft rejection, which are summarized in **Table 5** [28]. Strain rate analysis has a potential to detect even mild rejection. Kato TS et al. reported that the attenuation of LV longitudinal strain and the diastolic strain rate derived from TDI were associated with conventional ISHLT (International Society for Heart and Lung Transplantation) grade 1b or higher rejection without hemodynamic alterations (**Figure 10**) [32]. Marciniak et al. found significantly lower LV longitudinal and radial peak systolic strain and strain rate

http://dx.doi.org/10.5772/65095

values in patients with conventional ISHLT grade 1b or higher rejection. TDI-derived strain and strain rate potentially reflect abnormalities [33].

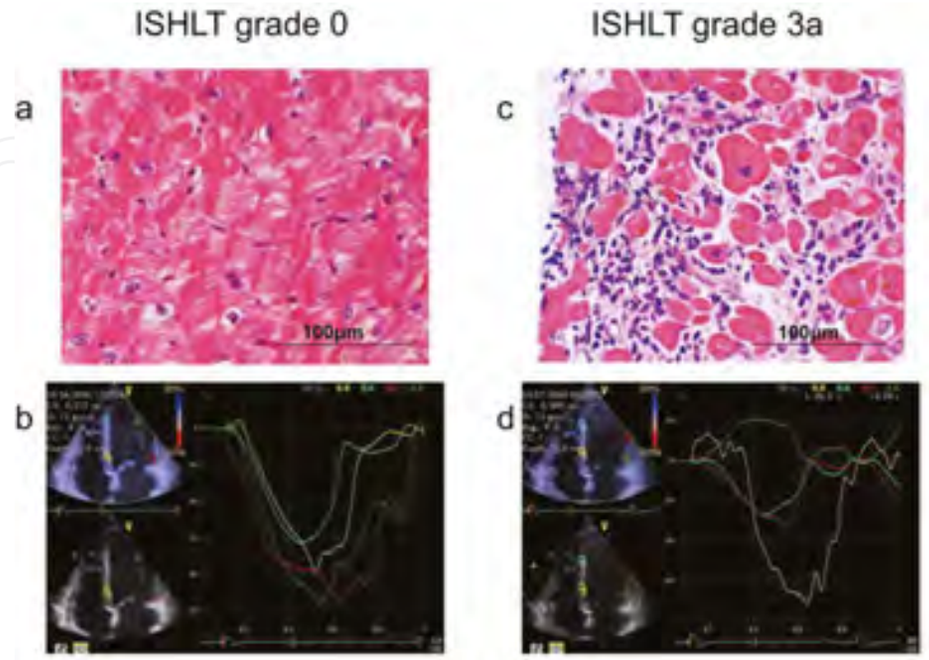

Figure 10. Representative TDI-derived strain analysis in a patient with and without rejection (quoted from Ref. [33]). Representative pathological findings for EMB specimens (a, b) and strain analysis (c, d) of HTx with ISHLT grade 0 (a, c) or 3a (b, d) rejection. Sections in (a) and (b) were stained with hematoxylin-eosin; scale bars, 100 mm. EMB, endomyocardial biopsies; HTx, heart transplant recipients; ISHLT, International Society for Heart and Lung Transplantation.

Two-dimensional speckle-tracking echocardiography (2D-STE) was developed as an angle-independent echocardiographic modality to evaluate cardiac mechanical function. The 2D-STE-derived parameters associated with rejection are also shown in **Table 5** [28]. The association between LV torsional deformation and rejection in transplant recipients has been reported since the 1980s. Sato et al. reported that 2D-STE-derived LV torsion values are decreased in patients with rejection, and the serial assessments of an intra-patients comparison showed that a cut-off value of a 25% reduction of LV torsion from the baseline is associated with ISHLT grade 2 or higher rejection, which returns to the baseline after adequate rejection treatment (**Figure 11**) [34]. LV global strains are also calculated using 2D-STE in an angle-independent manner. Sera F et al. reported that 2D-STE-derived LV global longitudinal strain was associated with treatment-requiring rejection [35] (**Figure 12**). In addition to its major advantage of angle independency, 2D-STE has other advantages over TDI, such as spatial resolution, translational artifacts, the sensitivity to signal noise, the time needed for data acquisition, and the necessity of employing expert readers. Three-dimensional (3D) STEs are useful echocardiographic modalities to assess various strain and rotation parameters more accurately than 2D-STE by tracking the same speckle throughout the cardiac cycle. However, it will take several years for the validation studies of 3D-STE to be performed to verify the value of rejection-detecting tools in heart transplant recipients.

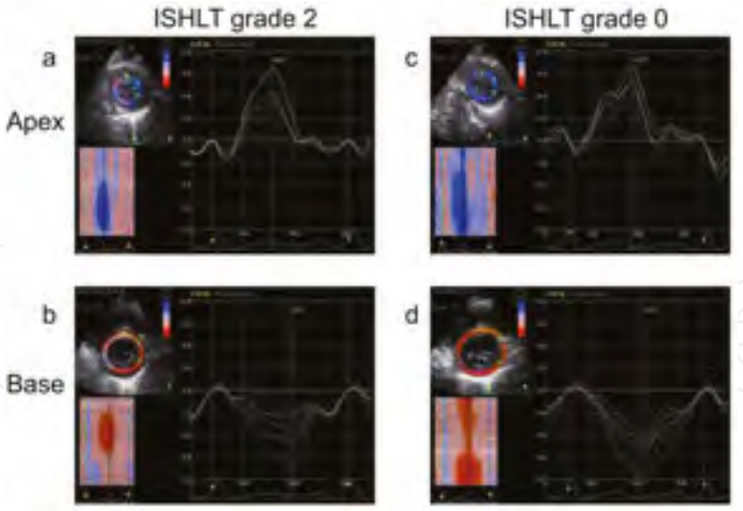

Figure 11. Representative 2D speckle-tracking echocardiogram and analysis of torsion in a patient with and without rejection. (quoted from Ref. [35]). Representative 2D-STE imaging with rotation curves obtained from the same recipient (a 32-year-old man) at LV short-axis views of the apex (a, c) and the base (b, d). Each color of the deformational curve represents one segment of the LV, and the dashed white curve depicts the mean rotation of six segments. The LV-tor, defined as the difference between apical basal end-systolic rotation when the patient had ISHLT grade 2 rejection, was 10.9 degrees (a, b). The LV torsion accompanied with ISHLT grade 0 after rejection treatment was 15.6 degrees (c, d). The % change of LV torsion in this patient at the time of rejection was approximately 30% decreased from his baseline. ISHLT, International Society for Heart and Lung Transplantation; LV, left ventricular; 2D-STE, 2D speckle-tracking echocardiography; EMB, endomyocardial biopsies; HTx, heart transplant recipients.

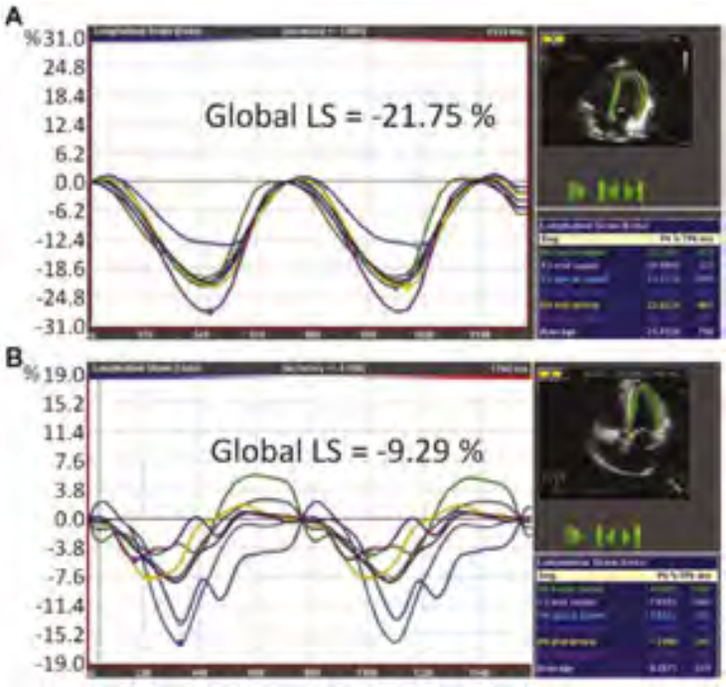

Figure 12. Representative 2D speckle tracking echocardiogram and analysis of global longitudinal strain in a patient with and without rejection (quoted from Ref. [36]). LS curves obtained from a patient without rejection (grade 0) (A) and another patient with grade 3a rejection (B). LS, longitudinal strain.

3.2.3. Transplant vasculopathy and echocardiography

Echocardiography is a helpful and an ideal noninvasive tool to detect transplant vasculopathy or chronic rejection as well. Dobutamine or/and exercise stress echocardiography has been used to detect allograft vasculopathy, especially for pediatric patients or those with renal insufficiency [36]. Decreases in strain and strain rates at rest and with dobutamine stress are also useful to detect significant transplant vasculopathy. Contrast echocardiography is another useful method.

Author details

1 Juntendo University School of Medicine, Heart Center, Tokyo, Japan
2 Tokyo Metropolitan Geriatric Hospital, Institute of Gerontology, Tokyo, Japan

References

[1] Lund LH, Edwards LB, Kucheryavaya AY, Benden C, Dipchand AI, et al. The Registry of the International Society for Heart and Lung Transplantation: Thirty-second Official Adult Heart Transplantation Report – 2015; Focus Theme: Early Graft Failure. J Heart Lung Transplant 2015; 34:1244–1254.

[2] Kirklin JK, Naftel DC, Pagani FD, Kormos RL, Stevenson LW, et al. Seventh INTERMACS annual report: 15,000 patients and counting. J Heart Lung Transplant 2015; 34:1495–1504.

[3] Jorde UP, Kushwaha SS, Tatooles AJ, Naka Y, Bhat G, et al; HeartMate II Clinical Investigators. Results of the destination therapy post-food and drug administration approval study with a continuous flow left ventricular assist device: a prospective study using the INTERMACS registry (Interagency Registry for Mechanically Assisted Circulatory Support). J Am Coll Cardiol. 2014; 63:1751–1757.

[4] Kukucka M, Stepanenko A, Potapov E, Krabatsch T, Kuppe H, Habazettl H. Impact of tricuspid valve annulus dilation on mid-term survival after implantation of a left ventricular assist device. J Heart Lung Transplant 2012;31:967–971.

[5] Dunlay SM, Deo SV, Park SJ. Impact of tricuspid valve surgery at the time of left ventricular assist device insertion on postoperative outcomes. ASAIO J 2015; 61:15–20.

[6] Han J, Takeda K, Takayama H, Kurlansky PA, Mauro CM, et al. Durability and clinical impact of tricuspid valve procedures in patients receiving a continuous-flow left ventricular assist device. J Thorac Cardiovasc Surg 2016;151:520–527.

[7] Cowger J, Rao V, Massey T, Sun B, May-Newman K, et al. Comprehensive review and suggested strategies for the detection and management of aortic insufficiency in patients with a continuous-flow left ventricular assist device. J Heart Lung Transplant 2015;34:149–157. doi: 10.1016/j.healun.2014.09.045. Epub 2014 Oct 24.

[8] Stulak JM, Tchantchaleishvili V, Haglund NA, Davis ME, Schirger JA, et al. Uncorrected pre-operative mitral valve regurgitation is not associated with adverse outcomes after continuous-flow left ventricular assist device implantation. J Heart Lung Transplant 2015;34:718–723.

[9] Taghavi S, Hamad E, Wilson L, Clark R, Jayarajan SN, et al. Mitral valve repair at the time of continuous-flow left ventricular assist device implantation confers meaningful decrement in pulmonary vascular resistance. ASAIO J 2013;59:469–473.

[10] Kitada S, Kato TS, Thomas SS, Conwell SD, Russo C, et al. Pre-operative echocardiographic features associated with persistent mitral regurgitation after left ventricular assist device implantation. J Heart Lung Transplant 2013;32:897–904.

[11] Mikus E, Stepanenko A, Krabatsch T, Loforte A, Dandel M, et al. Reversibility of fixed pulmonary hypertension in left ventricular assist device support recipients. Eur J Cardiothorac Surg. 2011;40:971–977.

[12] Kato TS, Jiang J, Schulze PC, Jorde U, Uriel N, et al. Serial echocardiography using tissue Doppler and speckle tracking imaging to monitor right ventricular failure before and after left ventricular assist device surgery. JACC Heart Fail 2013;1:216–222.

[13] Hayek S, Sims DB, Markham DW, Butler J, Kalogeropoulos AP. Assessment of right ventricular function in left ventricular assist device candidates. Circ Cardiovasc Imaging 2014;7:379–389.

[14] Puwanant S, Hamilton KK, Klodell CT, Hill JA, Schofield RS, et al. Tricuspid annular motion as a predictor of severe right ventricular failure after left ventricular assist device implantation. J Heart Lung Transplant 2008;27:1102–1107.

[15] Kukucka M, Stepanenko A, Potapov E, Krabatsch T, Redlin M, et al. Right-to-left ventricular end-diastolic diameter ratio and prediction of right ventricular failure with continuous-flow left ventricular assist devices. J Heart Lung Transplant 2011;30:64–69.

[16] Kato TS, Farr M, Schulze PC, Maurer M, Shahzad K, et al. Usefulness of 2-dimensional echocardiographic parameters of the left side of the heart to predict right ventricular failure after left ventricular assist device implantation. Am J Cardiol 2012;109:246–251.

[17] Grant AD, Smedira NG, Starling RC, Marwick TH. Independent and incremental role of quantitative right ventricular evaluation for the prediction of right ventricular failure after left ventricular assist device implantation. J Am Coll Cardiol 2012;60:521–528.

[18] Ammar KA, Umland MM, Kramer C, Sulemanjee N, Jan MF, et al. The ABCs of left ventricular assist device echocardiography: a systematic approach. Eur Heart J Cardiovasc Imaging 2012;13:885–899.

[19] Topilsky Y, Hasin T, Oh JK, Borgeson DD, Boilson BA, et al. Echocardiographic variables after left ventricular assist device implantation associated with adverse outcome. Circ Cardiovasc Imaging 2011;4:648–661.

[20] Uriel N, Morrison KA, Garan AR, Kato TS, Yuzefpolskaya M, et al. Development of a novel echocardiography ramp test for speed optimization and diagnosis of device thrombosis in continuous-flow left ventricular assist devices: the Columbia ramp study. J Am Coll Cardiol 2012;60:1764–1775.

[21] Kato TS, Maurer MS, Sera F, Homma S, Mancini D. Aortic regurgitation during systolic-phase accompanied by mitral regurgitation in patients with continuous-flow left ventricular assist device. Eur Heart J Cardiovasc Imaging 2013;14:1022.

[22] Kato TS, Oda N, Hashimoto S, Ikeda Y, Ishibashi-Ueda H, Komamura K. Assist device malfunction due to kinking of cannula between heart and chest wall. Asian Cardiovasc Thorac Ann 2010;18:598.

[23] Oda N, Kato TS, Niwaya K, Komamura K. Unusual cause of left ventricular assist device failure: pendulating mass in the cavity. Eur J Cardiothorac Surg 2007;32:533.

[24] Kato TS, Colombo PC, Nahumi N, Kitada S, Takayama H, et al. Value of serial echo-guided ramp studies in a patient with suspicion of device thrombosis after left ventricular assist device implantation. Echocardiography 2014;31:E5–E9.

[25] Gupta DK, Skali H, Rivero J, Campbell P, Griffin L, et al. Assessment of myocardial viability and left ventricular function in patients supported by a left ventricular assist device. J Heart Lung Transplant 2014;33:372–381.

[26] Hashimoto S, Kato TS, Komamura K, Hanatani A, Niwaya K, et al. Utility of echocardiographic evaluation of donor hearts upon the organ procurement for heart transplantation. J Cardiol 2011;57:215–222.

[27] Raichlin E, Edwards BS, Kremers WK, Clavell AL, Rodeheffer RJ, et al. Acute cellular rejection and the subsequent development of allograft vasculopathy after cardiac transplantation. J Heart Lung Transplant 2009;28:320–327.

[28] Kato TS, Homma S, Mancini D. Novel echocardiographic strategies for rejection diagnosis. Curr Opin Organ Transplant 2013;18:573–580.

[29] Valantine HA, Yeoh TK, Gibbons R, McCarthy P, Stinson EB, et al. Sensitivity and specificity of diastolic indices for rejection surveillance: temporal correlation with endomyocardial biopsy. J Heart Lung Transplant 1991;10:757–765.

[30] Sun JP, Abdalla IA, Asher CR, Greenberg NL, Popović ZB, et al. Non-invasive evaluation of orthotopic heart transplant rejection by echocardiography. J Heart Lung Transplant 2005;24:160–165.

[31] Leonard GT Jr, Fricker FJ, Pruett D, Harker K, Williams B, Schowengerdt KO Jr. Increased myocardial performance index correlates with biopsy-proven rejection in pediatric heart transplant recipients. J Heart Lung Transplant 2006;25:61–66.

[32] Kato TS, Oda N, Hashimura K, Hashimura K, Hashimoto S, et al. Strain rate imaging would predict subclinical acute rejection in heart transplant recipients. Eur J Cardiothorac Surg 2010;37:1104–1110.

[33] Marciniak A, Eroglu E, Marciniak M, Sirbu C, Herbots L, et al. The potential clinical role of ultrasonic strain and strain rate imaging in diagnosing acute rejection after heart transplantation. Eur J Echocardiogr 2007;8:213–221.

[34] Sato T, Kato TS, Komamura K, Hashimoto S, Shishido T, et al. Utility of left ventricular systolic torsion derived from 2-dimensional speckle-tracking echocardiography in monitoring acute cellular rejection in heart transplant recipients. J Heart Lung Transplant 2011;30:536–543.

[35] Sera F, Kato TS, Farr M, Russo C, Jin Z, et al. Left ventricular longitudinal strain by speckle-tracking echocardiography is associated with treatment-requiring cardiac allograft rejection. J Card Fail 2014;20:359–364.

[36] Dedieu N, Greil G, Wong J, Fenton M, Burch M, Hussain T. Diagnosis and management of coronary allograft vasculopathy in children and adolescents. World J Transplant 2014;24(4):276–293.

Chapter 9

Assessment of Right Ventricle by Echocardiogram

Gunjan Choudhary, Arushi A. Malik,
Dwight Stapleton and Pratap C. Reddy

Additional information is available at the end of the chapter

http://dx.doi.org/10.5772/64781

Abstract

Assessment of right ventricular (RV) function is important to ascertain clinical outcome in patients with symptoms of right ventricular failure manifested as lower extremity swelling and abdominal congestion. RV function is not routinely assessed and reported in clinical practice. Unlike the bullet-shaped left ventricle (LV), RV has a complex geometry with a triangular shape. RV is further divided into the inlet, trabecular apex, and infundibulum or conus. RV evaluation involves quantifying afterload and preload, assessing the mechanism and severity of tricuspid regurgitation (TR), and quantitative evaluation of RV performance. For quantification of RV size and function, we can use intravenous contrast for endocardial tracing of RV border to measure RV dimensions, tricuspid annular plane systolic excursion (TAPSE), fractional area change (FAC), Doppler index of myocardial performance (Tei index or myocardial performance index), pulsed wave or color Doppler tissue imaging systolic velocity [s'], or strain imaging. For qualitative evaluation of RV, the RV size is compared to the LV size in parasternal, short axis, and subcostal projections.

Keywords: right ventricle, functional evaluation, right heart hemodynamics, echocardiography, clinical significance

1. Introduction

Historically, the importance of right ventricle (RV) has been underestimated and overlooked in clinical practice and literature. Usually, left ventricle (LV) function is most commonly reported and signified. Only in recent years, the importance of assessment of RV size and function in clinical management and treatment of cardiopulmonary disorders has been recognized [1]. RV dysfunction is associated with adverse clinical outcome [2–8] in patients with LV dysfunction,

acute myocardial infarction, pulmonary embolism, pulmonary arterial hypertension, and congenital heart disease [9–11]. Hence, this has generated interest in the evaluation of RV function. RV dysfunction could be secondary to pressure or volume overload; from primary right heart disease or secondary to left heart diseases such as cardiomyopathy or valvular heart disease [12, 13] (**Tables 1** and **2**). RV dysfunction may affect by way of interventricular septal motion (ventricular interdependence) and by affecting LV preload.

RV cardiomyopathy
Arrhythmogenic right ventricular cardiomyopathy (ARVC)
Dilated cardiomyopathy
Endomyocardial fibrosis
Cirrhotic cardiomyopathy
Eosinophilic myocarditis
Peripartum cardiomyopathy
Uhl's anomaly
Sepsis
Viral myocarditis
Coronary artery disease

Table 1. Causes of RV contractile dysfunction.

RV pressure overload
All groups of pulmonary hypertension
Massive pulmonary embolism
ARDS
Eisenmenger syndrome
RV outflow obstruction
Pulmonic valve stenosis
Infundibular stenosis
(Tetralogy of Fallot, hypertrophic cardiomyopathy)
Mechanical ventilation
Hypoventilation
RV volume overload
Left to right shunt
Atrial septal defect
Anomalous pulmonary venous drainage
Pulmonary regurgitation
Tricuspid regurgitation
Primary
Infective endocarditis
Carcinoid syndrome
Rheumatic heart disease
Ebstein's anomaly
Secondary to tricuspid annular dilation from RV Dilation

Table 2. Causes of right ventricular overload.

http://dx.doi.org/10.5772/64781

Of all the noninvasive imaging modalities, echocardiography remains a mainstay in the evaluation of RV. Moreover, with advances in echocardiography the pathophysiology of RV has been better understood. In this chapter, we aim to review various methods to assess RV anatomy, function, and hemodynamics using two-dimensional (2D) echocardiography, color Doppler echocardiography, tissue Doppler imaging (TDI), three-dimensional (3D) echocardiography, and strain imaging echocardiography [12]. To identify RV pathology, guidelines have been published by the American Society of Echocardiography (ASE) on parameters and normal reference values (**Table 5**).

2. Location and anatomy of RV

The RV in the normal heart is the most anteriorly situated cardiac chamber located immediately behind the sternum and anterior to LV. It forms the majority of the anterior as well as the inferior border of the cardiac silhouette. Due to this unique anatomical location, assessment of RV size and function by transthoracic echocardiogram (TTE) may appear easy but assessment of RV function is challenging given the odd geometry of the crescent-shaped RV that wraps around conical LV. Furthermore, heavily trabeculated myocardium also limits the delineation of RV endocardial surface.

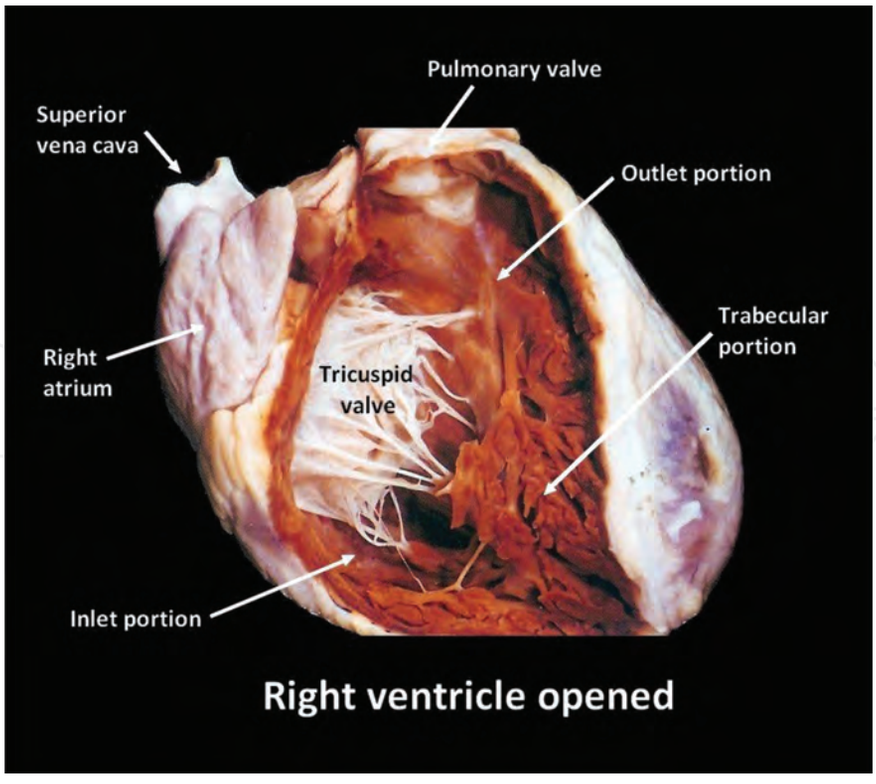

Figure 1. RV anatomy and myocardial fibers. The RV structure: illustrates the inlet, trabecular, and outlet components.

Unlike the LV that is ellipsoid or conical, the RV is crescent shaped or pyramidal, and its cavity has three components [14]: **Figure 1**

1. The muscular inlet comprising of the tricuspid valve, chordae tendineae, and three papillary muscles, which originate in ventricular wall and attach to anterior, posterior, and septal leaflets of the tricuspid valve via chordae tendineae.

2. Immobile apex with heavy, coarse trabeculations; two thick intracavitary muscle bands, the crista supraventricularis [15], and the moderator band attached to the right ventricular outflow tract (RVOT) extending from the interventricular septum (IVS) to the anterior RV wall. The apical part of the RV is heavily trabeculated and virtually an immobile part of the ventricle.

3. Smooth funnel-shaped myocardial outflow tract called infundibulum [14].

The RV is formed by free (anterior and posterior) wall and interventricular septum. Blood supply to the RV is by right coronary artery (equal in systole and diastole except in pressure overload and hypertrophy). The moderator band is supplied by the left anterior descending artery. The tricuspid valve has three papillary muscles and three cusps (anterior, posterior, and septal). The tricuspid valve is 2 mm more apical to the mitral valve. It is very important to be able to differentiate left ventricle from right ventricle based on morphology seen on an echocardiogram (**Table 3**).

Right ventricle is characterized by:
• More *apical position* of the tricuspid valve as compared to the mitral valve
• Presence of a moderator band
• Presence of more than three papillary muscles
• Three leaflets of the tricuspid valve with *septal* papillary attachments
• Presence of trabeculations (trabeculations can also be seen in the left ventricle in case of pathological noncompaction of the left ventricle)

Table 3. Morphological differences between the right ventricle from the left ventricle.

2.1. Musculature of ventricular wall

The RV has one-sixth the muscle mass of LV as it pumps against approximately one-sixth the resistance the LV encounters. However, the RV pumps equal cardiac output as LV. The RV ejection fraction (EF) is lower as RV end-diastolic volume is slightly larger than that of the left ventricle. Appropriately, the RV is adaptable as a volume pump but is likely to fail when subjected to acute pressure overload. The muscular wall of the RV excluding trabeculations is

3–5 mm thick [16]. RV is relatively thin walled having superficial subepicardial circumferential myofibers parallel to the atrioventricular groove that encircles the subpulmonary infundibulum and deeper subendocardial longitudinal myofibers. Unlike the relatively thick-walled LV, the RV lacks the third layer of spiral/oblique myofibers. Longitudinal fibers contract to result in inward/radial thickening. The septal motion is considered to contribute to both LV and RV function [17, 18] and is a major determinant of overall RV performance [17–19].

2.2. RV area

The RV area is measured in the apical four-chamber window at end-diastole by planimetry of the RV cavity. Delineation of the RV endocardium is challenging and should exclude trabeculations or moderator band; however, one should include the apex of the RV to avoid erroneous estimation. The normal reference limit for RV end-diastolic area is ≤24 cm^2 in men and ≤20 cm^2 in women [14].

2.3. RV wall thickness

The RV wall thickness can be measured by M-mode or 2D echocardiography from either the left parasternal window or subcostal window at the level of the tip of the anterior tricuspid leaflet. RV hypertrophy is seen in infiltrative and hypertrophic cardiomyopathy, whereas RV wall thinning is seen in Uhl anomaly and arrhythmogenic RV cardiomyopathy. When measuring the RV wall thickness, it is essential to exclude RV trabeculations, papillary muscle, thickened pericardium, and epicardial fat. The normal cutoff is 0.5 cm from either parasternal long axis (PLAX) or subcostal windows.

2.4. RV linear dimensions

RV size can be measured from the apical four-chamber view at end-diastole wherein RV should appear almost two-thirds of the size of LV on qualitative assessment. The RV is enlarged in acute pressure and volume overload. The absence of standard reference points in RV imaging serves as a limitation in using transthoracic echocardiogram. The RV may appear viable in size when RV imaging is done through various cut planes depending on the probe rotation [20]. In the four-chamber view, the focus should be on the right ventricular chamber "RV Focused view" for better imaging of the RV lateral wall and to maximize the RV size. One should adjust the transducer to attain maximal plane to avert underestimation and to avoid overestimation by positioning the transducer over the cardiac apex with the plane through the left ventricle in the center of the cavity. The basal diameter is the maximal short-axis dimension in the basal, one-third of the right ventricle. The mid-cavity diameter is measured at the level of the LV papillary muscles in mid-third of the RV, and the longitudinal dimension is measured from the plane of the tricuspid annulus to the RV apex. ASE guidelines for the right heart assessment recommend measurement of the following dimensions: RV basal-apical four-chamber view, RV wall thickness (subcostal long axis view), proximal RVOT PSAX (parasternal short axis) view at the great vessels level, and distal RVOT PLAX view (**Figure 2**).

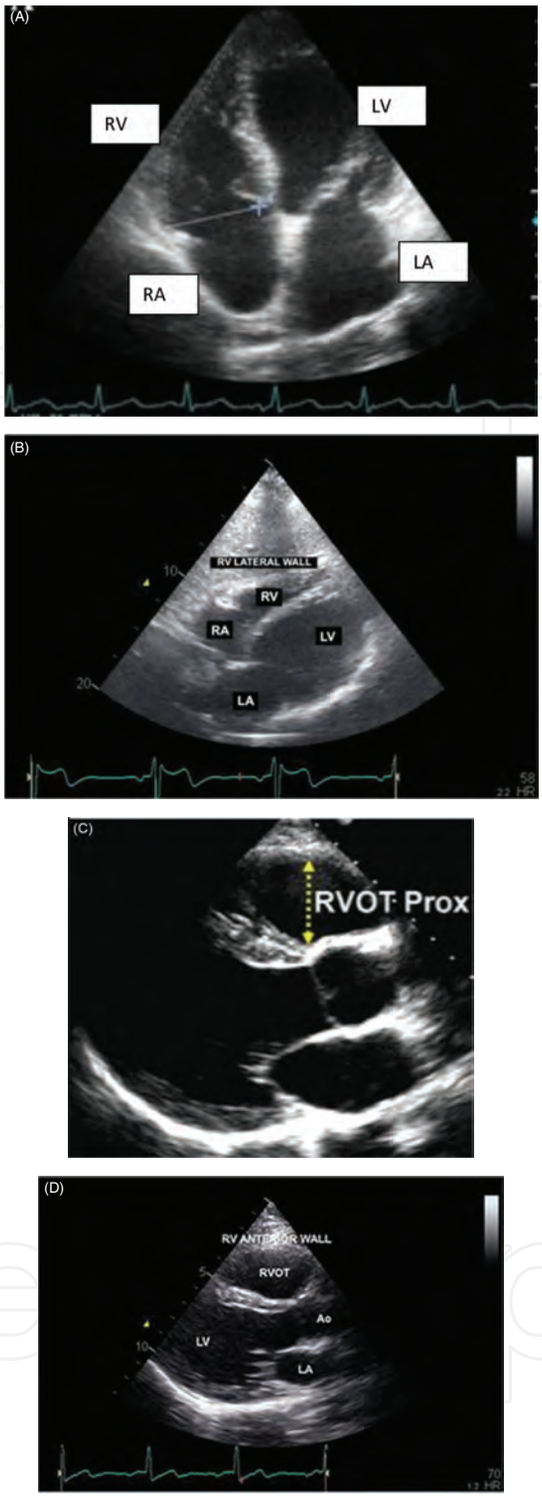

Figure 2. (A) RV basal apical four-chamber view: illustrating the plane of the tricuspid valve and RV endocardial border. **(B) RV wall thickness** (subcostal long axis view): illustrates the LA, left atrium; LV, left ventricle; RA, right atrium; RV, right ventricle; and RV lateral wall. **(C) Proximal RVOT** (parasternal short-axis view PSAX at the great vessels level): illustrates the Ao, aorta; PA, pulmonary artery; LV, left ventricle; RVOT, right ventricular outflow tract; and RV anterior wall. **(D) Distal RVOT** (parasternal long axis view PLAX): illustrates the Ao, aorta; LA, left atrium; LV, left ventricle; RVOT, right ventricular outflow tract, RV anterior wall.

2.5. Right ventricular outflow tract

The RVOT includes the pulmonic valve and subpulmonary infundibulum or conus that extends from the crista supraventricularis to the pulmonary valve [21, 22]. RVOT is usually imaged from the left parasternal short axis view. In patients with congenital heart disease and arrhythmogenic RV dysplasia, parasternal long axis view may be added to assess the proximal and distal diameter of RVOT. There is no standard window for measurement of RVOT size; oblique imaging may interfere in the accurate estimation of its size. The upper reference limit for the PSAX distal RVOT diameter is 27 mm and for PLAX is 33 mm (**Table 5**).

2.6. Interventricular septal morphology

Normally the LV has circular shape throughout the cardiac cycle. During systole, the LV protrudes into the RV. Compliance of one ventricle can modify the other through diastolic ventricular interaction. However, interventricular septum gets flattened and curved into LV cavity secondary to volume and pressure overload of the RV. The LV cavity, therefore, appears D-shaped at end-systole and end-diastole in RV pressure overload and RV volume overload (e.g., tricuspid regurgitation), respectively [17, 19] (**Figure 3**).

2.7. Volumetric assessment of RV

Two-dimensional TTE approximates complex RV geometry and underestimates MRI-derived RV volume. Assessment of RV volume using 3D TTE is superior and more accurate because 3D echo uses disc summation and apical rotational methods for RV volume and EF assessment [20]. However, the accuracy of RV volume assessment is less definite when the RV is dilated.

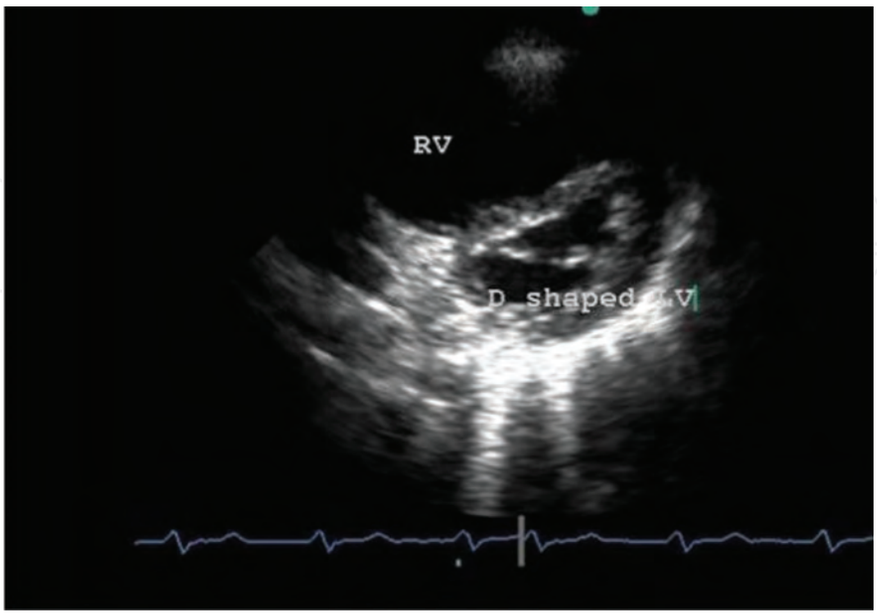

Figure 3. Example of RV with D-shaped LV cavity. RV, right ventricle; LV, left ventricle.

3. Intracardiac pressure measurement

Echocardiography can provide an estimate of right heart hemodynamics.

3.1. Estimated right atrial (RA) pressure

Estimation of right atrial pressure can be derived from the size of the inferior vena cava (IVC) and its response to changes in spontaneous respiration [23, 24]. Using a dilated IVC to assess elevated RA pressures is not accurate in mechanically ventilated patients. However, a small IVC of less than 1.2 cm in mechanically ventilated patient is 100% specific for an RA pressure of less than 10 mm Hg. Normal IVC is <2 cm in diameter, approximately 1 cm from RA-IVC junction and collapses by at least 50% with inspiration or sniff. A flat IVC indicates low RA pressure [0–5 mm Hg]. IVC <2 cm with normal inspiratory collapse indicates RA pressure of 5 mm Hg, and an IVC of >2 cm with normal inspiratory collapse suggests an RA pressure of 10 mm Hg. IVC <2 cm but without inspiratory collapse suggests 15 mm Hg RA pressure; IVC >2 cm but without inspiratory collapse suggests an RA pressure of 20 mm Hg. The normal RA pressure is 0–5 mm Hg.

3.2. Pulmonary artery systolic pressure (PASP)

Pulmonary artery (PA) systolic pressure can be determined from tricuspid regurgitation peak velocity. Provided there is no tricuspid valve obstruction, peak TR velocity depends on the pressure gradient between the right ventricle and right atrium [the difference between peak right ventricular systolic pressure (RVSP) and RA pressure] (**Table 4**). Therefore, estimated RVSP is equal to pressure difference (determined from peak TR velocity using Bernoulli equation) and estimated RA pressure [25]. (**Figure 4**) When there is no obstruction across the pulmonic valve, RVSP will be similar to PASP. PASP = 4 × peak TR velocity^2 + estimated RA pressure. For example, if TR velocity is 2.5 m/sec and IVC is normal in size and collapses with inspiration the estimated PASP would be 33 mm Hg [4(2.5)^2 mm Hg = 25 mm Hg + 5 mm Hg (estimated RA pressure)]. If the estimated PASP is >35 to 40 mm Hg, pulmonary HTN is considered to be present.

3.3. Pulmonary artery diastolic pressure (PADP)

Pulmonary regurgitation (PR) represents the pressure difference between pulmonary artery and right ventricle. Hence, the end-diastolic pulmonary regurgitation velocity can be utilized to measure the end-diastolic pressure difference between PA and right ventricle. PA diastolic pressure can be estimated from the spectral Doppler signal of pulmonary regurgitation. The right ventricular end-diastolic pressure is the same as RA pressure; therefore, PADP can be estimated by addition of the estimated RA pressure to the end-diastolic pressure difference between PA and right ventricle. Thus, PADP = 4 × (end-diastolic pulmonary regurgitation velocity)^2 + estimated RA pressure.

Color flow regurgitant jet area of 30% or more of RA area
Annulus dilation (≥4 cm) or inadequate cusp coaptation
Late systolic concave configuration of the continuous-wave signal
Late systolic flow reversals in the hepatic vein
ERO of 0.4 cm^2 or larger
Regurgitant volume of 45 mL or more
Width of vena contracta of 6.5 mm or more

Abbreviations: ERO, effective regurgitant orifice; RA, right atrium.

Table 4. Severe TR is defined by echocardiography on the basis of the following criteria.

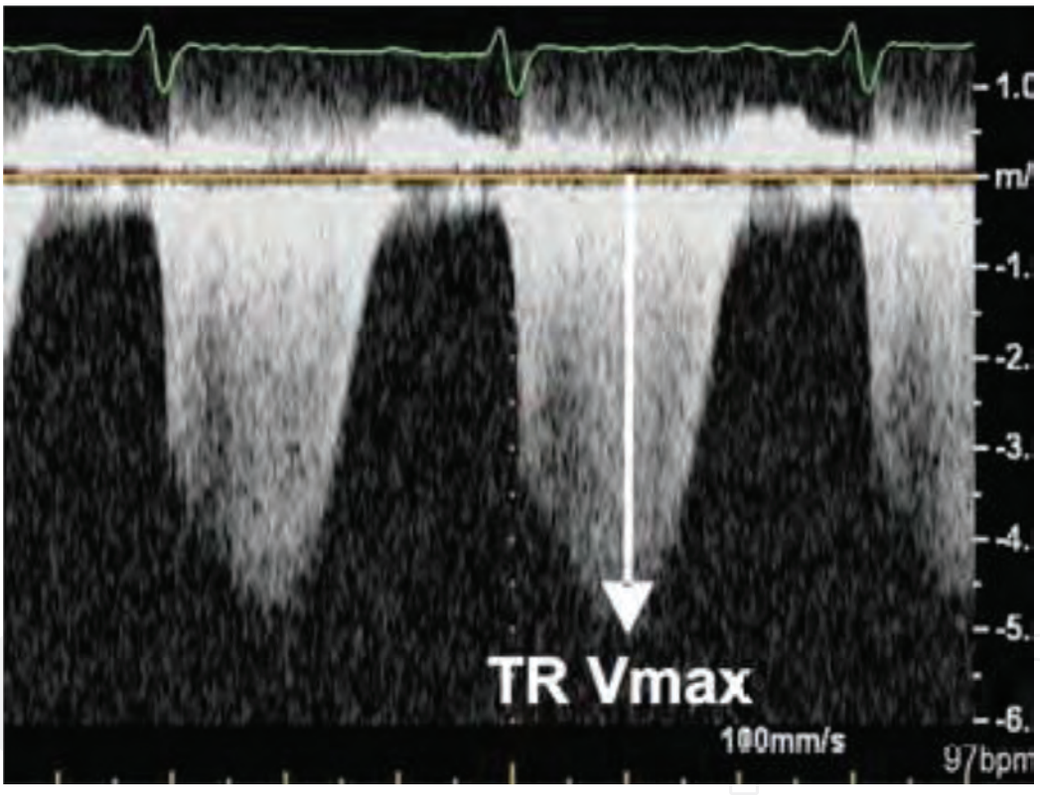

Figure 4. Peak TR velocity. RVSP = $4(V_{max})^2$ + RAP. In the absence of pulmonic stenosis: RVSP = PASP. Peak TR velocity depends on pressure gradient between right ventricle and right atrium [difference between peak RVSP and RA pressure] provided there is no tricuspid valve obstruction. TR, tricuspid regurgitation; RAP, right atrium pressure; RVSP, right ventricle systolic pressure; V_{max}, peak TR velocity.

3.4. Mean pulmonary artery pressure

There are various formulae to estimate mean PA pressure [26–28]. Mean PA pressure = 1/3(PASP) + 2/3 (PADP). Mean PA pressure can be estimated by pulmonary acceleration time

(AT) measured by pulsed Doppler of the pulmonary artery in systole. Mean PA pressure = 79 × (0.45 × AT) or if AT <120 ms, mean PA pressure = 90 – (0.62 × AT). Mean PA pressure = 4 × (early PR velocity)^2 + estimated RA pressure. Mean PA pressure = estimated RA pressure + velocity-time integral of the TR jet to calculate a mean systolic pressure.

3.5. Pulmonary vascular resistance (PVR)

As per the formula $P = QR$, where pressure (P) equals the product of flow (Q) and resistance (R), PASP can be elevated in the setting of increased stroke volume without PVR being elevated. PVR can be calculated by the ratio of peak TR velocity (m/s) to RVOT VTI (velocity time integral) (cm) [29, 30]. PVR = [(TR velocity/RVOT VTI) × 10] + 0.16. PVR value is in Woods units (WU) and correlates well with invasively measured PVR up to approximately 8 WU [30]. However, when PVR is >8 WU by invasive hemodynamic measurement the relationship is not reliable. This method is not validated and should not be used for routine clinical purposes in place of invasive hemodynamic measurements. It can be used when PASP is elevated from increased stroke volume or PASP is low (despite increased PVR) from decreased stroke volume.

4. Assessment of RV function

Most of the RV contraction occurs longitudinally from base to apex (contributing to most of the RV stroke volume), along with radial thickening/inward motion. The following techniques are used to assess RV function [15, 16, 31, 32].

4.1. Tricuspid annular planar systolic excursion (TAPSE)

TAPSE is a diagnostic and prognostic tool of mortality and morbidity in patients with precapillary pulmonary hypertension, RV infarction associated with inferior myocardial infarction, and chronic left-sided heart failure [33, 34]. TAPSE is assessed in an apical four-chamber view by placing the M-mode on the lateral tricuspid annulus; maximum systolic excursion of the lateral annulus along its longitudinal plane toward the apex is recorded [33, 35]. The displacement of the basal segment from the reference point reflects longitudinal contraction of the RV. Normal reference limit is TAPSE of >1.6 cm [36, 37]. This is the most commonly used method as it is a simple, easily obtainable, reproducible with a low interobserver variability. For accurate estimation of TAPSE, one should place M-mode cursor parallel to the plane of longitudinal motion carefully measuring the magnitude of displacement from the M-mode image. The limitations of this method are that TAPSE estimates only the longitudinal contraction within one segment of RV and hypothesizes that the function of a single RV segment reflects the entire RV function which is not true in conditions like RV infarction and pulmonary embolism (**Figure 5**).

http://dx.doi.org/10.5772/64781

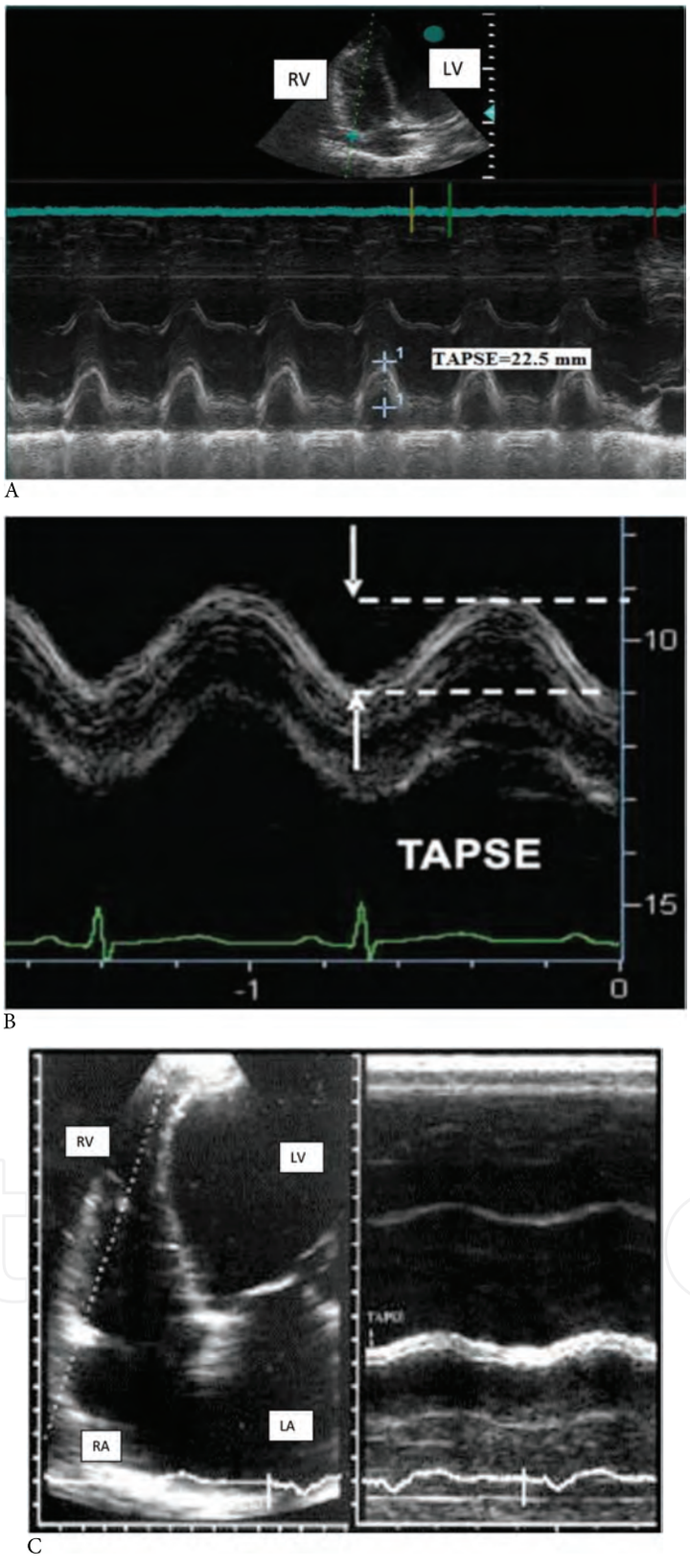

Figure 5. A: Example of a normal TAPSE (tricuspid annular planar systolic excursion) value >1.6 cm; B: normal TAPSE; C: reduced TAPSE.

4.2. Tricuspid annular velocity S'

The tricuspid annular velocity is also known as systolic excursion velocity S'. In an apical four-chamber view, the cursor of pulsed tissue Doppler or color-coded tissue Doppler is placed on the lateral tricuspid annulus to measure the longitudinal velocity of excursion of basal-free wall segment and tricuspid annulus in systole. Normal reference limit (**Table 5**) of S′ is >9.5 cm/s. Color-coded tissue Doppler yields lower velocities and is analyzed off-line on specific platforms. The advantages and disadvantages are similar to TAPSE.

RV systolic dysfunction
TAPSE ≤ 1.6 cm
Pulse Doppler peak annular velocity at tricuspid annulus S′ <9.5 cm/s
2D RV FAC <35%
Tei index/RIMP >0.40 by pulsed Doppler and >0.55 by tissue Doppler
RVEF 3D ≤44%
RV diastolic dysfunction
E/A <0.8 by tissue Doppler
E/A >2.1 by tissue Doppler
Dilated RV chamber
Basal RV diameter >4.2 cm
Mid-level diameter >3.5 cm
Longitudinal dimension >8.6 cm
Abnormal RVOT value
RVOT in PSAX distal diameter >2.7 cm
RVOT in PLAX proximal diameter >3.3 cm
Increased RV subcostal wall thickness >0.5 cm

Abbreviations: 2D, two-dimensional; 3D, three-dimensional ; FAC, fractional area change; MPI, myocardial performance index; PLAX, parasternal long-axis; PSAX, parasternal short-axis; RA, right atrium; RV, right ventricle; RVOT, right ventricular outflow tract; TAPSE, tricuspid annular plane systolic excursion; RIMP, right ventricular index of myocardial performance.

Table 5. Echocardiographic parameters for assessment of right ventricle based on ASE recommendations.

4.3. Myocardial performance index (MPI)

The myocardial performance index is also denoted as the right ventricular index of myocardial performance (RIMP) or right ventricular Tei index. It is an index of global ventricular function and is independent of the geometry of the ventricle [38]. The MPI is calculated by the ratio of isovolumetric time interval over ventricular ejection time as follows: MPI = (isovolumetric

http://dx.doi.org/10.5772/64781

relaxation time + isovolumetric contraction time)/ventricular ejection time = (tricuspid closure to opening time – ejection time)/ejection time. Lower MPI values indicate healthy RV function as less time is utilized in isovolumetric state and more time is consumed in ejecting blood. MPI can be measured through pulsed Doppler or tissue Doppler methods (**Figure 6**).

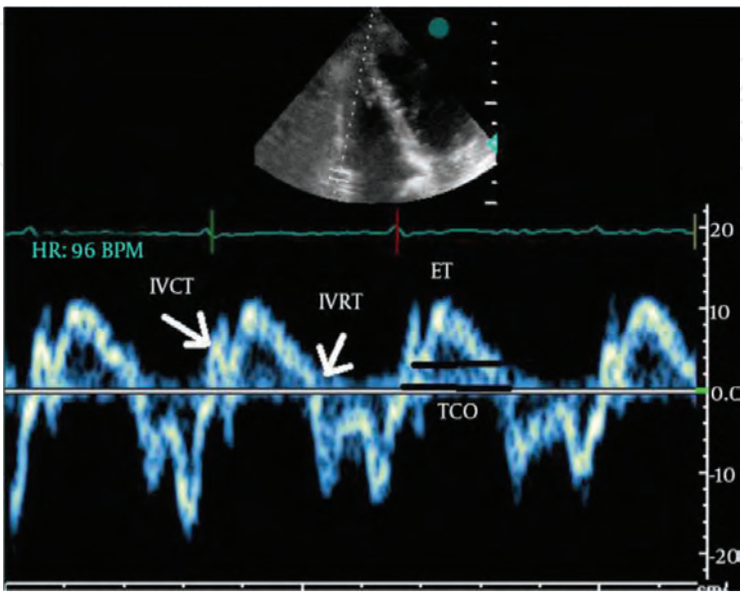

Figure 6. Pulse Doppler MPI. Calculation of RIMP by pulse tissue Doppler imaging RIMP = (TCO - ET)/ET or IVRT + IVCT/ET. RIMP, right ventricular index of myocardial performance; TCO, tricuspid valve closure to opening time; IVCT, isovolumetric contraction time; IVRT, isovolumetric relaxation time; ET, ejection time.

4.3.1. Pulsed Doppler method

In the pulsed Doppler method, pulsed wave Doppler tracing of the distal RVOT is used to obtain ejection time, while the tricuspid-closure-opening time is calculated from the pulsed wave Doppler tracing of the tricuspid inflow (time from end of the A wave to the onset of the following E wave) or the continuous wave Doppler tracing of the tricuspid regurgitation jet. The total isovolumetric time is calculated from the difference between the tricuspid-closure-opening time and the ejection time. The normal reference limit for the pulsed Doppler MPI is <0.40.

4.3.2. Tissue Doppler method

Tissue Doppler method obtains the ejection time, tricuspid-closure-opening time, and total isovolumetric time from the pulsed tissue Doppler tracing of the lateral tricuspid annulus. The normal reference limit for the tissue Doppler MPI is <0.54.

MPI is a sensitive parameter to evaluate subclinical or early RV dysfunction even in poorly visualized RV because it depends on time intervals [39]. However, MPI is observer dependent as delineating time intervals can be challenging [40].

4.4. Fractional area change (FAC)

FAC is the percent change in RV area from diastole to systole.

FAC = [(end-diastolic RV area – end-systolic RV area)/end-diastolic RV area] × 100. FAC is best correlated with MRI-derived RVEF. RV endocardium is traced both in systole and diastole from the annulus, along the free wall to the apex and then back to the annulus, along the interventricular septum. The RV wall should be carefully traced under the trabeculations. FAC has prognostic value and is an independent predictor of all-cause mortality in patients with acute myocardial infarction and low left ventricular ejection fraction. The reference value for normal RV systolic function is >35%.

5. Pulse Doppler MPI

5.1. Three-dimensional echocardiogram

3D echo combined with intravenous contrast agents can improve endocardial border delineation and RV end-diastolic and end-systolic volumes.

$$\text{RVEF} = \left[\text{end} - \text{diastolic RV volume} - \text{end} - \text{systolic RV volume}\right] / \text{end} - \text{diastolic RV volume.} \quad (1)$$

The RV volumes measured by 3D echo use disk summation or surface modeling method. Although 3D echo-derived RVEF correlates well with MRI-derived RVEF, the method is complex, time-consuming, and very much dependent on image quality [20]. The normal reference limit for 3D-derived RVEF is >45%.

5.2. Strain imaging by 2D

The strain is the degree of myocardial deformation, while strain rate represents the rate of myocardial deformation over time [38]. In echocardiography, RV longitudinal strain can be assessed reliably from apical views, whereas the assessment of radial strain is challenging from the parasternal views because of near-field artifacts and extremely small computational distance. The crescent shape of thin-walled RV contributes to inhomogeneous strain rate and values with the highest values in the apical segments and outflow tract. One-dimensional strain is measured using a tissue Doppler (angle-dependent) [18], while 2D strain is measured by speckle tracking (non-angle-dependent). 2D strain imaging estimates global and regional RV function, reflects intrinsic contractility of the RV (with contractility defined as the less stress-strain interplay), and evaluates diastolic properties [39, 41].

Disadvantages are a dearth of normative data, challenges in the adequate image acquisition and analysis requiring high frame rates, high signal-to-noise ratio, minimal image dropout, and most notably the need for experienced observers for reproducible measurements. As it is

not highly reproducible, this technique is not recommended for routine use. Given high variability, no reference limits are available [40].

6. Clinical and prognostic significance of assessment of right ventricle

Quantitative assessment of RV size and function has prognostic value regarding exercise tolerance and outcome in various cardiac and pulmonary diseases [3, 36, 42, 43]. RV pump function depends on contractility, afterload, preload, heart rate, rhythm, and valve function. Being a thin-walled chamber, it is not suited to sustain high pressure (**Tables 1** and **2**). RV dysfunction can be acute or chronic, secondary to RV volume overload, pressure overload, or decreased contractility.

6.1. RV overload

RV overload can be related to pressure overload or volume overload. RV overload, in turn, reduces LV diastolic function and causes higher filling pressures.

6.1.1. Volume overload

Volume overload can result from tricuspid regurgitation, pulmonary regurgitation, ASD, and VSD and is assessed through the movement of IVS. Normally during systole, IVS thickens and moves into the left ventricle and during diastole, it moves into the RV cavity. In RV volume overload, RA and RV are enlarged, and IVS is pushed into the LV during end-systole and early diastole as RV pressure exceeds LV pressure. This leads to IVS flattening and a D-shaped LV only during early diastole. At the outset of systole, LV contraction increases LV pressure pushing the IVS in the direction of RV cavity [12].

6.1.2. Pressure overload

Pressure overload can be acute or chronic. Acute pressure overload can be from adult respiratory distress syndrome (ARDS) or massive pulmonary embolism. Echocardiographic findings of RV pressure overload are the same as volume overload. RA and RV are enlarged with no hypertrophy of RV-free wall; there is a flattening of the IVS in diastole. The peak RV systolic pressures rarely exceed 50 mm Hg in acute pressure overload. Chronic pressure overload is secondary to chronic lung diseases, chronic thromboembolism, or chronic pulmonary venous hypertension from left heart pathology. RV is enlarged with thickening of the RV-free wall and increased trabeculation. The RV can generate higher peak systolic pressures, usually exceeding 50 mm Hg. The IVS remains flattened into the LV cavity during the entire cardiac cycle.

6.2. Right ventricular diastolic function

RV diastolic dysfunction has prognostic value and has been associated with both acute and chronic conditions. RV diastolic function is assessed like that of the left ventricle. Techniques

used are Doppler velocities of the trans tricuspid flow (E, A, E/A), tissue Doppler velocities of the tricuspid annulus (E', A', and E'/A'), deceleration time, and isovolumetric relaxation time [20, 40]. Estimation of RA pressure by measurement of IVC diameter and collapse with inspiration is to be considered while determining the RV diastolic function.

6.3. Cardiac rhythm and the RV

RV function is dependent on cardiac rhythm. RV function is compromised by atrial fibrillation and ventricular tachycardia originating from the RV examples of which are arrhythmogenic RV dysplasia, RV myocardial infarction, idiopathic ventricular tachycardia, or ventricular tachycardia occurring after surgical repair of congenital heart disease [44].

6.4. Cardiac markers

The elevated B-type natriuretic peptide is associated with RV failure secondary to pulmonary hypertension, congenital heart disease, or pulmonary disease [45–47]. Elevated troponin levels indicate poor prognosis in pulmonary embolism and pulmonary hypertension [48].

6.5. Evaluation of pulmonary arterial hypertension

Pulmonary arterial hypertension is a clinical entity that is seen as a consequence of both left heart disease and pulmonary pathology, as well as occurring without an underlying etiology such as primary pulmonary arterial hypertension. Estimation of pulmonary artery pressure can be performed by TTE in the majority of patients [37, 49].

6.6. Evaluation of patients with pulmonary embolism

Pulmonary embolism is associated with high mortality and morbidity; hence, prompt diagnosis and treatment is imperative. When a patient has had a large pulmonary embolism, this may place acute pressure overload on the right ventricle. The right ventricle handles pressure poorly and may undergo acute dilation with decreased right ventricular systolic function as a result of an acute increase in afterload. Usually, peak systolic pressures in the pulmonary artery do not exceed 50 mm Hg unless there is a baseline chronic RV pressure overload. The size and function of the RV are among the most important factors in determining the initiation of either thrombolysis or referral for surgical embolectomy. A classic pattern of RV systolic dysfunction in acute pulmonary embolism has been described. This is known as McConnell sign and is characterized by akinesis of the free wall of the right ventricle with sparing of the apical segment. This phenomenon has 77% sensitivity and 94% specificity for the diagnosis of acute pulmonary embolism (**Figure 7**).

6.7. Evaluation of RV dyssynchrony

Echocardiographic indices of dyssynchrony are assessed by measuring time delay in mechanical activity between segments. Tissue Doppler imaging is limited to the assessment of the septum-RV free wall.

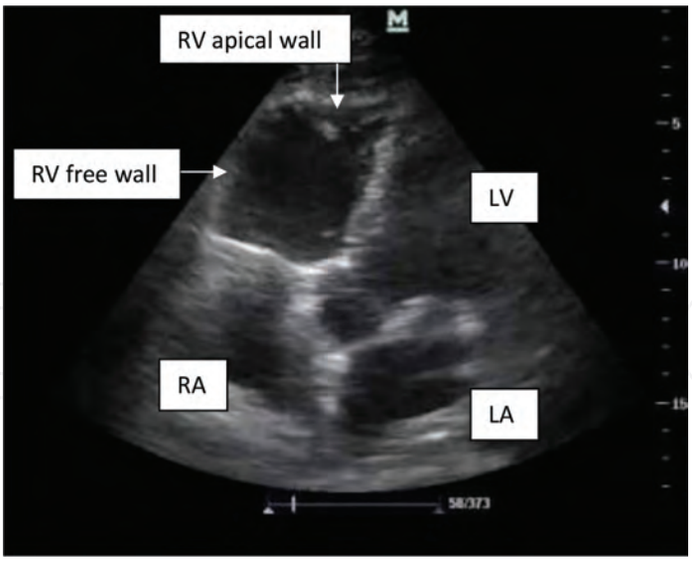

Figure 7. McConnell sign. McConnell sign: akinesis of the free wall of the right ventricle with sparing of the apical segment seen in acute pulmonary embolism causing right ventricle systolic dysfunction.

7. Conclusion

Accurate quantitative assessment of right ventricular size and function remains difficult given its unique shape despite significant advances in echocardiography. RV dysfunction is an important diagnostic and prognostic indicator in many cardiac and pulmonary diseases [42, 43, 50, 51]. Qualitative evaluation of RV systolic function is through visual assessment. For quantitative assessment of RV, FAC, TAPSE, pulsed tissue Doppler S', and MPI are available and at least one of them should be routinely performed and reported as recommended by the ASE. If more than one of these measurements is used in conjunction, RV function can be more reliably and accurately assessed [36, 40, 52].

Author details

©2016 Gunjan Choudhary1*, Arushi A. Malik2, Dwight Stapleton1 and Pratap C. Reddy3 *.

1 Robert Packer Hospital/Guthrie Clinic, Sayre, USA

2 Dr. S.N. Medical College, Jodhpur, India

3 Louisiana State University Health Science Center, Shreveport, USA

References

[1] Ghio S, Klersy C, Magrini G, et al. Prognostic relevance of the echocardiographic assessment of right ventricular function in patients with idiopathic pulmonary arterial hypertension. Int J Cardiol 2010; 140:272.

[2] Graham T P, Jr, Bernard Y D, Mellen B G, et al. Long-term outcome in congenitally corrected transposition of the great arteries: a multi-institutional study. J Am Coll Cardiol 2000; 36:255–261.

[3] Burgess M I, Mogulkoc N, Bright-Thomas R J, et al. Comparison of echocardiographic markers of right ventricular function in determining prognosis in chronic pulmonary disease. J Am Soc Echocardiogr 2002; 15:633–639.

[4] D'Alonzo G E, Barst R J, Ayres S M, et al. Survival in patients with primary pulmonary hypertension. Results from a national prospective registry. Ann Intern Med 1991; 115:343–349.

[5] Mehta S R, Eikelboom J W, Natarajan M K, et al. Impact of right ventricular involvement on mortality and morbidity in patients with inferior myocardial infarction. J Am Coll Cardiol 2001; 37:37–43.

[6] Zehender M, Kasper W, Kauder E, et al. Eligibility for and benefit of thrombolytic therapy in inferior myocardial infarction: focus on the prognostic importance of right ventricular infarction. J Am Coll Cardiol 1994; 24:362–369.

[7] de Groote P, Millaire A, Foucher-Hossein C, et al. Right ventricular ejection fraction is an independent predictor of survival in patients with moderate heart failure. J Am Coll Cardiol 1998; 32:948–954.

[8] Gavazzi A, Berzuini C, Campana C, et al. Value of right ventricular ejection fraction in predicting short-term prognosis of patients with severe chronic heart failure. J Heart Lung Transplant 1997; 16:774–785.

[9] Afilalo J, Flynn AW, Shimony A, et al. Incremental value of the preoperative echocardiogram to predict mortality and major morbidity in coronary artery bypass surgery. Circulation 2013; 127:356.

[10] Hamon M, Agostini D, Le Page O, et al. Prognostic impact of right ventricular involvement in patients with acute myocardial infarction: meta-analysis. Crit Care Med 2008; 36:2023.

[11] Rudski LG, Lai WW, Afilalo J, et al. Guidelines for the echocardiographic assessment of the right heart in adults: a report from the American Society of Echocardiography endorsed by the European Association of Echocardiography, a registered branch of the European Society of Cardiology, and the Canadian Society of Echocardiography. J Am Soc Echocardiogr 2010; 23:685.

[12] Bleeker G B, Steendijk P, Holman E R, Yu C M, Breithardt O A, Kaandorp T A, et al. Assessing right ventricular function: the role of echocardiography and complementary technologies. Heart 2006; 92:19–26.

[13] Nagel E, Stuber M, Hess O M. Importance of the right ventricle in valvular heart disease. Eur Heart J 1996; 17:829–836.

[14] Ho S Y, Nihoyannopoulos P. Anatomy, echocardiography, and normal right ventricular dimensions. Heart 2006; 92(Suppl 1): i2–i13.

[15] Ostenfeld E, Flachskampf FA. Assessment of right ventricular volumes and ejection fraction by echocardiography: from geometric approximations to realistic shapes. Echo Res Pract 2015; 2(1):R1–R11.

[16] Haddad F, Hunt SA, Rosenthal DN, Murphy DJ. Right ventricular function in cardiovascular disease, part I: anatomy, physiology, aging, and functional assessment of the right ventricle. Circulation 2008; 117:1436.

[17] Kaul S. The interventricular septum in health and disease. Am Heart J 1986; 112:568–581.

[18] Lindqvist P, Morner S, Karp K, Waldenstrom A. New aspects of septal function by using 1-dimensional strain and strain rate imaging. J Am Soc Echocardiogr 2006;19:1345–1349.

[19] Klima U, Guerrero JL, Vlahakes GJ. Contribution of the interventricular septum to maximal right ventricular function. Eur J Cardiothorac Surg 1998; 14:250–255.

[20] Lang RM, Badano LP, Tsang W, et al. EAE/ASE recommendations for image acquisition and display using three-dimensional echocardiography. J Am Soc Echocardiogr 2012; 25:3.

[21] Grant RP, Downey FM, MacMahon H. The architecture of the right ventricular outflow tract in the normal human heart and in the presence of ventricular septal defects. Circulation 1961; 24:223–235.

[22] Foale R, Nihoyannopoulos P, McKenna W, et al. Echocardiographic measurement of the normal adult right ventricle. Br Heart J 1986; 5:633–644.

[23] Brennan JM, Blair JE, Goonewardena S, et al. Reappraisal of the use of inferior vena cava for estimating right atrial pressure. J Am Soc Echocardiogr 2007; 20:857.

[24] Beigel R, Cercek B, Luo H, Siegel RJ. Noninvasive evaluation of right atrial pressure. J Am Soc Echocardiogr 2013; 26:1033.

[25] Yock PG, Popp RL. Noninvasive estimation of right ventricular systolic pressure by Doppler ultrasound in patients with tricuspid regurgitation. Circulation 1984; 70:657.

[26] Abbas AE, Fortuin FD, Schiller NB, et al. Echocardiographic determination of mean pulmonary artery pressure. Am J Cardiol 2003; 92:1373.

[27] Mahan G, Dabestani A, Gardin J, Allfie A, Burn C, Henry W. Estimation of pulmonary artery pressure by pulsed Doppler echocardiography. Circulation 1983;68:367.

[28] Dabestani A, Mahan G, Gardin JM, Takenaka K, Burn C, Allfie A, et al. Evaluation of pulmonary artery pressure and resistance by pulsed Doppler echocardiography. Am J Cardiol 1987; 59:662–668.

[29] Rajagopalan N, Simon MA, Suffoletto MS, et al. Noninvasive estimation of pulmonary vascular resistance in pulmonary hypertension. Echocardiography 2009; 26:489.

[30] Abbas AE, Franey LM, Marwick T, et al. Noninvasive assessment of pulmonary vascular resistance by Doppler echocardiography. J Am Soc Echocardiogr 2013; 26:1170.

[31] Lindqvist P, Calcutteea A, Henein M. Echocardiography in the assessment of right heart function. Eur Heart J 2008; 9(2):225–234.

[32] Kaul S, Tei C, Hopkins JM, Shah PM. Assessment of right ventricular function using two-dimensional echocardiography. Am Heart J 1984; 107:526.

[33] Ghio S, Recusani F, Klersy C, et al. Prognostic usefulness of the tricuspid annular plane systolic excursion in patients with congestive heart failure secondary to idiopathic or ischemic dilated cardiomyopathy. Am J Cardiol 2000; 85:837.

[34] Damy T, Kallvikbacka-Bennett A, Goode K, et al. Prevalence of, associations with, and prognostic value of tricuspid annular plane systolic excursion (TAPSE) among out-patients referred for the evaluation of heart failure. J Card Fail 2012; 18:216.

[35] Alam M, Wardell J, Andersson E, et al. Right ventricular function in patients with first inferior myocardial infarction: assessment by tricuspid annular motion and tricuspid annular velocity. Am Heart J 2000; 139:710.

[36] Miller D, Farah MG, Liner A, et al. The relation between quantitative right ventricular ejection fraction and indices of tricuspid annular motion and myocardial performance. J Am Soc Echocardiogr 2004; 17:443.

[37] Sato T, Tsujino I, Ohira H, et al. Validation study on the accuracy of echocardiographic measurements of right ventricular systolic function in pulmonary hypertension. J Am Soc Echocardiogr 2012; 25:280.

[38] Blanchard DG, Malouf PJ, Gurudevan SV, et al. Utility of right ventricular Tei index in the noninvasive evaluation of chronic thromboembolic pulmonary hypertension before and after pulmonary thromboendarterectomy. JACC Cardiovasc Imaging 2009; 2:143.

[39] López-Candales A, Rajagopalan N, Dohi K, et al. Abnormal right ventricular myocardial strain generation in mild pulmonary hypertension. Echocardiography 2007; 24:615.

[40] Lang RM, Badano LP, Mor-Avi V, et al. Recommendations for cardiac chamber quantification by echocardiography in adults: an update from the American Society of Echocardiography and the European Association of Cardiovascular Imaging. J Am Soc Echocardiogr 2015; 28:1.

[41] D'hooge J, Heimdal A, Jamal F, Kukulski T, Bijnens B, Rademakers F, Hatle L, Suetens P, Sutherland GR. Regional strain and strain rate measurements by cardiac ultrasound: principles, implementation and limitations. Eur J Echocardiogr. 2000; 1:154–170.

[42] Mendes LA, Dec GW, Picard MH, Palacios IF, Newell J, Davidoff R. Right ventricular dysfunction: an independent predictor of adverse outcome in patients with myocarditis. Am Heart J 1994; 128:301–307.

[43] Ghio S, Gavazzi A, Campana C, Inserra C, Klersy C, Sebastiani R, et al. Independent and additive prognostic value of right ventricular systolic function and pulmonary artery pressure in patients with chronic heart failure. J Am Coll Cardiol 2001; 37:183–188.

[44] Hoch DH, Rosenfeld LE. Tachycardias of right ventricular origin. Cardiol Clin 1992; 10:151–164.

[45] Nagaya N, Nishikimi T, Uematsu M, Satoh T, Kyotani S, Sakamaki F, Kakishita M, Fukushima K, Okano Y, Nakanishi N, Miyatake K, Kangawa K. Plasma brain natriuretic peptide as a prognostic indicator in patients with primary pulmonary hypertension. Circulation 2000; 22;102:865–870.

[46] Yap LB, Mukerjee D, Timms PM, Ashrafian H, Coghlan JG. Natriuretic peptides, respiratory disease, and the right heart. Chest 2004; 126:1330–1336.

[47] Oosterhof T, Tulevski II, Vliegen HW, Spijkerboer AM, Mulder BJ. Effects of volume and/or pressure overload secondary to congenital heart disease (tetralogy of Fallot or pulmonary stenosis) on right ventricular function using cardiovascular magnetic resonance and B-type natriuretic peptide levels. Am J Cardiol 2006; 1(97):1051–1055.

[48] Konstantinides S, Geibel A, Olschewski M, Kasper W, Hruska N, Jackle S, Binder L. Importance of cardiac troponins I and T in risk stratification of patients with acute pulmonary embolism. Circulation 2002; 106:1263–1268.

[49] Kittipovanonth M, Bellavia D, Chandrasekaran K, et al. Doppler myocardial imaging for early detection of right ventricular dysfunction in patients with pulmonary hypertension. J Am Soc Echocardiogr 2008; 21:1035.

[50] Kjaergaard J, Akkan D, Iversen KK, et al. Right ventricular dysfunction as an independent predictor of short- and long-term mortality in patients with heart failure. Eur J Heart Fail 2007; 9:610.

[51] Baker BJ, Wilen MM, Boyd CM, Dinh H, Franciosa JA. Relation of right ventricular ejection fraction to exercise capacity in chronic left ventricular failure. Am J Cardiol 1984; 54:596–599.

[52] Tamborini G, Pepi M, Galli CA, Maltagliati A, Celeste F, Muratori M, et al. Feasibility and accuracy of a routine echocardiographic assessment of right ventricular function. Int J Cardiol 2007; 115:86–89.

IntechOpen

Chapter 10

Role of Echocardiography in the Critically Ill Patients

Manivannan Veerasamy

Additional information is available at the end of the chapter

http://dx.doi.org/10.5772/65068

Abstract

Since its inception in 1950s, echocardiography has evolved significantly. Its role has expanded beyond cardiology into operating theaters, intensive care units, and emergency departments. It is an easy, inexpensive, noninvasive, and portable technique, which can be rapidly performed at bedside. It is devoid of complications and, for the most part, universally available. This review focuses on growing importance of echocardiography for critically ill patients in the intensive care and high dependency unit settings including indications, modalities, measurements, and therapeutic impact. Literature review of echocardiography use for the cardiovascular assessment of the critically ill patients was done and various indications are discussed including appropriate use scores. Methods being used include transthoracic and transesophageal echo with various modes. This does include assessment of volume status of the hemodynamically unstable patients, myocardial function, global left ventricular systolic function, regional wall motion abnormalities, cardiac output, cardiac tamponade, valvular function, left ventricular outflow obstruction, and right ventricular function. Other diagnostic assessments include aortic dissection, thromboembolisms, pleural effusions, and septal defects. Echocardiography is now considered as an indispensable tool for diagnosis and management including hemodynamic monitoring in critically ill patients. It provides advantages including noninvasiveness and real-time anatomical and functional assessment of the cardiovascular system.

Keywords: echocardiography, critically ill, ventricular function, hemodynamics

1. Introduction

Echocardiography (echo) is one of the most powerful diagnostic and monitoring tools available to the modern emergency/critical care practitioner. The provision of echo is fundamental to the management of patients with acute cardiovascular disease. Since its inception

in 1950s, echocardiography has evolved significantly. Its role has expanded beyond cardiology into operating theaters, intensive care units, and emergency departments [1]. It is an easy, inexpensive, noninvasive, and portable technique, which can be rapidly performed at bedside. It is devoid of complications and, for the most part, universally available. This review focuses on growing importance of echocardiography for critically ill patients in the intensive care and high dependency unit settings including indications, modalities, measurements, and therapeutic impact.

Echocardiography has been included in international guidelines regarding the management of cardiac arrest and in the universal definition of acute myocardial infarction (AMI). In the acutely ill and critical care settings, echocardiography can be used to measure/monitor cardiac output (CO) and to determine abnormalities of cardiac physiology and coronary perfusion, as well as providing more standard anatomical information related to diagnosis.

This chapter is not intended to be a comprehensive review of echocardiographic techniques. Instead, it focuses on the indications, therapeutic impact, and some of the most common scenarios (**Table 1**) where dilemmas can be answered using echocardiography in critically ill patients.

Hypovolemia/hypotension
Hemodynamic instability
Ventricular dysfunction
Evaluation of cardiac thrombus or embolus
Pulmonary embolism infective endocarditis
Acute valvular regurgitations
Pericardial effusions/cardiac tamponade
Complications after cardiac procedures/cardiothoracic surgery
Acute aortic syndromes

Table 1. General indications for echocardiographic examination in the intensive care unit.

2. Types of echo

The challenges of imaging in the acute settings are well studied and may influence echocardiographic findings and interpretation in critically ill patients. These include a number of factors such as filling status, metabolic status, patient habitus and positioning, positive pressure ventilation, intubation/mechanical ventilation, different ventilation modalities, weaning inotropic status, lung injury, the presence of lines/dressings and/or drains, and extracorporeal support. The echocardiographic data should be interpreted in the case scenario of the acutely/critically ill patient, particularly when time-specific factors further challenge the echocardiographer (i.e., cardiac arrest).

http://dx.doi.org/10.5772/65068

2.1. Transthoracic echocardiography

Transthoracic echocardiography (TTE) is a widely available, inexpensive tool, which is generally the initial imaging modality in the assessment of acute cardiac conditions (**Table 2**). It is used in the majority of clinical scenarios associated with cardiac emergencies. Findings can be overlooked if the study is restricted to standard imaging only. The study should be comprehensive and undertaken with a fully equipped echocardiographic machine. The easiest and least invasive way to image cardiac structures is echocardiography using the transthoracic approach [2]. This noninvasive imaging modality is of great value in the critical care settings because of its portability, widespread availability, and rapid diagnostic capability.

Indication	AUS
Assessment of volume status in critically ill patient	U
Hypotension/hemodynamic instability of uncertain or suspected cardiac etiology	A
Suspected complication of MI	A
Acute chest pain with suspected MI, inconclusive ECG during pain	A
Respiratory failure/hypoxemia of uncertain etiology	A
Respiratory failure/hypoxemia when noncardiac etiology is already established	U
To guide therapy of known acute PE	A
To establish diagnosis of suspected PE	I
Reevaluation of known PE change RV function and PAP after therapy	A
Routine surveillance of prior PE, with normal RV function and PAP	I
No chest pain but laboratory and/or other features indicative of MI	A
Severe deceleration injury/chest trauma with suspected or possible pericardial effusion, valvular, or cardiac injury	A
Routine evaluation in mild chest trauma without ECG or biomarker changes	I

Note: I: inappropriate test for that indication (not generally acceptable and not a reasonable approach. Score 1–3 out of 9); U: uncertain for specific indication (may be acceptable and may be a reasonable approach. Also implies that further patient information/research needed to classify indication definitively. Score 4–6 out of 9); A: appropriate test for that indication. (Test is generally acceptable and is a reasonable approach for the indication. Score 7–9 out of 9.) MI: myocardial infarction, PE: pulmonary embolism, RV: right ventricle, PAP: pulmonary arterial pressure.

Table 2. Indications for echocardiography in acute care settings, evaluated using appropriate use scores (AUS).

2.2. Transesophageal echocardiography

A nondiagnostic TTE usually requires a transesophageal echocardiography (TEE). TEE allows better imaging of the posterior structures and heart in general, due to the position of the probe and better acoustic transmission. Certain situations that warrant TEE include acute aortic syndromes, unexplained hypotension, trauma, morbid obesity, prosthetic valve dysfunction, valvular regurgitations/vegetation, and mechanical ventilation with high-level positive end-

expiratory pressure and source of cardiac emboli. TEE should be done cautiously in patients with coagulopathy, potential trauma to airway or esophagus, and in patients who are unable to protect their own airways or severely hypoxic without mechanical ventilation. During the study, the airway and hemodynamics should be monitored. In the ICU, transthoracic echocardiography (TTE) may, in certain cases, fail to provide adequate image quality because of different factors that can potentially hinder the quality of the ultrasound signal, be it air, bone, calcium, a foreign body, or any other type of interposed structure.

Other imaging modalities include contrast echocardiography, 3D-echo, lung ultrasound examination, focused cardiac ultrasound, and pocket imaging devices.

3. Hemodynamic evaluation

3.1. Ventricular function

3.1.1. Left ventricular systolic function

Patients may present with a spectrum of conditions ranging from cardiogenic shock, acute pulmonary edema, isolated RV dysfunction, or heart failure (HF) complicating an ACS. Since HF is not a diagnosis *per se*, but rather a syndrome, additional investigations are required to determine the underlying cause. Rapid diagnosis of the underlying cause, and distinction between HF due to systolic versus isolated diastolic dysfunction, should be obtained since identification of these features determines immediate treatment in the acute settings.

Assessment of the left ventricular (LV) systolic function is an integral part of the medical management of hemodynamically unstable critically ill patients. Assessment of the global LV function can be quickly obtained by "eyeballing" from the parasternal long- and short-axis, apical two- and four-chamber, and subcostal views and real-time visualization of the kinetics and size of the cardiac cavities, a combination of ejection fraction/fractional shortening, Doppler patterns of ventricular filling and tissue. Doppler imaging supplements to the information from the echocardiogram. Assessment of the chamber size and LV wall thickness is also done. Findings may include increase in the left ventricular end-systolic and diastolic volume, increase in end-systolic and diastolic diameter and abnormal wall motion. Two other modes of imaging that are relatively easy to obtain for the assessment of the LV function are the atrioventricular plane displacement (AVPD) and systolic tissue Doppler velocities (sTD) [3].

TTE was shown to be an excellent diagnostic tool for assessment of the LV function in the ICU, even when positive end expiratory pressure was present [4]. However, if the TTE provides suboptimal imaging for evaluation of ventricular function, TEE can be obtained for better assessment. It is important to remember that significant LV dysfunction is common in critically ill patients and the "normal" values quoted from noncritical care studies may not be valid.

http://dx.doi.org/10.5772/65068

3.1.1.1. Sepsis-related cardiomyopathy

Bedside echocardiography is an important tool for identification of the cause of hemodynamic instability (which may be of cardiogenic, hypovolemic, or distributive origin) and for the further management (i.e., administration of fluid, vasoactive, or inotropic agent infusion). Classically, septic shock has been considered to be a hyperdynamic state characterized by normal or high cardiac output (CO). But echocardiographic studies indicate that ventricular performance is often diminished in those patients. LVEF might not be a reliable index of LV systolic function in patients with early septic shock.

3.1.1.2. Stress-induced cardiomyopathy (Takotsubo syndrome)

Defined as a transient, stress-induced dysfunction of the LV apex, it predominantly affects female patients (90%). Takotsubo cardiomyopathy mimics an ACS, echo findings show a reversible LV dysfunction with regional wall motion abnormalities, but these patients have no angiographic evidence of ACS. Akinesia has also been demonstrated in the LV mid-cavity, LV base, and RV, with or without sparing of the other LV segments (**Figure 1**). Echo is a useful tool for the follow-up as the LV function must completely recover over time to confirm the diagnosis.

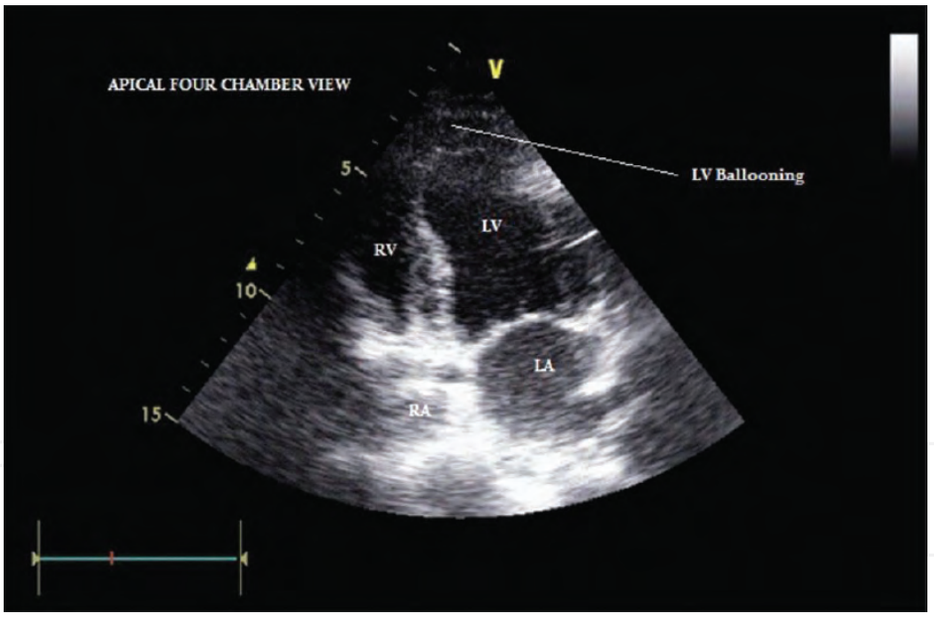

Figure 1. Takotsubo's cardiomyopathy.

LV measurements also provide data on myocardial injury, cardiomyopathies, and fluid status. The left atrial size is evaluated as an enlarged Left atrium (LA) may indicate significant valvular disease, intra-atrial shunting and atrial fibrillation, all of which may in turn cause hemodynamic instability. Finally, the aortic and mitral valves are assessed to complete the examination of left ventricular function. Two-dimensional speckle tracking echocardiography (STE) offers potentially useful information in acute HF patients with underlying cardiomyopathies.

3.1.2. LV diastolic function

In the ICU, when EF is normal or supernormal and ventricular filling pressure (pulmonary artery occlusion pressure) is elevated, diastolic dysfunction should be suspected. The filling patterns related to the diastolic function can be influenced by different factors such as heart rate, ischemia, left atrial pressure, ventricular hypertrophy, and valvular pathologies. In patients with an abnormal relaxation pattern (E/A < 1), and peak E velocity <50 cm/s, LV filling pressures are usually normal [5]. With restrictive filling (E/A ≥ 2, mitral E deceleration time <150 ms), mean LA pressure is often increased. Patients with heart failure with preserved LV ejection fraction (HFpEF) present with signs and/or symptoms of HF and several echocardiographic findings.

In both acute systolic and diastolic HF, interstitial edema may be diagnosed at the bedside by the demonstration of an abnormally high number of bilateral sonographic B-lines (also called ultrasound lung comets). Two-dimensional speckle tracking echocardiography offers diagnostic data in acute heart failure associated with cardiomyopathies, specifically when ejection fraction appears preserved [5].

3.1.3. Cardiac arrest

Echo is a very useful tool in the management of critically ill patients with cardiac arrest. The use of echo in an advanced cardiac life support (ACLS) is supported by international evidence-based recommendations. Peri-resuscitation echocardiography does not impact upon high-quality cardiopulmonary resuscitation (CPR) when appropriately applied and requires special training in advanced cardiac life support (ACLS) compliant manner. Images should be obtained only during the pulse/rhythm check. It can provide data to diagnose or exclude certain potential reversible causes of cardiac arrest (including severe LV/RV dysfunction, myocardial infarction, hypovolemia, pulmonary embolism (PE), tension pneumothorax, or tamponade). Echo is particularly useful in situations of pulseless electrical activity (electromechanical dissociation—EMD) to differentiate between pseudo-EMD and true EMD. Though there is extensive data, we need further recommendations regarding how to use echo during a code situation and specific guidelines for termination of resuscitation.

3.2. Right ventricular function

Right ventricular (RV) function can be altered by massive pulmonary embolism and acute respiratory distress syndrome (ARDS), the two main causes of acute cor pulmonale, in the critical care settings [6]. Other causes of acute RV dysfunction include RV infarction associated with inferior myocardial infarction, myocardial contusion, fat or air embolism, acute sickle-cell crisis, and sepsis. In unstable critically ill patients, specifically those with massive PE and acute respiratory distress syndrome, a diagnosis of RV dysfunction may guide therapy (e.g., use of thrombolytics, vasopressors, volume resuscitation, and catheter-directed interventional therapy). RV size and function are frequently evaluated by visual comparison with the left ventricle. RV kinetics of the cavity and septum, and diastolic dimensions are also measured, using either TTE or TEE. Measuring the ratio between the RV and LV end diastolic areas from

http://dx.doi.org/10.5772/65068

apical four-chamber view is one of the best ways to evaluate RV dilation [7]. The diastolic ventricular ratio of 0.6–1.0 is consistent with moderate RV dilation and a ratio of 1 is consistent with severe RV dilation. Tricuspid regurgitation, right atrial dilation, and inferior vena caval dilation are commonly associated with RV diastolic enlargement.

3.2.1. Pulmonary embolism

Though pulmonary angiography remains the gold standard for diagnosis of pulmonary embolism (PE), other available imaging modalities include ventilation-perfusion scanning, spiral computed tomography (CT), and magnetic resonance imaging (MRI) angiography. TTE can help to establish a prompt diagnosis to identify patients with high-risk features, especially if the patient is hemodynamically unstable. Overall, the sensitivity of TTE for the diagnosis of pulmonary embolism is about 50–60% while the specificity is around 80–90%. In some situations, that is, in critically ill patients, TEE may improve the sensitivity.

The main indirect findings for pulmonary embolism (**Table 3**) are the consequences of acutely increased pulmonary artery/right heart pressures [5]. In pulmonary embolism, RV hypokinesia is not necessarily global but can be limited to the mid-RV free wall while the contraction of the RV apex may be normal or hyperdynamic (McConnell sign) (**Figure 2**).

Thrombus into right chambers
RV systolic dysfunction/global RV hypokinesia
Dilatation RA, RV (end-diastolic RV/LV diameter.0.6 or area.1.0)
Mild to severe TR
Pulmonary arterial dilatation
Abnormal septal motion toward LV
McConnell sign—mid-RV wall hypokinesia with apical sparing
Pulmonary hypertension around 40–50 mm Hg (60 mm Hg in the case of pre-existing pulmonary hypertension)
Lack of respiratory variation of the inferior vena cava

Table 3. Echocardiographic finding in pulmonary embolism.

As other clinical conditions can produce acute cor pulmonale in the ICU, better visualization of the pulmonary arteries is needed to achieve high accuracy for the diagnosis of PE. This goal can be achieved by using TEE. TEE helps to achieve a better visualization of the pulmonary arteries and detecting emboli that are lodged in the main and right pulmonary arteries. The diagnosis is made when an embolus is visualized. When the index of suspicion for PE is high and TEE is negative, then pulmonary angiography or helical computed tomography should be considered as the next step. The demonstration of acute cor pulmonale with echocardiography has important prognostic and therapeutic implications. The presence of cor pulmonale with massive PE is associated with increased mortality, whereas the absence of RV dysfunction is associated with a better prognosis.

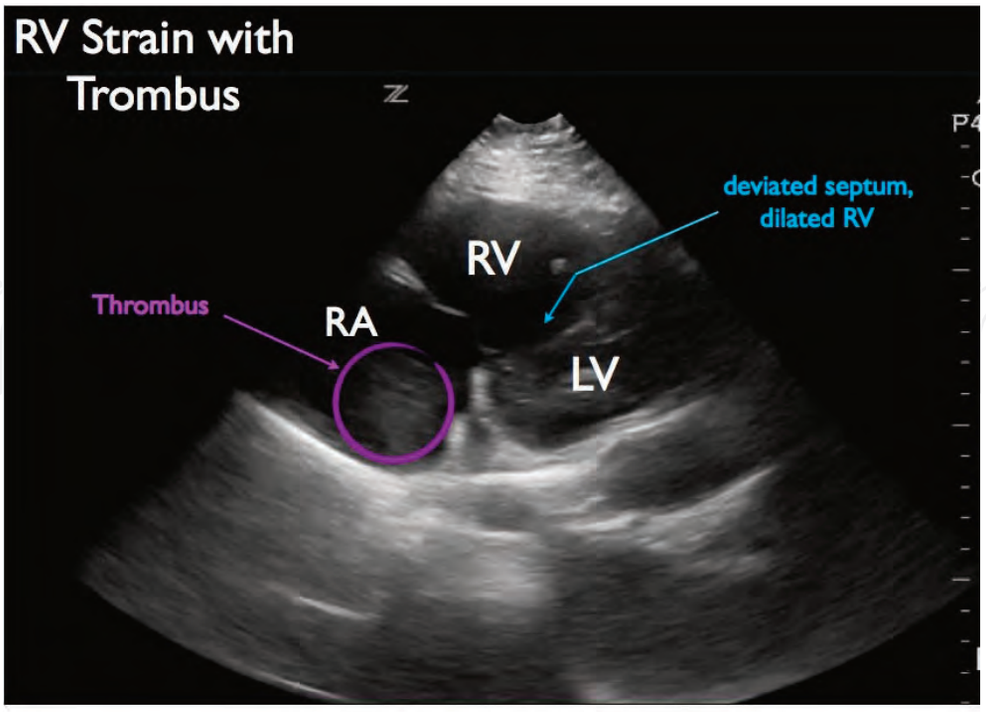

Figure 2. Thrombus in the right ventricle.

3.3. Assessment of cardiac output (CO)

Measurement of CO is an important data in the assessment of critically ill patients with unstable hemodynamics. Cardiac output and stroke volume can be established by combining Doppler data derived from blood flow velocity through a conduit and the cross-sectional area of the conduit. The most common and most reliable technique is using the left ventricular outflow tract and aortic valve. Another method using an esophageal probe inserted in sedated patients, to measure blood flow velocity waveforms in the descending aorta combined with a nomogram, is particularly useful in adult patients to provide continuous monitoring of cardiac function.

3.4. Assessment of filling pressures and volume status

Accurate measurement of volume status and LV preload is important for management of critically ill patients. Besides, invasive pressure measurements to assess LV filling may not correlate well with LV volume. Echo can be very useful in adequately evaluating preload. Measurements from two-dimensional and Doppler echo include LV end-diastolic volume (EDV), LV end-diastolic area (EDA), transmitral diastolic filling pattern, and mitral and pulmonary venous flow.

"Eyeballing" LV end-diastolic (LVED) and end-systolic (LVES) areas provide a quick assessment of intracardiac volume status. Findings in hypovolemic patients include hyperdynamic LV with a reduced end-diastolic volume and "kissing" papillary muscles in systole, suggesting an increased ejection fraction with an empty ventricle at end-systole. Septic patients tend to

have a reduced afterload, which is usually demonstrated by a normal LVED area, but a reduced LVES area. Patients with chronic cardiac failure have a dilated LV and may be hypovolemic even with a higher LVED area.

Right atrial pressure measurement is also helpful in the evaluation of the circulating volume status and often measured by the diameter and change in caliber with inspiration of the inferior vena cava. A dilated vena cava (diameter of 20 mm) without a normal inspiratory decrease in caliber (50% with gentle sniffing) usually indicates elevated right atrial pressure. Available data suggest inferior vena cava diameter variation with inspiration can be used a guide to fluid therapy [8]. A small vena cava in mechanically ventilated patient excludes the presence of elevated right atrial pressure, as these patients usually have dilation of the inferior vena cava [9].

3.5. Assessment of pulmonary artery pressure

Pulmonary hypertension is usually diagnosed when systolic pulmonary pressure is ~35 mm Hg, diastolic pulmonary pressure is ~15 mm Hg, and mean pulmonary pressure is ~25 mm Hg. Critically ill patients commonly have pulmonary arterial hypertension, possibly from various cardiac, pulmonary, and systemic processes. Several echocardiographic methods have been validated for noninvasive estimation of pulmonary artery pressure [10], which are useful in critically ill patients. A large number of ICU patients have some degree of tricuspid and pulmonary regurgitation, which are needed to measure pulmonary arterial pressure. The tricuspid and pulmonary regurgitation velocities determine systolic and diastolic pulmonary artery pressures.

3.6. Assessment of valvular function

Significant valvular abnormalities can be present in the critically ill patient without being clinically recognized. In the ICU, TTE can provide valuable information concerning valvular integrity and function [11] but may be suboptimal and TEE may be indicated. Adequate and accurate evaluation of the valvular structures may often be required in the critically ill patients. The most common indications for bedside echocardiography for evaluation of the valvular apparatus in this population are for suspected endocarditis, acute valvular stenosis or regurgitation, critical aortic stenosis, significant mitral stenosis, or prosthetic valve dysfunction including regurgitation and obstruction. Information regarding etiology, pathogenesis, and severity of the valvular lesions, valvular anatomy and function, chamber size, function, and wall thickness of the ventricles can be readily obtained by echo. Abnormalities such as vegetation, thrombus, fibrosis, calcification, immobile, or prolapsing leaflets or prosthetic valve dehiscence can be detected by echo [5].

3.7. Evaluation of the pericardial space

Suspected tamponade is the most common indication for assessment of the pericardium in the critically ill patient. The pericardial space can be filled with a variety of substances including fluid, pus, blood, or air. Presence of fluid in this space is detected as an echo-free space. TTE

easily detects pericardial effusion (**Figure 3**), usually in the parasternal long and short-axis and the apical views. But, given higher chances of suboptimal TTE in critically ill patients, TEE may be warranted, particularly in patients with poor acoustic windows or post cardiothoracic surgical patients.

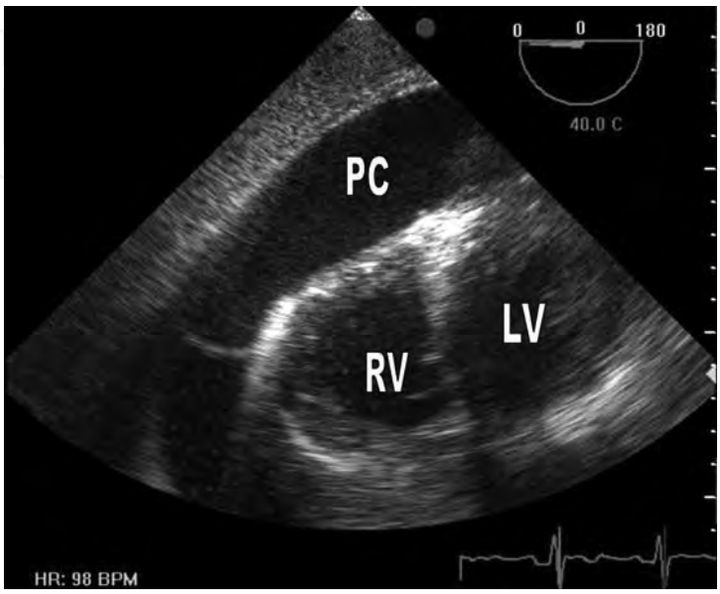

Figure 3. Pericardial effusion.

Echocardiography is also useful in the management of pericardial effusion, as pericardiocentesis can be performed safely under echocardiographic guidance [12]. Echocardiography also can be used to accurately place the needle during the drainage, immediately monitor the results of the pericardiocentesis, and serially monitor to evaluate the reaccumulation of the effusion.

3.7.1. Cardiac tamponade in the ICU

The most common causes of cardiac tamponade in the ICU are listed in **Table 4**.

Complication of myocardial infarction (e.g., ventricular rupture)
Blunt or penetrating chest trauma
Proximal ascending aortic dissection
Myocardial or coronary perforation secondary to catheter-based interventions (i.e., after
intravenous pacemaker lead insertion, central catheter placement, or percutaneous coronary interventions)
Uremic or infectious pericarditis
Compressive hematoma after cardiac surgery
Pericardial involvement by metastatic disease or other systemic processes

Table 4. Common causes of cardiac tamponade in intensive care unit.

http://dx.doi.org/10.5772/65068

There are several 2D-echo findings that suggest a hemodynamically significant pericardial fluid collection (**Table 5**). The rate of accumulation of the pericardial fluid, and collection and size of the collection determine the intrapericardial pressure. Although diastolic RV collapse (inward diastolic motion of the RV free wall) occurs later, it is a more specific sign and is best appreciated from the parasternal or subcostal long-axis views [13] (**Figure 4**).

Usually large pericardial effusion
Swinging heart
RA collapse (rarely LA)
Diastolic collapse of the anterior RV-free wall (rarely LV)
IVC dilatation (no collapse with inspiration)
TV flow increases and MV flow decreases during inspiration (reverse in expiration)
Systolic and diastolic flows are reduced in systemic veins in expiration and reverse flow with atrial contraction is increased

Table 5. Echo findings of hemodynamically significant pericardial effusion.

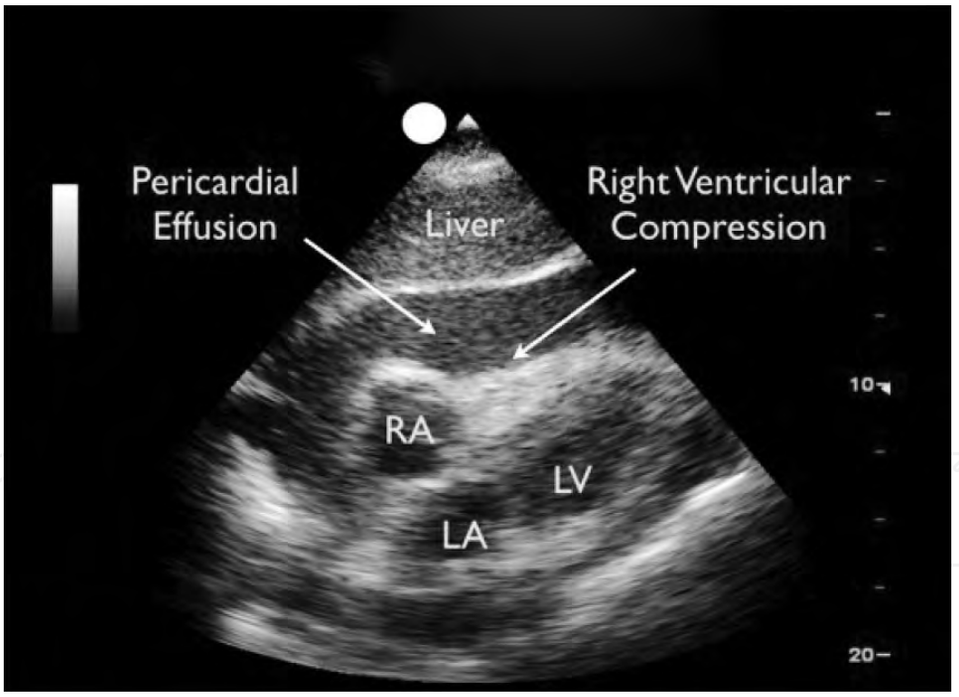

Figure 4. Cardiac tamponade.

If the patient's condition requires urgent pericardiocentesis, the procedure may be echocardiographically guided, as this has been shown to reduce complications. Echocardiography can additionally be used to verify whether the collection has been completely drained. TEE is rarely indicated in this setting.

4. Some other common conditions/scenarios

4.1. LVOT obstruction

In patients who develop dynamic Left Ventricular Outflow Tract (LVOT) obstruction with resultant decrease in cardiac output, particularly the ones who fail to respond to inotropic support, echo is a valuable diagnostic tool. In these patients, right heart catheterization can often be misleading, resulting in inappropriate management.

4.2. Cardiogenic shock

The commonest cause of cardiogenic shock is severe systolic dysfunction from acute myocardial infarction and echo remains an excellent initial diagnostic tool. Shock due to LV dysfunction remains the leading cause of mortality in AMI (50–70%) [14]. Other etiologies include mechanical complications of AMI, myocarditis, cardiomyopathy, valvular heart disease, RV dysfunction, myocardial contusion, and acute aortic dissection. TTE should be obtained first in this set of patients and TEE may be warranted when TTE is suboptimal. Common findings of cardiogenic shock complicating acute myocardial infarction are shown in **Table 6**.

LV dysfunction	Depressed EF, regional wall motion abnormalities, decrease in stroke volume, CO, elevated LV pressures, mitral regurgitation infarction
RV infarction	RV dilatation, dyssynergy, paradoxical septal motion, and McConnell sign, decrease of tricuspid annulus systolic excursion (TAPSE)
Free ventricular wall rupture	Obvious cardiac tamponade or only pericardial collection in subacute free wall rupture (30% of rupture)
Acute mitral regurgitation	Complete or partial rupture of the posterior papillary muscle with partial or complete flail of the mitral valve. Also from acute systolic anterior motion of the mitral valve secondary to dynamic LVOT obstruction

Table 6. Echo findings in cardiogenic shock complicating acute myocardial infarction.

4.3. Complications after cardiac surgery/procedures

In patients with hemodynamic instability after cardiothoracic operations, bedside echocardiography has been shown as a valuable tool in the critical care management [15]. TTE is often suboptimal and TEE is warranted as it obtains information that can help determine the etiology of hypotension in this set of patients. Most frequently encountered echocardiographic findings of LV dysfunction, cardiac tamponade, RV failure, hypovolemia, and valvular dysfunction have been described in earlier sections of this chapter.

Echo is useful in other situations such as evaluation of coronary arteries in suspected coronary disruption, RV dysfunction, and TAPSE (pre-, intra-, and postoperative TAPSE) evaluation, immediately after heart transplant (to rule out early rejection, early RV dysfunction, tamponade, or other causes of instability). Echo is an initial modality of imaging in patients who

http://dx.doi.org/10.5772/65068

underwent catheterization/electrophysiology procedures presenting with potential acute complications include ventricular failure, cardiogenic shock, tamponade, displacement of implanted devices, and occlusion of coronary stents.

4.4. Extracorporeal support

Extracorporeal support is increasingly used to support critically ill patients with severe cardiac and/or respiratory failure. Echocardiography for extracorporeal support is highly specialized. Thus echocardiography has a vital role in excluding any potentially treatable underlying cause for cardiorespiratory failure, essential to determine the requirement for the RV and/or LV support and level of support required, mandatory to exclude cardiovascular contraindications for initiation of the support. Echocardiography subsequently has a vital role in its successful implementation, including confirming/guiding correct cannula placement, ensuring the goals of support are met, detecting complications, and assessing tolerance to assistance. Finally, in patients requiring extracorporeal cardiac support, various echocardiographic parameters have been proposed to be used in conjunction with clinical and hemodynamic assessment in order to attempt to predict those patients who can be successfully weaned.

4.5. Cardiac arrhythmias

In the critically ill patient population, heart rates of 100–120/min may be required to maintain adequate cardiac output.

4.5.1. Atrial arrhythmias

Atrial arrhythmias, common in the acute settings, present challenging conditions for assessing cardiac function and hemodynamics, especially when irregular (as in atrial fibrillation). Use of echo in critically ill patients is done with caution. In atrial fibrillation, measurements are obtained from an average of about 10 consecutive heartbeats, to permit the use of echocardiographic parameters usually used in sinus rhythm, to predict elevated filling pressures. The "index beat" method using the measurement performed on the cardiac cycle following a pair of equal preceding cardiac cycles, is also being used in practice.

4.5.2. Ventricular arrhythmias

Echocardiography is one of the first investigations to be performed as soon as the arrhythmia is successfully terminated. Etiologies include ischemic and nonischemic causes that require echocardiographic evaluation.

4.6. Assessment of the aorta

TTE is a good initial investigation tool for evaluation of the proximal aorta (ascending aorta and arch). Because of the close anatomic relationship between the thoracic aorta and the esophagus, TEE allows optimal visualization of the entire thoracic aorta.

4.6.1. Aortic dissection and rupture

Diagnosis and management of aortic dissection is an emergency and these patients are often critically ill. Of the various available imaging modalities, echo, particularly TEE has been recommended for evaluation of suspected aortic dissection (**Figure 5**). TEE has the ability to assess the following, including extension of dissection into the proximal coronary arteries, the point of entry and exit between the true and false lumens, the presence of thrombus in the false lumen, the presence of pericardial or mediastinal hematoma or effusion, severity, and mechanism of associated aortic valve regurgitation, and ventricular function.

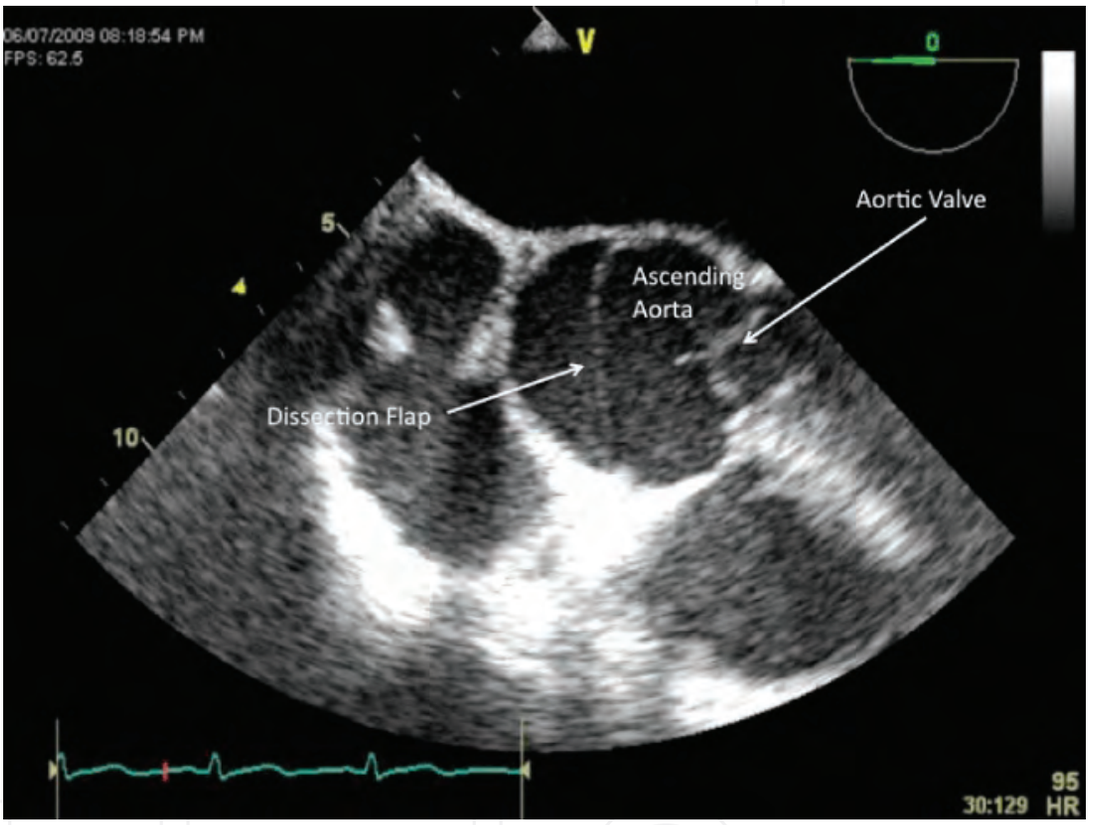

Figure 5. Ascending aortic dissection on TEE.

4.6.2. Intraaortic balloon pump

TEE is useful in various phases of management including evaluation of aortic regurgitation as a contraindication prior to insertion, to confirm the position of the catheter, to ensure correct functioning of the balloon, and to rule out complications such as aortic dissection.

4.6.3. Traumatic injuries of the heart and aorta

Blunt or penetrating chest trauma may cause severe injury to the heart and great vessels. A rapid, focused assessment with echocardiography can detect pericardial collection, myocardial contusion, mediastinal hematomas, aortic intramural hematomas, aortic dissection or

http://dx.doi.org/10.5772/65068

transection, and pleural collections. Both TTE and TEE play an important role in the assessment of patients with chest trauma, and TEE may be indicated in patients with polytrauma and/or on mechanical ventilation or when a traumatic, acute aortic syndrome is suspected. It is important to distinguish aortic from cardiac injuries. Also, traumatic pseudoaneurysms must be differentiated from true aneurysms. Trauma may cause aortic rupture, dissection, or intramural hematoma. Partial disruption of the aortic wall may lead to pseudoaneurysm. Once pericardial tamponade is excluded, a standard echocardiogram is useful in other conditions, like cardiac contusion/dysfunction, myocardial rupture, septal and valvular injury. Acute MI from coronary artery dissection and arrhythmias in acute trauma patients warrant echocardiographic evaluation.

4.7. Infective endocarditis

Febrile illness in critically ill patients warrants evaluation including infective endocarditis. See section on valvular lesions evaluations. Echocardiography is the test of choice for the noninvasive diagnosis of endocarditis. The echocardiographic findings may include new valvular regurgitation, an oscillating intracardiac mass on a valve or supporting structure or in the path of a regurgitant jet or an iatrogenic device, valve abscesses and new partial dehiscence or vegetation of a prosthetic valve. TEE has also been clearly shown to be superior to TTE for diagnosing complications of endocarditis, such as aortic root abscess, fistulas, and ruptured chordae tendineae of the mitral valve.

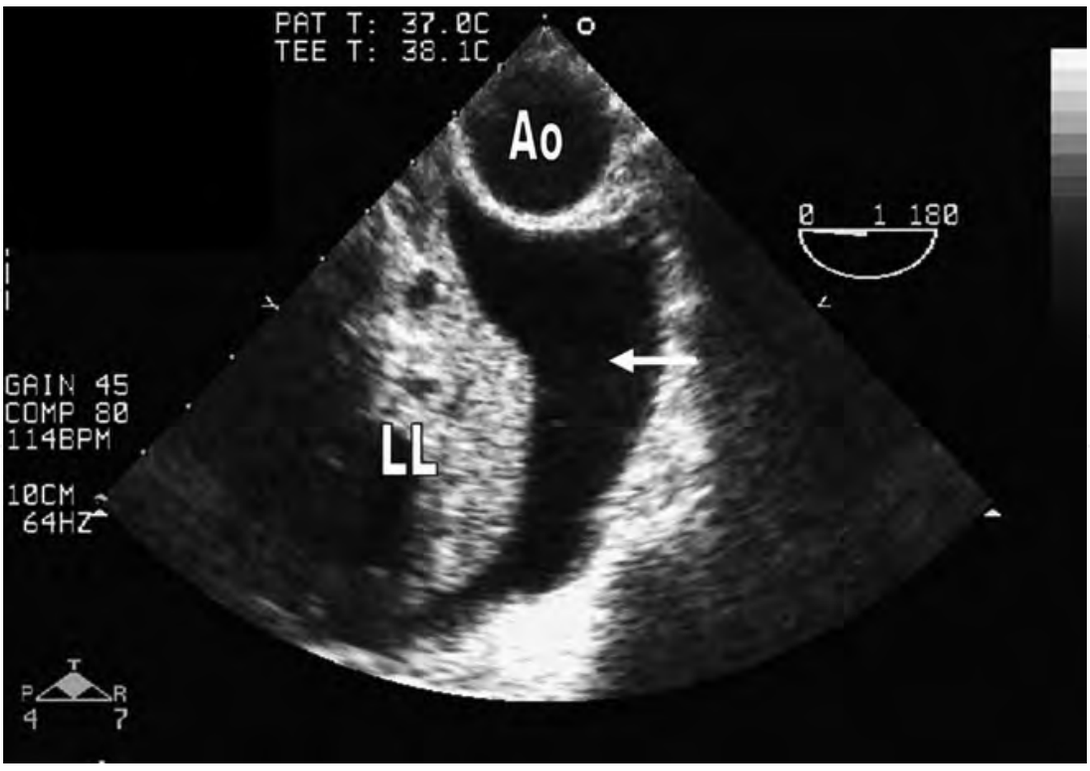

Figure 6. Pleural effusion on echo.

4.8. Pleural effusions

Echocardiogram often finds the presence of pleural effusions (**Figure 6**) and can be used as a diagnostic tool while evaluating the cardiovascular system, especially in patients with acute dyspnea and decompensated heart failure.

4.9. Assessment for intracardiac and intrapulmonary shunts

In critically ill patients with unexplained embolic stroke or refractory hypoxemia, the presence of a right-to-left shunt needs to be excluded. Common positions of right-to-left shunt are atrial septal defect or patent foramen ovale at the cardiac level, arteriovenous fistula at the pulmo-nary level and pulmonary arteriovenous fistulas. Bubble study, color Doppler studies, and contrast-enhanced studies are done to increase the detection rate of intracardiac shunt.

4.10. Source of embolus

Patients presenting with acute unexplained embolic stroke and arterial occlusions, echocardiography should be obtained to investigate a potential embolic source of cardiac origin. In this situation, TEE is the preferred imaging of choice. Possible cardiac sources of emboli include thrombus in the left atrial or appendage, LV thrombus, valvular vegetation, right-sided clots (right atrium, right ventricle, vena cava) combined with a right-to-left intracardiac shunt (leading to a paradoxical embolus), thoracic atheromatosis, and cardiac tumors. TEE is a valuable tool in evaluating the left atrium and appendage for the presence of thrombus, for patients with atrial fibrillation or flutter in whom cardioversion is considered.

5. Conclusion

Echocardiography is now considered as an indispensable tool and primary imaging modality for diagnosis and management of hemodynamic monitoring in critically ill patients. However, echocardiography is subject to variations in interpretation, which can potentially lead to errors, as with any diagnostic and monitoring tool and caution need to be undertaken during interpretation. Nevertheless, it provides advantages including noninvasiveness and rapid and accurate real-time anatomical and functional assessment of the cardiovascular system under stressful situations and is very useful in assisting therapeutic procedures.

Author details

References

[1] Roscoe, A., Strang, T. (2008). Echocardiography in intensive care. *Continuing Education in Anaesthesia, Critical Care & Pain, 8* (2), 46–49. doi: 10.1093/bjaceaccp/mkn002

[2] Poelaert, J., Schmidt, C., Colardyn, F. (1998). Transoesophageal echocardiography in the critically ill. *Anaesthesia, 53*(1), 55–68. doi:10.1111/j.1365-2044.1998.00285

[3] Parker, M.M., Suffredini, A.F., Natansan, C., et al. (1989). Responses of left ventricular function in survivors and nonsurvivors in septic shock. *Journal of Critical Care, 4*, 19–25. doi:10.1016/0883-9441(89)90087-7

[4] Beaulieu, Y. (2007). Bedside echocardiography in the assessment of the critically ill. *Critical Care Medicine, 35*(5 Suppl), S235–S249. doi:10.1097/01.CCM.0000260673.66681.AF

[5] Lancellotti, P., Price, S., Edvardsen, T., Cosyns, B., Neskovic, A.N., Dulgheru, R., et al. (2015). The use of echocardiography in acute cardiovascular care: Recommendations of the European association of cardiovascular imaging and the acute cardiovascular care association. *European Heart Journal Cardiovascular Imaging, 16*(2), 119–146. doi: 10.1093/ehjci/jeu210

[6] Vieillard-Baron, A., Schmitt, J.M., Augarde, R., Fellahi, J.L., Prin, S., Page, B., et al. (2001). Acute cor pulmonale in acute respiratory distress syndrome submitted to protective ventilation: Incidence, clinical implications, and prognosis. *Critical Care Medicine, 29*(8), 1551–1555. doi:10.1007%2Fs00134-013-3045-2

[7] Vieillard-Baron, A., Prin, S., Chergui, K., Dubourg, O., Jardin, F. (2002). Echo-doppler demonstration of acute cor pulmonale at the bedside in the medical intensive care unit. *American Journal of Respiratory and Critical Care Medicine, 166*(10), 1310–1319. doi: 10.1164/rccm.200202-146CC

[8] Feissel, M., Michard, F. et al. (2004). The respiratory variation in inferior vena cava diameter as a guide to fluid therapy. *Intensive Care Medicine, 30* (9), 1834–1837. doi: 10.1007/s00134-004-2233-5

[9] Jardin, F., Vieillard-Baron, A. (2006). Ultrasonographic examination of the venae cavae. *Intensive Care Medicine, 32*(2), 203–206. doi:10.1007/s00134-005-0013-5

[10] Stevenson, J.G. (1989). Comparison of several non-invasive methods for estimation of pulmonary artery pressure. *Journal of American Society Echocardiography, 2*, 157–171. doi: 10.1016/S0894-7317(89)80053-7

[11] Alam, M. (1996). Transesophageal echocardiography in critical care units: Henry ford hospital experience and review of the literature. *Progress in Cardiovascular Diseases, 38*(4), 315–328. doi: S0033-0620(96)80016-8

[12] Callahan, J. A., Seward, J. B. (1997). Pericardiocentesis guided by two-dimensional echocardiography. *Echocardiography (Mount Kisco, N.Y.), 14*(5), 497–504. doi/10.1111/j.1540-8175. 1997.tb00757

[13] Troianos, C.A., Porembka, D.T. (1996). Assessment of left ventricular function and hemodynamics with transesophageal echocardiography. *Critical Care Clinics, 12*(2), 253–272. doi :10.1016/S0749-0704(05)70248-7

[14] Klein, T., Ramani, G.V. (2012). Assessment and management of cardiogenic shock in the emergency department. *Cardiology Clinics, 30*(4), 651–664. doi:10.1016/j.ccl.2012.07.004

[15] Wake, P.J., Ali, M., Carroll, J., Siu, S.C., Cheng, D.C. (2001). Clinical and echocardiographic diagnoses disagree in patients with unexplained hemodynamic instability after cardiac surgery. *Canadian Journal of Anaesthesia, 48*(8), 778–783. doi:10.1007/BF03016694

8

Detection of Intracardiac and Intrapulmonary Shunts at Rest and During Exercise Using Saline Contrast Echocardiography

Andrew T. Lovering and Randall D. Goodman
University of Oregon, Oregon Heart & Vascular Institute, USA

1. Introduction

Ultrasound has become a valuable tool for making non-invasive physiological measurements that are clinically important, one of which is detection of anatomic shunts using saline contrast echocardiography. Right-to-left intrapulmonary and intracardiac shunts are clinically relevant for two reasons. First, they allow deoxygenated blood to mix with oxygenated blood, thereby reducing the overall efficiency of pulmonary gas exchange. Thus, the opening of either intrapulmonary or intracardiac shunts at rest and/or during exercise may play a role in determining pulmonary gas exchange efficiency (Sun *et al.*, 2002; Stickland & Lovering, 2006; Lovering *et al.*, 2011). The opening of these shunts may also explain why some people with pulmonary diseases such as chronic obstructive pulmonary disease (COPD) desaturate so profoundly during even mild exercise (Miller *et al.*, 1984; Dansky *et al.*, 1992). The second reason that these pathways are clinically relevant is that anatomic right-to-left shunts may allow for thrombi to bypass the pulmonary capillary filter. Indeed, a patent foramen ovale and pulmonary arteriovenous malformations are associated with increased risk for neurological sequelae such as migraines, transient ischemic attacks and stroke (Movsowitz *et al.*, 1992; Petty *et al.*, 1997; De Castro *et al.*, 2000; Lamy *et al.*, 2002).

Where there is a right-to-left shunt it is likely that there may also be a left-to-right shunt following the same path but during a different phase of the cardiac and/or respiratory cycle. Left-to-right shunts are clinically relevant because they can result in right heart volume overload and irreversible pulmonary hypertension (Mulder, 2010). Thus, evidence of right heart chamber enlargement or right-to-left shunt by saline contrast echocardiography is sufficient reason for further investigation to rule out significant left-to-right shunting.

This chapter will focus on the ultrasound measurements used for detecting anatomic right-to-left shunts at rest, during exercise and during pharmacological-induced stress in both clinical and research settings. We also include a section on recent findings from our lab and others using saline contrast to detect right-to-left shunts in healthy human subjects and subjects with COPD.

2. Right-to-left intrapulmonary and intracardiac shunt

Intracardiac shunts include patent foramen ovale (PFO), atrial septal defects (ASD) and ventricular septal defects (VSD). It is generally accepted that 25 to 30% of the general population has a probe-patent foramen ovale (Hagen *et al.*, 1984). Interestingly, recent estimates of the prevalence of PFO using saline contrast echocardiography suggest a slightly higher prevalence of approximately 40% (Woods *et al.*, 2010; Elliott *et al.*, 2011b). The association of PFO with neurological sequelae such as migraine, transient ischemic attack and stroke make these pathways highly clinically relevant (Homma *et al.*, 1997; Petty *et al.*, 1997; De Castro *et al.*, 2000; Lamy *et al.*, 2002; Carpenter *et al.*, 2010).

It has been documented for over 70 years that anatomic right-to-left intrapulmonary shunts exist in normal human lungs. The studies that established the existence of these pathways used solid, large diameter microspheres to prove that there are large diameter pathways that bypass pulmonary capillaries (von Hayek, 1940; Tobin & Zariquiey, 1950; Tobin, 1966). More recent studies by our group have used microspheres to demonstrate the existence of large diameter (>25 to 50 μm) intrapulmonary arteriovenous anastomoses in isolated, ventilated and perfused healthy human and baboon lungs under physiologic conditions (Lovering *et al.*, 2007).

Intrapulmonary right-to–left pathways can be pulmonary arteriovenous malformations (PAVMs), grossly distended capillaries or arteriovenous anastomoses. The prevalence of PAVMs and grossly distended capillaries that result from rare diseases such as hepatopulmonary syndrome and hemorrhagic hereditary telangiectasia is considered to be very small, on the order of 1 in 50,000 (Khurshid & Downie, 2002; Liu *et al.*, 2010). However, we have found that greater than 95% of healthy humans have intrapulmonary arteriovenous anastomoses that are closed at rest but open up during exercise (Stickland & Lovering, 2006; Lovering *et al.*, 2010). Furthermore, the existence of these pathways in baboon lungs suggests that they may not be evolutionary disadvantageous since humans, gorillas and chimpanzees diverged from the old world monkeys (baboons, macaques, etc.) approximately 25 to 30 million years ago (Purvis, 1995; Goodman *et al.*, 1998; Stewart & Disotell, 1998). Although there is a high prevalence of these pathways in healthy humans, a significant impact on physiologic processes has not yet been proven.

3. Echocardiography for the detection of anatomic right-to-left shunt at rest

Saline contrast echocardiography is a proven non-invasive technique for the detection of right-to-left shunts at rest. This technique is used in both clinical and research settings, although certified ultrasonographers are typically required to obtain images of diagnostic quality. We strongly suggest that all recommendations by the American Society for Echocardiography for performance, interpretation and application of saline contrast echocardiography be followed accordingly (Waggoner *et al.*, 2001; Mulvagh *et al.*, 2008).

3.1 Theory

Echocardiography used as a technique for the detection of right-to-left shunts assumes that intravenously-infused saline contrast bubbles are filtered out by the pulmonary capillaries or collapse before reaching the left side of the heart (Yang, 1971; Yang *et al.*, 1971a, b; Meltzer

et al., 1980a; Meltzer *et al.*, 1980b; Meltzer *et al.*, 1981; Bommer *et al.*, 1984; Woods & Patel, 2006). Thus, large diameter bubbles do not reach the left side of the heart unless they travel through large diameter pathways such as pulmonary arteriovenous malformations (PAVMs) or a PFO. Saline contrast echocardiography is therefore considered to be the most sensitive test for detection of intracardiac shunts (Belkin *et al.*, 1994). With a prevalence of 30 to 40%, it is difficult to argue the existence of a PFO if intravenously injected saline contrast bubbles appear in the left heart. Alternatively, saline contrast echocardiography as a technique for intrapulmonary right-to-left shunts remains less well established, despite the fact that it is more sensitive than pulmonary angiography for detection of even the smallest right-to-left intrapulmonary shunts (Cottin *et al.*, 2004; van Gent *et al.*, 2009).

3.2 Equipment, instrumentation & technique

Subjects are instrumented with an intravenous catheter (i.v.) in a peripheral vein for the introduction of the contrast agent, which is normally air and sterile saline. Typically, 0.5-1 ml of air and 4-10 ml of saline are used to manually agitate between two syringes connected by stopcocks for a total injection volume of 10 ml (Otto, 2004; Feigenbaum, 2005; Woods *et al.*, 2010). In a research setting, equal success has been achieved in detecting right-to-left shunts via intrapulmonary arteriovenous anastomoses using 0.5-1 ml of air and 3-5 ml of saline, for a total injection volume of 5 ml (Stickland & Lovering, 2006; Laurie *et al.*, 2010; Lovering *et al.*, 2010; Elliott *et al.*, 2011a). The agitated saline mix solution should be injected as a bolus, forcibly by hand. Simultaneously, a well-trained sonographer should be acquiring a four chamber apical view of the heart. For superior image quality, the resting subject should be positioned in the left lateral decubitus position so that the heart moves anteriorly and laterally within the chest cavity. If necessary, the left arm should be folded upwards behind the head to expand the ribcage. A mattress cutout/drop-down is beneficial when the subject must be rolled steeply onto their left side to reduce lung artifact during inspiration. The echocardiograph should be preset to digitally acquire a 20-beat loop and the sonographer should employ settings that achieve high resolution without compromising penetration. The focal zone should be set near the base of the heart.

Technique and timing are important for a successful agitated saline contrast echocardiogram with a Valsalva maneuver. The subject should be instructed in the Valsalva maneuver and it is often helpful if they practice it a few times prior to contrast injection. The sonographer should position the patient and locate the best apical imaging window. The patient is asked to inhale a small breath, stop breathing, tighten the stomach muscles and sustain this effort for a minimum of ten seconds. The sonographer should move the imaging plane (typically inferiorly and medially) with the heart during the maneuver and then follow the heart back to the original window upon release of the maneuver. During the maneuver, a second caregiver forcibly agitates the saline mixture by plunging it back and forth between two syringes. When the 10 second maneuver is nearly completed, the contrast is quickly injected. Image acquisition should commence the moment contrast is injected. Immediately following injection, the subject is instructed to release the Valsalva maneuver and take small breaths. Upon release of Valsalva a rush of contrast will quickly opacify the right heart. Additional injections are performed if initial findings are equivocal.

Transesophageal echocardiography (TEE) provides image resolution that is superior to transthoracic echocardiography (TTE). Saline contrast injections are a routine element of

every TEE and intracardiac shunt pathways are often easily identified as contrast passes through them. Patient sedation can prevent adequate Valsalva maneuvers during TEE so right-to-left shunts across a patent foramen ovale may go undetected (Fisher *et al.*, 1995).

3.3 Differentiating between intrapulmonary and intracardiac shunt

Once the agitated saline contrast mix is injected as a bolus, forcibly by hand, timing becomes critical in differentiating between intrapulmonary and intracardiac right-to-left shunts. After the appearance of saline contrast on the right side of the heart, timing of the appearance of saline contrast bubbles on the left heart will determine whether an intrapulmonary or intracardiac shunt is suspected. In general, if bubbles appear on the left side of the heart in ≤ 3 heart beats, then an intracardiac shunt is suspected, e.g. patent foramen ovale, atrial septal defect (Meltzer *et al.*, 1980a; Woods & Patel, 2006). If an intracardiac shunt is suspected, then a second contrast injection should be performed upon the subject's release of a Valsalva maneuver (Woods & Patel, 2006). Performing and releasing the Valsalva maneuver transiently elevates right heart pressure, which reverses the pressure gradient between the atria, creating conditions favorable for right-sided contrast to move to the left side of the heart across the intracardiac shunt. The second injection should confirm the presence of an intracardiac shunt if there is increased contrast and/or if the contrast bubbles continue to appear in the left heart in ≤ 3 heartbeats. Alternatively, if saline contrast bubbles appear in the left heart in > 3 heartbeats after their appearance in the right heart, then an intrapulmonary shunt is suspected, e.g., pulmonary arteriovenous malformation, pulmonary arteriovenous anastomoses (Nanthakumar *et al.*, 2001; Lee *et al.*, 2003; van Gent *et al.*, 2009; Elliott *et al.*, 2011a). The different types of intracardiac and intrapulmonary shunts are outlined in detail below.

3.3.1 Intracardiac shunts

The most common intracardiac shunt pathway is the PFO. Unlike ASDs, a PFO is a feature of normal cardiac development. Although the foramen is no longer patent in the majority of adults, a PFO is detectible in 25 to 40% of the general population (Hagen *et al.*, 1984; Woods *et al.*, 2010; Elliott *et al.*, 2011b). A PFO typically has the echocardiographic appearance of a valve-like flap of tissue covering the foramen ovale in the middle portion of the interatrial septum. This flap can be seen opening intermittently into the left atrium whenever right atrial pressure exceeds left atrial pressure. If fusion of the flap provides a nearly complete seal, the remaining orifice is shaped more like a narrow slit or tunnel. Standard TTE views for visualizing a PFO include the parasternal short-axis view at the level of the aortic valve, the right parasternal bicaval view and the subcostal bicaval view. The atrial septum is best imaged by TEE and a small PFO may only be visualized using this technique. However, saline contrast TTE during the release of a Valsalva maneuver has been found to be even more sensitive than TEE for revealing a PFO (Lam *et al.*, 2010; Gonzalez-Alujas *et al.*, 2011). To achieve the highest sensitivity for intracardiac right-to-left shunting, one should always coordinate contrast injection with the release of a Valsalva maneuver.

Right-to-left shunting may also occur through an ASD. The most common type is a secundum ASD. Unlike a PFO, a secundum ASD typically has the appearance of a hole with defined edges. Similar to a PFO, a secundum defect is located in the middle of the interatrial

septum and may be quite small and difficult to visualize. It is best viewed using the same imaging planes one would use to view a PFO, and might only be detected by a saline contrast injection. Three-dimensional imaging, either TTE or TEE, is a useful method of examining the true shape and area of the defect. It is important to differentiate between a PFO and an ASD because an ASD is less likely to restrict left-to-right shunting and therefore may present a greater risk of right heart volume overload and associated sequelae.

An ostium primum ASD results from the incomplete fusion of the inferior and superior endocardial cushions and therefore is located in the inferior portion of the interatrial septum. An ostium primum ASD may exist in isolation and may be referred to as a partial AV canal. Commonly it is paired with an inlet ventricular septal defect, in which case it bears the name atrioventricular septal defect (AVSD) or complete AV canal. A distinguishing feature of AVSD is that both atrioventricular valves share the same annulus and valve plane. This valvular alignment is visible by TTE in the apical four-chamber view. This is easily distinguishable from normal heart alignment because the normal tricuspid valve plane is displaced towards the apex relative to the mitral valve plane.

A defect adjoining the atria near the junction of the superior or inferior vena cava with the right atrium is a sinus venosus ASD. It most often involves the superior and posterior portion of the interatrial septum and is commonly associated with partial anomalous pulmonary venous return. It can be difficult to detect using standard TTE views but is readily visible by TEE in the bicaval view. An effort should be made to rule out sinus venosus ASD if a substantial and early right-to-left shunt is detected by saline contrast injection without evidence of defects in the secundum or primum septum.

The absence of separation between the roof of the coronary sinus and the floor of the left atrium (coronary sinus defect) has often been categorized as an atrial septal defect because it effectively provides a shunt pathway between the atria via the coronary sinus. This defect is sometimes associated with a common thoracic venous abnormality known as persistent left superior vena cava (PLSVC). A PLSVC provides venous return from the left upper extremity (or both if the right SVC is absent) into the right atrium via the coronary sinus resulting in coronary sinus dilatation. For direct visualization of a coronary sinus defect, TEE is superior to TTE. However, a customized saline contrast TTE can uncover both PLSVC and coronary sinus defect with one injection. Whenever a dilated coronary sinus is detected (usually an incidental finding), a PLSVC and/or coronary sinus defect should be suspected as the cause and a saline contrast injection should be performed (Goyal *et al.*, 2008). The sonographer images the heart using an inferiorly tilted apical four-chamber view to reveal coronary sinus drainage into the right atrium. Once contrast appears within the coronary sinus, the sonographer quickly tilts the scanhead anteriorly to the standard apical four-chamber view. If a PLSVC is present, contrast will be seen in the coronary sinus before it reaches the right atrium. If both a PLSVC and a coronary sinus defect are present, contrast will appear within the left atrium and right atrium simultaneously. If contrast appears within the left atrium shortly following opacification of the right atrium, a PFO is likely but a coronary sinus defect is effectively ruled-out.

Saline contrast echocardiography should not be used to rule out suspected small ventricular septal defects (VSD). Shunting through a small VSD is primarily systolic, left-to-right, and because of the high-pressure gradient they are readily apparent by color flow Doppler on

the right ventricular side of the septum. If a small VSD is suspected by 2D imaging, but there is no high-velocity systolic color jet on the right side of the septum and right ventricular systolic pressure is normal, VSD has been effectively ruled out.

3.3.2 Intrapulmonary shunts

As listed above, the interrogator should count the number of cardiac cycles between right atrial opacification and the arrival of contrast in the left atrium. If the delay is > 3 cardiac cycles, the passage of microbubbles followed a transpulmonary pathway. Intrapulmonary pathways include pulmonary arteriovenous malformations (PAVMs) and intrapulmonary arteriovenous anastomoses. Although PAVMs are considered to be rare, and associated with diseases states, more recent work suggests a prevalence of ~20% in the general population (Woods *et al.*, 2010; Elliott *et al.*, 2011b). Whether or not these pathways detected by Woods and colleagues are truly PAVMS or intrapulmonary arteriovenous anastomoses is unknown. Preliminary findings from our lab suggest that they are the latter (Elliott *et al.*, 2011b), however further research into this area is needed.

Clinically, subjects lay in the supine position for ultrasound imaging. In a research setting, subjects can be in a supine, upright or reclined position, however interpretation of the echocardiograms should take into account body positioning during ultrasound imaging. Specifically, there are data suggesting that intrapulmonary arteriovenous anastomoses are patent in the supine position, but not in the upright position (Stickland *et al.*, 2004; Elliott *et al.*, 2011b). Also, Tobin & Zariquiey demonstrated that intrapulmonary arteriovenous anastomoses 20 to 500 μm in functional diameter are located in the apex of the human lung (Tobin & Zariquiey, 1950). Together, these data support the idea that perfusion of the apices of the lung may open these vessels. Thus, if the goal is to identify the presence of intrapulmonary right-to-left shunts, then subjects should be screened in the supine position. When subjects are in the reclined position, it is recommended that they be rotated 45 degrees on their left side to allow for optimal imaging conditions.

In summary, the chance to detect either an intracardiac or an intrapulmonary right-to-left shunt in healthy human subjects at rest is approximately 60% (40% PFO + 20% intrapulmonary). In subjects with a PFO, it is not possible to unequivocally detect intrapulmonary right-to-left shunts. The reason for this is that bubbles may cross over the inter-atrial septum at any time during echocardiographic imaging. Thus, if bubbles appear in the left ventricle after 10 heartbeats in subjects with a PFO, there is no way to determine if those bubbles crossed the atrium via an intracardiac or intrapulmonary shunt pathway.

3.4 Semi-quantification of right-to-left shunt

There are numerous scoring methods used in both clinical and research settings for *semi-quantification* of right-to-left shunt with saline contrast bubbles (Barzilai *et al.*, 1991; Lovering *et al.*, 2008b; La Gerche *et al.*, 2010; Laurie *et al.*, 2010). These scoring methods take into account the density and spatial distribution of saline contrast bubbles in the left heart. As such, a score of 0 typically represents no saline contrast bubbles, while increasing numbers indicate increasing amounts of saline contrast (Figure 1). Better anatomic approaches to quantification of right-to-left shunts use radiolabeled albumin macroaggregates in

conjunction with nuclear medicine imaging (Whyte *et al.*, 1992; Lovering *et al.*, 2009b), but this topic is beyond the scope of the current chapter.

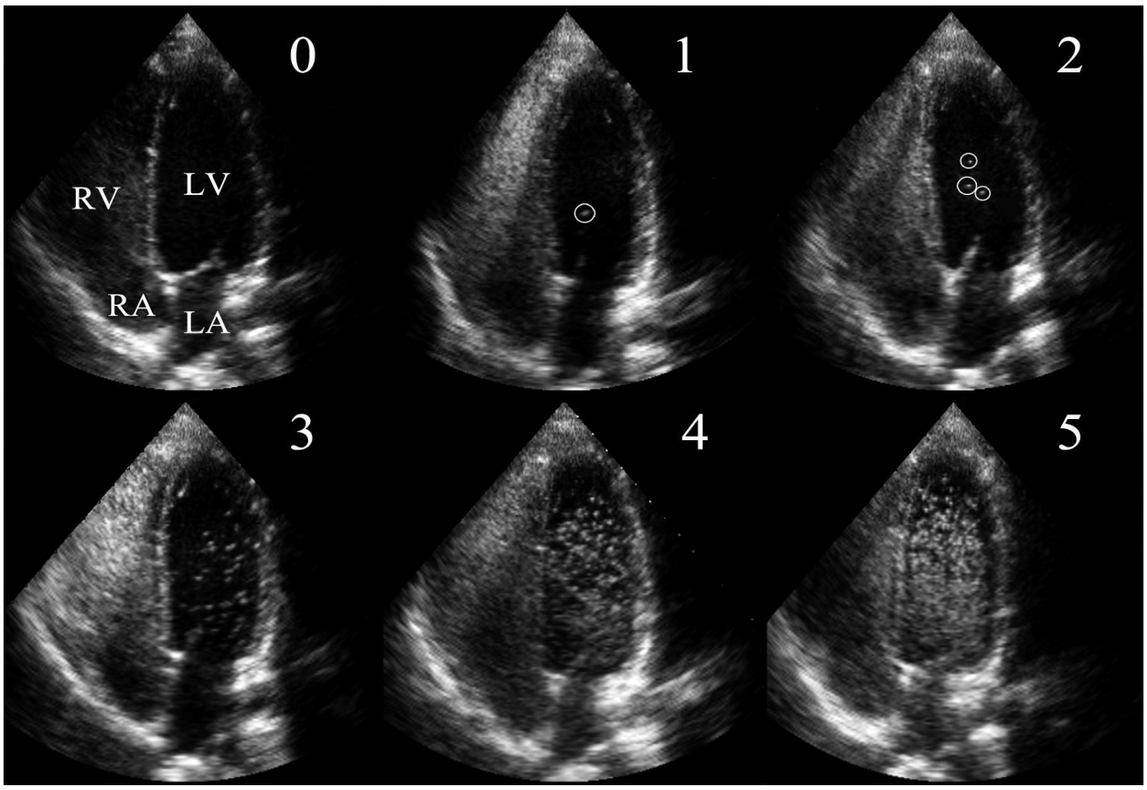

Fig. 1. Representative echocardiograms of bubble scores. Scores are assigned based on both the density and spatial distribution of microbubbles in the left ventricle from the frame with the largest amount of contrast. A score of 0 = 0 microbubbles; 1 = 1 – 3 microbubbles; 2 = 4 – 12 microbubbles; 3 = more than 12 microbubbles in a bolus; 4 = more than 12 microbubbles heterogeneously distributed throughout the left ventricle; 5 = more than 12 microbubbles homogeneously distributed throughout the left ventricle. Scores 1 and 2 have bubbles circled for clarity. RA, LA = right & left atrium; RV, LV = right & left ventricle.

4. Echocardiography for the detection of anatomic right-to-left shunt during exercise & stress

Stress echocardiography is a proven non-invasive technique frequently used to test for flow-limiting coronary artery disease in patients with symptoms of angina. Less commonly, it is used in combination with Doppler techniques to evaluate the effect of stress on valvular lesions and outflow tract obstruction. Saline contrast is also useful during exercise to enhance the Doppler signal or to assess the effect of exercise on right-to-left shunting. Performing echocardiography on an individual during exercise is a challenge to the skill of the sonographer. Obtaining images of diagnostic quality is made more difficult by respiratory artifact, motion of the patient, exaggerated cardiac motion, and tachycardia. It is recommended that only experienced sonographers be selected for the performance of these tests. Furthermore, we strongly suggest that all recommendations by the American Society

for Echocardiography for performance, interpretation and application of stress echocardiography be followed accordingly (Pellikka *et al.*, 2007).

4.1 Technical considerations for echocardiographic measurements during exercise

The ultrasound equipment required for saline contrast echocardiography during exercise are the same as those listed above for resting imaging. Continuous 12-lead electrocardiography is often performed during exercise testing. Depending upon the locations of the imaging windows in an individual during rest and exercise, some of the precordial EKG leads may need to be relocated to allow for echocardiographic imaging. This varies significantly between individuals, but the leads most likely to be affected are V2, V4 and V5. If they must be moved, V2 can be moved to a higher rib space and V4 and V5 can be moved to a lower rib space to accommodate echocardiographic imaging (Figure 2).

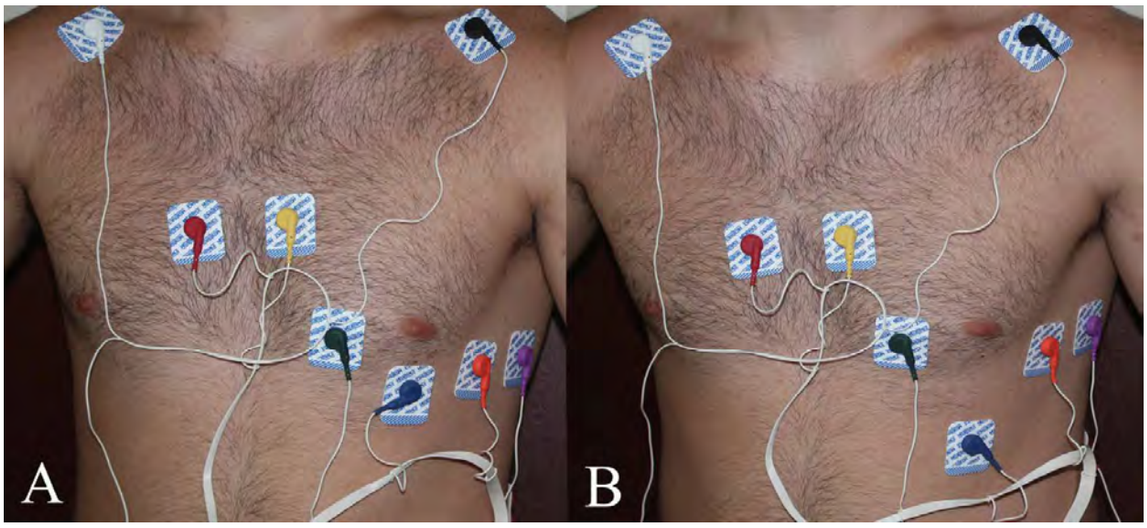

Fig. 2. Placement of 12 lead electrodes for use with ultrasound imaging during exercise. A) normal configuration, B) adaptive configuration example.

4.2 Treadmill versus cycle ergometer exercise:

Most stress echocardiograms are performed using a treadmill and three minute stages of increasing workload. Treadmill exercise has the advantage in that it allows most patients to achieve their target heart rate (85% of the age-predicted maximum) on a treadmill. However, it bears the significant disadvantage that echocardiographic images cannot be acquired during exercise. Images must be acquired immediately following exercise during the recovery phase on an exam table, and for this reason, transient exercise-induced cardiac abnormalities, and right-to-left shunting, can be missed.

Supine and/or recumbent cycle ergometers are popular in many clinical settings because echocardiographic imaging can be performed during exercise (Stickland *et al.*, 2004). The cycling apparatus is built into an exam table so that an individual is able to exercise while lying in the supine or recumbent position. These tables normally include the capacity to be tilted sideward and are equipped with a drop-down section to expose the apical imaging

window. These features permit high quality imaging during various levels of exercise. The primary disadvantage of supine cycle stress is that some patients find it difficult to exercise well in that position and are consequently unable to achieve the target heart rate.

We have considerable experience successfully performing diagnostic contrast-enhanced spectral Doppler studies during exercise and evaluations of right-to-left shunting during exercise on subjects in the forward-leaning upright bike arrangement, or "Aerobar" position (Lovering *et al.*, 2008b; Elliott *et al.*, 2011a) (Figure 3). The "Aerobar" position has several advantages: One, subjects are able to lean forward resting their forearms on bars that allow them to maintain a relatively still upper body during exercise. Two, the apex of the heart falls forward in this position allowing for superior image quality during exercise. Three, this is a more comfortable and more natural position for exercise than the supine bike, so the likelihood of achieving the target heart rate is greater than in supine exercise. Four, evaluation of global and regional left and right ventricular wall motion may also be successfully performed during exercise in this position. A disadvantage is that it can be difficult to image a patient during exercise in this position if they have abdominal obesity. To date, similar results have been found when comparing right-to-left shunt during recumbent and upright exercise (Stickland *et al.*, 2004; La Gerche *et al.*, 2010; Elliott *et al.*, 2011a). There are no published data examining intrapulmonary shunting during supine exercise. We would suggest that body positioning be taken into consideration when making these measurements in the supine position during exercise given the fact that previous work has shown differences in patency of intrapulmonary arteriovenous anastomoses at rest (see **3.3.2 Intrapulmonary Shunts** above). Thus it seems appropriate to use the cycle ergometer-testing paradigm that best suits the investigator needs.

4.3 Non-exercise stress modalities

In addition to cycle ergometer exercise, pharmacologic-induced stress can be used in lieu of "true exercise." Pharmacological stress echocardiography allows for better image quality than any of the competing exercise modalities because the patient is lying still in a position best suited for imaging while the heart is stressed chemically. The most common protocol calls for continuous infusion of dobutamine that increases in three to five minute stages with atropine injections performed during the later stages if necessary to reach the target heart rate (Pellikka *et al.*, 2007). Pharmacological stress echocardiography is the preferred method when a patient is physically unable to exercise or when valvular lesions or outflow tract obstructions need to be assessed. The disadvantage of pharmacological stress is that it is not true exercise. Additionally, many patients do not tolerate the drugs well.

5. Recent research advancements using echocardiography in healthy humans & patient populations

5.1 Research using echocardiography in healthy humans during exercise

Work by our group and others have focused on detection of intrapulmonary and intracardiac shunting at rest and during exercise using saline contrast echocardiography. Succinylated gelatin has been used to detect patent intrapulmonary arteriovenous anastomoses (La Gerche *et al.*, 2010) but there are no data suggesting that this contrast agent is superior to using air and saline alone. Given the fact that additives may increase the risk

of adverse reactions in research subjects, the use of saline and air seems to be the best choice (Bommer *et al.*, 1984; Mulvagh *et al.*, 2008). Commercially available contrast agents contain microbubbles small enough to transit pulmonary capillaries and opacify the left ventricle. By design these agents opacify all four cardiac chambers preventing the viewer from detecting an intracardiac shunt. They are also specifically contraindicated for use when there is a known or suspected intracardiac shunt (Mulvagh *et al.*, 2008).

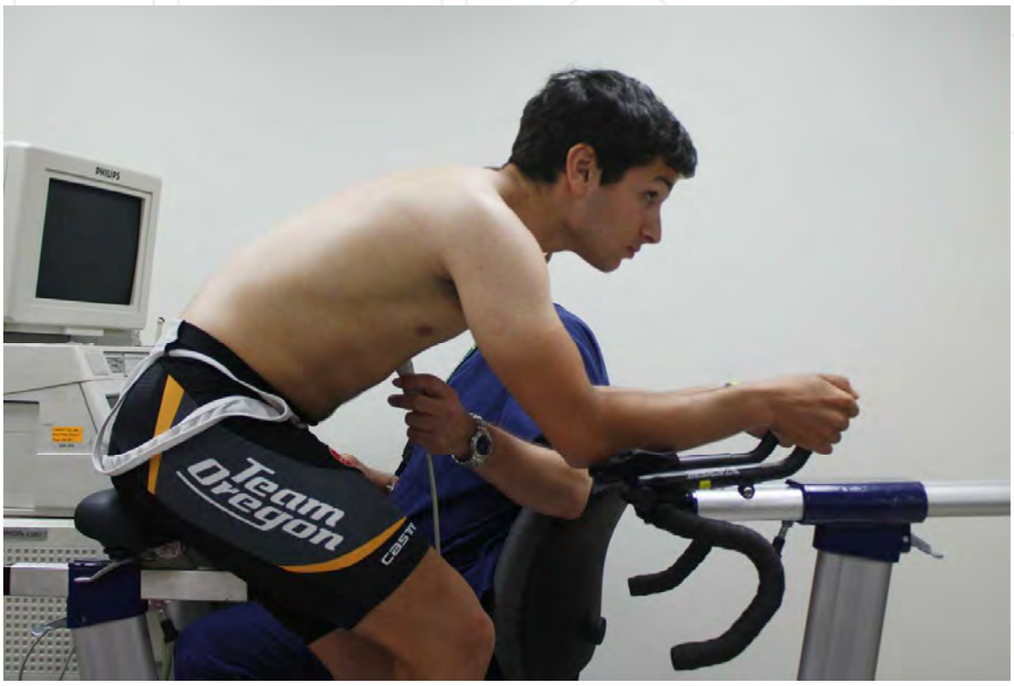

Fig. 3. Subject in the "aerobar" position. Note aerobars on the cycle ergometer with subject in the forward leaning position.

It has been demonstrated that exercise opens intrapulmonary arteriovenous anastomoses that were closed at rest in healthy humans (Eldridge *et al.*, 2004; Stickland *et al.*, 2004; La Gerche *et al.*, 2010; Elliott *et al.*, 2011a). Furthermore, increasing exercise intensity increases the amount of saline contrast that is detected in the left ventricle, which is indicative of increased intrapulmonary shunting (Stickland *et al.*, 2004). It has been suggested that blood flowing through intrapulmonary arteriovenous anastomoses is acting as a "true" shunt (Stickland & Lovering, 2006; Lovering *et al.*, 2009a), however the physiologic role of these vessels remains highly controversial and as of yet, unproven (Hopkins *et al.*, 2009).

The effect of inspired oxygen concentration is another intervention that has been shown to have a modulatory effect on the patency of intrapulmonary arteriovenous anastomoses. We have demonstrated that breathing hyperoxic gas closes intrapulmonary arteriovenous anastomoses at rest and during exercise (Elliott *et al.*, 2011a). This may play a role in detecting intrapulmonary arteriovenous anastomoses at rest in patients with lung disease or healthy human subjects (Elliott *et al.*, 2011b). Conversely, we have also demonstrated that breathing hypoxic gas mixtures will open intrapulmonary arteriovenous anastomoses in healthy humans at rest and will increase the degree of shunting during exercise compared to

exercise in normoxia (Lovering *et al.*, 2008a; Elliott *et al.*, 2011a) (Figure 4). Since arterial hypoxemia is associated with patent intrapulmonary arteriovenous anastomoses in healthy humans, this may have an effect on patient populations with arterial hypoxemia (see below).

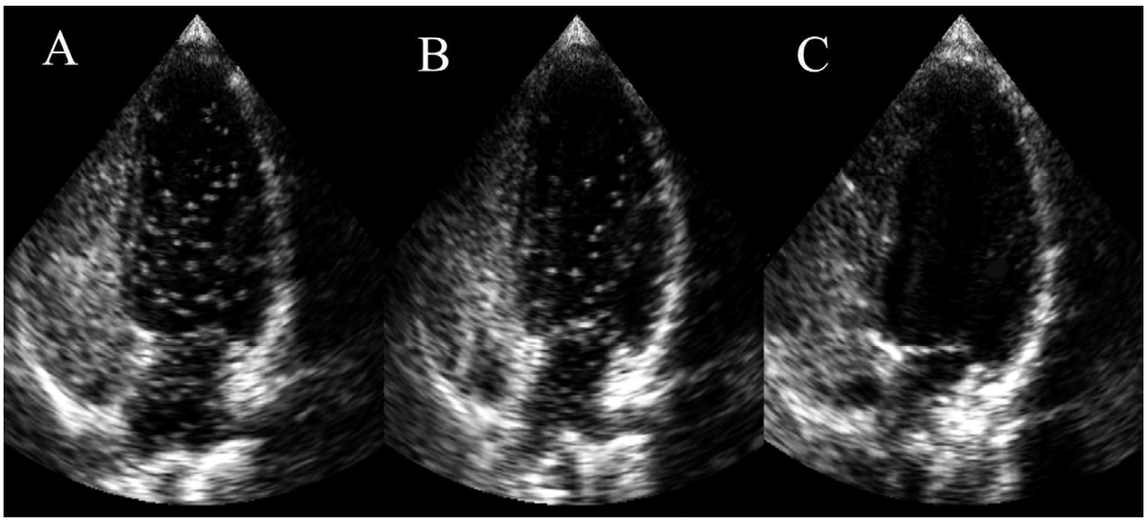

Fig. 4. Echocardiograms during exercise in hypoxia (A), normoxia (B) and hyperoxia (C). Note left side contrast is greatest in hypoxia (A) but is absent during in hyperoxia (C).

Of note, it has been argued that changing inspired oxygen tension may affect the external partial pressure environment (i.e. PO_2 of the blood) such that breathing hyperoxia may shorten the lifespan of saline contrast bubbles whereas hypoxia may lengthen the life span of saline contrast bubbles (Van Liew & Vann, 2010). Although this argument follows mathematical modeling and theoretical calculations, when this question was directly addressed *in vivo* using various inspired gases and saline contrast bubbles made of 100% carbon dioxide, 100% nitrogen, 100% helium, 100% room air or 100% oxygen, it was found that there was no effect on either the bubble score or the sensitivity of the technique (Elliott *et al.*, 2011a). Thus, any effect on inspired oxygen tension is likely a direct effect on the pulmonary vasculature rather than an effect on *in vivo* gas bubble dynamics. These data are further supported by the fact that ventilating dogs with low and high oxygen mixtures results in increased and decreased intrapulmonary shunt fractions, respectively (Niden & Aviado, 1956). In these studies the authors detected right-to-left shunting using solid microspheres (60 to 420 μm in diameter), which clearly would not be affected by altered *in vivo* external partial pressure environments.

5.2 Research using echocardiography in patients with lung disease at rest

Special considerations are suggested when examining certain patient populations. For example, patients with chronic obstructive pulmonary disease (COPD) who also have arterial hypoxemia are likely to have patent intrapulmonary right-to-left shunts at rest (Miller *et al.*, 1984; Dansky *et al.*, 1992). Preliminary work in our lab using saline contrast echocardiography has detected these pathways in subjects with COPD who do not have a PFO (Figure 5). Interestingly, administration of supplemental oxygen to these subjects with COPD closes intrapulmonary pathways suggesting that they are actively regulated.

Other diseases associated with arterial hypoxemia such as hepatopulmonary syndrome and hereditary hemorrhagic telangiectasia are known to have arteriovenous malformations that will allow for the transpulmonary passage of saline contrast bubbles under resting conditions (Woods & Patel, 2006). Thus, patients with underlying lung diseases and arterial hypoxemia, may desaturate further as a result of the opening of hypoxia-induced intrapulmonary arteriovenous anastomoses. It is unknown whether or not hyperoxia would close intrapulmonary arteriovenous anastomoses in these patients, but data from healthy humans suggests that it would be possible (Lovering *et al*., 2008b; Elliott *et al*., 2011a).

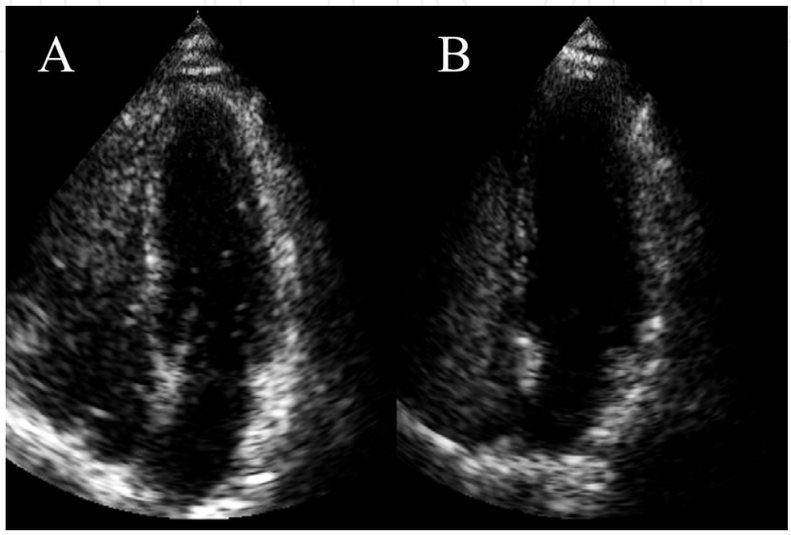

Fig. 5. Intrapulmonary arteriovenous anastomoses in COPD subjects. A) left side contrast in subject at rest with arterial saturation of 94%, B) absence of left side contrast in the same subject breathing 100% O_2 with a saturation of 100%.

6. Conclusion

In conclusion, saline contrast echocardiography is a non-invasive technique that can be used to detect right-to-left shunts in healthy humans and in various patient populations. Timing of the appearance of saline contrast bubbles in the left heart can be used to differentiate intracardiac shunts (e.g. PFOs) from intrapulmonary shunts (e.g. PAVMs) in subjects who do not have both. Special considerations should be taken with the interpretation of the echocardiograms depending on the subject's body positioning, the fraction of inspired oxygen the subject is breathing and the disease status of the patient.

7. Acknowledgement

We thank Kara M. Beasley, BS for assistance with preparation of figures. Andrew Lovering thanks John Hokanson, MD for introducing him to saline contrast echocardiography. Financial support: Oregon Health & Science University Medical Research Foundation Grant, American Lung Association in Oregon Research Grant, University of Oregon/Peace Health Oregon Region Translational Research Award, American Physiological Society's Giles F. Filley Memorial Award for Excellence in Respiratory Physiology & Medicine.

8. References

Barzilai B, Waggoner AD, Spessert C, Picus D & Goodenberger D. (1991). Two-dimensional contrast echocardiography in the detection and follow-up of congenital pulmonary arteriovenous malformations. *Am J Cardiol* 68, 1507-1510.

Belkin RN, Pollack BD, Ruggiero ML, Alas LL & Tatini U. (1994). Comparison of transesophageal and transthoracic echocardiography with contrast and color flow Doppler in the detection of patent foramen ovale. *American heart journal* 128, 520-525.

Bommer WJ, Shah PM, Allen H, Meltzer R & Kisslo J. (1984). The safety of contrast echocardiography: report of the Committee on Contrast Echocardiography for the American Society of Echocardiography. *J Am CollCardiol* 3, 6-13.

Carpenter DA, Ford AL & Lee JM. (2010). Patent foramen ovale and stroke: Should PFOs be closed in otherwise cryptogenic stroke? *Curr Atheroscler Rep* 12, 251-258.

Cottin V, Plauchu H, Bayle JY, Barthelet M, Revel D & Cordier JF. (2004). Pulmonary arteriovenous malformations in patients with hereditary hemorrhagic telangiectasia. *American journal of respiratory and critical care medicine* 169, 994-1000.

Dansky HM, Schwinger ME & Cohen MV. (1992). Using contrast material-enhanced echocardiography to identify abnormal pulmonary arteriovenous connections in patients with hypoxemia. *Chest* 102, 1690-1692.

De Castro S, Cartoni D, Fiorelli M, Rasura M, Anzini A, Zanette EM, Beccia M, Colonnese C, Fedele F, Fieschi C & Pandian NG. (2000). Morphological and functional characteristics of patent foramen ovale and their embolic implications. *Stroke; a journal of cerebral circulation* 31, 2407-2413.

Eldridge MW, Dempsey JA, Haverkamp HC, Lovering AT & Hokanson JS. (2004). Exercise-induced intrapulmonary arteriovenous shunting in healthy humans. *J Appl Physiol* 97, 797-805.

Elliott JE, Choi Y, Laurie SS, Yang X, Gladstone IM & Lovering AT. (2011a). Effect of initial gas bubble composition on detection of inducible intrapulmonary arteriovenous shunt during exercise in normoxia, hypoxia, or hyperoxia. *Journal of Appl Physiol* 110, 35-45.

Elliott JE, Nigam SM, Lauire SS, Yang X, Beasley KM, Goodman RD, Gladstone IM & Lovering AT. (2011b). Pulmonary arteriovenous malformations or intrapulmonary arteriovenous anastomoses in healthy humans at rest. Unpublished Observations.

Feigenbaum H. (2005). *Feigenbaum's Echocardiography*. Lippincott Williams & Wilkins, Philadelphia.

Fisher DC, Fisher EA, Budd JH, Rosen SE & Goldman ME. (1995). The incidence of patent foramen ovale in 1,000 consecutive patients. A contrast transesophageal echocardiography study. *Chest* 107, 1504-1509.

Gonzalez-Alujas T, Evangelista A, Santamarina E, Rubiera M, Gomez-Bosch Z, Rodriguez-Palomares JF, Avegliano G, Molina C, Alvarez-Sabin J & Garcia-Dorado D. (2011). Diagnosis and quantification of patent foramen ovale. Which is the reference technique? Simultaneous study with transcranial Doppler, transthoracic and transesophageal echocardiography. *Rev Esp Cardiol* 64, 133-139.

Goodman M, Porter CA, Czelusniak J, Page SL, Schneider H, Shoshani J, Gunnell G & Groves CP. (1998). Toward a phylogenetic classification of Primates based on DNA evidence complemented by fossil evidence. *MolPhylogenetEvol* 9, 585-598.

Goyal SK, Punnam SR, Verma G & Ruberg FL. (2008). Persistent left superior vena cava: a case report and review of literature. *Cardiovasc Ultrasound* 6, 50.

Hagen PT, Scholz DG & Edwards WD. (1984). Incidence and size of patent foramen ovale during the first 10 decades of life: an autopsy study of 965 normal hearts. *Mayo ClinProc* 59, 17-20.

Homma S, Di Tullio MR, Sacco RL, Sciacca RR, Smith C & Mohr JP. (1997). Surgical closure of patent foramen ovale in cryptogenic stroke patients. *Stroke* 28, 2376-2381.

Hopkins SR, Olfert IM & Wagner PD. (2009). Last Word on Point:Counterpoint: Exercise-induced intrapulmonary shunting is imaginary vs. real. *J Appl Physiol* 107, 1002.

Khurshid I & Downie GH. (2002). Pulmonary arteriovenous malformation. *Postgrad Med J* 78, 191-197.

La Gerche A, Macisaac AI, Burns AT, Mooney DJ, Inder WJ, Voigt JU, Heidbuchel H & Prior DL. (2010). Pulmonary transit of agitated contrast is associated with enhanced pulmonary vascular reserve and right ventricular function during exercise. *J Appl Physiol*.

Lam YY, Yu CM, Zhang Q, Yan BP & Yip GW. (2010). Enhanced detection of patent foramen ovale by systematic transthoracic saline contrast echocardiography. *International journal of cardiology*.

Lamy C, Giannesini C, Zuber M, Arquizan C, Meder JF, Trystram D, Coste J & Mas JL. (2002). Clinical and imaging findings in cryptogenic stroke patients with and without patent foramen ovale: the PFO-ASA Study. Atrial Septal Aneurysm. *Stroke* 33, 706-711.

Laurie SS, Yang X, Elliott JE, Beasley KM & Lovering AT. (2010). Hypoxia-induced intrapulmonary arteriovenous shunting at rest in healthy humans. *J Appl Physiol* 109, 1072-1079.

Lee WL, Graham AF, Pugash RA, Hutchison SJ, Grande P, Hyland RH & Faughnan ME. (2003). Contrast echocardiography remains positive after treatment of pulmonary arteriovenous malformations. *Chest* 123, 351-358.

Liu FY, Wang MQ, Fan QS, Duan F, Wang ZJ & Song P. (2010). Endovascular embolization of pulmonary arteriovenous malformations. *Chin Med J (Engl)* 123, 23-28.

Lovering AT, Eldridge MW & Stickland MK. (2009a). Counterpoint: Exercise-induced intrapulmonary shunting is real. *J Appl Physiol* 107, 994-997.

Lovering AT, Elliott JE, Beasley KM & Laurie SS. (2010). Pulmonary pathways and mechanisms regulating transpulmonary shunting into the general circulation: An update. *Injury* 41S2, S16-S23.

Lovering AT, Haverkamp HC, Romer LM, Hokanson JS & Eldridge MW. (2009b). Transpulmonary passage of 99mTc macroaggregated albumin in healthy humans at rest and during maximal exercise. *J Appl Physiol* 106, 1986-1992.

Lovering AT, Romer LM, Haverkamp HC, Pegelow DF, Hokanson JS & Eldridge MW. (2008a). Intrapulmonary shunting and pulmonary gas exchange during normoxic and hypoxic exercise in healthy humans. *J ApplPhysiol* 104, 1418-1425.

Lovering AT, Stickland MK, Amann M, Murphy JC, O'Brien MJ, Hokanson JS & Eldridge MW. (2008b). Hyperoxia prevents exercise-induced intrapulmonary arteriovenous shunt in healthy humans. *J Physiol* 586, 4559-4565.

Lovering AT, Stickland MK, Amann M, O'Brien MJ, Hokanson JS & Eldridge MW. (2011). Effect of a patent foramen ovale on pulmonary gas exchange efficiency at rest and during exercise. *Journal of applied physiology* 110, 1354-1361.

Lovering AT, Stickland MK, Kelso AJ & Eldridge MW. (2007). Direct demonstration of 25- and 50- μm arteriovenous pathways in healthy human and baboon lungs. *Am J Physiol Heart CircPhysiol* 292, H1777-H1781.

Meltzer RS, Sartorius OE, Lancee CT, Serruys PW, Verdouw PD, Essed CE & Roelandt J. (1981). Transmission of ultrasonic contrast through the lungs. *Ultrasound MedBiol* 7, 377-384.

Meltzer RS, Tickner EG & Popp RL. (1980a). Why do the lungs clear ultrasonic contrast? *Ultrasound Med Biol* 6, 263-269.

Meltzer RS, Tickner EG, Sahines TP & Popp RL. (1980b). The source of ultrasound contrast effect. *J ClinUltrasound* 8, 121-127.

Miller WC, Heard JG & Unger KM. (1984). Enlarged pulmonary arteriovenous vessels in COPD. Another possible mechanism of hypoxemia. *Chest* 86, 704-706.

Movsowitz C, Podolsky LA, Meyerowitz CB, Jacobs LE & Kotler MN. (1992). Patent foramen ovale: a nonfunctional embryological remnant or a potential cause of significant pathology? *J Am Soc Echocardiogr* 5, 259-270.

Mulder BJ. (2010). Changing demographics of pulmonary arterial hypertension in congenital heart disease. *Eur Respir Rev* 19, 308-313.

Mulvagh SL, Rakowski H, Vannan MA, Abdelmoneim SS, Becher H, Bierig SM, Burns PN, Castello R, Coon PD, Hagen ME, Jollis JG, Kimball TR, Kitzman DW, Kronzon I, Labovitz AJ, Lang RM, Mathew J, Moir WS, Nagueh SF, Pearlman AS, Perez JE, Porter TR, Rosenbloom J, Strachan GM, Thanigaraj S, Wei K, Woo A, Yu EH & Zoghbi WA. (2008). American Society of Echocardiography Consensus Statement on the Clinical Applications of Ultrasonic Contrast Agents in Echocardiography. *Journal of the American Society of Echocardiography : official publication of the American Society of Echocardiography* 21, 1179-1201; quiz 1281.

Nanthakumar K, Graham AT, Robinson TI, Grande P, Pugash RA, Clarke JA, Hutchison SJ, Mandzia JL, Hyland RH & Faughnan ME. (2001). Contrast echocardiography for detection of pulmonary arteriovenous malformations. *Am Heart J* 141, 243-246.

Niden AH & Aviado DM, Jr. (1956). Effects of pulmonary embolism on the pulmonary circulation with special reference to arteriovenous shunts in the lung. *CircRes* 4, 67-73.

Otto C. (2004). *Textbook of Clinical Echocardiography*. Saunders, Philadelphia.

Pellikka PA, Nagueh SF, Elhendy AA, Kuehl CA & Sawada SG. (2007). American Society of Echocardiography recommendations for performance, interpretation, and application of stress echocardiography. *Journal of the American Society of Echocardiography : official publication of the American Society of Echocardiography* 20, 1021-1041.

Petty GW, Khandheria BK, Chu CP, Sicks JD & Whisnant JP. (1997). Patent foramen ovale in patients with cerebral infarction. A transesophageal echocardiographic study. *Arch Neurol* 54, 819-822.

Purvis A. (1995). A composite estimate of primate phylogeny. *PhilosTransRSocLond B BiolSci* 348, 405-421.

Stewart CB & Disotell TR. (1998). Primate evolution - in and out of Africa. *CurrBiol* 8, R582-R588.

Stickland MK & Lovering AT. (2006). Exercise-induced intrapulmonary arteriovenous shunting and pulmonary gas exchange. *ExercSport SciRev* 34, 99-106.

Stickland MK, Welsh RC, Haykowsky MJ, Petersen SR, Anderson WD, Taylor DA, Bouffard M & Jones RL. (2004). Intra-pulmonary shunt and pulmonary gas exchange during exercise in humans. *J Physiol* 561, 321-329.

Sun XG, Hansen JE, Oudiz RJ & Wasserman K. (2002). Gas exchange detection of exercise-induced right-to-left shunt in patients with primary pulmonary hypertension. *Circulation* 105, 54-60.

Tobin CE. (1966). Arteriovenous shunts in the peripheral pulmonary circulation in the human lung. *Thorax* 21, 197-204.

Tobin CE & Zariquiey MO. (1950). Arteriovenous shunts in the human lung. *Proc Soc Exp Biol Med* 75, 827-829.

van Gent MW, Post MC, Luermans JG, Snijder RJ, Westermann CJ, Plokker HW, Overtoom TT & Mager JJ. (2009). Screening for pulmonary arteriovenous malformations using transthoracic contrast echocardiography: a prospective study. *Eur Respir J* 33, 85-91.

Van Liew HD & Vann RD. (2010). Sonic echocardiography: what does it mean when there are no bubbles in the left ventricle? *J Appl Physiol* 110, 295; author reply 296-7.

von Hayek H. (1940). öber einen Kurzschlusskreislauf (arterio-venîse Anastomosen) in der menschlichen Lunge. *ZtschrfAnatuEntwklsg* 110, 412-422.

Waggoner AD, Ehler D, Adams D, Moos S, Rosenbloom J, Gresser C, Perez JE & Douglas PS. (2001). Guidelines for the cardiac sonographer in the performance of contrast echocardiography: recommendations of the American Society of Echocardiography Council on Cardiac Sonography. *Journal of the American Society of Echocardiography : official publication of the American Society of Echocardiography* 14, 417-420.

Whyte MK, Peters AM, Hughes JM, Henderson BL, Bellingan GJ, Jackson JE & Chilvers ER. (1992). Quantification of right to left shunt at rest and during exercise in patients with pulmonary arteriovenous malformations. *Thorax* 47, 790-796.

Woods TD, Harmann L, Purath T, Ramamurthy S, Subramanian S, Jackson S & Tarima S. (2010). Small and Moderate Size Right-to-Left Shunts Identified By Saline Contrast Echocardiography Are Normal and Unrelated To Migraine Headache. *Chest*.

Woods TD & Patel A. (2006). A critical review of patent foramen ovale detection using saline contrast echocardiography: when bubbles lie. *J Am SocEchocardiogr* 19, 215-222.

Yang WJ. (1971). Dynamics of gas bubbles in whole blood and plasma. *J Biomech* 4, 119-125.

Yang WJ, Echigo R, Wotton DR & Hwang JB. (1971a). Experimental studies of the dissolution of gas bubbles in whole blood and plasma. I. Stationary bubbles. *J Biomech* 4, 275-281.

Yang WJ, Echigo R, Wotton DR & Hwang JB. (1971b). Experimental studies of the dissolution of gas bubbles in whole blood and plasma. II. Moving bubbles or liquids. *J Biomech* 4, 283-288.

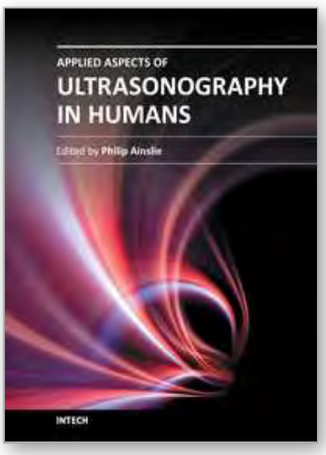

Applied Aspects of Ultrasonography in Humans

Edited by Prof. Philip Ainslie

ISBN 978-953-51-0522-0

Hard cover, 190 pages

Publisher InTech

Published online 25, April, 2012

Published in print edition April, 2012

Written by international experts, this publication provides the reader with the present knowledge and future research directions of diagnostic and therapeutic ultrasound and spectroscopy. Focused topics include Duplex ultrasound, transcranial color Duplex, MRA guided Doppler ultrasonography and near-infrared spectroscopy. New directions in the use and application of transcranial and color Duplex ultrasound are provided, as well as the use of ultrasound and arterial stiffness for measuring human vascular health and circulatory control. Novel use of ultrasound for the detection of intra-cardiac and intra-pulmonary shunts is also described along with its utility for the assessment of gastric regulation and emptying.

InTech Europe
University Campus STeP Ri
Slavka Krautzeka 83/A
51000 Rijeka, Croatia
Phone: +385 (51) 770 447
Fax: +385 (51) 686 166
www.intechopen.com

InTech China
Unit 405, Office Block, Hotel Equatorial Shanghai
No.65, Yan An Road (West), Shanghai, 200040, China
中国上海市延安西路65号上海国际贵都大饭店办公楼405单元
Phone: +86-21-62489820
Fax: +86-21-62489821

IntechOpen